Self-assembled Transition Metal Coordination Frameworks of Carbohydrazone and Thiocarbohydrazone Ligands: Structural, Spectral, Magnetic and Anticancer Properties

Thesis submitted to

Cochin University of Science and Technology

In partial fulfillment of the
requirements for the degree of

DOCTOR OF PHILOSOPHY

Under the Faculty of Science

By

Manoj E.

Department of Applied Chemistry
Cochin University of Science and Technology
Kochi - 682 022

October 2007

to the lotus feet of Sree Padmanabha

Phone Off. 0484-2575804
Phone Res. 0484-2576904
Telex: 885-5019 CUIN
Fax: 0484-2577595
Email: mrp@cusat.ac.in
mrp_k@yahoo.com

DEPARTMENT OF APPLIED CHEMISTRY
COCHIN UNIVERSITY OF SCIENCE AND TECHNOLOGY
KOCHI - 682 022, INDIA

Dr. M.R. Prathapachandra Kurup
`Professor of Inorganic Chemistry`

18th October 2007

CERTIFICATE

This is to certify that the thesis entitled **"Self-assembled Transition Metal Coordination Frameworks of Carbohydrazone and Thiocarbohydrazone Ligands: Structural, Spectral, Magnetic and Anticancer Properties"** submitted by Mr. Manoj E., in partial fulfillment of the requirements for the degree of Doctor of Philosophy, to the Cochin University of Science and Technology, Kochi-22, is an authentic record of the original research work carried out by him under my guidance and supervision. The results embodied in this thesis, in full or in part, have not been submitted for the award of any other degree.

M.R. Prathapachandra Kurup
(Supervisor)

DECLARATION

I hereby declare that the work presented in this thesis entitled **"Self-assembled Transition Metal Coordination Frameworks of Carbohydrazone and Thiocarbohydrazone Ligands: Structural, Spectral, Magnetic and Anticancer Properties"** is entirely original and was carried out independently under the supervision of Professor M.R. Prathapachandra Kurup, Department of Applied Chemistry, Cochin University of Science and Technology and has not been included in any other thesis submitted previously for the award of any other degree.

Manoj E.

18-10-07
Kochi-22

PREFACE

In its method, chemistry is a science of interactions, of transformations and of models. In its object, the molecule and the material, chemistry expresses its creativity. Chemical synthesis has the power to produce new molecules and new materials, with new properties. The appearance of supramolecular chemistry in the late 20th century stimulated new thinking about the relationship of chemistry with biology, that biology and other higher sciences may be considered as emerging out of this new chemistry. The roots of supramolecular chemistry extend into organic chemistry, coordination chemistry and metal ion ligand complexes, physical chemistry, material science and biology. These wide horizons of supramolecular science are a challenge and a stimulus to the creative imagination of the chemist. However, chemistry is not limited to systems similar to those found in biology, but is free to create novel species and to invent processes.

This Ph. D. thesis is mainly concerned with the coordination chemistry of some novel selected transition metal complexes of suitably substituted carbohydrazones and thiocarbohydrazones, with a view to self-assembled molecular square grid architectures, carried out during the period of my research from January 2004 to October 2007. The work presentation comprises reports of relevant related results published so far into a consistent and useful structure as far as that are possible. I hope the work comes up to its premises and proves useful though there remains, however, a lot to be done. Interesting anticipation are due to ideal opportunities that it can provide some steps into the fascinating world of supramolecular chemistry through symmetrical metallosupramolecular square grid complexes and related studies.

Symmetry is everywhere we look in nature. Nature like symmetry as there seems to be a lot of symmetrical objects. In lines to those beautiful symmetrical structures of macro world, building beautiful framework molecules is a subject of keen interest in all branches of synthetic chemistry especially because of their potential applications. The current work focuses on building beautiful molecular

square grid complexes and is reported as a beginning for carbohydrazones. We found many openings for further research and have marked some of them at different places, with auspicious future for similar kinds of work.

Novel magnetic materials and biologically active metal chelates have been the subject of two different but widely interesting area of an Inorganic Chemist. Magnetic materials have a vital role in day-to-day life of mankind. On the other hand, metallo-pharmaceutical compounds have spurred a great interest in the present day medicine. The present work includes the magnetochemistry and preliminary anticancer studies of relevant novel compounds with anticipation of providing routes for novel materials for making life more humane.

The thesis has been divided into six chapters. In Chapter 1, a brief account of self-assembled coordination frameworks with relevance to metallosupramolecular squares along with a general overview of carbohydrazones and thiocarbohydrazones, their chemistry and applications upto their recent developments are described. The introductory chapter also comprises physico-chemical techniques used and some general aspects that found appropriate. Chapter 2 deals with the syntheses and characterization of ligands with a view to spectral and structural features of carbohydrazones and their corresponding thiocarbohydrazones as a comparative study. Syntheses and structural, spectral and magnetic studies of novel nickel, copper and manganese framework complexes are discussed in Chapters 3, 4 and 5 respectively. Anticancer *in vitro* study of selected compounds are described in Chapters 2 and 4. Chapter 6 describes the syntheses and characterizations of zinc and cadmium compounds. A brief summary and conclusion are also added at the last part.

CONTENTS

CHAPTER 3
Ni(II) complexes of carbohydrazone, thiocarbohydrazone and thiosemicarbazone ligands: Structural, spectral and magnetic properties

CHAPTER 4
Cu(II) complexes of carbohydrazone and thiocarbohydrazone ligands: Spectral, magnetic and anticancer studies

CHAPTER 5
Spectral and magnetic studies of Mn(II) molecular frameworks of carbohydrazone and thiocarbohydrazone ligands

CHAPTER 6
Self-assembled Zn(II) and Cd(II) molecular frameworks: Structural and spectral properties

Introduction to carbohydrazones, thiocarbohydrazones and self-assembled transition metal coordination frameworks

1.1. General introduction

Chemistry occupies a unique middle position in the scientific arena, between physics and mathematics on the one side and biology, ecology, sociology and economics on the other [1]. Chemistry is the science of matter and of its transformations, and life is its highest expression [2]. According to reductionist thinking biology is reducible into chemistry, chemistry into physics, and ultimately physics into mathematics. Reductionism implies the ease of understanding one level in terms of another. Mathematics, considered as the language of science, is in analogy to Sanskrit, the language of the Gods. Both these languages are precise and accurate, and yet remain aloof [1]. The extrapolation from physics to chemistry and articulation of chemistry as an independent subject was mainly the handiwork of the great scientist Linus Pauling [3]. However, in moving from the covalent to the non-covalent world we obtain a new chemistry, one that is a starting point for the emergence of the soft sciences. Living systems are viewed as autonomous self-reproducing entities that operate upon information, that originates at the molecular level by covalent chemistry, transferred and processed through non-covalent chemistry, expanded in complexity at the system level and are ultimately changed through reproduction and natural selection [4]. Biology may be considered as emerging out of this new non-covalent chemistry, which in itself cannot be reduced into physics and mathematics as was the case for chemistry thus far practiced. This dualistic nature of chemistry, reducible and

irreducible, is a new development but nevertheless one that ensures that the subject will remain robust in the foreseeable future [1].

Chemistry is oceanic with respect to factual information. In a broad context, the science of chemistry may be viewed as comprised of (i) a conceptual foundation of principles and theoretical, often hypothetical, relationships, (ii) an experimental base of currently available methods and techniques for manipulating and evaluating matter, and (iii) the chemical content, an enormous data base of specific information about individual chemicals, chemical systems, and chemical reactions [5]. Molecular chemistry, the chemistry of the covalent bond, is concerned with uncovering and mastering the rules that govern the structures, properties, and transformations of molecular species [6]. The appearance of supramolecular chemistry stimulated new thinking about the relationship of chemistry with biology and it opens up a huge discontinuity from physics [1]. Supramolecular chemistry, literally means chemistry beyond the molecules, provides a convenient introduction to chemists about the notion of complexity. Since complexity is a temporal attribute what is complex today might become merely complicated tomorrow, or even trivial [1]. Supramolecular chemistry is full of emergent phenomena, as the whole is difficult to predict from the properties of individual parts. The scope and possibilities of this new subject were clearly enunciated by Jean-Marie Lehn [2,6]. The developments in molecular and supramolecular science and engineering offer exciting perspectives at the frontiers of chemistry with physics and biology. Emergence and reductionism are nearly antithetical. Emergent properties are more easily understood in their own right than in terms of lower level properties. So in terms of emergence, a useful way of looking at chemistry and its relationship to mathematics and natural sciences, biology emerges out of chemistry, which emerges out of physics, which emerges out of mathematics, which emerges out of the mind contemplating the Absolute, like Sankara's doctrines of *advaita* [1].

1.2. Coordination frameworks - A brief introduction

In the intervening period of coordination chemistry, which marked from Alfred Werner's seminal article 'Beitrag zur Konstitution anorganischer Verbindungen' [7], this discipline has metamorphized from the province of inorganic chemists to the domain of a broad constituency of researchers, ranging from biochemists to materials scientists [8]. The chemistry of multinuclear coordination metal complexes, especially coupled systems is of special interest in various fields of science including physics, material science, biotechnology, etc. The main reason probably due to the phenomenon of interaction between metal centers lies at the crossover point of two widely separated areas, namely the physics of the magnetic materials and the role of polynuclear reaction sites in biological processes [9]. The growth of coordination chemistry has been three dimensional, encompassing breadth, depth, and applications. The spawning of, or key roles in, new fields is an inevitable consequence of the foundational position of coordination chemistry in the chemical sciences. Complexes containing two or more metal ions are of increasing interest because of their relevance to biological systems also, as evidenced by the many multinuclear complexes in biology [10]. Conversely, in the last two decades, reports of various self-assembled supramolecular transition metal architectures have made a great stimulus in the modern inorganic chemistry in general, and supramolecular coordination chemistry in particular. The past decade has seen a proliferation in the reports of complexes displaying distinct, nonsimple architectures. For example, coordination compounds exhibiting motifs reminiscent of grids, racks, ladders, triangles, squares, hexagons and other polygons, various polyhedra/boxes, cylinders, rods, metallodendrimers, coordination oligomers, rotaxanes, catenanes, knots, circular helicates, etc are known today [11]. The definition of coordinate bonds as supramolecular interactions tends to be limited to those cases where they result in particularly unusual or elaborate molecular architectures [12]. The self-assembly

process offers a valuable means of preparing, in an often rational and highly selective manner, coordination compounds whose structural complexity starts to approach that common in biology. As in biology, such compounds may exhibit novel physical and chemical properties with interesting and useful associated applications. The greatest importance of coordination chemistry in the future will almost certainly be in bringing higher levels of molecular organization into the design of molecules and complicated molecular systems [5].

The primary objective and key step in present study is the design of suitable ditopic ligands with the anticipation of using them as building blocks for transition metal coordination frameworks, mainly molecular square grid complexes. However, the work involves other coordination frameworks like mononuclear, dinuclear, trinuclear and tetranuclear complexes of these ligands also. The reason behind the anticipation and selection of molecular squares is their increasing attention in the current period of coordination chemistry. Metallosupramolecular squares are one of the simplest but nonetheless interesting members of the family of polygons. They have now been considered as versatile substitutes of the conventional organic macrocycles [13]. The synthesis and characterization of molecular squares have achieved growing interest during the last decade especially because of their wide spectrum of applications in science and technology. The first step towards this direction was explored by Fujita *et al.* [14] by making use of the *cis*-protected square planar Pd^{II} and linear bidentate ligand 4,4'-bipyridine. The initial purpose for the construction of molecular squares was to utilize them as artificial receptors [13].

Self-assembly and kinetically controlled macrocyclization are major strategies for the construction of such architectures. Of these, self-assembly is a powerful and simple approach to build up interesting multidimensional frameworks often having versatile magnetic properties and endowed with special functional properties. A more important aspect in this area is that the self-assembled complexes may exhibit new and unexpected properties particularly owing to the binding abilities of the receptor

4

frameworks and the redox or magnetic properties of the metals [15]. Also, with their potential application as functional materials and molecular devices of interdisciplinary area made a rapid development in the synthesis and structural characterization of novel compounds. The inclusion of magnetic metal ions with these polynuclear complexes added a new dimension, which leads nanometer-sized magnetic clusters of versatile magnetic properties. Of these, the grid structures are of special interest in information storage and processing technology [16]. At the same time, the self-assembly process driven by noncovalent interactions are considered as crucial in the proliferation of all biological organisms [17], they can serve as biological models. Stang *et al.*[17] have reported many different molecular square complexes based on square planar coordinated metal centers. The most frequently used metal ions for octahedral centers include Fe(II), Co(II) and Ni(II) [15] and are rare for self-assembled molecular squares of multidentate ligands.

Wurthner *et al.* in 2004 [13] have reported a valuable account of metallosupramolecular squares from their structure to function in detail. One of the main attractive features of molecular squares is their suitability for various functional applications. On the one hand, functionalities can be readily introduced onto metallosupramolecular squares by employing functional ligands and/or metal corners in the assembly processes. Upon square formation these functions may interact leading to a higher level of functionality. Additionally, cavities are created which may accommodate guest molecules. On the other hand, macrocycles containing transition metals are generally more sensitive and responsive on electro- and photochemical stimuli compared to metal-free organic macrocyclic molecules. Therefore, the employment of metallosupramolecular squares may open up new opportunities to develop novel molecular switches and devices [13]. Different molecular functional squares include: (a) squares for molecular recognition by varying the cavity sizes, (b) chiral molecular squares for enantioselective recognition, sensing and catalysis, (c) photoluminescent molecular squares for molecular sensing and as artificial light

5

harvesting systems, (d) redox active molecular squares for electrochemical sensing and (e) molecular squares as catalysts. Due to the photo- and electrochemical activities of incorporated transition metals and chromophoric ligands, metallosupramolecular squares possess also considerable potential for applications in molecular electronics [18]. Through metal-mediated self-assembly, it should be possible to move from discrete molecular squares to more complex infinite 2D square grids and networks, which might involve in the promising application as porous functional materials also.

1.2.1. The method of self-assembly

The term 'self-assembly' is generally agreed to involve the spontaneous assembly of molecules into stable, noncovalently joined aggregates displaying distinct 3-D order [11,19]. While coordinate bonds are highly directional and of greater strength (bond energies ca. 10-30 kcal mol^{-1}) than the weak interactions of biology (bond energies ca. 0.6-7 kcal mol^{-1}), they are nevertheless noncovalent in nature. Indeed, they can be considered to have intermediate properties when compared to covalent bonds (strong and kinetically inert) and the interactions of biology (weak and kinetically labile) [11]. Supramolecular chemistry can be defined as the chemistry beyond the covalent bond or the chemistry of associates with a well-defined structure [6,20]. In this regard, in supramolecular coordination chemistry, self-assembly is a powerful approach which involves the encoding of coordination information into a ligand, and then using a metal ion to interpret and use this information, according to its own coordination preferences, in order to organize the growth of large polynuclear metal ion arrays. Strategies to produce desired self-assembled coordination frameworks of transition metal centers include design and synthesis of a polyfunctional ligand and judicial utilization of its organizing ability to suitable metal ions. Building grids or supramolecular architectures of nanoscopic dimensions from

individual subunits using sequential bond formation methodologies on the other hand is time-consuming and results in low yields.

Grid-like two-dimensional arrangements of metal centers offer significant benefits to random clusters, in that flat surface arrays are possible. The organization of paramagnetic metal centers into regular grid like arrangements has been achieved using the ligand directed self-assembly approach and examples of 2×2 and 3×3 grid structures have been produced [21]. The success of this approach relies on the fact that the structural attributes necessary for the formation of a specific grid arrangement are pre-programmed into the ligand itself and the grid formed by a self-assembly process in which the donor groupings of the ligand are read by the metal ions in terms of their coordination algorithms as the polynuclear structure is built [21].

A characteristic feature of all "strict" or "thermodynamic" self-assembly processes is that a kinetically rapid, reversible thermodynamic equilibrium exists between the starting materials and the products at all times and for all steps [11]. The proportion of each product obtained in the final mixture is then determined by its relative thermodynamic stability. As the equilibrium is reversible, the process is self-correcting; a bond, which is initially formed "incorrectly" can therefore dissociate and reassociate "correctly". To be practically useful, however, a thermodynamic self-assembly process should generate one product, which is substantially more stable than any of its competitors; this ensures a near-quantitative yield of that substance. While thermodynamic self-assembly is particularly common in coordination chemistry, other forms of self-assembly also exist. From the biological literature, Lindsey [22] has identified six further self-assembly processes: (i) irreversible self-assembly, (ii) assisted self-assembly, (iii) directed self-assembly, (iv) precursor modification followed by assembly, (v) self-assembly with post-modification and (vi) self-assembly with intermittent processing.

The requirements for a thermodynamic self-assembly of a metallocycle are that (i) coordination bonds must form between the donor and acceptor elements

7

involved, (ii) the bonds must be kinetically labile so as to allow self-correction and (iii) the desired assembly must be thermodynamically more favorable than any competing species. Several studies have examined the role of thermodynamic factors in the self-assembly of metallocyclic compounds [11]. These have generally concluded that cyclic structures are preferred over linear ones for enthalpic reasons, while small cycles are favored over large cycles (at low concentrations) for entropic reasons. In coordination chemistry, the enthalpic driving forces in a self-assembly reaction invariably dominate the entropic ones because of the large enthalpy of coordinate bond formation.

The size of large polymetallic clusters is difficult to control, and these systems are invariably obtained serendipitously through self-assembly reactions. Controlling the nuclearity for clusters of large numbers of metals is very difficult, and requires an ingenious approach to the design of a single ligand. A more practical approach is based on the propensity of metal ions, given the right coordination environment, to self-assemble into a cluster. This occurs readily with simple bidentate ligands, which do not fully satisfy the coordination requirements of a single metal, and the vacant coordination sites are filled by spare donor fragments from a neighboring subunit as the overall cluster forms in a self-assembly process [23]. However, a significant amount of control can be exerted over the formation of relatively low nuclearity molecular clusters ($<M_6$) by the use of polyfunctional and polytopic ligands with well-defined and appropriately positioned coordination pockets. If the pockets form a contiguous linear array the outcome of the self-assembly process can lead to grids, with the possibility of significant magnetic exchange between adjacent paramagnetic metal centers if appropriate bridging groups are included. The advantage is that ligand design features can be pre-programmed into a system to generate a polynuclear system of specific size, and possibly with tailored magnetic properties [24].

8

1.2.2. Metallosupramolecular squares

Cyclic tetranuclear metal complexes with ~90° angles at the corners (molecular squares or molecular boxes) are of great interest [25]. The complexes having an 'array of metal centers at the vertices of a (approximate) square lattice' is the reason behind the name. 'Polytopic' ligands, with well defined and appropriately separated coordination compartments, in principle have a better chance of control over the outcome of a self-assembly process to produce a cluster with a predefined nuclearity. Here, the ligands have two potential coordination pockets (ditopic) and involve monatomic bridging groups. Thermodynamically favored grid complexes are formed by self-assembly process in high yield as suggested by so far obtained results [13], with homoleptic and non-homoleptic examples.

Based on rapid chemical exchanges among starting materials, intermediates (*e.g.* oligomers and polymers) and final ensembles during the coordinative assembling processes the composition of the final products depends primarily on the thermodynamic parameters of the possible products and intermediates. Such exchange provides an efficient mechanism for error correction, which may result in the conversion of thermodynamically unfavorable intermediates into a single final product. However, thermodynamic control only affords the formation of a single product if this product has a sufficient thermodynamic advantage over the other possible species. For many metallosupramolecular systems, two or more species are in equilibrium because no clear thermodynamic preference for one species is given. From the viewpoint of thermodynamics, enthalpy favors the formation of squares, which have less conformational strain (90° corner) than triangles (60° corner), while entropy favors the formation of triangles, which are assembled from fewer components than squares. As a consequence, both the triangular and square species may co-exist in solution. However, the reversibility of metal–ligand coordination

plays a pivotal role in the formation of metallosupramolecular squares in high yields by avoiding other macrocyclic or polymeric by-products [13].

Taking together all the information available on metal-directed self-assembly, it can be concluded that the formation of metallosupramolecular squares is a more complex process than simple chemical equations of their preparation disclose [13]. For a typical self-assembly process, open polymeric intermediates have to be considered which can be transformed to a specific macrocyclic product only under the conditions of reversibility. The possible equilibria in such a self-assembly process are schematically presented [13] in Fig. 1.1. As can be seen, the coordinative interactions between metals and ligands lead initially to the formation of openchain oligomers (n = 1, 2, 3,...∞), which may be transformed to the corresponding cyclic products through a macrocyclization process. In this context, the generation of a specific macrocycle depends on its thermodynamic advantage compared to other cyclic species. In order to achieve this desired situation, the building blocks must be designed properly.
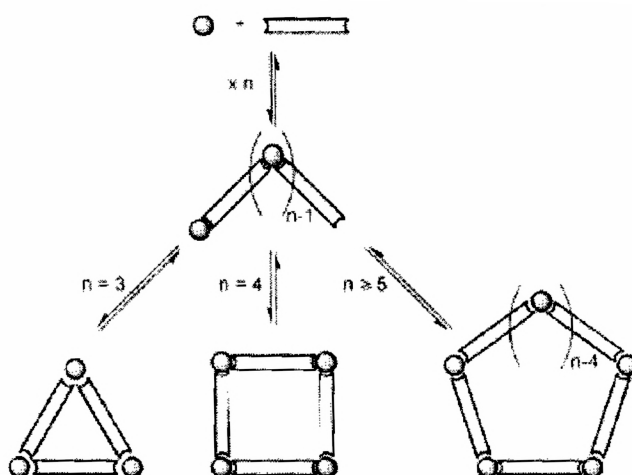
Fig. 1.1. Possible equilibria between linear and cyclic oligomeric species in the self-assembly process (metal corners shown as circles, ditopic ligands shown as connecting the corners).

According to some studies [26,27] regarding the physical basis of self-assembly macrocyclization for the 1:1 model system, the formation of macrocyclic species can only be accomplished in a certain concentration range between the lower self-assembly concentration (lsac) and the effective molarity (EM) of the self-assembled macrocycle; since monomer and linear oligomers prefer to exist in the lower and higher concentration ranges, respectively. In a qualitative manner, this distribution of various self-assembled species as a function of concentration is illustrated [13] in Fig. 1.2. The parameter EM is a measure for the concentration at which open polymeric structures start to compete with the respective macrocycles (here the squares), while lsac refers to the concentration at which the macrocycle is half-assembled from the initial building blocks.
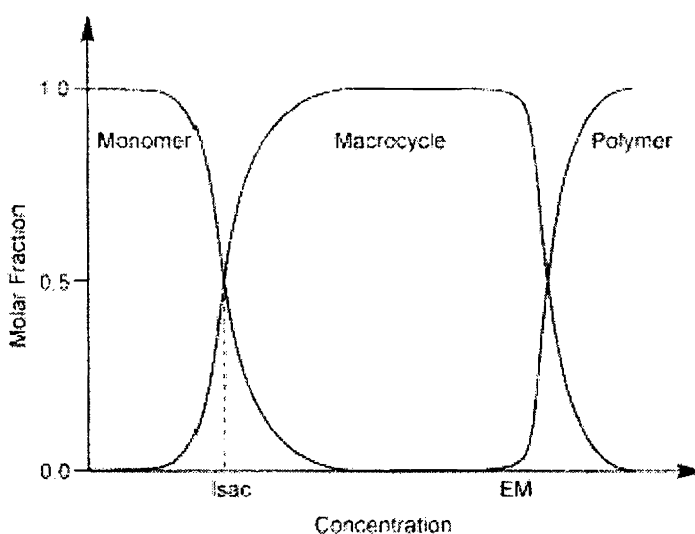
Fig. 1.2. The distribution of self-assembly species as a function of concentration.

According to this thermodynamic analysis of self-assembly macrocyclization, desired macrocyclic products exist as major species only within a limited range of concentration under given temperature and solvent conditions [13]. In order to accomplish self-assembly already at low concentration, the coordinative bonds should

exhibit considerable thermodynamic stability. To achieve this, the binding constant (and the related Gibbs free energy) for the respective monotopic model building blocks should be high. A large EM is desired for the square macrocycle to avoid transformation into metallosupramolecular polymers even at high concentrations. Finally, other cyclic species should exhibit much smaller EM values than that of the square to provide a clear thermodynamic advantage for square macrocycles. To accomplish these goals rigid building blocks are required whose structural predisposition affords square macrocycles that are free of strain.

Molecular design and chemical templates will help provide the species and processes that create order. It is as it has always been that the enemy is the second law of thermodynamics. The job of coordination chemists is, within the systems that are their focus, to confound the second law. That is the essence of molecular organization, and, within limits specified in the concept of a coordination entity, the broad mission of the complete coordination chemistry [5]. It may appear obvious that the self-assembly of geometrically shaped polygons and polyhedra must involve ligands which are somewhat conformationally inflexible. However square complexes, which employ linkers that are generally considered flexible or semiflexible are known. Molecular squares involving these ligands are typically stabilized by (i) conformational restraints inherent to the motif itself, (ii) steric or repulsive interactions to minimize crowding, (iii) attractive π-interactions, or (iv) the presence of bridging atoms/groups on the sides of squares [11]. For example, the first molecular square of a thiocarbohydrazone [28] is stabilized by bridging thiocarbohydrazide S-atoms on each side; as this molecule contains a large central cavity surrounded by a lattice-like arrangement of ligands, it can also be considered a grid [11]. So by using rigid building blocks of suitably substituted thiocarbohydrazones and taking advantage of octahedral geometries of metal centers, molecular square grids [28-31] can be readily achieved.

1.2.2.1. Characterization of molecular squares

Proper characterization of metallosupramolecular square compounds is not a trivial task and the unequivocal characterization of these self-assembled species requires different complementary methods such as NMR, IR, UV-vis, XRD, mass spectrometry etc. This is because the structure and stability of coordination squares are critically dependant on various factors such as the nature of ligand, metal ions, solvent, concentration, temperature and even counterions [13].

For diamagnetic complexes, NMR can provide the basic structural information about coordination sites, components and symmetry of the assembly. Usually a single set of proton signals in ¹H NMR spectra indicates symmetrical geometry of the species. However, the molecular squares may deviate from symmetric geometry and results to increase in number of signals and assignments become a rigorous task. A charge neutral molecular square of Cd(II) of 1,5-bis(6-methyl-2-pyridyl-methylene) thiocarbohydrazone have been studied [31] by ¹H NMR and identified the presence of lower molecular weight oligomers. The single crystal X-ray analysis, undoubtedly, the most reliable and effective method for the characterization of assemblies in the solid state provides directly structural details. However the solid-state structure of a thermodynamically controlled system may not necessarily be identical with the structure that prevails in solution. Also, characterization of molecular squares based on X-ray crystallography is often hampered by difficulties in growing high-quality single crystals, especially for those with large cavities [13]. Mass spectroscopy may provide information on molecular size, stability and fragmentation pathway. The most widely used ionization modes for the analysis of supramolecular structures by MS include fast atom bombardment (FAB), electrospray ionization (ESI) and matrix-assisted laser desorption ionization (MALDI). These relatively soft ionization methods are suited particularly for weakly bound noncovalent species. Nevertheless, it is often not possible to ionize such self-

assemblies to generate sufficient ion abundance without fragmentation. Also, the assignments of square structures based on mass signals need caution, since triangle or unspecific aggregates may generate during ionization processes [32]. So several complimentary analysis methods are necessary for the unequivocal characterization of these assemblies.

1.3. A preface on carbohydrazones and thiocarbohydrazones

Carbohydrazones and thiocarbohydrazones are condensation products of carbohydrazide and its thio analogue thiocarbohydrazide respectively with carbonyl compounds. Carbohydrazide and thiocarbohydrazide are next symmetric homologue of urea, the compound most directly associated with the foundation of organic chemistry, and thiourea respectively. Curtius and Heidenreich have described in 1894 and more fully in 1895 [33] the synthesis and characterization, by its conversion into suitable derivatives, of carbohydrazide by the hydrazinolysis of diethyl carbonate. In 1908 Stolle, formerly Curtius' assistant, discovered thiocarbohydrazide by continuing the work [34]. In between and in the next decades the mono and di condensation derivatives of carbohydrazide and thiocarbohydrazide with aldehydes and ketones, carbohydrazones and thiocarbohydrazones, were reported by various research groups [34-36]. A comprehensive and critical account of the chemistry of carbohydrazide and thiocarbohydrazide and their relevant derivatives have been provided by Frederick Kurzer and Michael Wilkinson in 1970 [36]. The systematic review covers historical works and all subsequent corrected works of previous studies to the end of that period with then state of knowledge. Conversely, the crystal and molecular structure of thiocarbohydrazide was reported by Braibanti *et al.* [37]. The crystal structure of carbohydrazide was reported by Domiano *et al.* [38] and later along with electron deformation density distribution [39] and ab initio molecular orbital studies [40].

Carbohydrazide and thiocarbohydrazide possess a number of synonyms. The various names of carbohydrazide include 1,3-diaminourea, N,N'-diaminourea,

14

carbazic acid hydrazide, carbazide, carbodihydrazide, carbonic acid dihydrazide, carbonic dihydrazide, carbonohydrazide, carbonylbis-hydrazine, carbonyldi-hydrazine, N-aminohydrazinecarboxamide, hydrazinecarboxylic acid hydrazide and 4-aminosemicarbazide while thiocarbohydrazide includes TCH, 1,3-Diamino-2-thiourea, thiocarbazide, thiocarbonohydrazide, thiocarbonic dihydrazide, carbonothioic dihydrazide and hydrazinecarbohydrazonothioic acid. The names carbonohydrazide (preferred to carbohydrazide or carbazide) and thiocarbonohydrazide are as per IUPAC rules [41]. The numbering scheme of carbohydrazide and thiocarbohydrazide are given in Scheme 1.1. The derivatives formed by the removal of both hydrogens on N^1 or N^5 using aldehyde or ketone may be named by adding the word 'carbohydrazone or thiocarbohydrazone' after the name of the aldehyde or ketone.
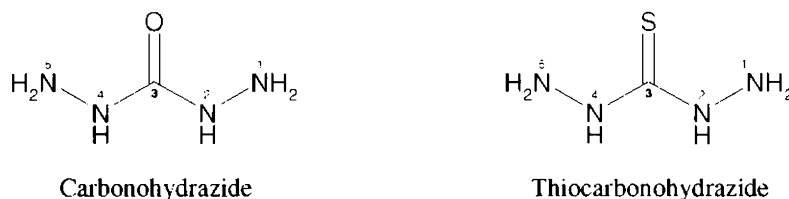
Scheme 1.1. Structure and numbering of carbohydrazide and thiocarbohydrazide.

The aldehyde and ketone disubstituted carbohydrazide compounds are thus named as bis(aldehyde or ketone) carbohydrazone or more correctly 1,5-bis(aldehyde or ketone) carbohydrazone and likewise for substituted thiocarbohydrazides.

Thiourea, thiosemicarbazide and thiocarbohydrazide are known to form complexes with different transition metals [42]. Many closely related compounds like bis(salicylidene) carbonohydrazide [43,44], substituted carbazones [45,46] and their complexes [47-50] have been reported. Thiocarbohydrazides usually behave as neutral or uninegative ligands and bind the metal through one sulfur atom and one hydrazinic nitrogen atom [51]. Carbohydrazide and thiocarbohydrazide have the coordination ability to form mononuclear or even dinuclear coordination compounds [52]. Reports

15

of mono or dinuclear dioxomolybdenum [51,53], tin [54] and niobium [55] complexes of different thiocarbohydrazones are reported. Similarly, oxovanadium(IV) [56], La(III) and Pr(III) [57] complexes of some carbohydrazones and other complexes of related substituted carbohydrazides [58,59] are reported. Also, many reports of substituted carbohydrazides and thiocarbohydrazides are in patent literature [60-64].

The (thio)carbohydrazones are next higher homologue of (thio)semicarbazones with a possible extra metal binding domain. Their coordination chemistry towards transition metal ions are found least studied compared to lower homologues. Reports of some interesting compounds of suitably substituted thiocarbohydrazones in the last decade [28-31, 65-68] provided a new dimension to the chemistry of thiocarbohydrazones and carbohydrazones, and is mainly behind our interest. We designed some flexible ligands, suitably substituted carbohydrazones and thiocarbohydrazones, mainly having two potential coordination pockets (ditopic). Coordination frameworks of these ligands towards selected metal ions and their important features are the subjects of our study.

1.3.1. Applications of carbohydrazones and thiocarbohydrazones

Carbohydrazones and thiocarbohydrazones are an important class of compounds and has been achieved the attention of various fields of biology and different branches of chemistry. The attention of applications of carbohydrazones and thiocarbohydrazones were arrived, ever since their discovery, as an extension of the application studies of their precursors carbohydrazide and thiocarbohydrazide. In short, carbohydrazide and thiocarbohydrazide are found useful in biochemical [69], pharmacological and related properties like convulsant, anticarcinogenic, antibacterial, fungicidel, etc [36]. Carbohydrazide and thiocarbohydrazide are used for the formation of industrially important various polymers, in photography, and for various miscellaneous uses [36]. Carbohydrazones and thiocarbohydrazones have also been reported with most of these applications [36]. They have been found a variety of

16

industrial uses, many of which are covered by the patent literature [60-64]. The chelating ability of some thiocarbohydrazones have been reported as useful analytical reagent for the quantitative extraction of different divalent metals like Co(II), Ni(II), Cu(II), Zn(II), Cd(II), etc and photometric and fluorimetric determinations [70,71].

Carbohydrazones and thiocarbohydrazones are the next higher homologues of potential biologically important compounds after semicarbazones and thiosemicarbazones. However little is known about the biological properties of thiocarbohydrazones [68,72] and likewise for carbohydrazones. Carbohydrazones and thiocarbohydrazones of various unsaturated ketones and Mannich bases were evaluated for their cytotoxic properties [73]. Some thiocarbohydrazones are reported to have antimicrobial activity towards bacteria and fungi [58,68,72,74]. Of these, the bisthiocarbohydrazones possess the highest antibacterial activity compared to their monothiocarbohydrazones and are potentially useful as antimicrobial agents against *Gram-positive bacteria* [68]. It is reported that many monocarbohydrazone ligands act as mutagenic agents, whereas bis substituted derivatives are devoid of mutagenic properties [68]. As an inactivator of *HSV-1 ribonucleotide reductase* a series of 2-acetylpyridine thiocarbohydrazones are found to possess better activity than that of corresponding thiosemicarbazones [75,76]. Thiosemicarbazones have been extensively studied since their biological activities were first reported in 1946 [77]. They have drawn great interests for their high potential biological activity especially their antitumor activity [78] and is still gaining high attention [79,80]. Antitumor functions of 1,2-naphtho-quinone-2-thiosemicarbazone (NQTS) and its metal complexes {Cu(II), Pd(II), and Ni(II)} against the MCF-7 human breast cancer cells and the possible mechanisms of action were determined [81] and there are reports that the substituents in these compounds affect their antitumor activities strongly. Several other reports of thiosemicarbazones and their metal complexes as anticancer drugs have been reported [82-85]. In this regard, the higher homologues, especially Cu(II) complexes, are anticipated as anticancer drug analogues [66,67].

1.3.1.1. Anticancer drugs-A brief report

Cancer chemotherapy uses compounds that can differentiate to some degree between normal tissue cells and cancer cells. Mechlorethamine, a derivative of the chemical warfare agent nitrogen mustard, was first used in the 1940s in the treatment of cancer and was shown to be effective in treating lymphomas. Since then, many antineoplastic drugs have been developed and used with much success. Because cancer cells are similar to normal human cells, the anticancer agents are generally toxic to normal cells and can cause numerous side effects, some of which are life threatening. These adverse effects may require that the drug dosage be reduced or the antineoplastic drug regimen be changed to make the drug tolerable to the patient [86].

Alkylating agents were the first anticancer drugs used, and, despite their hazards, they remain a cornerstone of anticancer therapy. Some examples of alkylating agents are nitrogen mustards (chlorambucil and cyclophosphamide), cisplatin, nitrosoureas (carmustine, lomustine, and semustine), alkylsulfonates (busulfan), ethyleneimines (thiotepa) and triazines (dacarbazine). These chemical agents are highly reactive and bind to certain chemical groups (phosphate, amino, sulfhydryl, hydroxyl, and imidazole groups) commonly found in nucleic acids and other macromolecules. These agents bring about changes in the deoxyribonucleic acid (DNA) and ribonucleic acid (RNA) of both cancerous and normal cells. The result is that the nucleic acid will not be replicated. Either the altered DNA will be unable to carry out the functions of the cell, resulting in cell death (cytotoxicity), or the altered DNA will change the cell characteristics, resulting in an altered cell (mutagenic change). This change may result in the ability or tendency to produce cancerous cells (carcinogenicity). Normal cells may also be affected and become cancer cells. Alkylating agents have found use in the treatment of lymphoma, leukemia, testicular cancer, melanoma, brain cancer, and breast cancer. They are most often used in combination with other anticancer drugs [86].

1.4. Importance of carbohydrazones and thiocarbohydrazones

Metal complexes of Schiff bases have played a central role in the development of coordination chemistry. The substitution by aldehydes or ketones having extra coordinating groups can increase their diversity towards forming coordination compounds. There are reports of monosubstituted carbohydrazones and their mononuclear metal complexes [65]. However, when substituting both sides with pyridine like coordinating groups lead to two tricoordinating pockets and thereby it offers various possibilities. The thiocarbohydrazones with suitable substituents as ditopic ligands using bridging sulfur atoms are capable of generating self-assembled molecular squares as evidenced by the four publications so far [28-31]. This potential class of building blocks thus offers a precise pathway for molecular frameworks in a controlled manner. However there was no report of their oxygen analogue acting as building blocks for molecular frameworks through self-assembly. The carbohydrazones are not much studied like thiocarbohydrazones perhaps due to a possibility of degradation of the carbonyl group. With the anticipation that suitable carbohydrazones can also produce metallosupramolecular squares we selected both thiocarbohydrazones and carbohydrazones as the building blocks.

(Thio)carbohydrazone ligands are generally in the (thio)keto form in solid state. However, in solution they can exist in (thio)keto or (thio)enol tautomeric forms. Moreover, the (thio)enol tautomers can exist as *syn* and *anti* geometric isomers as a consequense of the double bond character of the central N–C linkage. The different tautomeric forms of carbohydrazones and thiocarbohydrazones are as given in Scheme 1.2. In the *syn* (thio)enol tautomeric form and in the (thio)keto form (thio)carbohydrazones are capable to act as building units for square grids, while in the *anti* form the ligands are potentially hexadentate with two sets of nonequivalent coordination sites.

(Thio)ketone form (X=O, S)   (Thio)enol form, syn (X=O, S)

(Thio)enol form, anti (X=O, S)
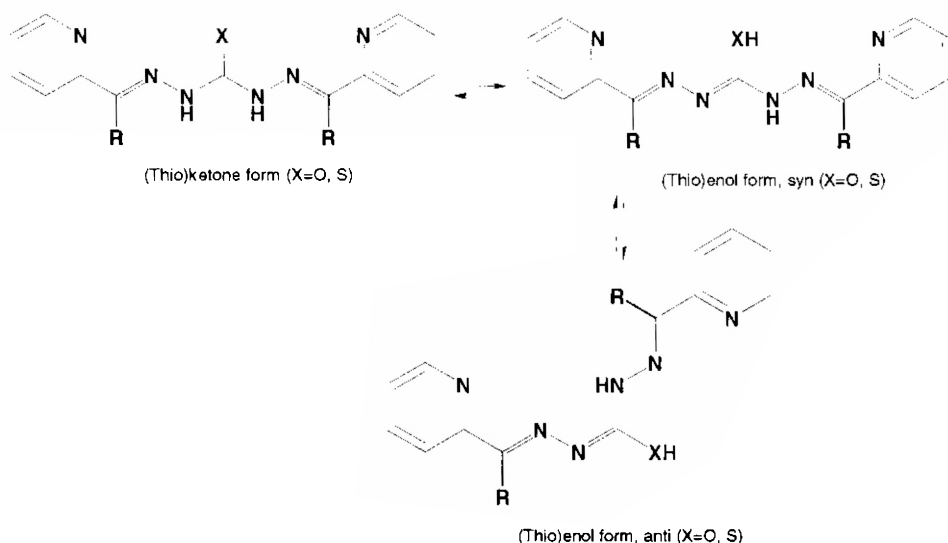
Scheme 1.2. Different tautomeric forms of (thio)carbohydrazones.

The geometrical constraints that prevails within the self-assembly of metals are of greatest importance for controlled assembly process. Suitably substituted thiocarbohydrazone ligands favors cyclic tetramers for octahedral metal centers as the most possible compound [31]. The bridging sulfur donor requires pairs of metal ions to assemble in a *syn* manner when coordinated within each M_2L (or M_2HL or M_2H_2L) moiety. It follows that, for six-coordination to be achieved at each center, only an equal and even number of metal ions and thiocarbohydrazones can lead to closure of a cyclic oligomer. All other combinations of metals and ligands must be open-chain. However only a 4:4 metal/ligand assembly enables an *orthogonal* coordination of the two tridentate N, N, X units, leading to the least distorted six-coordinate geometry [31]. For example, a 6:6 cyclic hexamer would require a 30° twist of each N, N, X chelate away from orthogonality (with respect to its companion ligand), which would introduce considerable non-bonded repulsion.

Crystal structures of all thiocarbohydrazone ligands reported so far [29,65,68,87] are in amidothioketone tautomeric form. Similar is the case with

carbohydrazone [65] as it shows amidoketone tautomeric form. However, the enol tautomer (in solution) can adopt a *syn* or *anti* configuration as a consequence of the double-bond character of the central N–C linkage. The *syn* configuration is essential for getting molecular square architectures of thiocarbohydrazone derived octahedral centers. So far reported square complexes [28-31] are all formed with *syn* configuration of respective ligands in deprotonated forms.

1.5. Objectives of the present work

Since the properties of any material are largely due to its structure, control over the structure allows to manipulate these properties. By judicious choice of preferred ligand and metal coordination geometries, control over the topology can be gained. On the other hand, therapeutic applications of inorganic chemistry in medicine are varied, encompassing many aspects of the introduction of metal ions into the body. These successful developments of metallo-pharmaceutical compounds also have prompted many researchers to provide other types of therapeutic agents using the unique and characteristic properties of metal ions. Carbohydrazone and thiocarbohydrazone structures are found to show different specific properties like different potential biological activities, energetic materials (as they are derivatives of energetically important hydrazines), etc and are least studied, in addition to the capability to act as building blocks for metal-organic frameworks. Keeping these in mind we undertook the present work with the following objectives.

➤ design, synthesize and characterize some chelating ligands, carbohydrazones and thiocarbohydrazones, and compare their spectral features

➤ study the coordination behavior of these ligands towards selected metal ions

➤ to use these ligands as building blocks to synthesize novel self-assembled molecular square grid complexes

➤ better understanding of the structural and spectral properties of the complexes

> ➤ establishing the structure of the complexes mainly by mass and single crystal X-ray crystallography

> ➤ to investigate the magnetic characteristics of complexes and possible magnetostructural correlation study

> ➤ and to study anticancer properties of selected compounds

1.6. Physico-chemical techniques

The characterization of organic ligands and their metal complexes takes advantage of several conventional and modern physico-chemical techniques. A brief account of these methods used in the present study is discussed below.

1.6.1. Elemental analyses and conductivity measurements

Elemental analyses of all compounds were carried out using an Elementar Vario EL III CHNS analyzer at SAIF, Kochi, India. The molar conductivities of the metal complexes in organic solutions at room temperature were measured using a direct reading conductivity meter. TG scans in air atmosphere using a Perkin Elmer, Diamond TG/DTA at SAIF, Kochi.

1.6.2. NMR spectra

^{1}H NMR, ^{13}C NMR and DCTB135 spectra of compounds in $CDCl_3$ or DMSO-d_6 were recorded using Bruker AMX 400/500 FT-NMR spectrometer using TMS as the internal standard at National Chemical Laboratory, Pune, India. The 135° decouple pulse sequence of DCTB produces a carbon spectrum with methyl (CH_3) and methyne (CH) carbons are up, but methane (CH_2) carbons are down.

1.6.3. Electronic spectra

Electronic spectra of organic ligands and their metal complexes (200-900 nm) were recorded on a Varian, Cary 5000 version 1.09 UV-vis spectrophotometer.

22

1.6.4. IR spectra

Infrared spectra of organic ligands and their metal complexes in the range 4000–400 cm^{-1} were recorded on a Thermo Nicolet, Avatar 370 DTGS model FT-IR spectrophotometer with KBr pellets and ATR technique at SAIF, Kochi. The far IR spectra of metal complexes were recorded using polyethylene pellets in the 500–100 cm^{-1} region on a Nicolet Magna 550 FTIR instrument at the Sophisticated Analytical Instrumentation Facility, Indian Institute of Technology, Bombay, India.

1.6.5. Single crystal X-ray crystallography

The technique of single crystal X-ray crystallography is used to determine the arrangement of atoms within a crystal, which provides positions of atoms very precisely. This has led to a better understanding of chemical bonds and non-covalent interactions. The first atomic-resolution structure to be solved (in 1913) was that of table salt [88], which proved the existence of ionic compounds and that crystals are not necessarily comprised of molecules. X-Ray crystallography had a pioneering role in the development of supramolecular chemistry, particularly in clarifying the structures of the crown ethers and the principles of host-guest chemistry. As of 1st January 2007 the Cambridge Structural Database (CSD), the principal product of the Cambridge Crystallographic Data Centre (CCDC) contains 400977 structures [89].

The crystallographic data of present work were collected at (i) the X-ray Crystallography Unit, School of Physics, Universiti Sains Malaysia, Penang, Malaysia, (ii) the Analytical Sciences Division, Central Salt and Marine Chemicals Research Institute, Bhavnagar, Gujarat, India, (iii) the Department of Inorganic and Physical Chemistry, Indian Institute of Science, Bangalore, India and (iv) the National Single Crystal X-ray Diffraction Facility, Indian Institute of Technology, Bombay, India.

1.6.6. MALDI MS spectrometry

MALDI (matrix-assisted laser desorption/ionization), a laser based soft ionization method, developed in the late 1980s, has proven to be one of the most successful ionization methods for mass spectrometric analysis and investigation of large molecules. The most important applications of MALDI mass spectrometry are (in decreasing order of importance): peptides and proteins, synthetic polymers, oligonucleotides, oligosaccharides, lipids, inorganics. Compared to the large number of applications for organic (especially bioorganic) compounds the use of the matrix assisted laser ionization method for the analysis of inorganic compounds is relatively rare [90]. Nevertheless there is a good chance to get useful MALDI mass spectra from many inorganic compounds with the appropriate choice of the matrix. However, with metal complexes the matrix may occupy a coordination site and additional peaks are expected. Also the acidic nature of many matrices is destructive to proton sensitive compounds.

In the present study, High-resolution MALDI spectra were measured by the MS-service, Laboratorium fur Organische Chemie, ETH Zurich, Switzerland on an IonSpec HiResMALDI apparatus in a DCTB {T-2-[3-(4-t-butyl-phenyl)-2-methyl-2-propenylidene]malononitrile} matrix and dichloromethane solvent. All spectra were taken in positive ion mode. Simulation of isotropic distribution patterns were carried out using a free demo version of ChemSW Mass Spec Calculator.

1.6.7. EPR spectroscopy

Electron Paramagnetic Resonance (EPR) phenomenon was discovered by Zavoisky in 1944 and in the beginning it was used by physicists to study the paramagnetic metal ions in crystal lattices. It is based on the absorption of electromagnetic radiation, usually in the microwave region, which causes transitions between energy levels produced by the action of a magnetic field on an unpaired electron. For example, in the case of a Cu(II) ion, it has an effective spin of $S = \frac{1}{2}$ and

is associated with a spin angular momentum $m_s = +\frac{1}{2}$, leading to a doubly degenerate spin state in the absence of a magnetic field. When a sufficient magnetic field is applied, this degeneracy is removed, and the energy difference between two resultant states is given [91] by,

$$\Delta E = h\nu = g\beta H$$

where h is Planck's constant, ν is the frequency, g is the Lande splitting factor, β is the electron Bohr magneton and H is the magnetic field.

The static spin Hamiltonian used to describe the energies of states of a paramagnetic species in the ground state with an effective electron spin S and m nuclei with spins I is given by [92]

$$\hat{H}_0 = \hat{H}_{EZ} + \hat{H}_{ZFS} + \hat{H}_{HF} + \hat{H}_{NZ} + \hat{H}_{NQ}$$

Where, $\hat{H}_{EZ}$ - electron Zeeman interaction, $\hat{H}_{ZFS}$ - zero-field splitting, $\hat{H}_{HF}$ - hyperfine interactions between the electron spins and the m nuclear spins, $\hat{H}_{NZ}$ - nuclear Zeeman interactions and $\hat{H}_{NQ}$ - nuclear quadrupole interactions for $I > \frac{1}{2}$.

EPR is an important spectroscopic tool in experimental studies of systems containing unpaired electrons. The traditional application areas for EPR include studies of transition metal complexes, stable organic radicals, transient reaction intermediates, as well as solid state and surface defects. EPR spectroscopy measures differences between magnetic energy levels and this is the principal difference from the magnetic susceptibility measurements, which measures the Boltzmann occupation of all energy levels [93]. In many cases, the extreme sensitivity of EPR allows experimental access to electronic structure and molecular environment parameters, which would be impossible to measure otherwise. The structure of the EPR spectrum depends upon (a) the g-tensor anisotropy, (b) the presence of the hyperfine interaction of the central atom nuclear spin with the electron spin (the A^M-tensor), (c) the presence of the superhyperfine interaction of the ligand donor atom nuclear spins with the

electron spin (the A^l-tensors), (d) the appearance of satellites among which the forbidden transitions may occur, (e) the nuclear quadrupole effects, (f) the zero-field splitting (ZFS) and (g) the exchange (spin-spin) interactions of the magnetic centers [93].

Several factors influence the line-width of the EPR spectra, as the dipolar interaction, the exchange interaction, and the zero field splitting. The effect of the dipolar interaction is the broadening of the main line of the spectrum. When the exchange interaction is present, a narrowing of the bands could be observed. If the dipolar interaction is more important than the exchange interaction, a broadening of the spectra will be attended. Additional broadening mechanisms are the hyperfine coupling and the single-ion ZFS effects [94].

EPR spectrum of a compound reveals some distinct features of the structure of the paramagnetic molecule. For example, for Cu(II) complexes, the factors that determine the type of EPR spectrum observed are: (a) nature of the electronic ground state (b) the symmetry of the effective ligand field about the Cu(II) ion (c) the mutual orientations of the local molecular axes of the separate Cu(II) chromophores in the unit cell. The factors (a) and (b) deal with the mode of splitting of the five-fold degenerate 3d orbitals by crystal fields of octahedral and tetrahedral symmetries which are inverse of each other. The orbital sequences of the various stereochemistries determine their ground states. The vast majority of Cu(II) complexes give rise to orbitally non-degenerate ground states involving a static form of distortion and a $d_{x^2-y^2}$ ground state; a substantial number of complexes have a d_{z^2} ground state and a few have a d_{xy} ground state. It depends on the nature of the ligands regarding their π bonding potential. The third factor (c) determines the amount of exchange coupling present, which is the major factor in reducing the amount of stereochemical information available from the EPR spectra [95].

EPR spectra of the present work {Cu(II) and Mn(II) complexes} were carried out on a Bruker ElexSys E500 @9.6 GHz X band cw EPR spectrometer at EPR@ETH, ETH, Zurich, Switzerland. The spectra were recorded in powder form at room temperature as well as in frozen DMF solution at 77 K. Also, few spectra were recorded on a Varian E-112 EPR spectrometer using TCNE as the standard at SAIF, IIT, Bombay, India.

1.6.8. Magnetochemistry

Magnetochemistry is the study of the magnetic properties of materials. Magnetism has been known to mankind for millenia but only in 20th century quantum mechanics successfully explained its origin. The relationship between magnetism and structure is a subject of interest for more than six decades because it provides an approach to estimate the extent of exchange coupling [96]. The need for new materials that have more diversified and more sophisticated properties is continuously increasing. Opportunities offered by the flexibility of inorganic chemistry led to blossoming of new research fields in inorganic molecular materials. Two systems with the same core topology, but with different coordination environments can exhibit different magnetic behaviour [97]. The magnetic properties of multinuclear coordination complexes can be modulated by the nature of metal centers, their number, the nature of the bridging ligand and also by the whole structure and environment created by the supramolecular arrangement of the building blocks [98]. Additional physical properties can be introduced by different ways viz. (a) the ligand can be the center of this phenomenon when bearing a specific property, for example optic in the case of an optically active ligand, magnetic when the ligand is a free radical, (b) by using different building blocks and one of them can possess a specific property like chirality or fluorescence activity and (c) when the material comprise two- sub-lattices (hybrid materials), one of them can bring out the magnetic properties while the other one brings a different property [98].

Traditional magnets are based on metallic or ionic systems, but recently it has been discovered that even individual molecules can behave like tiny magnets. Magnetic molecules are a new class of fascinating materials. These molecules contain a finite number of interacting spin centers (e.g. paramagnetic ions) and thus provide ideal opportunities to study basic concepts of magnetism. One of the characteristic features of molecular magnetism is its deeply interdisciplinary character, bringing together organic, organometallic and inorganic synthetic chemists as well as theoreticians from both the chemistry and physics communities, and materials and life-science specialists. This interdisciplinary nature confers a special appeal to this field. Nobody alone can make a crucial contribution [99].

Paramagnetic metal ions with covalent radii of the order of 1 Å (0.1 nm) can be brought into close proximity with suitable diamagnetic single atom bridging ligands, and with appropriate magnetic orbital overlap situations can produce parallel or antiparallel alignment of the metal centered spins (ferromagnetic or antiferromagnetic behavior respectively). Increasing the number of spin centers in a polynuclear bridged arrangement is more of a challenge, but can be achieved using polydentate ligands of various types. One approach uses well-defined polydentate ligands to impose specific geometries on the resulting arrays, while another approach uses simple ligands, and essentially is controlled by properties of the metal ion. An intermediate approach uses coordinatively flexible ligands [21].

Magnetic measurements can be performed in *ac* or *dc* modes. In the *dc* mode a static magnetic field H is applied, and the induced magnetization, M, is studied as a function of this magnetic field and of temperature [99]. In the present study variable temperature and field dependent magnetization were carried out in *dc* mode at the Department of Physics, Boise State University, Boise, USA in the powder state on a Quantum Design PPMS superconducting magnetometer at 500 Oe field strength. Diamagnetic corrections were made using Pascal's constants [100].

28

References

1. G.R. Desiraju, Curr. Sci. Special section: Mathematics 88 (2005) 374.
2. J.-M. Lehn, Supramolecular Chemistry. Concepts and Perspectives, Wiley VCH (1995).
3. G.R. Desiraju, Nature 408 (2000) 407.
4. D.H. Lee, K. Severin, M.R. Ghadiri, Curr. Opin. Chem. Biol. 1 (1997) 491.
5. D.H. Busch, Chem. Rev. 93 (1993) 847.
6. J.-M. Lehn, Angew. Chem. Int. Ed. Engl. (Nobel lecture) 27 (1988) 89.
7. A. Werner, Z. Anorg. Chem. 3 (1893) 267.
8. J. Gladysz, J. Michl, Chem. Rev. 93 (1993) 845.
9. O. Khan, Angew. Chem. Int. Ed. Engl. 24 (1985) 834.
10. A. Messerschmidt, R. Huber, T. Poulos, K. Wieghardt, (eds.) Handbook of Metalloproteins, John Wiley & Sons, Chichester, U.K. (2001).
11. G.F. Swiegers, T.J. Malefetse, Chem. Rev. 100 (2000) 3483.
12. M.D. Ward, Annu. Rep. Prog. Chem. Sec. A 96 (2000) 345.
13. F. Wurthner, C.-C. You, C.R. Saha-Moller, Chem. Soc. Rev. 33 (2004) 133.
14. M. Fujita, J. Yazaki, K. Ogura, J. Am. Chem. Soc. 112 (1990) 5645.
15. M. Fujita, Chem. Soc. Rev. 27 (1998) 417.
16. L.K. Thompson, L. Zhao, Z. Xu, D.O. Miller, W.M. Reiff, Inorg. Chem. 42 (2003) 128.
17. P.J. Stang, B. Olenyuk, Acc. Chem. Res. 30 (1997) 502 and refs therein.
18. C.S. Lent, Science 288 (2000) 1597.
19. L.F. Lindoy, I.M. Atkinson, Self-Assembly in Supramolecular Systems, Royal Society of Chemistry, Cambridge (2000).
20. F.C.J.M. van Veggel, W. Verboom, D.N. Reinhoudt, Chem. Rev. 94 (1994) 279.

21. L.K. Thompson, O. Waldman, Z. Xu, Chap 5. Magnetism: Molecules to materials, J.S. Miller, M. Drillon, Wiley-VCH (2001).

22. J. S. Lindsey, New J. Chem. 15 (1991) 153.

23. C.J. Matthews, K. Avery, Z. Xu, L.K. Thompson, L. Zhao, D.O. Miller, K. Biradha, K. Poirier, M.J. Zaworotko, C. Wilson, A.E. Goeta, J.A.K. Howard, Inorg. Chem. 38 (1999) 5266.

24. C.J. Matthews, L.K. Thompson, S.R. Parsons, Z. Xu, D.O. Miller, S.L. Heath, Inorg. Chem. 40 (2001) 4448.

25. Y. Zhang, S. Wang, G.D. Enright, S.R. Breeze, J. Am. Chem. Soc. 120 (1998) 9398.

26. G. Ercolani, J. Phys. Chem. B102 (1998) 5699.

27. X. Chi, A.J. Guerin, R.A. Haycock, C.A. Hunter, L.D. Sarson, J. Chem. Soc., Chem. Commun. (1995) 2567.

28. C.-y. Duan, Z.-h. Liu, X.-z. You, F. Xue, T.C.W. Mak, Chem. Commun. (1997) 381.

29. C. He, C.-y. Duan, C.-j. Fang, Y.-j. Liu,Q.-j. Meng, J. Chem. Soc., Dalton Trans. (2000) 1207.

30. G. Han, D. Guo, C. -y. Duan, H. Mo, Q. -j. Meng, New J. Chem. 26 (2002) 1371.

31. M.A. Ali, P.V. Bernhardt, C.L. Keim, A.H. Mirza, Aust. J. Chem. 57 (2004) 409.

32. C.A. Schalley, Mass Spectrom. Rev. 20 (2001) 253.

33. T. Curtius, K. Heidenreich, J. Prakt. Chem. 52 (1895) 454.

34. R. Stolle, P.E. Bowles, Chem. Ber. 41 (1908) 1099.

35. P. C. Guha, S.C. De, J. Ind. Chem. Soc. 2 (1926) 225.

36. F. Kurzer, M. Wilkinson, Chem. Rev. 70 (1970) 111.

37. A. Braibanti, A. Tirjpicchio, M.T. Camellini, Acta. Cryst. B25 (1969) 2286.

38. P. Domiano, M.A. Pellinghelli, A. Tiripicchio, Acta. Cryst. B28 (1972) 2495.

39. T. Ottersen, H. Hope, Acta. Cryst. B35 (1979) 373.

40. G.A. Geffrey, J.R. Ruble, R.G. Nanni, A.M. Turano, J.H. Yates, Acta. Cryst. B41 (1985) 354.

41. http://www.acdlabs.com/iupac/nomenclature/79/r79_673.htm

42. G.R. Burns, Inorg. Chem. 7 (1968) 277 and refs therein.

43. R.L. Dutta, M.M. Hossain, Ind. J. Chem. 22A (1983) 201.

44. J. Dan, S. Seth, S. Chakraborty, Acta. Cryst. C43 (1987) 1114.

45. J.-P. Xiao, Y.-L. Wang, Q.-X. Zhou, Synth. Commun. 31 (2001) 661.

46. X.-C, Li, Y.-L. Wang, J.-Y. Wang, Synth. Commun. 32 (2002) 3285.

47. A.H.M. Siddalingaiah, S.G. Naik, H.D. Patil, Spectrochim. Acta. Part A 60 (2004) 2499 and refs therein.

48. A.H.M. Siddalingaiah, S.G. Naik, J. Mol. Struct. (Theochem) 582 (2002) 129 and refs therein.

49. A.H.M. Siddalingaiah, S.G. Naik, Synth. React. Inorg. Met. –Org. Chem. 31 (2001) 1675.

50. S.A. Hiremath, A.F. Dodamani, S.G. Naik, Trans. Met. Chem. 27 (2002) 47.

51. G.R. Bustos, O. Burdkhardt, R. Schrebler, D. Carrilo, Inorg. Chem. 29 (1990) 3996.

52. H.-Y. Chen, T.-L. Zhang, J.-G. Zhang, K.-B. Yu, Struct. Chem. 16 (2005) 657.

53. A. Rana, R. Dinda, P. Sengupta, S. Ghosh, L.R. Falvello, Polyhedron 21 (2002) 1023.

54. M. Carcelli, D. Delledonne, A. Fochi, G. Pelizzi, M.C. Rodriguez-Arguelles, U. Russo, J. Organomet. Chem. 544 (1997) 29.

55. H.S. Chabanur, V.K. Revankar, V.B. Mahale, Synth. React. Inorg. Met.-

Org. Chem. 31 (2001) 339.

56.   O.P. Pandey, Polyhedron 5 (1986) 1587.

57.   A. Tripathi, A. Sinha, O.P. Pandey, S.K. Sengupta, Synth. React. Inorg. Met. -Org. Chem. 30 (2000) 139.

58.   D.P. Singh, R. Kumar, P. Tyagi, Trans. Met. Chem. 31 (2006) 970.

59.   O.V. Mikhailov, M.A. Kazymova, T.A. Shumilova, S.S. Solovieva, Trans. Met. Chem. 28 (2003) 665.

60.   H.S. Silvester, US Patent (1951) 2706180.

61.   G.M. Haist, W.J. Humphlet, US Patent (1971) 3615625.

62.   D.M. Wiles, T. Suprunchuk, US Patent (1973) 3734757.

63.   D.G. Kelley, D.M. Rogers, S.J. Swiecinski, US Patent (1993) 5258125.

64.   L.D. Albin, M. Jacobsen, D.B. Olson, US Patent (1994) 5376451.

65.   A. Bacchi, A. Bonini, M. Carcelli, F.J. Farraro, J. Chem. Soc., Dalton Trans. (1996) 2699.

66.   B. Moubaraki, K.S. Murray, J.D. Ranford, X. Wang, Y. Xu, Chem. Commun. (1998) 353.

67.   B. Moubaraki, K.S. Murray, J.D. Ranford, J.J. Vittal, X. Wang, Y. Xu, J. Chem. Soc., Dalton Trans. (1999) 3573.

68.   A. Bacchi, M. Carcelli, P. Pelagatti, C. Pelizzi, G. Pelizzi, F. Zani, J. Inorg. Biochem. 75 (1999) 123.

69.   J. A. Gordon, W.P. Jencks, Biochem. 2 (1963) 47.

70.   M.T.S. Cordero, A.G. de Torres, J.M.C. Pavon, Talanta 40 (1993) 691 and refs therein.

71.   F. Alvarez, F. de Pablos, J.L.G. Ariza, Talanta 35 (1988) 493 and refs therein.

72.   A.A.A. Abu-Hussen, A.A.A. Emara, J. Coord. Chem. 57 (2004) 973.

73.   J.R. Dimmock, P. Kumar, T.M. Allen, G.Y. Kao, S. Halleran, J. Balzarini,

de Clercq, Pharmazie 52 (1997) 182.

74. Z.H. Chohan, H. Pervez, K.M. Khan, C.T. Supuran, J. Enz. Inhib. Med Chem. 20 (2005) 81.

75. T. Spector, J.A. Harrington, R.W. Jr Morrison, C.U. Lambe, D.J. Nelson, D.R. Averett, K. Biron, P.A. Furman, Proc. Natl. Acad. Sci. USA. 86 (1989) 1051.

76. T.A. Blumenkopf, J.A. Harrington, C.S. Kolbe, D.D. Bankston, R.W. Morrison, E.C. Bigham, V.L. Styles, T. Spector, J. Med. Chem. 35 (1992) 2306.

77. G. Domagk, R. Behnisch, F. Mietzsch, H. Schmidt, Naturewissenschaften 33 (1946) 315.

78. W.-x. Hu, W. Zhou, C.-n. Xia, X. Wen, Bioorg. Med. Chem. Lett. 16 (2006) 2213.

79. M. Whitnall, J. Howard, P. Ponka, D.R. Richardson, Proc. Nat. Acad. Sci. 103 (2006) 14901.

80. D.S. Kalinowski, Y. Yu, P.C. Sharpe, M. Islam, Y.-T, Liao, D.B. Lovejoy, N. Kumar, P.V. Bernhardt, D.R. Richardson, J. Med. Chem. 50 (2007) 3716.

81. C. Junnan, Y.-W. Huang, L. Guanshu, Z. Afrasiabi, E. Sinn, S. Padhye, M. Yinfa, Toxicol. Appl. Pharmacol. 197 (2004) 40.

82. A. Kraker, S. Krezoski, J. Schneider, D. Mingel, D.H. Petering, J. Biol. Chem. 260 (1985) 13710.

83. Z. Iakovidou, A. Papageorgiou, M.A. Demertzis, E. Mioglou, D. Mourelatos, A. Kotsis, P.N. Yadav, D. Kovala-Demertzi, Anti-Cancer Drugs 12 (2001) 65.

84. J.L. Buss, B.T. Greene, J. Turner, F.M. Torti, S.V. Torti, Curr. Topic. Med. Chem. 4 (2004) 1623.

85. S. Padhye, Z. Afrasiabi, E. Sinn, J. Fok, K. Mehta, N. Rath, Inorg. Chem. 44 (2005) 1154.

86. I.S. Snyder, J.L. Stringer, drug. Encyclopædia Britannica from Encyclopædia Britannica 2007 Ultimate Reference Suite (2007).

87. Z. Lin, H. Chen, J. Zhuang, Y. Wu, Y. Lin, J. Incl. Phen. Mol. Recog. Chem. 30 (1998) 13.

88. W.L. Bragg, Proc. Roy. Soc. London A89 (1913) 248.

89. http://www.ccdc.cam.ac.uk/products/csd/statistics/

90. Sigma-Aldrich, Analytix, 6 (2001).

91. B.J. Hathaway, Coord. Chem. Rev. 53 (1983) 87.

92. C. Calle, A. Sreekanth, M.V. Fedin, J. Forrer, I. Garcia-Rubio, I.A. Gromov, D. Hinderberger, B. Kasumaj, P. Léger, B. Mancosu, G. Mitrikas, M.G. Santangelo, S. Stoll, A. Schweiger, R. Tschaggelar, J. Harmer, Helv. Chim. Acta 89 (206) 2495.

93. R. Boca, Coord. Chem. Rev. 248 (2004) 757.

94. A. Bencini, D. Gatteschi, EPR of exchange Coupled Systems, Springer-Verlag, Berlin (1990).

95. B.J. Hathaway, D.E. Billing, Coord. Chem. Rev. 5 (1970) 143.

96. G.V.R. Chandramouli, T.K. Kundu, P.T. Manoharan, Aust. J Chem. 56 (2003) 1239.

97. G.A. Seisenbaeva, M. Kritikos, V.G. Kessler, Polyhedron 22 (2003) 2581.

98. W. Linert, M. Verdaguer (eds.), Molecular Magnets: Recent Highlights, Springer (2003).

99. J.-P. Sauvage, C. Dietrich-Buchecker (eds.) Molecular Catenanes, Rotaxanes and Knots, Wiley-VCH (1999).

100. R.L. Dutta, A. Syamal, Elements of Magnetochemistry, EWP (1993).

****

Carbohydrazone, thiocarbohydrazone and thiosemicarbazone ligands: Structural, spectral and anticancer properties

2.1. Introduction

The design and synthesis of a polyfunctional ligand of versatile coordinating ability to behave as building blocks is the key step for producing self-assembled macrocyclic molecular architectures. The symmetry and the overall shape of the resulting macrocyclic assembly are defined solely by the type and properties of the multidentate building units uses [1]. Among the macrocycles derived, molecular squares have received the highest attention. The synthesis and characterization of metallosupramolecular squares have achieved growing interest for the last decade especially because of their wide spectrum of applications in science and technology. Of these, the grid structures of magnetic metal ions are of special interest in information storage and processing technology [2]. The design and synthesis of projected coordination frameworks, mainly 2×2 molecular square grids, begin from the synthesis of novel ligands. Owing to the presence of different kinds of potential donor sites, we selected carbohydrazones and thiocarbohydrazones as ligand building blocks.

Interestingly, Schiff bases particularly those containing sulfur or oxygen atoms have received a renewed attention as important class of ligands because of their various biological applications. Conversely, the self-assembly process driven by noncovalent interactions are considered as crucial in the proliferation of all biological organisms [1]. Various antimicrobial applications of carbohydrazones and thiocarbohydrazones [3-5] along with the reports of Maubaraki *et al.* [6,7] about the

anticipation of Cu(II) complexes of bis(pyridine-2-aldehyde) thiocarbohydrazone as anticancer drug analogues of corresponding thiosemicarbazone complexes also prompted us to select these potential class of ligands.

Carbohydrazones and thiocarbohydrazones have previously served as chelating ligands to form mononuclear and dinuclear complexes [4,7-9]. The capability of thiocarbohydrazones, with suitable substituents and reaction condition for generating molecular squares were first reported by Duan *et al.* in 1997 [10] and his groups [11,12] and later by Akbar Ali *et al.* [13]. Recently, two octanuclear Cu(II) complexes have been reported with 1,5-bis(2-hydroxybenzaldehyde) thiocarbohydrazone ligand [14], where six of the seven donor atoms of tetradeprotonated ligand in *anti* tautomeric form are linked with two metal ions to form a dicopper(II) unit. The assembly of four such units into a metallo macrocyclic array takes place by coordination of the seventh donor atom of each unit. However, there was no earlier report of their oxygen analogues, carbohydrazones, acting as building blocks for molecular frameworks through self-assembly [15]. With the anticipation that carbohydrazones can also act as building blocks for self-assembly, like thiocarbohydrazones, when suitable conditions are employed, we selected carbohydrazones with suitable substituents. Conversely, the feel that it would be worthwhile to study a comparison of the spectral behaviour and coordinating properties between carbohydrazones and thiocarbohydrazones lead us to the synthesis, structural and spectral studies of the following six ligands (Scheme 2.1).

1. 1,5-Bis(di-2-pyridyl ketone) thiocarbohydrazone (H_2L^1)
2. 1,5-Bis(2-benzoylpyridine) thiocarbohydrazone (H_2L^2)
3. 1,5-Bis(quinoline-2-carbaldehyde) thiocarbohydrazone (H_2L^3)
4. 1,5-Bis(di-2-pyridyl ketone) carbohydrazone (H_2L^4)
5. 1,5-Bis(2-benzoylpyridine) carbohydrazone (H_2L^5)
6. 1,5-Bis(quinoline-2-carbaldehyde) carbohydrazone (H_2L^6)
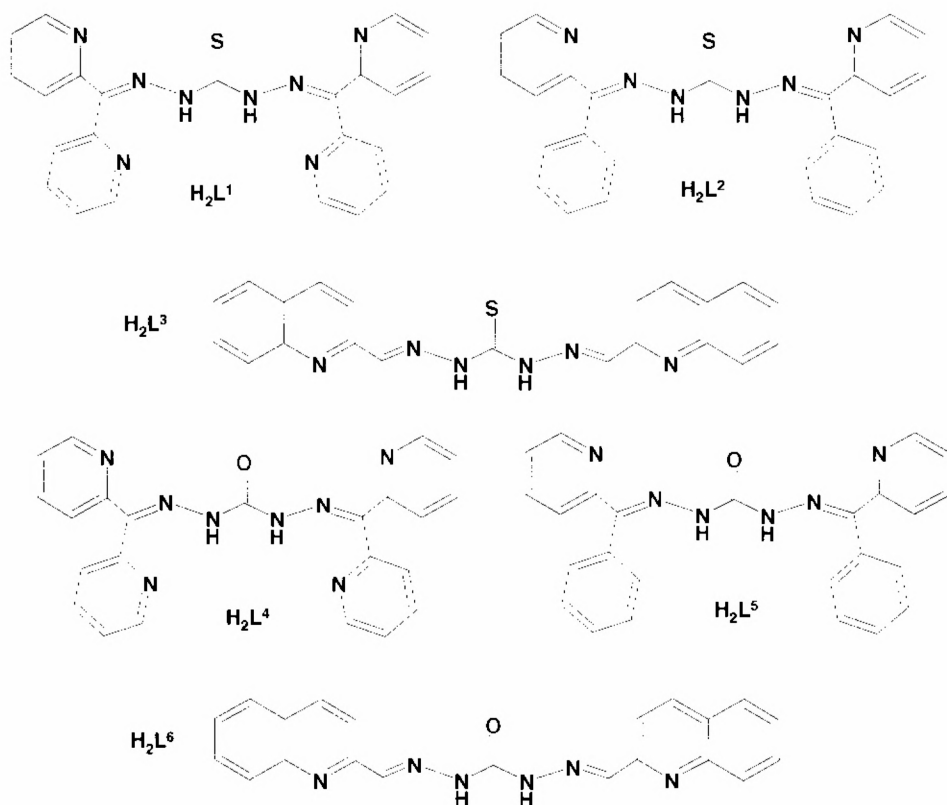
Scheme 2.1. Thiocarbohydrazone and carbohydrazone ligands.

The carbohydrazones and thiocarbohydrazones are next higher homologues of potentially active semicarbazones and thiosemicarbazones with a possible extra metal binding domain; a preliminary study of spectral and coordinating properties of thiosemicarbazones are found useful. Also, as the quinoline-2-carbaldehyde has not yet studied as a substituent of thiosemicarbazide, it is found relevant to prove the coordinating properties of a quinoline-2-carbaldehyde derived thiosemicarbazone. Keeping these in mind, we synthesized the following two thiosemicarbazones (Scheme 2.2) also.

1. Quinoline-2-carbaldehyde $N(4),N(4)$-(butane-1,4-diyl) thiosemicarbazone (HL^7)

2. 2-Benzoylpyridine-$N(4),N(4)$-(butane-1,4-diyl) thiosemicarbazone (HL^8)
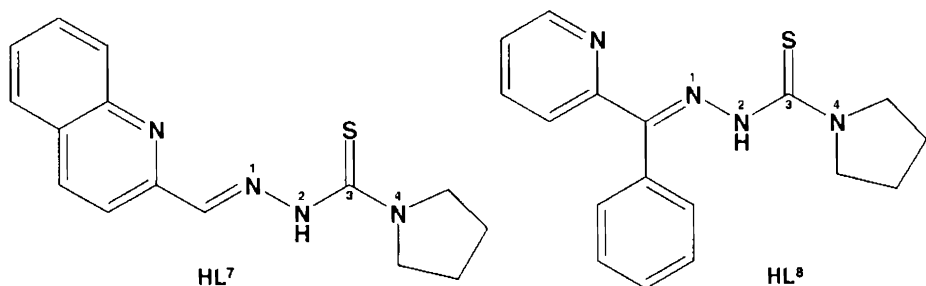
Scheme 2.2. Thiosemicarbazone ligands with general atom numbering scheme.

The synthesis of H_2L^1 was reported [10] meagerly, without any spectral studies. Synthesis and crystal structure of H_2L^2 have been reported simultaneously [4,11]. The spectral data for H_2L^2 was reinvestigated here for a comparison with that of other compounds, as there were contradictions in the two reports [4,11]. Also there is a report of synthesis of H_2L^5 [4] but without much study. However, there are no further reports of their coordination chemistry. The other two carbohydrazones and thiocarbohydrazone H_2L^3 are new ligands. We have reported the synthesis and structure of the ligand H_2L^4 [16]. Synthesis and structural and spectral studies of thiosemicarbazone HL^8 and its iron(III) [17], Cu(II) [18] and Mn(II) complexes [19] have been reported from our laboratory. But their coordination towards other transition metals like Ni(II) haven't reported. However, the ligand HL^7 is a newly synthesized one. The synthesis and studies of these thiosemicarbazone ligands are found relevant as a supporting study. For studying their coordinating properties and for a comparison with that of their higher homologue thiocarbohydrazone ligands also prompted us to study these thiosemicarbazones.

2.2. Experimental

2.2.1. Materials

Quinoline-2-carbaldehyde (Aldrich), di-2-pyridyl ketone (Aldrich), 2-benzoylpyridine (Aldrich), thiocarbohydrazide (Aldrich), carbohydrazide (Fluka), carbon disulfide (Merck), N-methylaniline (Loba Chemie), pyrrolidine (Aldrich), sodium hydroxide (Merck), sodium chloroacetate (Merck), hydrazine hydrate (98%, Glaxo), HCl (Rankem) and absolute ethanol (S.D.fine) were used as supplied and solvents acetonitrile (Rankem), methanol (Merck), chloroform (S.D.fine), etc were purified by standard procedures before use.

2.2.2. Synthesis of ligands

The carbohydrazone and thiocarbohydrazone ligands were prepared by a general method (Scheme 2.3) of direct condensation of carbohydrazide or thiocarbohydrazide with two equivalents of respective aldehyde or ketone in acid medium. The thiosemicarbazone ligands were synthesized by adapting a reported procedure of Scovill [20].
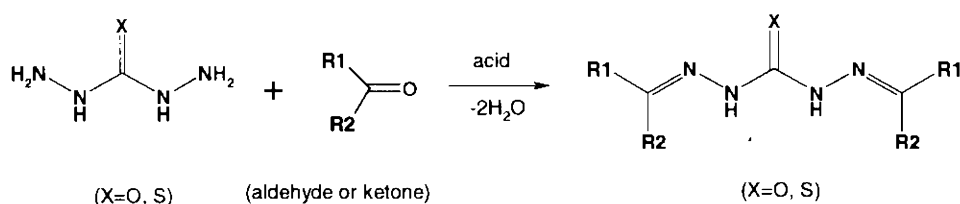
Scheme 2.3. Reaction scheme for (thio)carbohydrazones.

1,5-Bis(di-2-pyridyl ketone) thiocarbohydrazone (H_2L^1)

Di-2-pyridyl ketone (0.391 g, 2.1 mmol) in 10 ml methanol was added to thiocarbohydrazide (0.011 g, 1 mmol) dissolved in hot methanol (30 ml). After adding a drop of HCl, the solution was refluxed for 1 h and on cooling a yellow mass precipitated. It was then filtered, washed with methanol and ether, recrystallized in

chloroform solution and dried over P_4O_{10} *in vacuo*. Yield: 80%. M.p. 188 °C. Elemental analysis: Found (calc.): C, 62.30 (63.00); H, 4.32 (4.14); N, 25.19 (25.55); S, 7.27 (7.31)%.

1,5-Bis(2-benzoylpyridine) thiocarbohydrazone (H₂L²)

2-Benzoylpyridine (0.800 g, 4.4 mmol) in 10 ml methanol was added to thiocarbohydrazide (0.216 g, 2 mmol), dissolved in hot methanol (40 ml). The solution was refluxed for 3 h after adding a drop of 6 M HCl, and on cooling a yellow crystalline solid precipitated. This was then filtered, washed with methanol and ether, recrystallized in chloroform solution and dried over P_4O_{10} *in vacuo*. Yield: 75%. Elemental analysis: Found (calc.): C, 68.70 (68.78); H, 4.62 (4.62); N, 19.25 (19.25); S, 7.07 (7.35)%.

1,5-Bis(quinoline-2-carbaldehyde) thiocarbohydrazone (H₂L³)

Quinoline-2-carboxaldehyde (0.680 g, 4.2 mmol) in 10 ml methanol was added to thiocarbohydrazide (0.216 g, 2 mmol) dissolved in hot methanol (70 ml). After adding a drop of hydrochloric acid, the solution was refluxed for 1 h and on cooling a yellow solid precipitated. It was then washed with methanol and ether, recrystallized in acetonitrile solution and dried over P_4O_{10} *in vacuo*. Single crystals suitable for X-ray analysis were obtained by slow evaporation of its acetonitrile solution. Yield: 75%, M.p 182 °C. Elemental analysis: Found (calc.): C, 65.27 (65.61); H, 4.30 (4.19); N, 22.18 (21.86); S, 8.18 (8.34)%.

1,5-Bis(di-2-pyridyl ketone) carbohydrazone (H₂L⁴)

Di-2-pyridyl ketone (0.391 g, 2.1 mmol) in methanol (10 ml) was added to carbohydrazide (0.092 g, 1 mmol) dissolved in hot methanol (30 ml). After adding 2 drops of glacial acetic acid, the resulting solution was refluxed for 2 h and on cooling yellow white crystals were precipitated. These crystals were filtered, washed with

methanol and diethyl ether, recrystallized in chloroform solution and dried over P_4O_{10} *in vacuo*. Single crystals suitable for X-ray analysis were obtained by slow evaporation of a methanol solution of H_2L^4. Yield: 85%, M.p. 210 °C. Elemental analysis: Found (calc.): C, 65.18 (65.39); H, 4.47 (4.29); N, 26.92 (26.53)%.

1,5-Bis(2-benzoylpyridine) carbohydrazone (H_2L^5)

To a solution of carbonohydrazide (0.184 g, 2 mmol) in hot methanol (50 ml), a solution of 2-benzoylpyridine (0.777 g, 4.2 mmol) in methanol (20 ml) was added. The solution was refluxed for 2 h after adding two drops of glacial acetic acid and on cooling a dull white powder precipitated. This was then filtered, washed with methanol and diethyl ether, recrystallized in chloroform solution and dried over P_4O_{10} *in vacuo*. Yield: 68%. Elemental analysis: Found (calc.): C, 70.85 (71.41); H, 5.09 (4.79); N, 20.26 (19.99)%.

1,5-Bis(quinoline-2-carbaldehyde) carbohydrazone trihydrate ($H_2L^6 \cdot 3H_2O$)

To a solution of carbohydrazide (0.184 g, 2 mmol) in hot methanol (50 ml), a solution of quinoline-2-carboxaldehyde (0.680 g, 4.2 mmol) in 10 ml methanol was added and refluxed for 2 h after adding two drops of glacial acetic acid. The white solid mass precipitated was filtered, washed with methanol and ether and dried over P_4O_{10} *in vacuo*. Yield: 87%. Elemental analysis: Found (calc.): C, 59.90 (59.71); H, 5.11 (5.25); N, 19.94 (19.89)%.

Quinoline-2-carbaldehyde N(4),N(4)-(butane-1,4-diyl) thiosemicarbazone (HL^7)

A solution of 1.000 g (5. 52 mmol) of 4-methyl-4-phenyl-3-thiosemicarbazide in 5 ml of acetonitrile was refluxed with 0.392 g (5. 52 mmol) of pyrrolidine and 0.894 g (5.52 mmol) of quinoline 2-carbaldehyde for 1½ h. The resulting solution was chilled (overnight) and the yellow mass that separated was collected and washed well

with acetonitrile. The compound was recrystallized from ethanol solution and dried *in vacuo* over P_4O_{10}. Yield 46%. Elemental analysis: Found (calc.): C, 63.15 (63.35); H, 5.99 (5.67); N, 19.66 (19.70); S, 11.26 (11.28)%.
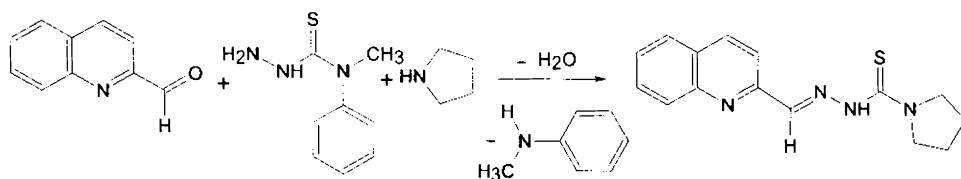
Scheme 2.4. Reaction scheme of thiosemicarbazone HL^7.

2-Benzoylpyridine-N(4),N(4)-(butane-1,4-diyl) thiosemicarbazone (HL^8)

To a solution of 1.000 g (5. 52 mmol) of 4-methyl-4-phenyl-3-thiosemicarbazide in 5 ml of acetonitrile, 0.392 g (5. 52 mmol) of pyrrolidine and 1.021 g (5.52 mmol) of 2-benzoylpyridine were added and refluxed for 1½ h. The solution was chilled (overnight) and the crystals that separated were collected and washed well with acetonitrile. The compound was recrystallized from ethanol solution and dried *in vacuo* over P_4O_{10}. Yield 40%, M.p. 186 °C. Elemental analysis: Found (calc.): C, 65.74 (65.78); H, 5.69 (5.84); N, 17.96 (18.05); S, 10.67 (10.33)%.

The compound 4-methyl-4-phenyl-3-thiosemicarbazide for the synthesis of HL^7 and HL^8 was prepared by the following two steps.

(i) Preparation of carboxymethyl N-methyl, N-phenyl dithiocarbamate

A mixture consisting of 12 ml (5.200 g, 0.20 mol) of carbon disulfide and 21.6 ml (21.200 g, 0.20 mol) of N-methylaniline was treated with a solution of sodium hydroxide (8.400 g, 0.21 mol) in 250 ml distilled water. This was then stirred at room temperature for 4 h to get a straw colored solution, after the complete disappearance of organic layer, and treated with 23.200 g (0.20 mol) of sodium chloroacetate and allowed to stand overnight (17 hours). The solution was acidified with 25 ml of conc.

HCl and the solid separated was filtered, washed well with distilled water and dried carefully to get the buff coloured product. Yield: 80%, M.p. 197 °C.
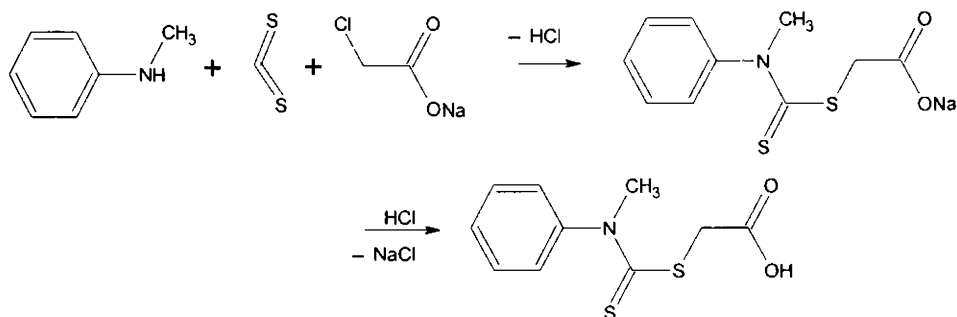
Scheme 2.5. Reaction scheme of carboxymethyl N-methyl, N-phenyl dithiocarbamate.

(ii) Preparation of N(4)-methyl, N(4)-phenyl 3-thiosemicarbazide

A solution of 17.700 g (0.073 mol) of carboxymethyl *N*-methyl, *N*-phenyl dithiocarbamate in 20 ml 98% hydrazine hydrate and 10 ml distilled water was heated on the rings of a steam bath at 85 °C. After 3 minutes crystals began to separate. Heating was continued for additional 22 minutes. The crystals were collected by filtration, washed well with distilled water and dried. This was then recrystallized from a mixture of 2:1 v/v absolute ethanol: distilled water to get the stout colored crystals of 4-methyl, 4-phenyl 3-thiosemicarbazide. Yield: 65%, M.p. 124 °C.
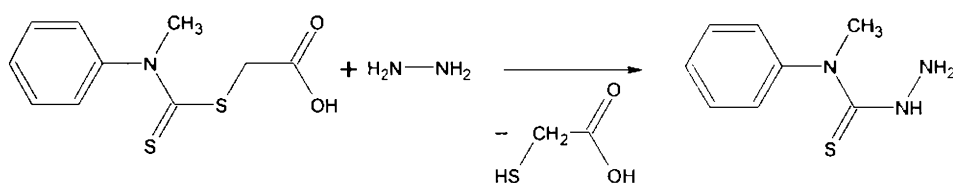
Scheme 2.6. Reaction scheme of N(4)-methyl, N(4)-phenyl 3-thiosemicarbazide.

2.3. Results and discussion

The syntheses of carbohydrazones and thiocarbohydrazones were done by condensation reaction in acid medium. The ratio of reagents, solvent, pH of the medium, etc are found affecting the reactions considerably. The syntheses of H_2L^2 [11] and H_2L^5 have been reported [4]. H_2L^5 was prepared according to reported procedure except that a 2 h refluxion could yield 67%, against 70% yield for 60 h. The syntheses of thiosemicarbazones HL^7 and HL^8 were done by adapting a reported procedure of Scovill [20]. 4-Methyl-4-phenyl-3-thiosemicarbazide was prepared as reported previously [20]. The synthesis of HL^7 and HL^8 from 4-methyl-4-phenyl-3-thiosemicarbazide comprises two processes namely condensation and transamination. The condensation reaction of 4-methyl-4-phenyl-3-thiosemicarbazide with 2-benzoylpyridine or quinoline-2-carbaldehyde results by the removal of a water molecule and transamination process involves the replacement of N-methylaniline with pyrrolidine. However both these were achieved in a single step reaction without any addition of acid, but in low yield compared to two-step reactions. The thiocarbohydrazones and thiosemicarbazones prepared are all yellow in color but the carbohydrazones all are found to be colorless. All compounds except H_2L^6 are soluble in chloroform and DMSO. H_2L^6 is readily soluble in DMF only and soluble in methanol slightly on heating.

2.3.1. IR spectral studies

The IR spectra of all compounds were recorded in the 4000-400 cm^{-1} range. (Thio)carbohydrazones, in principle, can exhibit (thio)ketone-(thio)enol tautomerism. Also, since the spectra are very much rich with bands, a comparison of spectra of all carbohydrazones and thiocarbohydrazones are also found useful to assign these bands, which are listed in Table 2.1.

Table 2.1. **IR** spectral data of the ligands (cm^{-1}).

c.	vN–H	vC–H	vC=N+ vC=C	vC–N /vHeter ocyclic	vC=S/ vC=O	vN–N	δC–H	py/qu
H$_2$L^1	3428br, 3068m	3049m, 3003m	1580m, 1487s, 1454vs, 1426vs	1303m, 1282m	1223s	1117s	996m, 872m, 800s, 738m	617m, 645m 470w
H$_2$L^2	3323m, 3266m	3050m	1568s, 1495vs, 1459vs, 1422s	1358m, 1300s	1225vs	1132vs	996s, 975m, 840s, 793s, 742m, 705s	607s, 663s 486s, 455m
H$_2$L^3	3442br	3035m, 2954br	1616m, 1575s, 1542m, 1482vs, 1412vs	1335m, 1293s	1209s	1126s	974m, 932m, 803s, 752m	613m, 685m 419s, 475s
H$_2$L^4	3428br, 3155m	3049m, 3003m	1580m, 1491s, 1456s, 1426s	1324s, 1279m	1704vs	1127vs	992m, 960m, 803s, 752m, 701m	613m, 636s 479m
H$_2$L^5	3451br, 3345s, 3155m	3054m, 3019m	1566m, 1501s, 1482s, 1459m, 1426m	1326m, 1256s	1697vs	1126s	803m, 791s, 743m	613m, 645s 456m
H$_2$L^6	3455br	3077m, 2938sh	1593m, 1533vs, 1501s, 1454m, 1431m	1329m, 1264s	1696vs	1126s	937m, 830m, 747s	622m, 648m 470m
HL^7	3442br	2970br, 2870s	1580s, 1543s, 1436s	1337m	1282s	1102s	934s, 897s, 820s, 760m	680m, 622m, 472s

c. = compounds, br = broad, sh = shoulder, s = strong, vs = very strong, m = medium, w = weak.

45

The carbohydrazone and thiocarbohydrazone compounds show some common features, and it is found that the main difference as carbohydrazones H_2L^4, H_2L^5 and H_2L^6 show strong bands in the range 1696-1704 cm^{-1} of C=O stretching vibrations instead of the strong bands seen in the range 1209-1225 cm^{-1} assigned to stretching mode of C=S vibrations for thiocarbohydrazones H_2L^1, H_2L^2 and H_2L^3. Apart from this, the spectra of carbohydrazones and thiocarbohydrazones show some marginal differences in the mixing patterns of common group frequencies. Many bands in the region 1400 to 1600 cm^{-1} are consistent with ν(C=N) and ν(C=C) mixing patterns. The ν(SH) band usually seen at ~2600 cm^{-1} is absent in the IR spectra of H_2L^1, H_2L^2 and H_2L^3, clear indication of the absence of thiol tautomers in the solid form of these compounds [11,21]. The strong bands at ~1700 cm^{-1} for carbohydrazones suggest the presence of ketone form in their solid state. These ketone and thione form in the solid state of compounds are in agreement with XRD studies of H_2L^3 and H_2L^4, will be discussed shortly. The broad bands at ~3400 cm^{-1} of NH protons are indicative of the presence of hydrogen bonding interactions as seen in the single crystal X-ray studies of H_2L^2 [11], H_2L^3 and H_2L^4 [16]. It is found that bands at ~1120 cm^{-1} are common in carbohydrazone, thiocarbohydrazone and thiosemicarbazone ligands, assigned to ν(N–N). Selected IR spectra of ligands are given in Figs 2.1 to 2.3.
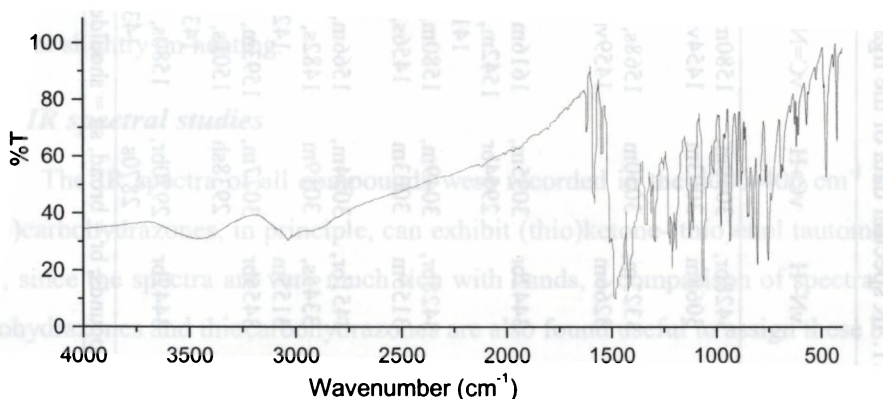
Fig. 2.1. IR spectrum of thiocarbohydrazone H_2L^3.
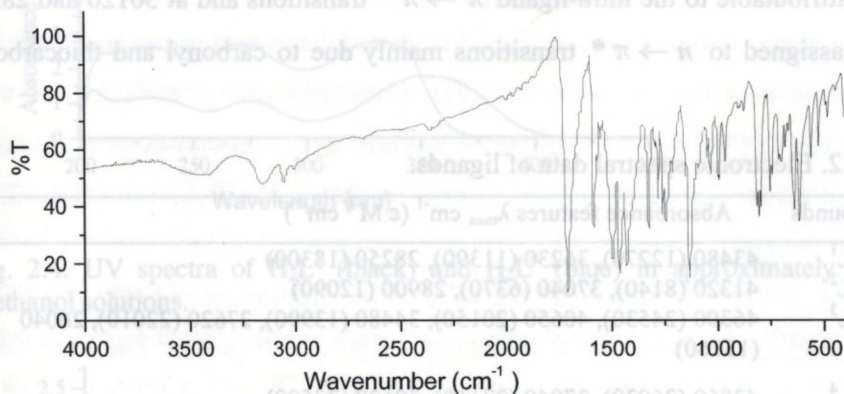
Fig. 2.2. IR spectrum of carbohydrazone H_2L^4.
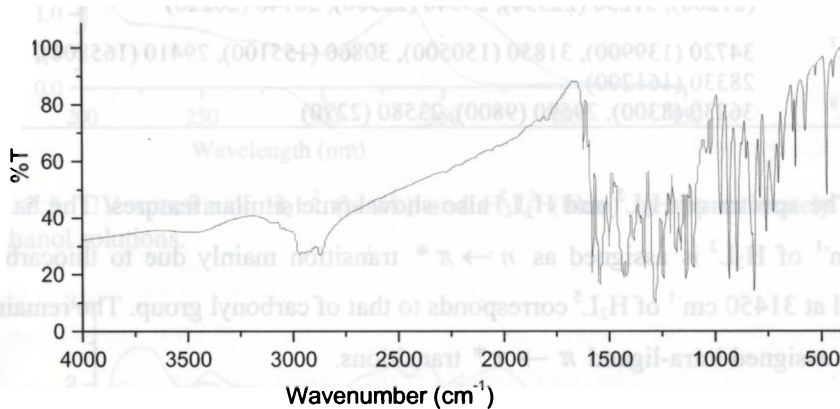
Fig. 2.3. IR spectrum of thiosemicarbazone HL^7.

2.3.2. Electronic spectral studies

The electronic spectra of carbohydrazones and thiocarbohydrazones were recorded in 10^{-4} M methanol solutions (Figs. 2.4 to 2.6) with a view to comparative study. The spectral features are summarized in Table 2.2. The thiocarbohydrazone H_2L^1 shows bands at 43480, 36230 and 28250 cm^{-1}, while its oxygen analogue H_2L^4 shows absorbances at 43860, 37040 and 30120 cm^{-1}. The bands at ~43600 and ~36600

cm^{-1} are attributable to the intra-ligand $\pi \rightarrow \pi *$ transitions and at 30120 and 28250 cm^{-1} are assigned to $n \rightarrow \pi *$ transitions mainly due to carbonyl and thiocarbonyl groups.

Table 2.2. Electronic spectral data of ligands.

Compounds	Absorbance features λ_{max} cm^{-1} (ε M^{-1} cm^{-1})
H$_2$L^1	43480 (12270), 36230 (11390), 28250 (18300)
H$_2$L^2	41320 (8140), 37040 (6370), 28900 (12090)
H$_2$L^3	46300 (24530), 40650 (20150), 34480 (13990), 27620 (22010), 26040 (15160)
H$_2$L^4	43860 (26030), 37040 (27110), 30120 (27500)
H$_2$L^5	42550 (15930), 37310 (13710), 31450 (18830)
H$_2$L^6	47170 (20270), 44640 (19140), 40650 (21610), 38020 (19760), 32260 (21280), 31250 (22330), 29940 (22500), 28740 (20220)
HL^7	34720 (139900), 31850 (150500), 30860 (155100), 29410 (165800), 28330 (161200)
HL^8	36230 (8300), 29590 (9800), 23580 (2270)

The spectra of H$_2$L^2 and H$_2$L^5 also show some similar features. The band at 28900 cm^{-1} of H$_2$L^2 is assigned as $n \rightarrow \pi *$ transition mainly due to thiocarbonyl group and at 31450 cm^{-1} of H$_2$L^5 corresponds to that of carbonyl group. The remaining bands are assigned intra-ligand $\pi \rightarrow \pi *$ transitions.

The electronic spectra of quinoline-derived compounds show many peaks compared to benzoylpyridine or di-2-pyridyl ketone derived compounds. H$_2$L^3 shows absorbances at 46300, 40650, 34480, 27620 and 26040 cm^{-1}, while H$_2$L^6 exhibits bands at 47170, 44640, 40650, 38020, 32260, 31250, 29940 and 28740 cm^{-1}. The bands at 27620 and 26040 cm^{-1} of H$_2$L^3 and 29940 and 28740 cm^{-1} of H$_2$L^6 are attributable to the intra-ligand $n \rightarrow \pi *$ transitions. Other bands are assigned to intra-ligand $\pi \rightarrow \pi *$ transitions.
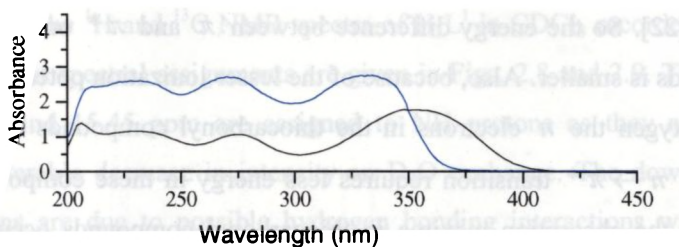
Fig. 2.4. UV spectra of H_2L^1 (black) and H_2L^4 (blue) in approximately 10^{-4} M methanol solutions.
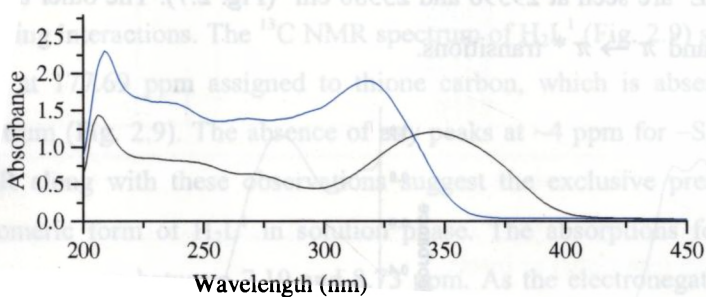
Fig. 2.5. UV spectra of H_2L^2 (black) and H_2L^5 (blue) in approximately 10^{-4} M methanol solutions.
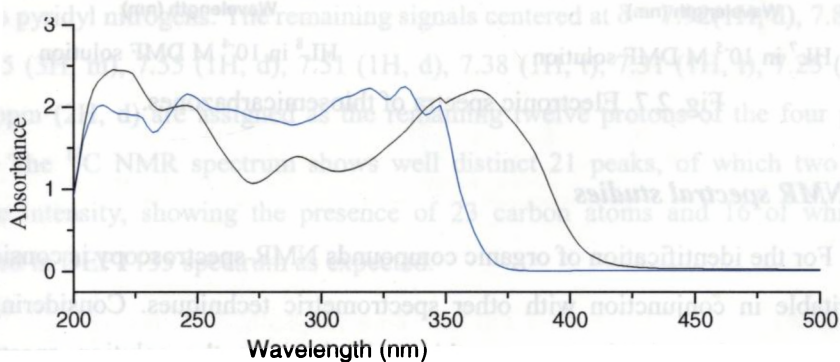
Fig. 2.6. UV spectra of H_2L^3 (black) and H_2L^6 (blue) in 10^{-4} M methanol solutions.

These differences in wavelengths can be explained on the basis of the weaker C=S π interaction in thiocarbonyl compounds compared to C=O π interaction in

49

carbonyl compounds [22]. So the energy difference between π and $\pi *$ orbitals in thiocarbonyl compounds is smaller. Also, because of the lesser ionization potential of sulfur compared to oxygen the n electrons in the thiocarbonyl compounds are of higher energy and the $n \rightarrow \pi *$ transition requires less energy in these compounds than in carbonyls. So the absorption maxima in thiocarbonyl compounds occur at longer wavelengths.

The thiosemicarbazone HL^7 shows $n \rightarrow \pi *$ transitions at 29410 and 28330 cm^{-1}, while that of HL^8 are seen at 29590 and 23580 cm^{-1} (Fig. 2.7). The other bands are assigned intra-ligand $\pi \rightarrow \pi *$ transitions.

HL^7 in 10^{-5} M DMF solution HL^8 in 10^{-4} M DMF solution
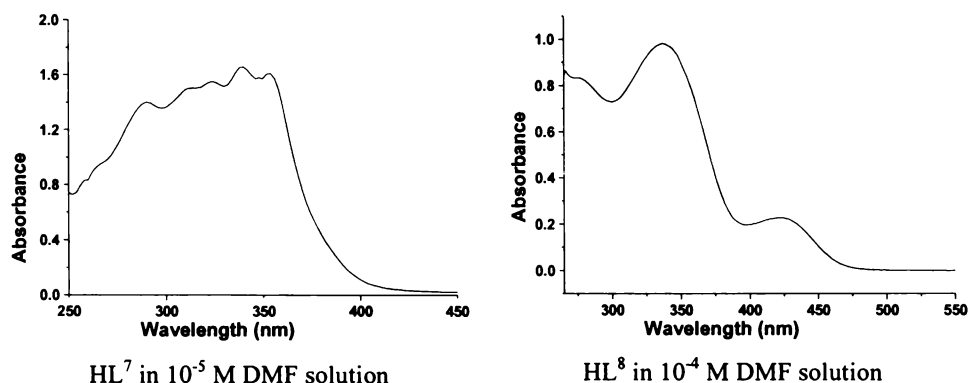
Fig. 2.7. Electronic spectra of thiosemicarbazones.

2.3.3. NMR spectral studies

For the identification of organic compounds NMR spectroscopy is considered as inevitable in conjunction with other spectrometric techniques. Considering the NMR spectra of semicarbazones or thiosemicarbazones the solution spectra of carbohydrazones and thiocarbohydrazones are much complicated. The thiocarbohydrazone ligands having better solubility in $CDCl_3$ or DMSO-d_6 are found to show well-resolved peaks compared to their oxygen counterparts.

The ^{1}H and ^{13}C NMR spectra of H_2L^1 in CDCl$_3$ recorded at 400 MHz, along with their spectral assignments are given in Figs. 2.8 and 2.9. The sharp peaks at δ = 14.56 and 15.45 ppm are assigned to NH protons as they are singlets and their considerable decrease in intensity on D$_2$O exchange. The downfield shifts of these protons are due to possible hydrogen bonding interactions with adjacent nitrogen atoms. Hydrogen bonding interaction decreases the electron density around the proton, and thus causes shifting of resonance absorption to a lower field [23]. The singlet nature of these peaks is attributed to the absence of any nearby protons for coupling interactions. The ^{13}C NMR spectrum of H_2L^1 (Fig. 2.9) shows a well distinct peak at 177.69 ppm assigned to thione carbon, which is absent in the DEPT135 spectrum (Fig. 2.9). The absence of any peaks at ~4 ppm for –SH proton [21] in ^{1}H NMR along with these observations suggest the exclusive presence of the thione tautomeric form of H_2L^1 in solution phase. The absorptions for pyridyl hydrogen atoms are seen between 7.19 and 8.73 ppm. As the electronegative pyridyl nitrogen atoms cause a downfield shift for adjacent protons, the peaks at 8.73 (1H, d), 8.62 (1H, d), 8.50 (1H, d) and 8.21 ppm (1H, d) are assigned due to the protons of carbons near to pyridyl nitrogens. The remaining signals centered at δ = 7.92(1H, d), 7.84 (1H, t), 7.75 (3H, m), 7.55 (1H, d), 7.51 (1H, d), 7.38 (1H, t), 7.31 (1H, t), 7.25 (1H, t), 7.20 ppm (2H, d) are assigned as the remaining twelve protons of the four pyridyl rings. The ^{13}C NMR spectrum shows well distinct 21 peaks, of which two are of double intensity, showing the presence of 23 carbon atoms and 16 of which are retained in DEPT135 spectrum as expected.
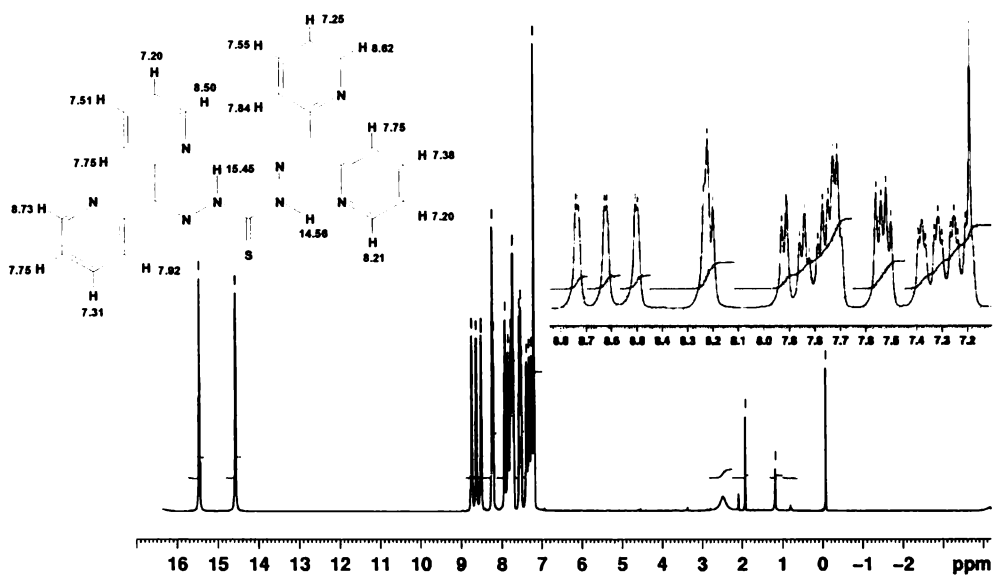
Fig. 2.8. ¹H NMR spectrum of H₂L¹ with its spectral assignment (top left) and aromatic proton peaks (top right) as insets.
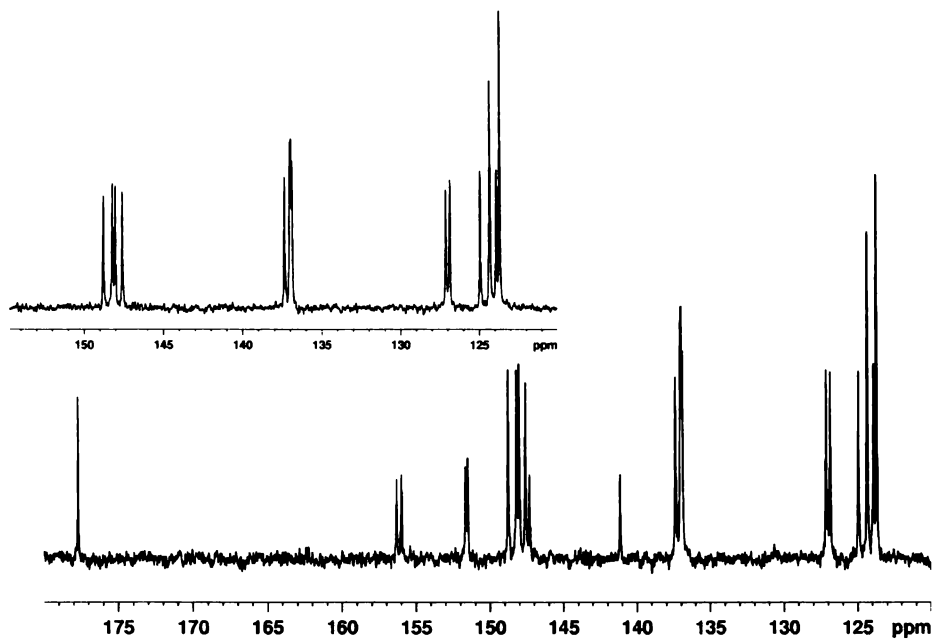
Fig. 2.9. ¹³C NMR spectrum of H₂L¹. The inset shows its DEPT135 spectrum.

The ^1H NMR spectrum of H_2L^3 in $CDCl_3$ recorded at 500 MHz (Fig. 2.10) shows two peaks at 16.84 and 15.76 ppm, found to loss its intensity on D_2O exchange. These downfielded peaks assigned to hydrogen bonded NH protons. The multiplet signals from 7.26 to 8.41 ppm are attributed to twelve protons of the two quinoline rings. These results suggest the presence of thione tautomer in solution phase. The ^{13}C NMR spectrum of H_2L^3 and ^1H NMR spectrum of H_2L^6 taken was of very poor quality for an assignment due to the poor solubility of these compounds.
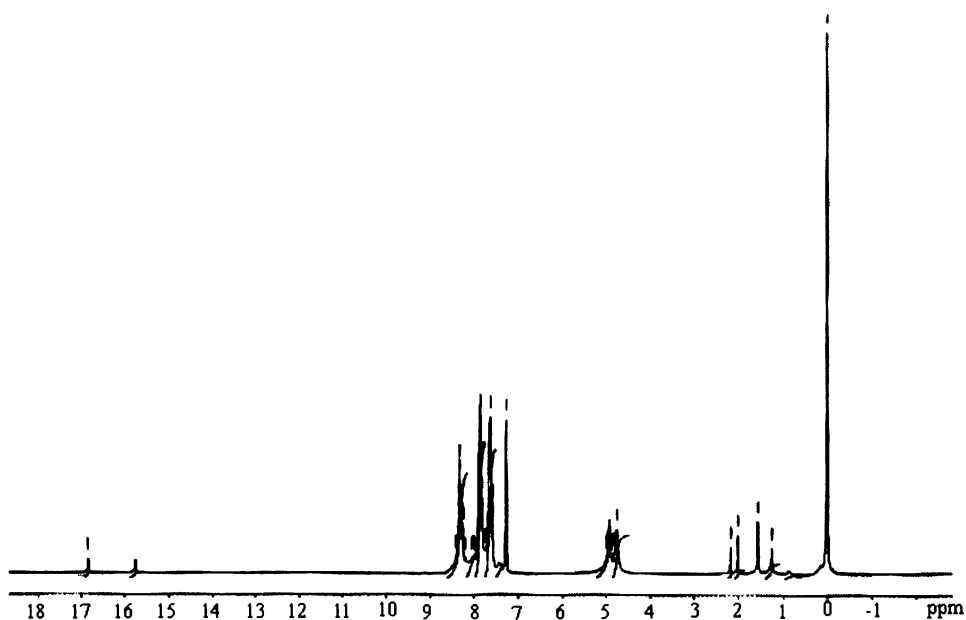
Fig. 2.10. ^1H NMR spectrum of H_2L^3.

The ^1H and ^{13}C NMR spectra of H_2L^2 in $CDCl_3$ recorded at 400 MHz (Figs. 2.11 & 2.12) are very difficult to interpret because of the crowding of peaks. The ^1H NMR spectrum of H_2L^2 in $CDCl_3$ has already been reported [4,11]. However the spectrum was reinvestigated, as there were contradictions like absence of thiol form [11] and presence of tautomers [4]. The downfield peaks at δ=15.18, 14.03, 13.67 and

53

10.92 ppm, attributed to hydrogen bonded NH protons, and a peak at 3.45 ppm, assigned to –SH proton are indicative of the presence of both thione and thiol tautomeric forms in the solution phase. The presence of more than thirtyfive peaks in the ^{13}C NMR spectrum and the disappearance of more than thirteen peaks in the DEPT135 spectrum (Fig. 2.13) also support the presence of both tautomeric forms. The possibility of *syn* and *anti* forms of thiol tautomer is also clear from the number of peaks. However, the intensities of various peaks confirm that the percentage of thione form is more compared to thiol forms in $CDCl_3$ solution. The ^{1}H NMR spectrum of its oxygen analogue H_2L^5 (Fig. 2.14) is also rich in peaks, but with the signs of much less amounts of enol tautomer compared to the tautomeric forms in H_2L^2 solution. Here the downfield singlets at δ= 14.27, 12.66, 12.25, 9.83 and 8.02 ppm are found to loss its intensity considerably on D_2O exchange showing the exchangeability of corresponding protons. The last one may be attributed due to –OH proton of the enol form and 12.25, 9.83 ppm peaks are assigned to hydrogen bonded NH protons of the ketone form, while the peak at 14.27 ppm is assigned to the same of the enol tautomer. The signal at 12.66 ppm is of insignificant intensity may be indicating both *syn* and *anti* confirmation of the enol form. The signals of the pyridine and phenyl hydrogens are seen in between 6.93 and 8.70 ppm. The ^{13}C NMR spectrum (Fig. 2.15), however requires a highly concentrated solution to show all signals of both tautomers, not showed much resolved signals which might be due to the low concentration of the enol tautomer in solution. The peak at 155.42 ppm is assigned to carbonyl group, and is absent in the DEPT135 spectrum. The DEPT135 spectrum retains more than 18 signals, with a new peak at 129.48 ppm, suggests the presence of the enol tautomer, and makes assignments difficult with the unequal intensities.
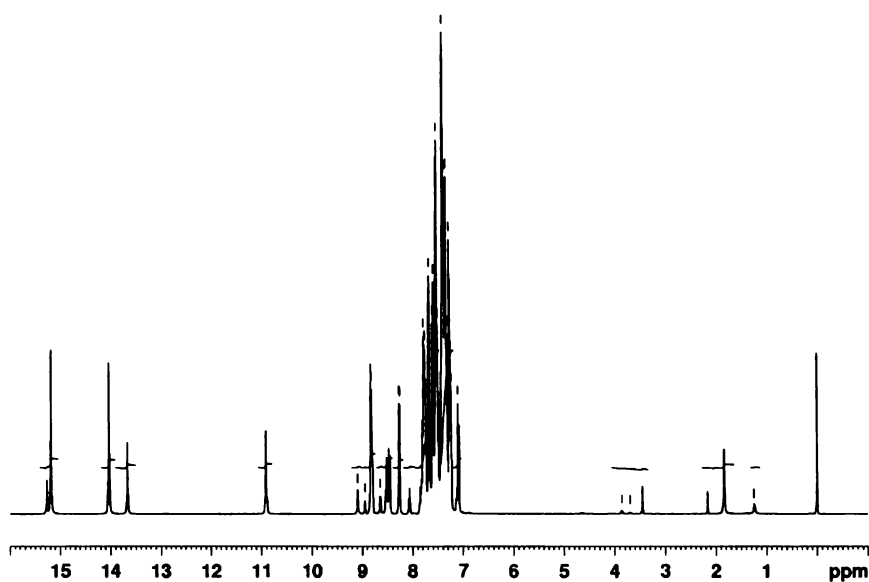
Fig. 2.11. ^{1}H NMR spectrum of H$_2$L^2.
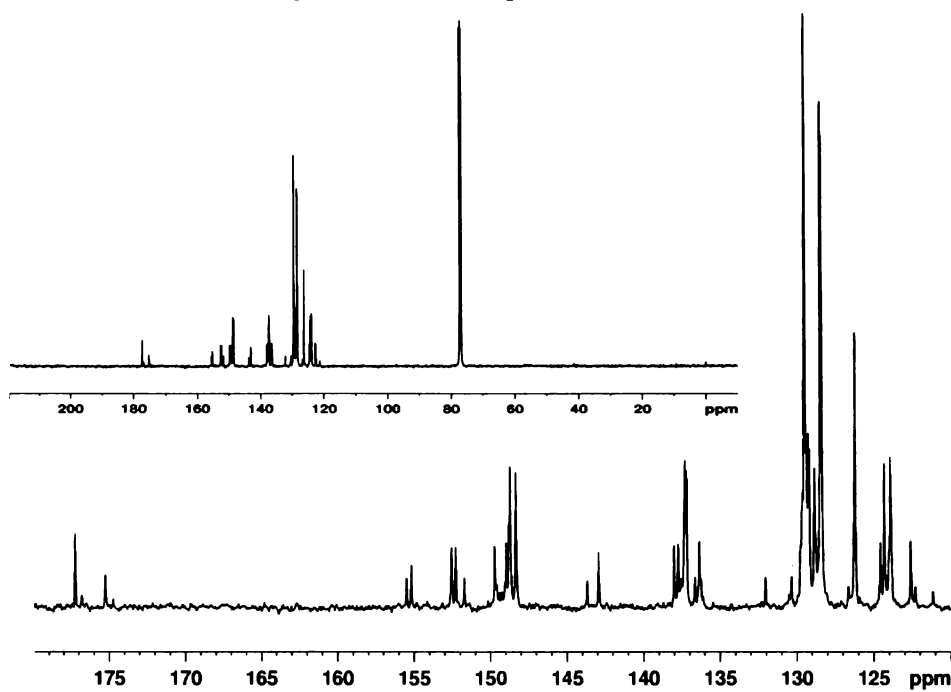
Fig. 2.12. ^{13}C NMR spectrum of H$_2$L^2 (inset shows the full spectrum).
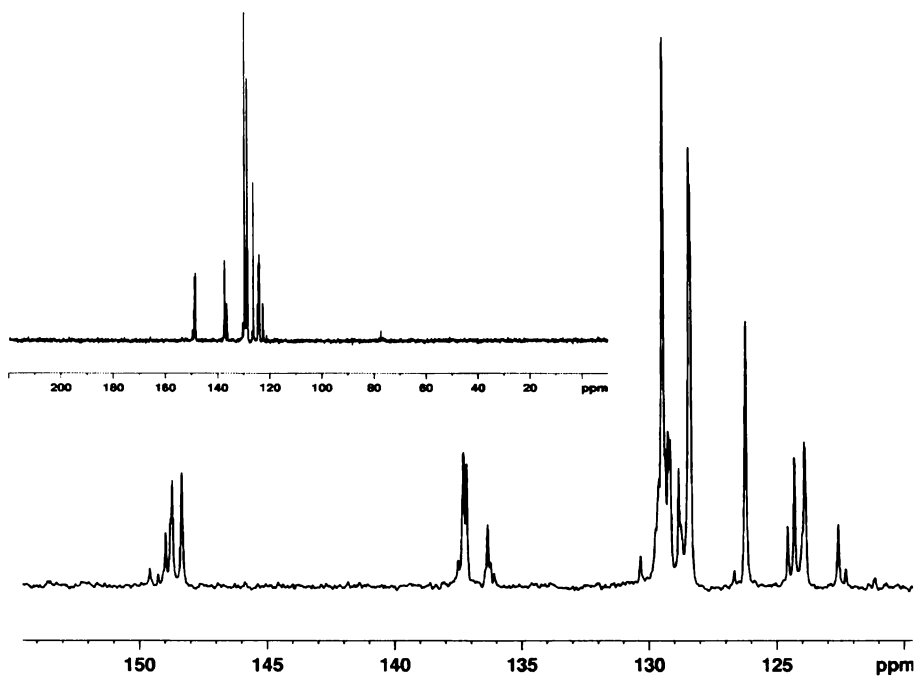
Fig. 2.13. DEPT135 NMR spectrum of H_2L^2 (inset shows the full spectrum).
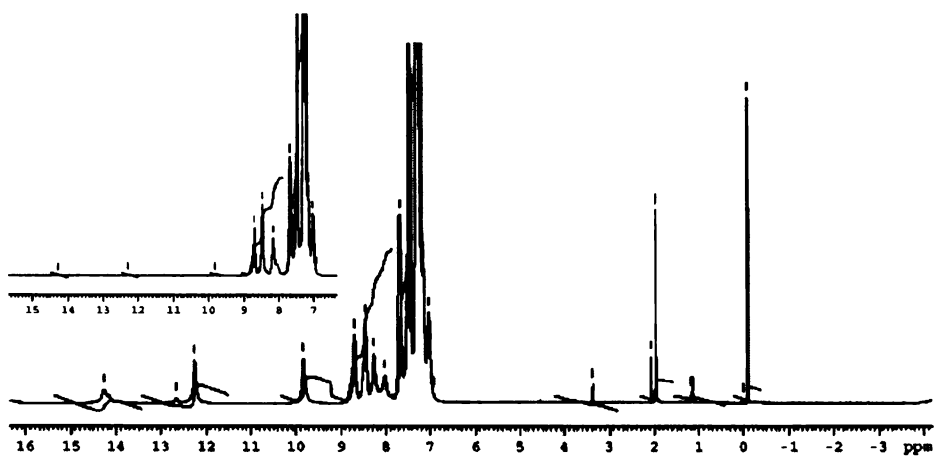
Fig. 2.14. ^1H NMR spectrum of H_2L^5 and its D_2O exchange spectrum as inset.
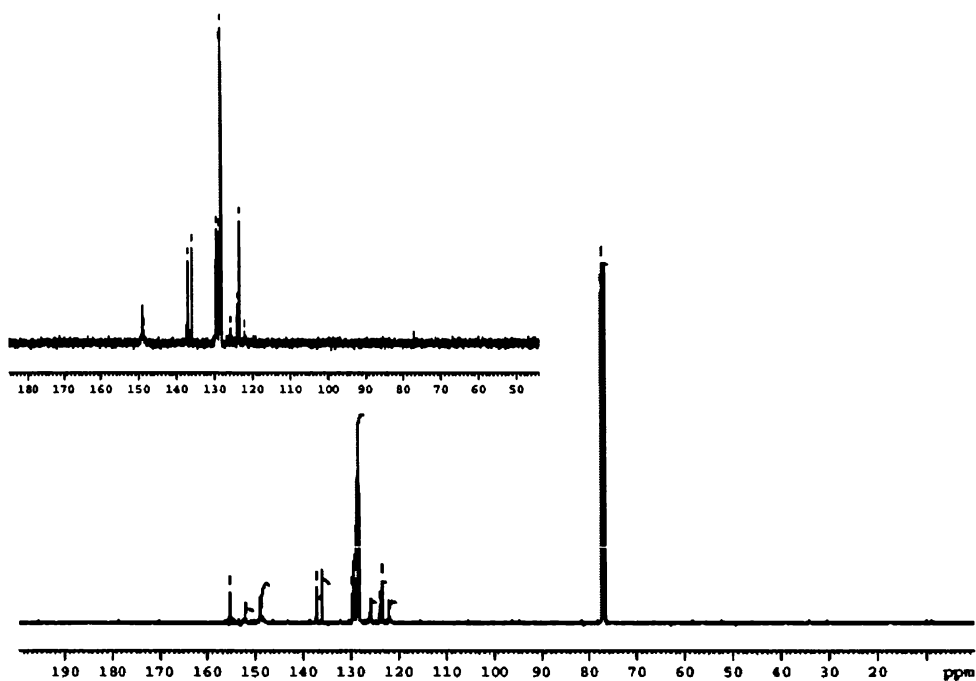
Fig. 2.15. ^{13}C NMR spectrum of H$_2$L^5 with its DEPT135 spectrum as inset.

2.3.4. Single crystal X-ray diffraction studies

The crystal structure data collection of H$_2$L^3 was done on a BRUKER SMART APEX CCD diffractometer at Analytical Sciences Division, Central Salt and Marine Chemicals Research Institute, Bhavnagar, Gujarat using graphite monochromated MoKα radiation (λ=0.71073 Å) at 273(2) K. A crystal with dimension 0.22 mm×0.18 mm×0.12 mm was used. The collected data were reduced using SAINT [24]. The structure was solved by direct methods with the program SHELXS-97 [25] and refined by full-matrix least squares on F^2 with SHELXTL-97. All non-hydrogen atoms were refined anisotropically. The hydrogen atoms were geometrically fixed and were treated as riding atoms on the parent C atoms, with C–H distances = 0.93 Å and N–H

0.86 Å with U_{iso} = 1.2 U_{eq} of the parent atoms, except H(3AN), H(4AN) and H(4BN) which were located from difference maps and were refined isotropically.

The data of H_2L^4 were collected at X-ray Crystallography Unit, School of Physics, Universiti Sains Malaysia, Penang, Malaysia using Bruker SMART APEX2 CCD area detector diffractometer equipped with graphite monochromated Mo Kα (λ = 0.71073 Å) radiation at temperature 297(2) K. The trial structure was solved using SHELXS-97 and refinement was carried out by full-matrix least squares on F^2 (SHELXTL-97). H atoms attached to N atoms were located in a difference map and refined isotropically. C-bound H atoms were placed in calculated positions and allowed to ride on their parent C atoms, with C–H = 0.93 Å and $U_{iso}(H)$ = 1.2U_{eq}(C).

The crystallographic data and structure refinement parameters for the compounds H_2L^3 and H_2L^4 are given in Table 2.3. The graphics tools used include ORTEP-III [26], PLATON [27], MERCURY [28] and DIAMOND version 3.0 [29].

2.3.4.1. Crystal structure of H_2L^3

The compound H_2L^3, $C_{21}H_{16}N_6S$, crystallizes in *triclinic* form with two independent molecules in the asymmetric unit and exists in the thione tautomeric forms. The two crystallographically independent molecules, A and B are depicted in Fig. 2.16 and their bond lengths and angles are given in Table 2.4, agree with each other and are within normal ranges [30]. Molecule A shows a *Z-Z* configuration about the C(10A)–N(2A) and C(12A)–N(5A) double bonds and molecule B shows the same about the C(10B)–N(2B) and C(12B)–N(5B) double bonds. A similar configuration was observed in the bisthiocarbohydrazone of 2-benzoylpyridine, H_2L^2 [11], while in 2-acetylpyridine analogue an *E-Z* configuration exists [9]. The thione S(1) atom is positioned *trans* to azomethine atom N(2) [The S(1)–C(11)–N(3)–N(2) torsion angle of -174.72(2)° for molecule A and 177.67(2)° for molecule B] and *cis* to azomethine atom N(5) [The S(1)–C(11)–N(4)–N(5) torsion angle of 4.26(3)° for molecule A and 1.43(3)° for molecule B] in both molecules.

58

Table 2. 3. Crystal data and structural refinement parameters of thiocarbohydrazone H_2L^3 and carbohydrazone H_2L^4.

Parameters	H_2L^3	H_2L^4
Empirical Formula	$C_{21}H_{16}N_6S$	$C_{23}H_{18}N_8O$
Formula weight (M)	384.47	422.45
Color, shape	Yellow, plate	Colorless, block
Temperature (T) K	273(2)	297(2)
Wavelength (Mo Kα) (Å)	0.71073	0.71073
Crystal system	*Triclinic*	*Triclinic*
Space group	*P1̄*	*P1̄*
Lattice constants		
a (Å)	11.331(2)	9.0963(2)
b (Å)	11.714(2)	9.1215(2)
c (Å)	15.116(3)	13.6215(3)
α (°)	100.369(4)	71.1360(10)
β (°)	109.512(4)	86.8990(10)
γ (°)	90.134(4)	72.4310(10)
Volume V (Å^3)	1856.1(6)	1018.42(4)
Z	4	2
$D_{calc.}$ (ρ) (Mg m^{-3})	1.376	1.378
Absorption coefficient μ (mm^{-1})	0.194	0.091
F(000)	800	440
Crystal size (mm^3)	0.22×0.18×0.12	0.31×0.26×0.19
θ Range for data collection	1.46 to 25.00	2.5 to 27.5
Limiting Indices	$-13 \leq h \leq 12$,	$-11 \leq h \leq 11$,
	$-13 \leq k \leq 11$,	$-11 \leq k \leq 11$,
	$-15 \leq l \leq 17$	$-16 \leq l \leq 17$
T_{max} and T_{min}	0.977 and 0.959	0.983 and 0.972
Reflections collected	9147	17391
Independent Reflections	6540 [R(int) = 0.0262]	4652 [R(int) = 0.0379]
Refinement method	Full-matrix least-squares on F^2	Full-matrix least-squares on F^2
Data / restraints / parameters	6396/0/517	4652/0/297
Goodness-of-fit on F^2	1.044	1.041
Final R indices [I > 2σ (I)]	R$_1$ = 0.0649, wR$_2$ = 0.1625	R$_1$ = 0.0450, wR$_2$ = 0.1018
R indices (all data)	R$_1$ = 0.1071, wR$_2$ = 0.1942	R$_1$ = 0.0702, wR$_2$ = 0.1168
Largest difference peak and hole (e Å^{-3})	0.495 and -0.489	0.146 and -0.209
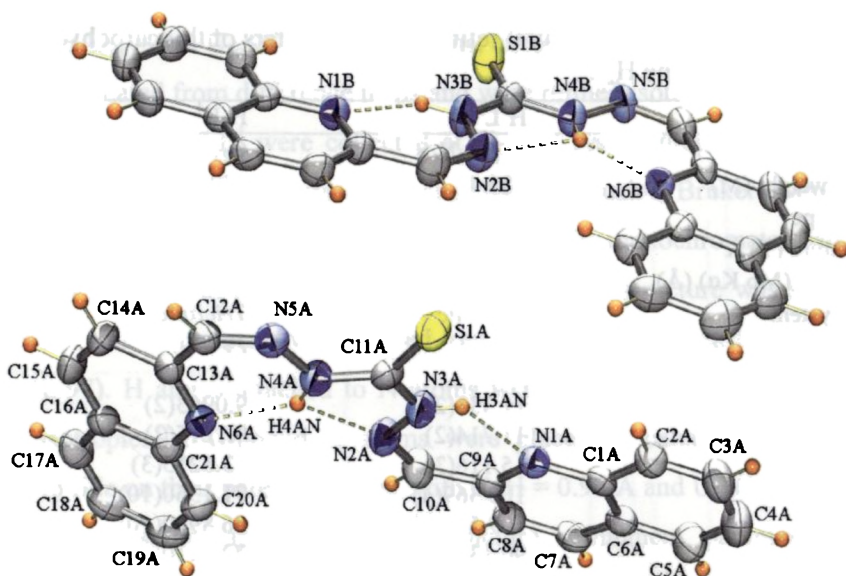
Fig. 2.16. ORTEP plot of the two independent molecules in the asymmetric unit of H_2L^3, with 50% probability displacement ellipsoids. H atoms are shown as small spheres of arbitrary radii and dashed lines denote the intramolecular N–H⋯N interactions.

Table 2.4. Selected bond lengths (Å) and angles (°) of H_2L^3.

S(1A)–C(11A)	1.657 (4)	C(11B)–N(4B)–N(5B)	120.0 (3)
S(1B)–C(11B)	1.651 (4)	N(2B)–N(3B)–C(11B)	120.3 (3)
N(4B)–C(11B)	1.345 (5)	C(12B)–N(5B)–N(4B)	116.5 (3)
N(4B)–N(5B)	1.365 (4)	C(11A)–N(3A)–N(2A)	120.4 (3)
N(3B)–N(2B)	1.358 (4)	C(10A)–N(2A)–N(3A)	118.3 (3)
N(3B)–C(11B)	1.362 (5)	C(11A)–N(4A)–N(5A)	119.9 (3)
N(5B)–C(12B)	1.292 (5)	C(12A)–N(5A)–N(4A)	116.5 (3)
N(3A)–C(11A)	1.353 (5)	C(10B)–N(2B)–N(3B)	117.7 (3)
N(3A)–N(2A)	1.355 (4)	N(4B)–C(11B)–N(3B)	113.0 (3)
C(13B)–C(12B)	1.457 (5)	N(4B)–C(11B)–S(1B)	126.6 (3)
N(2A)–C(10A)	1.290 (5)	N(3B)–C(11B)–S(1B)	120.4 (3)
N(4A)–C(11A)	1.347 (5)	N(4A)–C(11A)–N(3A)	112.5 (3)
N(4A)–N(5A)	1.366 (4)	N(4A)–C(11A)–S(1A)	127.0 (3)
N(5A)–C(12A)	1.286 (4)	N(3A)–C(11A)–S(1A)	120.5 (3)
C(9A)–C(10A)	1.454 (5)		
C(13A)–C(12A)	1.466 (5)		
N(2B)–C(10B)	1.289 (5)		
C(10B)–C(9B)	1.463 (5)		

The C–S bond distances of 1.6571(2) Å in molecule A and 1.6507(3) Å in molecule B agree well with those in related compounds [9,31,32] being intermediate between 1.82 Å for a C–S single bond and 1.56 Å for a C=S double bond [11]. The C(11)–N(3) and C(11)–N(4) bond distances in both molecules are, intermediate between 1.47 Å for a C–N single bond and 1.29 Å for a C=N double bond [33], indicative of some electron delocalization. Similarly the N(2)–N(3) [1.3545(2) Å and 1.3580(2) Å in molecules A and B respectively] and N(4)–N(5) [1.3663(2) Å and 1.3648(3) Å in molecules A and B respectively] bond distances are, intermediate between 1.45 Å for a N–N single bond and 1.25 Å for a N=N double bond [33], also indicative of extensive electron delocalization in the whole thiocarbohydrazone moiety. The extensive electron delocalization is similar to that seen in bis(2-benzoylpyridine) thiocarbohydrazone [11].

Each molecule is stabilized by three intramolecular hydrogen bonds. The intramolecular N(3)–H(3)···N(1) and N(4)–H(4)···N(6) hydrogen bonds form six-membered N(1)–C(9)–C(10)–N(2)–N(3)–H(3) and N(6)–C(13)–C(12)–N(5)–N(4)–H(4) rings respectively in both A and B molecules; while the intramolecular hydrogen bond N(4)–H(4)···N(2) forms a five-membered N(2)–N(3)–C(11)–N(4)–H(4) ring in both A and B molecules (Fig. 2.16 & Table 2.5). The thiocarbohydrazone moieties viz. C(10)/N(2)/N(3)/C(11)/S(1)/N(4)/N(5)/C(12) in A and B show some variations in planarity, as evidenced by a maximum deviation of 0.101(3) Å for N(4A) in molecule A and a maximum deviation of 0.028(3) Å for N(2B) in molecule B. This clearly shows that the central thiocarbohydrazone core is almost planar in molecule B and a slight deviation from planarity for the same core of molecule A. However the thiocarbohydrazide core N(2)/N(3)/C(11)/S(11)/N(4)/N(5) of molecule A is almost planar with a maximum deviation of -0.055(3) Å for N(4A).

Table 2.5. Hydrogen bonding geometry and C–H···π interactions of H_2L^3.

D–H···A	D–H (Å)	H···A (Å)	D···A (Å)	D–H···A (°)
N(3A)–H(3AN)···N(1A)	0.79(4)	2.15(4)	2.700(5)	128(4)
N(4A)–H(4AN)···N(6A)	0.85(3)	2.01(3)	2.688(5)	137(3)
N(4A)–H(4AN)···N(2A)	0.85(3)	2.21(3)	2.558(5)	105(3)
N(3B)–H(3BN)···N(1B)	0.86	2.02	2.692(5)	134
N(4B)–H(4BN)···N(6B)	0.85(4)	1.96(4)	2.646(4)	136(3)
N(4B)–H(4BN)···N(2B)	0.85(4)	2.20(4)	2.572(5)	107(3)
C(8A)–H(8A)···Cg(8)[a]	0.93	2.59	3.3821(44)	143
C(18A)–H(18A)···Cg(7)[b]	0.93	2.96	3.8008(46)	151
C(19A)–H(19A)···Cg(9)[b]	0.93	2.92	3.6909(45)	141

D= donor, A=acceptor; Symmetry codes: (a) -x, -y, 1 - z; (b) 1-x, 1-y, 1-z.

Each molecule contains two ten membered quinoline rings comprising atoms N(1), C(1)-C(9) and N(6), C(13)-C(21). There are eight centroids viz. Cg(1) and Cg(7) [comprising atoms N(1), C(1), C(6), C(7), C(8), C(9) with maximum deviations of 0.025(3) Å for C(9A) and 0.011(4) Å for C(9B)], Cg(2) and Cg(8) [comprising atoms N(6), C(13), C(14), C(15), C(16), C(21) with maximum deviations of 0.018(4) Å for C(21A) and -0.008(4) Å for C(15B)], Cg(3) and Cg(9) [comprising atoms C(1), C(2), C(3), C(4), C(5), C(6) with maximum deviations of 0.020(4) Å for C(1A) and -0.006(4) Å for C(2B)], and Cg(4) and Cg(10) [comprising atoms C(16), C(17), C(18), C(19), C(20), C(21) with maximum deviations of 0.019(5) Å for C(19A) and 0.014(4) Å for C(16B)], which are parts of four quinoline rings of the two forms A and B of compound H_2L^3. In molecule B each of the two quinoline rings are in separate planes, with maximum deviations of -0.018(4) Å for C8B and 0.034(4) Å for C(19B), and makes an angle of 5.19(11)° each other; while in molecule A both quinoline rings show slight deviation in planarity compared to that in molecule B. Here the quinoline rings, Cg(5) involving N(1A) and Cg(6) involving N(6A), show maximum mean plane deviations of 0.057(5) Å for C(4A) and 0.050(5) Å for C(19A) respectively. The dihedral angles 3.3(2)° between the mean planes of Cg(1) and Cg(3) and 2.7(2)°

between the planes of Cg(2) and Cg(4) also show slight tilted nature of quinoline rings in molecule A. The angle between the two quinoline rings in A shows considerable variation compared to that in B as evidenced by the dihedral angle of 17.49(12) Å.

In the crystal, A molecules are packed in the *bc* plane and B molecules are packed in the *ab* plane (Fig. 2.17). The C-H···Cg (π-ring) interactions (Table 2.5) involving Cg(7), Cg(8) and Cg(9) stabilize the packing in the unit cell. Only hydrogens of molecule A interact with centroids of molecule B, the reverse is not seen. The crystal structure cohesion is reinforced by various aromatic π···π stacking interactions (Table 2.6). We have reported these results recently [34].
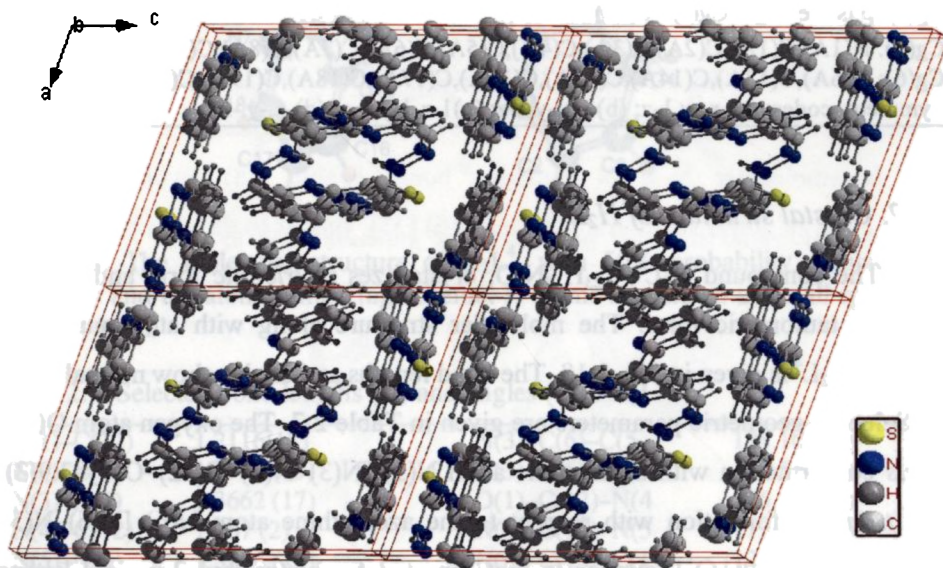
Fig. 2.17. Packing of thiocarbohydrazone H_2L^3 in the unit cells viewed along the *b* axis.

Table 2.6. $\pi \cdots \pi$ interactions of H_2L^3.

Cg(I)$\cdots$Cg(J)	Cg$\cdots$Cg (Å)	α (°)	β (°)
Cg(1)$\cdots$Cg(1)^a	3.492(2)	0.00	5.85
Cg(2)$\cdots$Cg(3)^b	3.849(3)	14.22	23.24
Cg(2)$\cdots$Cg(4)^c	3.638(3)	2.79	21.87
Cg(3)$\cdots$Cg(2)^b	3.848(3)	14.22	30.67
Cg(4)$\cdots$Cg(2)^c	3.638(3)	2.79	20.45
Cg(4)$\cdots$Cg(4)^c	3.582(3)	0.00	19.66
Cg(8)$\cdots$Cg(9)^d	3.557(2)	4.21	15.33
Cg(9)$\cdots$Cg(8)^d	3.557(2)	4.21	17.01
Cg(9)$\cdots$Cg(10)^d	3.819(2)	4.85	21.51
Cg(10)$\cdots$Cg(9)^d	3.820(2)	4.85	26.20

Cg$\cdots$Cg is the distance between ring centroids. Only $\pi \cdots \pi$ interactions with Cg$\cdots$Cg distances below 4 Å are included. α is the dihedral angle between the planes of Cg(I) and Cg(J). β is the angle Cg(I)$\cdots$Cg(J).

Cg(5): N(1A),C(1A),C(2A),C(3A),C(4A),C(5A),C(6A),C(7A),C(8A),C(9A)
Cg(6): N(6A),C(13A),C(14A),C(15A),C(16A),C(17A),C(18A),C(19A),C(20A),C(21A)
Symmetry codes: (a)-x,-y,1-z; (b)1-x,-y,1-z; (c)1-x,1-y,1-z; (d)-x,-y,-z.

2.3.4.2. Crystal structure of H_2L^4

The compound H_2L^4, $C_{23}H_{18}N_8O$, crystallizes in *triclinic* form and exists in the thione tautomeric form. The molecular structure along with atom numbering scheme of H_2L^4 is given in Fig. 2.18. The bond lengths and angles show normal values [30]. Selected geometric parameters are given in Table 2.7. The oxygen atom O(1) is in a *cis* conformation with azomethine atom N(3) [N(3)–N(4)–C(12)–O(1)=3.9(3)°] and a *trans* conformation with respect to the azomethine atom N(6) [N(6)–N(5)–C(12)–O(1)=170.20(16)°], similar to that reported for bis(methyl 2-pyridyl ketone) carbohydrazone [9]. As also observed in bis(methyl 2-pyridyl ketone) carbohydrazone [9] and in thiocarbohydrazones [9,11,32], the C(13)–N(6) and N(5)–C(12) bonds are in an *E* conformation with respect to the N(5)–N(6) bond and, similarly, the C(6)–N(3) and N(4)–C(12) bonds are in an *E* conformation about the N(3)–N(4) bond. The C(6)–N(3)–N(4)–C(12) [176.23(14)°] and C(13)–N(6)–N(5)–C(12) [179.44(15)°] torsion angles confirm the *EE* conformation. The C(12)–O(1) distance of 1.2116(18)

Å indicates a typical double-bond nature and the ketone form. The N–N and C–N bond lengths (Table 2.7) of the carbohydrazone core group are comparable to the corresponding lengths in bis(methyl 2-pyridyl ketone) carbohydrazone [9], indicate some electron delocalization in the N(3)/N(4)/C(12)/N(5)/N(6) moiety.
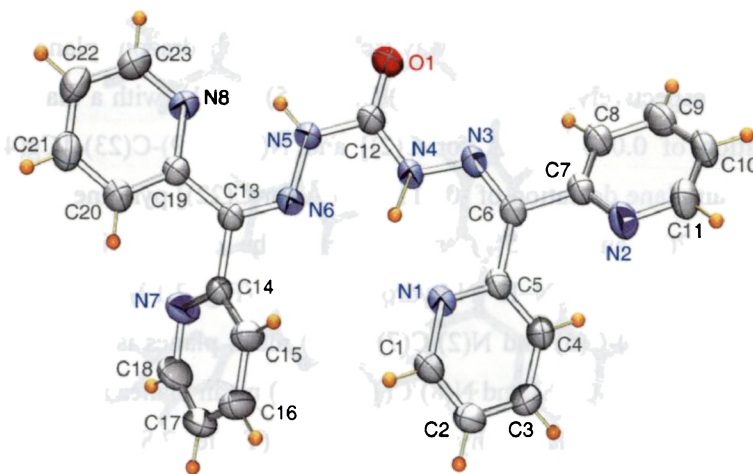
Fig. 2.18. The molecular structure of H_2L^4, with 50% probability displacement ellipsoids and the atom numbering scheme. H atoms are shown as small spheres of arbitrary radii.

Table 2.7. Selected bond lengths (Å) and angles (°) of H_2L^4.

O(1)–C(12)	1.2116(18)	N(3)–C(6)–C(5	128.10 (13)
N(3)–C(6)	1.2945 (19)	N(3)–C(6)–C(7	112.55 (13)
N(3)–N(4)	1.3662 (17)	O(1)–C(12)–N(4	125.56 (14)
N(4)–C(12)	1.367 (2)	N(4)–C(12)–N(5	113.51 (13)
N(5)–N(6)	1.3556 (17)	N(6)–C(13)–C(19	128.00 (13)
N(5)–C(12)	1.3799 (19)	N(6)–C(13)–C(14	113.27 (12)
N(6)–C(13)	1.2950 (18)	C(7)–C(6)–C(5	119.35(13)
C(5)–C(6)	1.489 (2)	O(1)–C(12)–N(5	120.93(15)
C(6)–C(7)	1.4903 (19)	C(19)–C(13)–C(14)	118.70(12)
C(13)–C(19)	1.482 (2)		
C(13)–C(14)	1.493 (2)		

65

The carbohydrazone moiety C(6)/N(3)/N(4)/C(12)/O(1)/N(5)/N(6)/C(13) is approximately planar, with a maximum mean plane deviation of -0.0937(16) Å for N(5), similar to bis(methyl 2-pyridyl ketone)carbohydrazone. The pyridine ring planes N(2)/C(7)-C(11) [Cg(2), having a maximum mean plane deviation of -0.0091(19) Å for C(10)] and N(7)/C(14)-C(18) [Cg(3), having a maximum mean plane deviation of 0.0065(19) Å for C(18)] are twisted away from the carbohydrazone plane by 40.88(5) and 50.10(4)° respectively, while the N(1)/C(1)-C(5) [Cg(1), with a maximum mean plane deviation of 0.0145(17) Å for C(2)] and N(8)/C(19)-C(23) [Cg(4), with a maximum mean plane deviation of -0.0110(18) Å for C(22)] pyridine ring planes are twisted by 23.92(7) and 21.45(7)° respectively. The decrease in the twisting is attributed to intramolecular N–H⋯N hydrogen bonds (Fig. 2.19). The dihedral angle between the N(1)/C(1)-C(5) and N(2)/C(7)-C(11) mean planes is 55.75(6)° and that between the N(7)/C(14)-C(18) and N(8)/C(19)-C(23) mean planes is 71.03(5)°.

Intramolecular N–H⋯N hydrogen bonds (Table 2.8) involving H(1N4) generate rings of graph-set motifs S(5) and S(6) [35], similar to those in bis(methyl 2-pyridyl ketone) carbohydrazone [9] and in related thiocarbohydrazones [9,11], while the N–H⋯N hydrogen bond involving H(1N5) generates a graph-set motif S(6), as seen in related thiocarbohydrazone [11]. As a consequence the angles subtended at C(6), C(12) and C(13) (Table 2.7) vary significantly. Molecules translated by one unit cell along the *a*-axis direction are linked by C(2)–H(2A)⋯O(1) and C(16)–H(16A)⋯O(1) (Table 2.8) hydrogen-bonding interactions, forming a chain (Fig. 2.20). These interactions together constitute a pair of bifurcated acceptor bonds. In addition, the crystal packing is reinforced by a weak C–H⋯π interaction (Table 2.8) involving the N(8)/C(19)-C(23) pyridine ring [centroid Cg(4)] and π⋯π stacking interactions involving the N(1)/C(1)-C(5) pyridine rings [centroid Cg(1)] at (x, y, z) and (2-x, 2-y, -z) [Cg⋯Cg distance=3.5804(9) Å]. Another week π⋯π stacking interactions between pyridine rings Cg(1) at (x, y, z) and Cg(4) at (2-x, 1-y, -z) [Cg⋯Cg distance =3.7785(10) Å] and its counterpart are also observed in the packing.

66
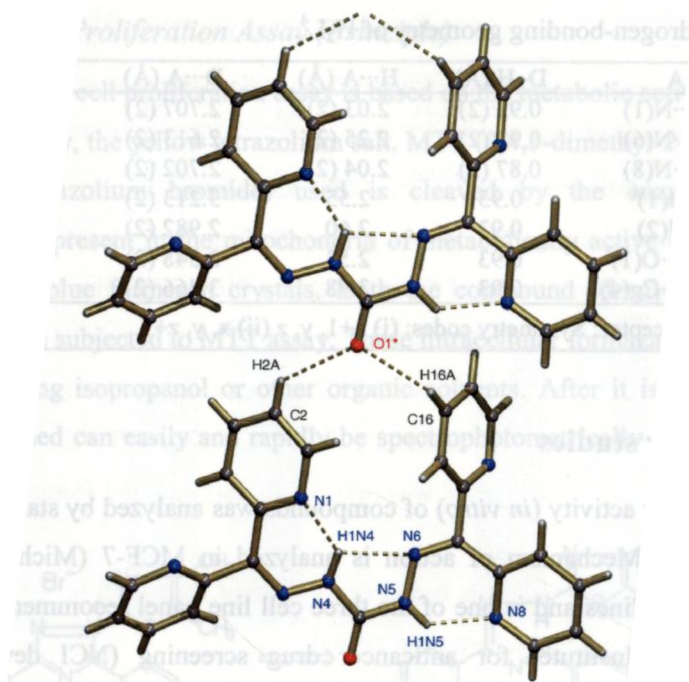
Fig. 2.19. A view of H_2L^4 showing intramolecular and intermolecular hydrogen bonds as dashed lines.
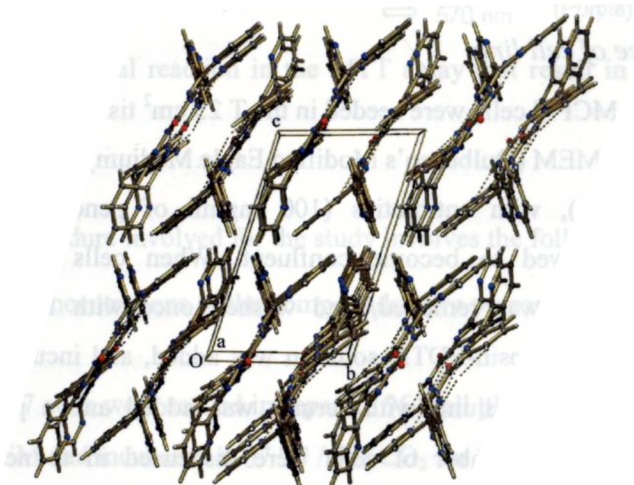
Fig. 2.20. The crystal packing of H_2L^4 viewed down the *a* axis. Hydrogen bonds are shown as dashed lines.

Table 2.8. Hydrogen-bonding geometry of H_2L^4.

D–H···A	D–H (Å)	H···A (Å)	D···A (Å)	D–H···A (°)
N(4)–H(1N4)···N(1)	0.92 (2)	2.03 (2)	2.707 (2)	130 (2)
N(4)–H(1N4)···N(6)	0.92 (2)	2.25 (2)	2.613 (2)	103 (1)
N(5)–H(1N5)···N(8)	0.87 (2)	2.04 (2)	2.702 (2)	132 (2)
C(2)–H(2A)···O(1)^i	0.93	2.55	3.213 (2)	128
C(4)–H(4A)···N(2)	0.93	2.60	2.982 (2)	105
C(16)–H(16A)···O(1)^i	0.93	2.53	3.348 (2)	146
C(11)–H(11A)···Cg(4)^{ii}	0.93	2.78	3.466 (2)	131

D= donor, A=acceptor; Symmetry codes: (i) x+1, y, z (ii) x, y, z+1.

2.4. Anticancer studies

Anticancer activity (*in vitro*) of compounds was analyzed by standard growth inhibitory assays. Mechanism of action is analyzed in MCF-7 (Michigan Cancer Foundation-7) cell lines and is one of the three cell line panel recommended by NCI (National Cancer Institute) for anticancer drug screening (NCI developmental therapeutic program). Determinations of the effectiveness of the compounds were achieved by MTT Cell Proliferation Assay.

2.4.1. Maintenance of cell line

The healthy MCF-7 cells were seeded in the T 25 cm^2 tissue culture flask with complete media i.e. DMEM (Dulbecco's Modified Eagle Medium) (Sigma), 10% FBS (Foetal Bovine Serum), with antibiotics (100 mg/ml of pencillin, 100 mg/ml streptomycin) and allowed to become confluent. When cells were grown to confluency, the medium was removed, and washed once with PBS (phosphate buffered saline). 0.25% Trypsin-EDTA solution was added, and incubated for 5-10 minutes at 37 °C. Fresh medium (with serum) was added and a pipette gently dispersed cells. A known number of cells were dispensed in to new flasks or microtitre plates for further experiments. The cells were incubated at 37 °C and 5% CO_2 atmosphere.

2.4.2. MTT Cell Proliferation Assay (Principle)

The MTT cell proliferation assay is based on the metabolic activities of viable cells. In this assay, the yellow tetrazolium salt, MTT (3,4,5-dimethyl-2-thiazolyl)-2,5-diphenyl-2,4-tetrazolium bromide) used is cleaved by the enzyme, succinate dehydrogenase, present in the mitochondria of metabolically active cells into water insoluble dark blue formazan crystals. Both the compound (drug)-treated and the control cells are subjected to MTT assay. These intracellular formazan crystals can be solubilized using isopropanol or other organic solvents. After it is solubilized, the formazan formed can easily and rapidly be spectrophotometrically quantified at 570 nm.

MTT
(Yellow)

MTT formazan

⇒ 570 nm (Purple)
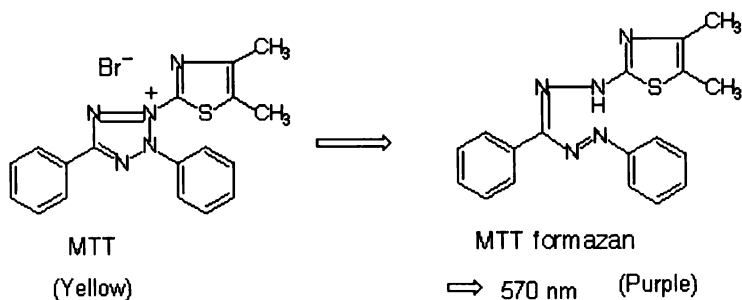
Scheme 2.7. Chemical reaction in the MTT assay that result in the formation of formazan crystals.

2.4.3. Procedure

The procedure involved for the study involves the following steps.

- Stock concentrations of the compounds were prepared in DMSO and stored at -70 °C.

- MCF-7 cells were seeded in separate 96-well plates (7000 cells/ well) in 10% DMEM and incubated at 37 °C / 5% CO_2 for 24 h.

- Once the cells had attached, the existing medium was removed and the cells were washed with PBS-EDTA solution.

69

- The compounds were then diluted in DMEM with 2.5% Fetal Bovine Serum.
- The drug-containing medium (100 µl of media with known concentrations of each compound) was added.
- The cells were incubated at 37 °C / 5% CO_2 for 48 h.
- Six wells, containing cells grown in drug-free medium were kept to determine the control cell survival and the percentage of live cells after culture.
- After incubation, the drug-containing medium was removed and 100 µl of 21% MTT (5 mg/ml) solution in 2.5% DMEM was added to each of the wells.
- The plates were kept for another 2½ h for incubation at 37 °C / 5% CO_2.
- The yellowish colored MTT was reduced to dark-colored formazan by viable cells only.
- Then, 100 µl of MTT lysis buffer (a mixture of 20% SDS in 50% DMF) was added to solubilize the formazan crystals.
- The color developed was quantified using an ELISA plate reader at 570 nm.
- Cell survival expressed as percentage and was calculated as:

Cell survival (CS) = (Mean OD $_{drug\text{-}treated\ cells}$ / Mean OD $_{control\ cells}$) × 100

A graph is plotted taking the concentration of the drug (X-axis) against the percentage viability (Y-axis). LD_{50} value (lethal dose of drug for killing 50% of cells) of the drug indicates the effectiveness of the compounds used; the lesser the value, the more effective the compounds are.

The ligands H_2L^1, H_2L^3, H_2L^4, H_2L^6 and HL^7 were independently tested using the above procedure towards MCF-7 cell lines for their unique features and the results are summarized in Table 2.9 and Fig. 2.21. It is seen that the thiocarbohydrazones (H_2L^1 and H_2L^3) and carbohydrazones (H_2L^4 and H_2L^6) show proliferation effect. However, the thiosemicarbazone HL^7 shows antiproliferation effect.

Table 2.9. Cell proliferation effect of compounds used.

Concentration	% cell proliferation of				
	HL^7	H_2L^1	H_2L^3	H_2L^4	H_2L^6
10 µM	73.35	82.76	85.66	98.74	87.74
100 µM	70.06	94.55	97.79	103.99	99.84
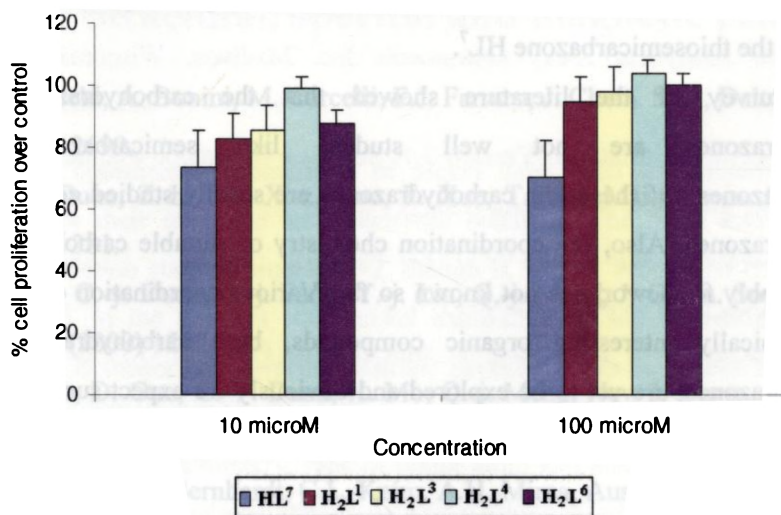
Fig. 2.21. Cell proliferation effect of compounds used at different concentration.

2.5. Concluding remarks

We have synthesized and physico-chemically characterized three carbohydrazones and three thiocarbohydrazones along with two thiosemicarbazones. All the thiocarbohydrazones and carbohydrazones possess two or more binding units and are capable of forming mono and dinuclear compounds in addition to serve as building blocks for tetranuclear molecular square grids. All the thiocarbohydrazones and carbohydrazones are found in the thione tautomeric form in the solid state. It is found that the compounds H_2L^2 and H_2L^5 exhibiting keto-enol tautomerism, while the compound H_2L^1 shows an exclusive presence of its thione tautomer in their CDCl₃ solutions. Single crystal X-ray diffraction studies of H_2L^3 and H_2L^4 are carried out, which support the spectral data. The N–N, N–C and the C=S bond distances of the

71

thiocarbohydrazide moiety in H_2L^3 and N–N, N–C and the C=O bond distances of the carbohydrazide moiety in H_2L^4 suggest extensive electron delocalization of the whole thiocarbohydrazone and carbohydrazone moieties. The thiocarbohydrazones and carbohydrazones, H_2L^1, H_2L^3, H_2L^4 and H_2L^6, were tested for *in vitro* anticancer properties and they show cell proliferation effect, but antiproliferation effect was observed for the thiosemicarbazone HL^7.

A survey of the literature showed that the carbohydrazones and thiocarbohydrazones are not well studied like semicarbazones and thiosemicarbazones. Of these, the carbohydrazones are scantly studied compared to thiocarbohydrazones. Also, the coordination chemistry of suitable carbohydrazones for self-assembly frameworks is not known so far. Various coordination compounds of these typically interesting organic compounds, both carbohydrazones and thiocarbohydrazones, are yet to be explored and obviously we expect such materials would find applications in various fields of science and technology.

References

1. P.J. Stang, B. Olenyuk, Acc. Chem. Res. 30 (1997) 502.

2. L.K. Thompson, L. Zhao, Z. Xu, D.O. Miller, W.M. Reiff, Inorg. Chem. 42 (2003) 128.

3. T.A. Blumenkopf, J.A. Harrington, C.S. Kolbe, D.D. Bankston, R.W. Morrison, E.C. Bigham, V.L. Styles, T. Spector, J. Med. Chem. 35 (1992) 306.

4. A. Bacchi, M. Carcelli, P. Pelagatti, C. Pelizzi, G. Pelizzi, F. Zani, J. Inorg. Biochem. 75 (1999) 123.

5. T. Spector, J.A. Harrington, R.W. Jr Morrison, C.U. Lambe, D.J. Nelson, D.R. Averett, K. Biron, P.A. Furman, Proc. Natl. Acad. Sci. USA. 86 (1989) 1051.

6. B. Moubaraki, K.S. Murray, J.D. Ranford, X. Wang, Y. Xu, Chem. Commun. (1998) 353.

7. B. Moubaraki, K.S. Murray, J.D. Ranford, J.J. Vittal, X. Wang, Y. Xu, J. Chem. Soc., Dalton Trans. (1999) 3573.

8. G.R. Bustos, O. Burdkhardt, R. Schrebler, D. Carrilo, Inorg. Chem. 29 (1990) 3996.

9. A. Bacchi, A. Bonini, M. Carcelli, F.J. Farraro, J. Chem. Soc., Dalton Trans. (1996) 2699.

10. C.-y. Duan, Z.-h. Liu, X.-z. You, F. Xue, T.C.W. Mak, Chem. Commun. (1997) 381.

11. C. He, C.-y. Duan, C.-j. Fang, Y.-j. Liu, Q.-j. Meng, J. Chem. Soc., Dalton Trans. (2000) 1207.

12. G. Han, D. Guo, C.-Y. Duan, H. Mo, Q.-j. Meng, New J. Chem. 26 (2002) 1371.

13. M.A. Ali, P.V. Bernhardt, C.L. Keim, A.H. Mirza, Aust. J. Chem. 57 (2004) 409.

14. D. Dragancea, V.B. Arion, S. Shova, E. Rentschler, N.V. Gerbeleu, Angew. Chem. Int. Ed. Engl. 44 (2005) 7938.

15. E. Manoj, M.R.P. Kurup, H.-K. Fun, Inorg. Chem. Commun. 10 (2007) 324.

16. E. Manoj, M.R.P. Kurup, H.-K. Fun, S. Chantrapromma, Acta. Cryst. E61 (2005) o4110.

17. A. Sreekanth, M.R.P. Kurup, Polyhedron 23 (2004) 969.

18. A. Sreekanth, M.R.P. Kurup, Polyhedron 22 (2003) 3321.

19. A. Sreekanth, M. Joseph, H.-K. Fun, M.R.P. Kurup, Polyhedron 25 (2006) 1408.

20. J.P. Scovill, Phosphorous Sulfur Silicon 60 (1991) 15.

21. M.A. Ali, A.H. Mirza, M.H.S.A. Hamid, F.H. Bujang, P.V. Bernhardt,

Polyhedron 23 (2004) 2405.

22. R.S. Drago, Physical Methods for Chemists, 2nd ed., Saunders, HBJ (1992).

23. R.M. Silverstein, G.C. Bassler, T.C. Morrill, Spectrometric Identification of Organic Compounds, 4th ed., John Wiley & Sons, New York (1981).

24. Siemens, SMART and SAINT, Area Detector Control and Integration Software, Siemens Analytical X-ray Instruments Inc. Madison, Wisconsin, USA (1996).

25. G.M. Sheldrick, SHELXTL Version 5.1, Software Reference Manual, Bruker AXS Inc. Madison, Wisconsin, USA (1997).

26. L.J. Farrugia, J. Appl. Cryst. 30 (1997) 565.

27. A.L. Spek, Acta Cryst. 36 (2003) 7.

28. C.F. Macrae, P.R. Edgington, P. McCabe, E. Pidcock, G.P. Shields, R. Taylor, M. Towler, J. van de Streek, J. Appl. Cryst. 39 (2006) 453.

29. K. Brandenburg, H. Putz, DIAMOND Version 3.0, Crystal Impact GbR, Postfach 1251, D-53002, Bonn, Germany (2004).

30. F.H. Allen, O. Kennard, D.G. Watson, L. Brammer, A.G. Orpen, R. Taylor, J. Chem. Soc. Perkin Trans. 2 (1987) S1.

31. Z. Lin, H. Chen, J. Zhuang, Y. Wu, Y. Lin, J. Incl. Phen. Mol. Recog. Chem. 30 (1998) 13.

32. S. Chantrapromma, I.A. Razak, H.-K. Fun, C. Karalai, H. Zhang, F.-X. Xie, Y.-P. Tian, W. Ma, Y.-H. Zhang, S.-S. Ni, Acta Cryst. C57 (2001) 289.

33. S.W. Benson, J. Chem. Edu. 42 (1965) 502.

34. E. Manoj, M.R.P. Kurup, E. Suresh, J. Chem. Cryst. DOI: 10.1007/s10870-007-9267-9

35. J. Bernstein, R.E. Davis, L. Shimoni, N.-L. Chang, Angew. Chem. Int. Ed. Engl. 34 (1995) 1555.

****

Ni(II) complexes of carbohydrazone, thiocarbohydrazone and thiosemicarbazone ligands: Structural, spectral and magnetic properties

3.1. Introduction

The coordination complexes of nickel have been the subject of interest especially for their magnetic and electronic behavior. The most stable and most common oxidation state of nickel is +2, though 0, +1, +3 and +4 Ni complexes are observed [1]. In the divalent state nickel exhibits wide and interesting variety of coordination numbers and stereochemistries. Several factors have been recognized to be particularly important in the stabilization of the +3 and +1 oxidation states, namely coordination number, geometry, type of donor atom and electronic characteristics of the ligand. Preparation of even zerovalent nickel complexes from elemental nickel has been reported [2]. Coming to the biomimetic chemistry, nickel is recognized as an essential trace element for bacteria, plants, animals and humans [3] and is one of the most toxic metal among transition metals [4]. It shows the toxicity even in low doses to both plants and animals. Epimediological data and animal study confirm that crystalline nickel compounds are carcinogenic, while amorphous nickel compounds are weak or non-carcinogenic. Ni complexes of some thiosemicarbazones and semicarbazones have been screened *in vitro* against MCF-7 breast cancer cell lines for their antiproliferation activity [5]. It is clearly observed that ligands on complexation with metal ion increase the inhibitory action on MCF-7 cell proliferation. Similar effect was observed upon complexation of some other thiosemicarbazones with nickel(II) ion [6]. The enhancement of antiproliferation activity by metal complexes

can be related to an increase in the lipophilicity, so they can penetrate into the cells more easily [5,7].

The idea of establishing control and predictability over molecular architectures is of much interest. Molecular squares are one of the simplest but nonetheless interesting members of the family of polygons and have received the highest attention. Strategies to produce molecular square grids of transition metal centers include judicial utilization of the organizing ability of a polyfunctional ligand to suitable metal ions. Ni(II) is one of the most frequently used metal ion for octahedral centers and are rare for self assembled molecular squares of multidentate ligands [8]. The inclusion of magnetic metal ions like Ni(II) with these polynuclear complexes added a new dimension, which leads nanometer-sized magnetic clusters of versatile magnetic properties. Of these, the grid structures are of special interest in information storage and processing technology [9]. Moreover, depending on the packing or metal centers with suitable ligands, such assemblies of grids may result molecular magnets. Nickel(II) is known to have a large single-ion zero-field splitting and often gives rise to ferromagnetic coupling [10], thus polynuclear nickel(II) complexes are potential candidates for single molecule magnets also.

Ni complexes of carbohydrazones and thiocarbohydrazones are least studied. Literature survey shows that mononuclear Ni(II) complexes of thiocarbohydrazide [11], 1,1'-diacetyl ferrocene-derived carbohydrazone [12], 1,1'-diacetyl ferrocene-derived thiocarbohydrazone [12], bis-(1,1'-disubstituted ferrocenyl) thiocarbohydrazone [13] and bis-(1,1'-disubstituted ferrocenyl) carbohydrazone [13] are reported. Mononuclear Ni(II) complexes derived from thiocarbohydrazide and benzil have also been reported [14]. In addition, a dinuclear Ni(II) complex of 5-chlorosalicylaldehyde thiocarbohydrazone has been reported recently [15]. A molecular square complex of bis(2-benzoylpyridine) thiocarbohydrazone (H_2L^2) [8] and another one of bis(2-acetylpyridine) thiocarbohydrazone [16] have also been reported. However, there are many reports of tetranuclear Ni(II) complexes [17-22]

76

and square grids [23,24] of other ligands, and they have made a great stimulus in the metallosupramolecular chemistry.

Paramagnetic Ni(II) complexes having sulfur/oxygen bridged are warranted as there are only few complexes that have been subjected to variable-temperature magnetic susceptibility studies. It has been shown that H_2L^2 [8] can connect two Ni(II) ions, generating sulfur-bridged molecular square complexes. However no magneto-structural correlation has yet been reported for these classes of complexes. Also, it is found desirable to construct new sulfur-bridged paramagnetic Ni(II) complexes. On the other hand, there are no reports of magnetically coupled Ni(II) molecular squares of carbohydrazone ligands. Transition metal template cyclizations have successfully produced some tetranuclear nickel complexes [17-20], in which the metal ions are bridged exclusively by oxygen donor groups. The anticipation that carbohydrazones can also produce Ni(II) molecular square grids when suitable conditions are employed by making use of oxygen bridge lead us to synthesize novel class of compounds. Also, the complexing ability of NNS thiosemicarbazones is closely related to that of thiocarbohydrazones as the former has one common coordination pocket with the latter. There are reports of octahedral complexes of Ni(II) thiosemicarbazones derived from di-2-pyridyl ketone [25]. So it is worthwhile to report the structural characterizations of few novel octahedral Ni(II) complexes of HL^7 and HL^8, having the same aldehydic or ketonic part of thiocarbohydrazone and carbohydrazone ligands (H_2L^2, H_2L^3, H_2L^5 and H_2L^6), as additional support for the formation of their higher class of compounds. This is found necessary especially to establish the coordination behaviour of novel quinoline-2-aldehyde derived ligand HL^7 and thereby to check any possibility of sterical hindrance for the formation of complexes having octahedral geometries with novel quinoline-2-aldehyde derived carbohydrazone and thiocarbohydrazone.

3.2. Experimental

3.2.1. Materials

Nickel(II) chloride hexahydrate (Merck), nickel(II) perchlorate hexahydrate (Merck) and ammonium hexafluorophosphate (Fluka) were used as supplied and solvents were purified by standard procedures before use.

Caution! Perchlorate complexes of metals with organic ligands are potentially explosive and should be handled with care.

3.2.2. Synthesis of Ni(II) complexes

[Ni(HL^1)]$_4$(PF$_6$)$_4$· 11H$_2$O (1)

To a hot solution of H$_2$L^1 (0.440 g, 1 mmol) in 50 ml methanol was added an equimolar amount of nickel(II) chloride hexahydrate (0.240 g) dissolved in 10 ml hot methanol. The brown colored mixture was refluxed for an hour and added NH$_4$PF$_6$ (2 mmol, 0.332 g) in 20 ml methanol and refluxed 2 more hours and allowed to stand at room temperature. The brown crystalline compound precipitated was filtered, washed with methanol and ether, recrystallized in acetonitrile: ethanol mixture and dried *in vacuo* over P$_4$O$_{10}$. Yield: 0.440 g (63%). Elemental Anal. Found (Calc.): C, 39.72 (40.00); H, 2.98 (3.28); N, 16.76 (16.22); S, 4.99 (4.64)%.

Crystals suitable for X-ray analysis were obtained by slow evaporation of a solution of the compound in ethanol-methanol mixture. The complex 1 crystallized as [Ni(HL^1)]$_4$(PF$_6$)$_4$· ½CH$_3$CH$_2$OH· 2.8H$_2$O (**1a**) and the relatively high R-factors of **1a** are due to the bad quality of the crystal. All attempts to get better quality crystals failed.

[Ni$_2$(HL^3)L^3]$_2$(PF$_6$)$_2$· 7H$_2$O (2)

The preparation of the compound **2** was carried out in a similar way as that of compound **1**, except that the ligand H$_2$L^3 (0.387 g, 1 mmol) was used instead of H$_2$L^1.

The reddish brown color on adding $NiCl_2$ was found to change into orange on adding NH_4PF_6, which changed to brown on refluxion. The brown powder precipitated after 2 days were filtered, washed with methanol and ether, recrystallized in acetonitrile: ethanol mixture and dried *in vacuo* over P_4O_{10}. Yield: 0.430 g (78%). Elemental Anal. Found (Calc.): C, 46.57 (46.22); H, 3.15 (3.33); N, 15.09 (15.40); S, 6.00 (5.88)%.

$[Ni(HL^4)]_4(PF_6)_4 \cdot 12H_2O$ (3)

To a hot solution of H_2L^4 (0.424 g, 1 mmol) in 50 ml methanol was added an equimolar amount of nickel(II) chloride hexahydrate (0.240 g) dissolved in 10 ml hot methanol. The mixture was refluxed for an hour and added NH_4PF_6 (2 mmol, 0.332 g) in 20 ml methanol and refluxed 2 more hours and allowed to stand at room temperature. The yellow powder precipitated after two days were filtered, washed with methanol and ether and dried *in vacuo* over P_4O_{10}. Yield: 0.236 g (35%). Elemental Anal. Found (Calc.): C, 40.22 (40.68); H, 2.76 (3.41); N, 16.98 (16.50)%.

$[Ni(HL^5)]_4(PF_6)_4 \cdot 9H_2O$ (4)

The preparation of the compound **4** was carried out in a similar way as that of compound **3**, except that the ligand H_2L^5 (0.424 g, 1 mmol) was used instead of H_2L^4. The greenish red color on adding $NiCl_2$ was found to change into yellowish brown on adding NH_4PF_6. The yellow powder precipitated after three days were filtered, washed with methanol and ether and dried *in vacuo* over P_4O_{10}. Yield: 0.357 g (54%). Elemental Anal. Found (Calc.): C, 44.77 (45.24); H, 3.56 (3.57); N, 13.35 (12.66)%.

$[Ni(HL^7)_2]Cl_2$ (5)

To a hot solution of HL^7 (0.142 g, 0.5 mmol) in 10 ml chloroform was added an equimolar amount of nickel(II) chloride hexahydrate (0.120 g) dissolved in 20 ml hot methanol. The mixture was refluxed for an hour and allowed to stand at room temperature. The reddish brown compound precipitated was filtered, washed with

methanol and ether and dried *in vacuo* over P_4O_{10}. Yield: 0.100 g (57%). Elemental analysis: Found (calc.): C, 51.46 (51.60); H, 5.01 (4.62); N, 16.17 (16.05); S, 9.09 (9.18)%.

Crystals suitable for X-ray analysis were obtained by slow evaporation of a methanol solution of **5** in air. The complex **5** crystallized as $[Ni(HL^7)_2]Cl_2 \cdot 2\frac{1}{2}H_2O$ (**5**·$2\frac{1}{2}H_2O$).

$[Ni(HL^8)L^8]ClO_4 \cdot 7H_2O$ (6)

To a hot solution of HL^8 (0.186 g, 0.6 mmol) in 10 ml chloroform was added an equimolar amount of nickel(II) perchlorate hexahydrate (0.220 g) dissolved in 20 ml hot methanol. The mixture was refluxed for an hour and allowed to stand at room temperature. The reddish brown crystals precipitated were filtered, washed with methanol and ether. It was then dried *in vacuo* over P_4O_{10}. Yield: 210 g (78%). Elemental analysis: Found (calc.): C, 44.65 (45.17); H, 5.32 (5.46); N, 12.28 (12.39); S, 6.83 (7.09)%.

XRD quality single crystals were obtained by slow evaporation of a solution of the compound in DMSO. The complex **6** got crystallized with deprotonation, of HL^8 in **6**, to form a new complex $[Ni(L^8)_2]$ (**6a**).

$[NiL^8Cl] \cdot \frac{1}{2}H_2O$ (7)

To a hot solution of HL^8 (0.186 g, 0.6 mmol) in 10 ml chloroform was added an equimolar amount of nickel(II) chloride hexahydrate (0.143 g) dissolved in 20 ml hot methanol. The mixture was refluxed for an hour and allowed to stand at room temperature. The reddish brown compound precipitated was filtered, washed with methanol and ether and then dried *in vacuo* over P_4O_{10}. Yield: 0.138 g (56%). Elemental analysis: Found (calc.): C, 49.94 (49.49); H, 4.15 (4.40); N, 13.75 (13.58); S, 7.72 (7.77)%.

3.3. Results and discussion

The novel complexes **1** to **4** were synthesized by equimolar reaction between $NiCl_2$ and corresponding ligands and by the metathetical displacement of chloride ions by PF_6^- anions. The complexes **3** and **4**, synthesized by carbohydrazone ligands, are first of its kind. The carbohydrazones having well defined and appropriately separated two coordination pockets, using the bridging mode of oxygen, in principle have a better chance of control over the outcome of a self-assembly process to produce the predefined Ni(II) nuclear molecular square, like Ni(II) thiocarbohydrazone grids. However the formation of these kinds of materials are hard to prove with common physico-chemical techniques, if the complexes lack stability. The Ni(II) grids **1** to **4**, fortunately seemed rigid framework even in solution phase, and soft ionization technique of MALDI MS spectra reveal the formation of tetranuclear molecular square natured structures. Molar conductivity measurement in 10^{-3} M DMF solution of **2** (147 $\Omega^{-1}cm^2mol^{-1}$) showed a 2:1 electrolyte [26]. For all the other three carbohydrazone and thiocarbohydrazone derived compounds the conductance values obtained were ~30 $\Omega^{-1}cm^2 \, mol^{-1}$ in 10^{-4} M DMF solution. The complex **2** was assigned the formula $[Ni_2(HL^3)L^3]_2(PF_6)_2 \cdot 7H_2O$ and **1**, **3**, and **4** were assigned a general formula $[Ni(HL)]_4[PF_6]_4 \cdot nH_2O$ (Scheme 3.1). The variable temperature magnetic studies reveal intramolecular antiferromagnetic couplings. The theoretical simulations of isotropic patterns of all molecular ion peaks and their fragmentation peaks of MALDI MS spectra could be achieved well, and confirm the proposed structural formulae. The structure of $[Ni(HL^1)]_4(PF_6)_4 \cdot \frac{1}{2}CH_3CH_2OH \cdot 2.8H_2O$ (**1a**) is confirmed by single crystal X-ray study and is in well agreement with mass spectral study of **1**.

The thiosemicarbazone complexes **5** and **6** are found to be six coordinate around Ni(II) centers based on spectral and room temperature magnetic susceptibility studies, while the compound **7** is four coordinate around Ni(II) center. The stoichiometries of the complexes are in agreement with the partial elemental analyses

and spectral studies. Infrared spectral evidences support the presence of coordination through thione form of HL^7 in compound **5**, through the thiolate form of HL^8 in **7** and through the thione and thiolate forms of HL^8 in **6**. Molar conductivity measurements in 10^{-3} M DMF solution showed non-electrolytic nature (8 $\Omega^{-1}cm^2mol^{-1}$) for complex **7**, a 1:1 electrolyte (89 $\Omega^{-1}cm^2mol^{-1}$) for **6** and a 2:1 electrolyte (138 $\Omega^{-1}cm^2mol^{-1}$) for **5** [26]. Like compound **6**, copper and cobalt complexes with both neutral and deprotonated forms of a thiosemicarbazone ligand in the same complexes with perchlorate ion have been reported [27]. The room temperature effective magnetic moments μ_{eff} of the three compounds **5**, **6** and **7** are found to be 2.80, 2.66 and 0.89 μ_B respectively. The anomalous magnetic moment of 0.89 μ_B shown by **7** is attributed to a four-coordinated Ni(II) center. For a perfect square planar complex of Ni(II), diamagnetism is expected. The low magnetic moment may be due to deviation from a perfect square planar geometry or presence of impurities. The structures of **5** and $[Ni(L^8)_2]$ (**6a**) are confirmed by single crystal X-ray diffraction study, and in the latter complex Ni(II) center is coordinated by two monodeprotonated ligands HL^8.
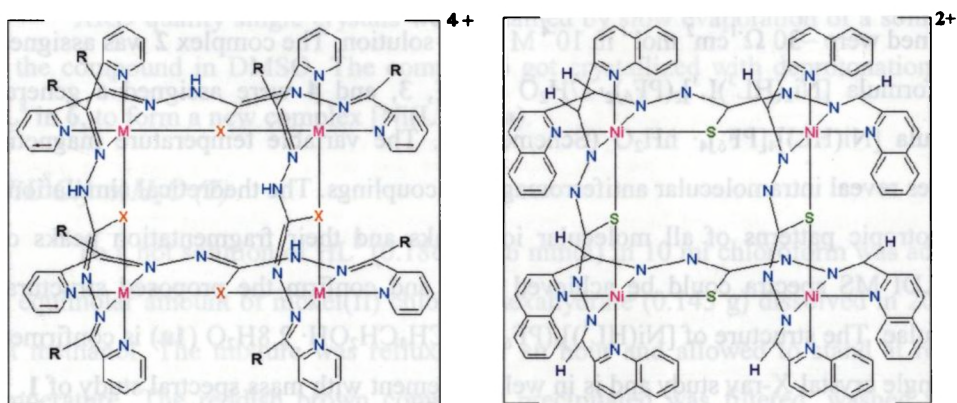
Scheme 3.1. General structure of the complex coordination part for compounds **1** to **3** (left). R=pyridyl and X= S for **1**, R=pyridyl, X= O for **3** and R=phenyl, X= O for **4**. The exact position of –NH hydrogens are uncertain for **3** and **4**, though they are shown. The tentative structural outline (most of the C–N bonds shown are double bonds and two –NH hydrogens are not shown) of cationic part of complex **2** (right).

3.3.1. MALDI MS spectral studies of molecular square grids

For the unequivocal characterization of large molecules, mass spectrometry was found useful as complementary. The structure and stability of coordination complexes under ionization conditions are dependent on various factures like the ligand itself, metal ions, counter ions, solvent, temperature, concentration, etc. MALDI mass spectra in dichloromethane as DCTB mix on positive ion mode have been found useful to get excellent results for stable Ni(II) square grids of both thiocarbohydrazones and carbohydrazones.

MALDI MS spectrum of compound **1** (Fig. 3.1) in dichloromethane shows the presence of three main peaks centered at m/z 495.0602, 991.1073 and 1981.2342. The peak centered at 1981.2342 is assigned as the molecular ion peak expected for $[Ni_4(HL^1)L^1_3]^+$ (calc. m/z 1981, Fig. 3.2), well agreement with the simulation. The base peak at m/z 495.0602 is assigned as $[Ni(HL^1)]^+$ (calc. 495) and the other major peak is assigned as $[Ni_2(HL^1)L^1]^+$ (calc. 991, Fig. 3.2).
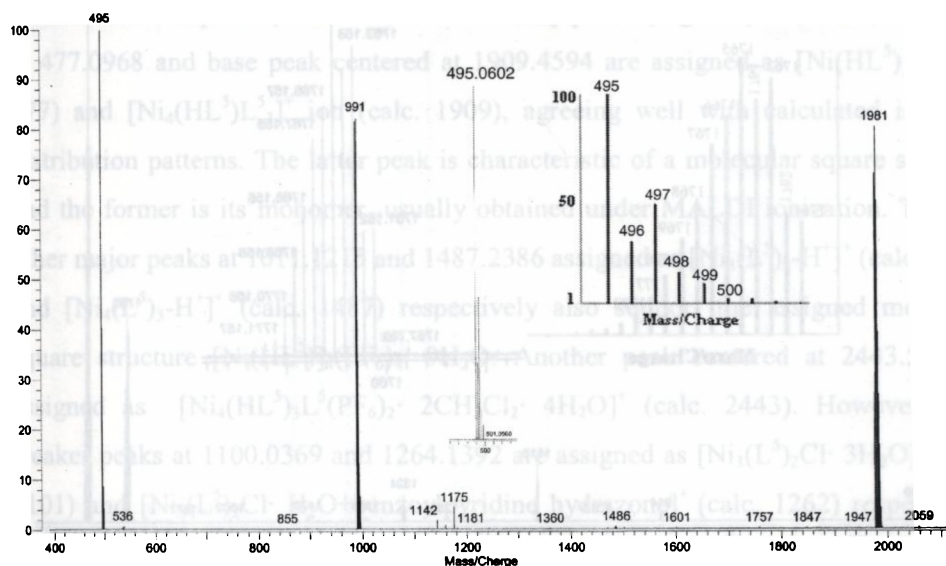
Fig. 3.1. MALDI mass spectrum of the compound **1**. The insets are isotropic distribution pattern of base peak (left) and its theoretical simulation (right).
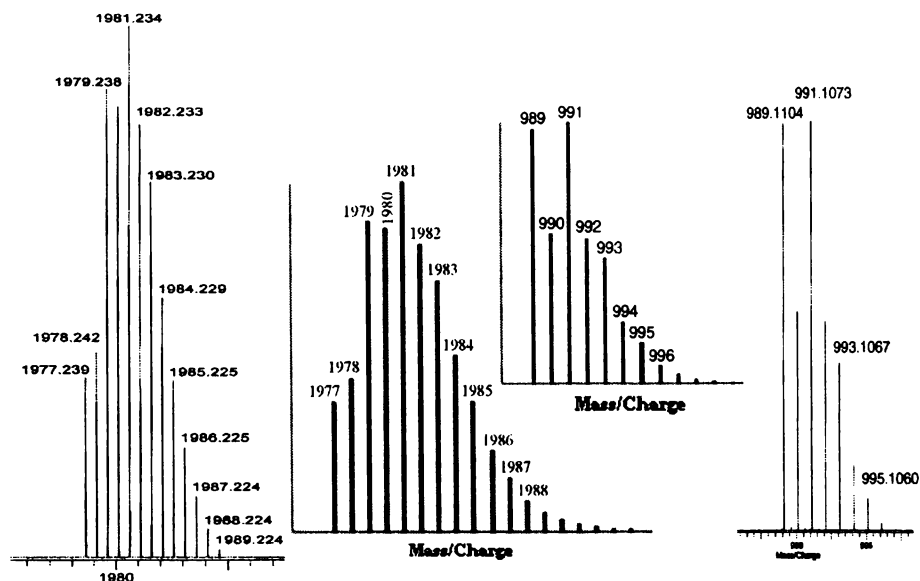
Fig. 3.2. The isotropic distribution patterns and their theoretical simulations of main peaks of $[Ni_4(HL^1)L^1{}_3]^+$ and $[Ni_2(HL^1)L^1]^+$ of complex **1**.
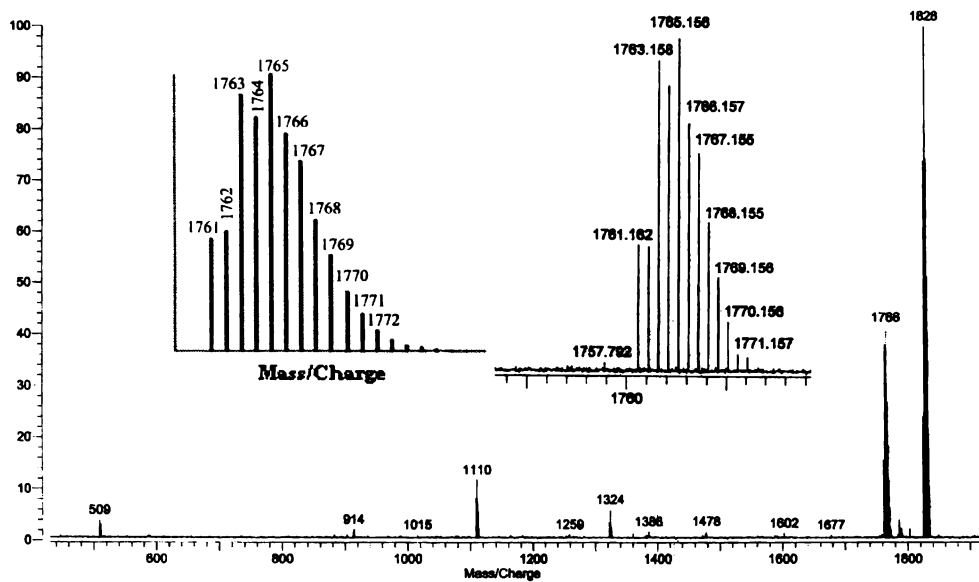
Fig. 3.3. MALDI mass spectrum of the compound **2**. The insets are the isotropic distribution pattern of $[Ni_4(HL^3)L^3{}_3]^+$ species and its simulation on the left side.

In the case of compound **2**, two major peaks are obtained at m/z 1827.1019 and 1765.1557 (Fig. 3.3). Here the peak at 1765.1557 is assigned as the $[Ni_4(HL^3)L^3{}_3]^+$ ion (calc. 1765). The base peak at 1827.1019 is assigned as the molecular ion peak with two methanol molecules (calc. 1827). The other peak at 1323.1211 is assigned as $[Ni_3(HL^3)L^3{}_2]^+$ (calc. 1323).

Considering the carbohydrazone compounds, the MALDI MS spectrum of compound **3** (Fig. 3.4) displays only two main peaks centered at m/z 479.0873, as base peak, and 1917.4364, the molecular ion peak. The former peak is assigned as $[Ni(HL^4)]^+$ (calc. 479) and the latter as $[Ni_4(HL^4)L^4{}_3]^+$ ion (calc. 1917) (Fig. 3.5), agreeing well with simulations and being characteristic results. The spectrum also implies the stability as evidenced by only two major peaks for assigned formula of $[Ni(HL^4)]_4(PF_6)_4 \cdot 12H_2O$. The small peaks centered at m/z 536 and 958 are assigned as $[Ni_2(L^4)-H^+]^+$ (calc. 535) and $[Ni_2(HL^4)L^4]^+$ (calc. 957) respectively, also agreeing well with calculated isotropic patterns.

The complex **4**, however, exhibits many peaks (Fig. 3.6). Of these, the peaks at 477.0968 and base peak centered at 1909.4594 are assigned as $[Ni(HL^5)]^+$ (calc. 477) and $[Ni_4(HL^5)L^5{}_3]^+$ ion (calc. 1909), agreeing well with calculated isotropic distribution patterns. The latter peak is characteristic of a molecular square structure and the former is its monomer, usually obtained under MALDI ionization. The two other major peaks at 1011.1215 and 1487.2386 assigned as $[Ni_3(L^5)_2-H^+]^+$ (calc. 1011) and $[Ni_4(L^5)_3-H^+]^+$ (calc. 1487) respectively also support the assigned molecular square structure $[Ni(HL^5)]_4(PF_6)_4 \cdot 9H_2O$. Another peak centered at 2443.5110 is assigned as $[Ni_4(HL^5)_3L^5(PF_6)_2 \cdot 2CH_2Cl_2 \cdot 4H_2O]^+$ (calc. 2443). However some weaker peaks at 1100.0369 and 1264.1392 are assigned as $[Ni_3(L^5)_2Cl \cdot 3H_2O]^+$ (calc. 1101) and $[Ni_3(L^5)_2Cl \cdot H_2O+benzoylpyridine\ hydrazone]^+$ (calc. 1262) respectively, may be due to the presence of impurity of chloride complex. All these isotropic patterns and their simulations are given in Figs. 3.7 to 3.9. These results, however, are indicative of the stability of Ni(II) molecular squares in the solution phase.

85
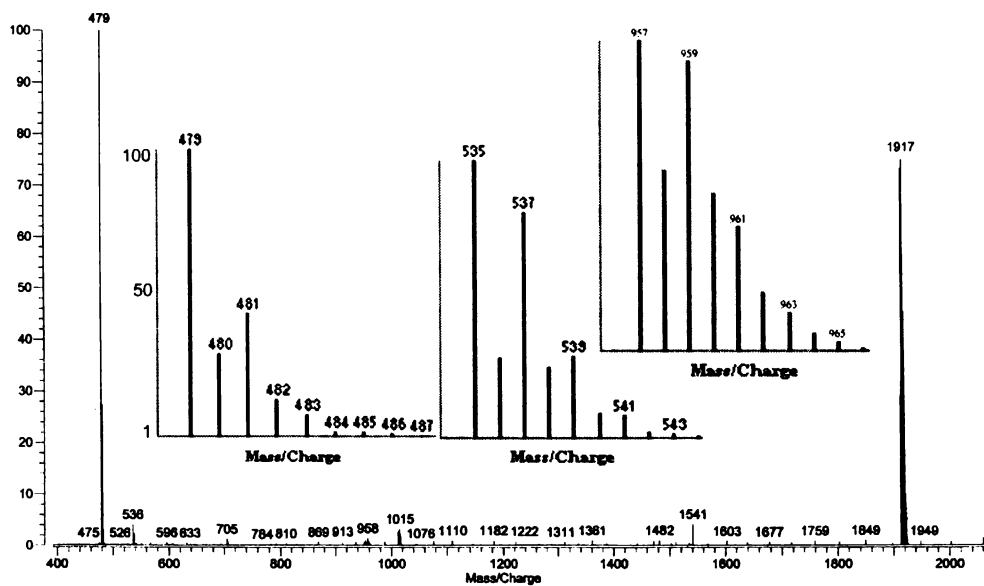
Fig. 3.4. MALDI mass spectrum of the compound **3**. The insets are the simulation patterns of base peak and other weaker peaks centered at m/z 536 and 958.
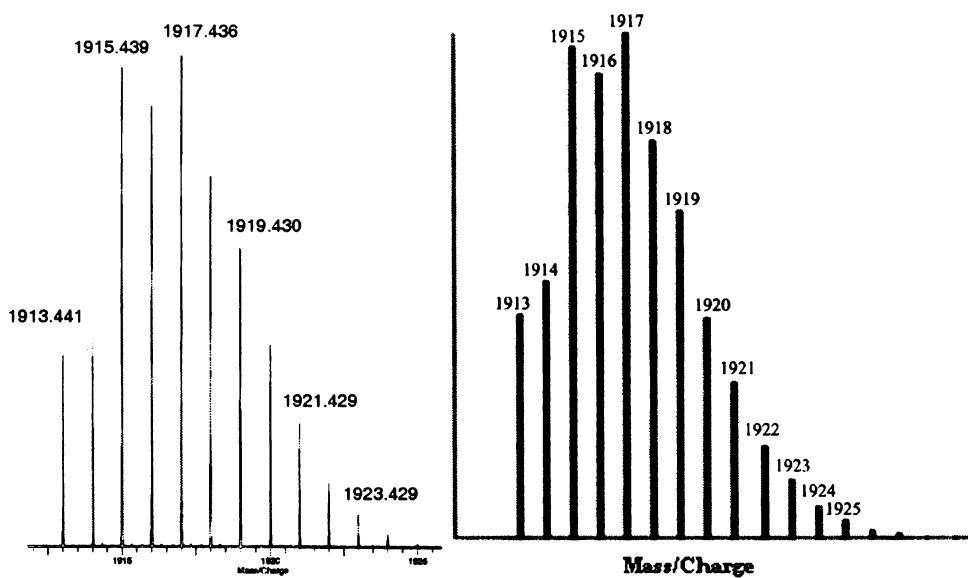
Fig. 3.5. The isotropic distribution pattern of the molecular ion peak of the compound **3** and its theoretical simulation on the right side.
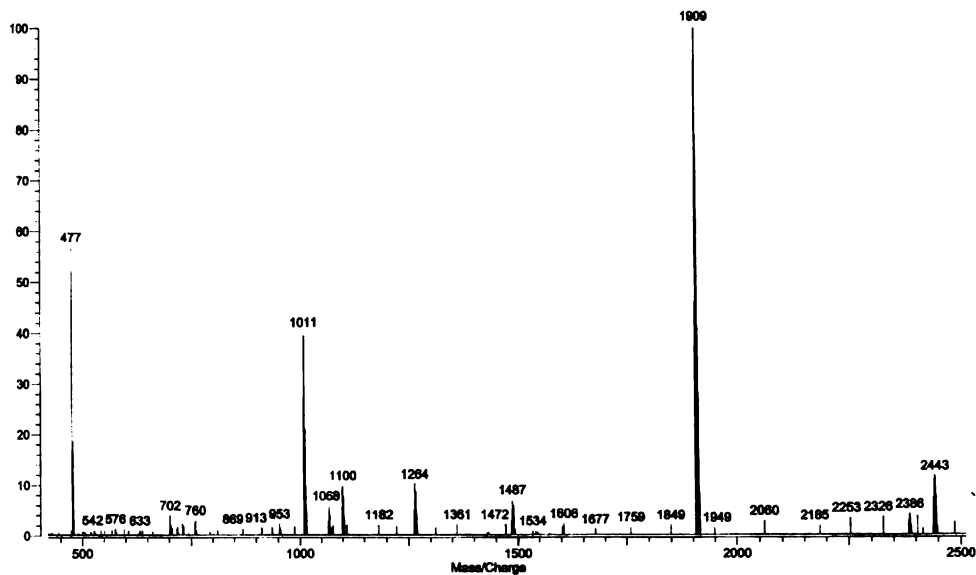
Fig. 3.6. MALDI mass spectrum of the Ni(II) carbohydrazone complex **4**.
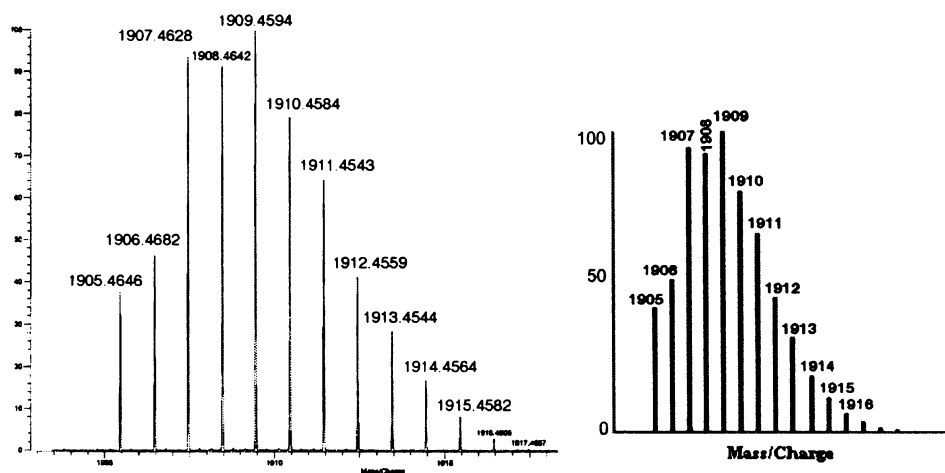
Fig. 3.7. The isotropic distribution pattern of $[Ni_4(HL^5)L^5_3]^+$ of the compound **4** and its theoretical simulation on the right side.
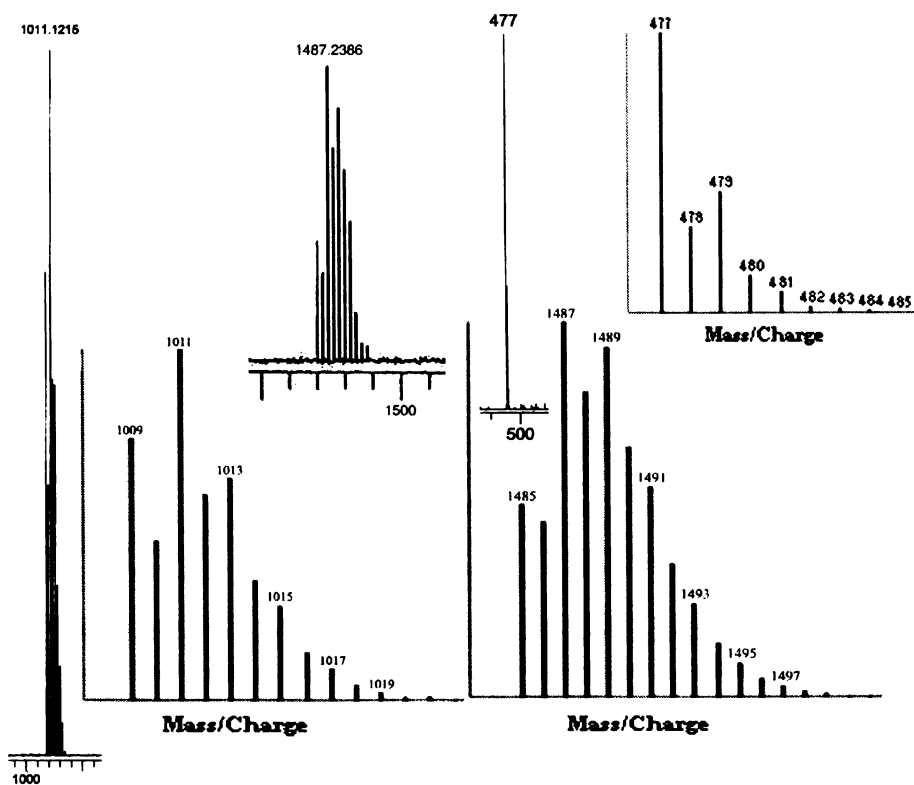
Fig. 3.8. The isotropic distribution patterns of the main peaks of the compound **4** and their theoretical simulations.
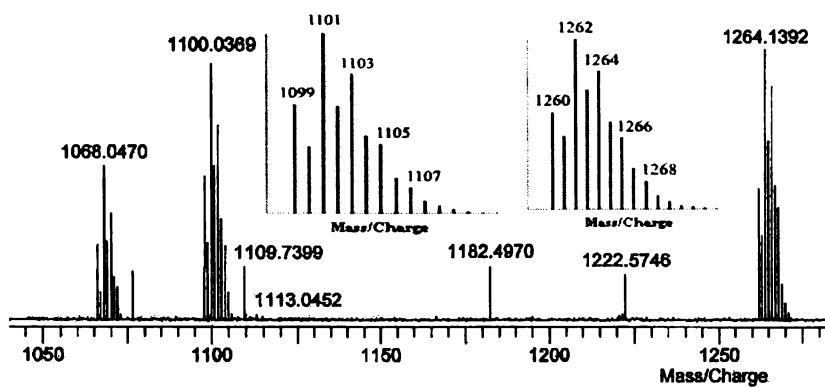
Fig. 3.9. The isotropic distribution patterns of the peaks obtained for the compound **4** and their theoretical simulations as insets.

3.3.2. IR and electronic spectral studies of square complexes

The IR spectral features of molecular square grids are different from that of their metal free ligands. The significant IR bands with tentative assignments of the Ni(II) square complexes are listed in Table 3.1. The absence of v(SH) bands at ~2600 cm^{-1} from the IR spectra of complexes **1** and **2** are clear indication of the absence of thiol tautomers in free or coordinated form in these compounds [8,29]. The change in frequencies for assigned bands and differences in mixing patterns of common group frequencies may be attributed to the coordination to metal center. For carbohydrazone complexes the carbonyl band at ~1700 cm^{-1} of free ligands disappear, confirming the absence of free ketonic group in the complexes, attributed to oxygen coordination. All the complexes show common broad bands in the region at ~3420 cm^{-1}, confirming the presence of lattice water [30], and the shift and broadness are attributable to possible hydrogen bonds. The v(P–F) band for all the four compounds are seen as sharp strong bands at ~842 cm^{-1} [8,16]. The spectra in the far IR region is rich with bands attributable to coordination to Ni(II) by pyridyl/quinolyl N (at ~260 cm^{-1}), azomethine N (at ~430 cm^{-1}) and sulfur/oxygen (at ~350 cm^{-1}). Selected IR and far IR spectra are given in Figs. 3.10 to 3.13.
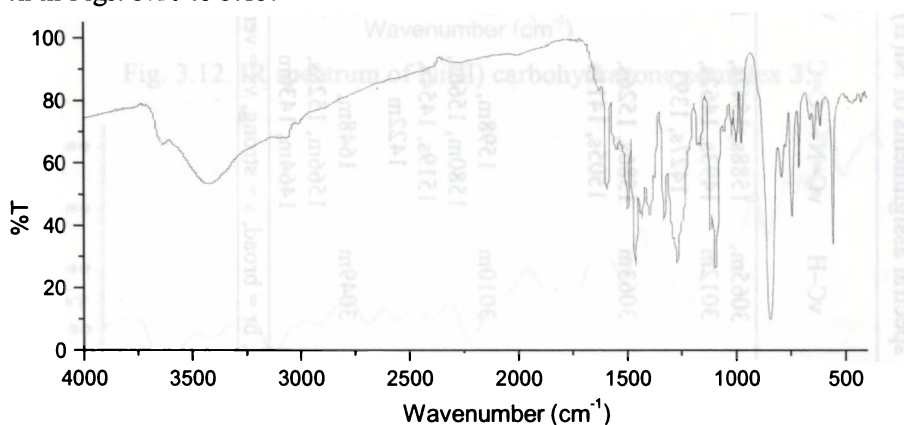
Fig. 3.10. IR spectrum of Ni(II) thiocarbohydrazone complex **1**.

Table 3.1. IR spectral assignments of Ni(II) molecular squares (cm⁻¹).

c.	vH$_2$O/ vN–H	vC–H	vC=N+ vC=C	vC–N/ vHetero cyclic	vC–S	vN–N	vC–O	δC–H	py/qu
1	3636m, 3422br	3065m, 3012m	1588s, 1547s, 1493s, 1462s, 1427s, 1393	1328m, 1267s	1094s	1161m, 1116m		998m, 978m, 789m, 742m, 710m	613m, 646m, 662m, 558s, 465m, 424m
2	3632m, 3414br, 3114w	3063m	1586s, 1526s, 1505s, 1411s	1350s, 1313s	1085vs	1212s, 1143s		989m, 782m, 747s	417m, 452m, 486m, 558s, 632m, 680m, 690m
3	3636m, 3413br, 3110m	3010m	1598m, 1580m, 1566s, 1519s, 1454s, 1422m	1362m, 1297m		1163m, 1126s, 1104s	1316vs	909m, 794m, 743s	696m, 627m, 558s, 479m, 451w
4	3632m, 3437br, 3211m	3049m	1648m, 1566m, 1528s, 1464m, 1436m	1295m, 1267m, 1212m		1154m, 1102s	1323s	789m, 743m, 704m	659m, 641m, 558s, 479m, 423m

c. = compounds, br = broad, s = strong, vs = very strong, m = medium, w = weak.
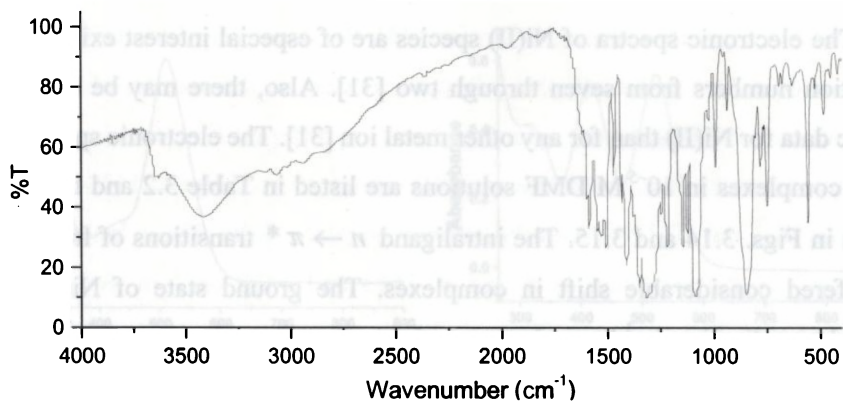
Fig. 3.11. IR spectrum of Ni(II) thiocarbohydrazone complex **2**.
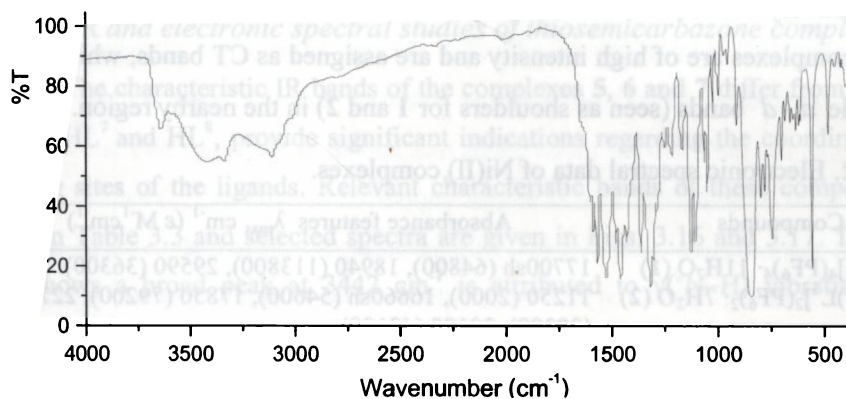
Fig. 3.12. IR spectrum of Ni(II) carbohydrazone complex **3**.
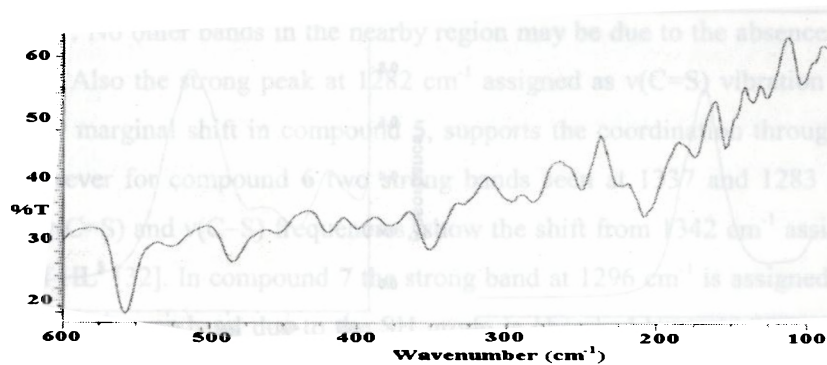
Fig. 3.13. Far IR spectrum of Ni(II) thiocarbohydrazone complex **2**.

91

The electronic spectra of Ni(II) species are of especial interest existing in all coordination numbers from seven through two [31]. Also, there may be exist more electronic data for Ni(II) than for any other metal ion [31]. The electronic spectral data of Ni(II) complexes in 10^{-5} M DMF solutions are listed in Table 3.2 and the spectra are given in Figs. 3.14 and 3.15. The intraligand $n \rightarrow \pi^*$ transitions of free ligands have suffered considerable shift in complexes. The ground state of Ni(II) in an octahedral coordination is $^3A_{2g}$ and expects three spin allowed transitions $^3T_{2g}(F) \leftarrow$ $^3A_{2g}(F)$ (v_1), $^3T_{1g}(F) \leftarrow ^3A_{2g}(F)$ (v_2) and $^3T_{1g}(P) \leftarrow ^3A_{2g}(F)$ (v_3) in the increasing order of energy generally fall within the ranges 7000-13000, 11000-20000 and 19000-27000 cm^{-1} respectively with low intensities [31]. However, the bands seen at ~18500 cm^{-1} in all the complexes are of high intensity and are assigned as CT bands, which masks the possible d-d bands (seen as shoulders for **1** and **2**) in the nearby region.

Table 3.2. Electronic spectral data of Ni(II) complexes.

Compounds	Absorbance features λ_{max} cm^{-1} (ε $M^{-1}cm^{-1}$)
[Ni(HL^1)]$_4$(PF$_6$)$_4$· 11H$_2$O (**1**)	17700sh (64800), 18940 (113800), 29590 (36300).
[Ni$_2$(HL^3)L^3]$_2$(PF$_6$)$_2$· 7H$_2$O (**2**)	11250 (2000), 16660sh (54600), 17850 (79200), 22730 (28300), 30120 (42100)
[Ni(HL^4)]$_4$(PF$_6$)$_4$· 12H$_2$O (**3**)	11390 (160), 19530 (222000), 22930 (60800), 29760 (83600)
[Ni(HL^5)]$_4$(PF$_6$)$_4$· 9H$_2$O (**4**)	11150 (500), 19080 (55900), 24210 (53300), 32050(41500)

1 in 10^{-5} M DMF

2 in 10^{-5} M DMF
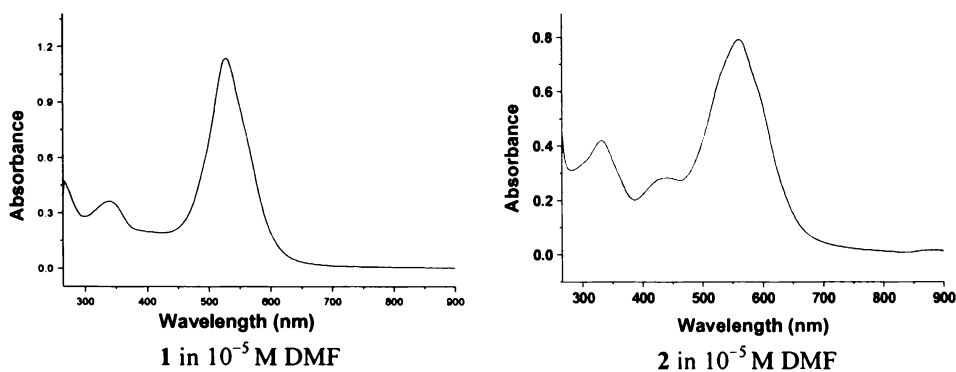
Fig. 3.14. Electronic spectra of Ni(II) thiocarbohydrazone complexes.

3 in 10^{-5} M DMF   4 in 10^{-5} M DMF
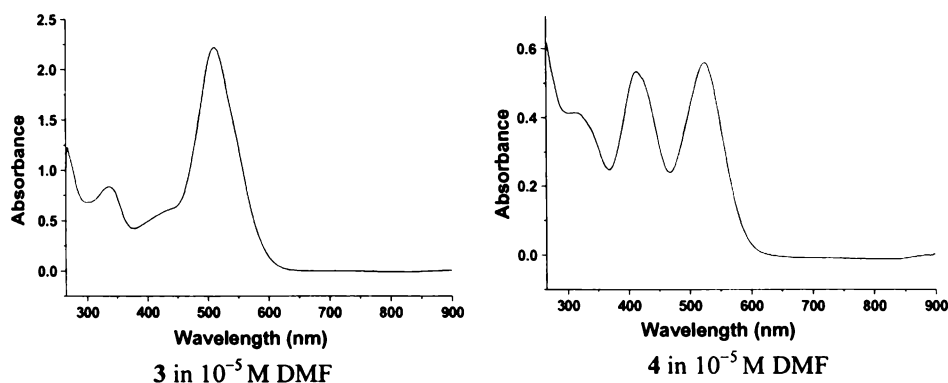
Fig. 3.15. Electronic spectra of Ni(II) carbohydrazone complexes.

3.3.2.1. IR and electronic spectral studies of thiosemicarbazone complexes

The characteristic IR bands of the complexes **5**, **6** and **7** differ from their free ligands HL^7 and HL^8, provide significant indications regarding the coordination and bonding sites of the ligands. Relevant characteristic bands of these compounds are listed in Table 3.3 and selected spectra are given in Figs. 3.16 and 3.17. The ligand HL^7 shows a broad peak at 3442 cm^{-1} is attributed to v(^{2}N–H) vibration with a possible hydrogen bond. In compound **5**, this peak is shifted slightly downwards but is indicative of the presence of ^{2}N-H. However in compounds **6** and **7** due to the presence of lattice water broad bands are seen at frequencies 3415 and 3440 cm^{-1} respectively. No other bands in the nearby region may be due to the absence of N–H hydrogens. Also the strong peak at 1282 cm^{-1} assigned as v(C=S) vibration for HL^7 shows only marginal shift in compound **5**, supports the coordination through thione form. However for compound **6** two strong bands seen at 1337 and 1283 cm^{-1} are assigned v(C=S) and v(C–S) frequencies, show the shift from 1342 cm^{-1} assigned for v(C=S) of HL^8 [32]. In compound **7** the strong band at 1296 cm^{-1} is assigned to v(C–S) band. Besides, no band due to the SH group is observed between 2600 and 2500 cm^{-1} [33], in agreement with the deprotonated thiolate form of the ligand in these complexes **6** and **7**. The bands seen at ~350 cm^{-1} for these complexes are assigned as

v(Ni–S), further supports sulfur coordination [34]. Bands ranging from 1600-1400 cm^{-1}, attributed to v(C=C) and v(C=N) vibration modes, in the spectra of complexes suffer significant shifts and their mixing patterns are different from that in the spectra of respective ligands. The azomethine v(C=N) vibrations at 1580 and 1630 cm^{-1} in the free ligands HL^7 and HL^8 respectively suffered negative shifts. These bands are seen at 1561 cm^{-1} in the spectrum of **5** and at 1553 and 1537 cm^{-1} in the spectra of compounds **6** and **7** respectively. The new bands at frequencies 1590 and 1594 cm^{-1} for **6** and **7** are assigned the vibration of newly formed v(^{2}N=C) bond and is absent in the spectrum of **5**. The coordination through azomethine nitrogen is further evidenced by the v(Ni–N$_{azo}$) [35] peaks at ~440 cm^{-1} for these compounds. The shifts in the v(N–N) frequencies also support the coordination through azomethine nitrogen in all the complexes. Coordination of the pyridine nitrogen atom is seen by the shift in frequencies of the deformation mode bands that appear in the range 649 and 455 cm^{-1} in the spectrum of HL^8 [32]. This is further supported by v(Ni–N$_{py/qu}$) bands [36] seen at ~250 cm^{-1} for all these compounds. The perchlorate complex **6** shows a broad band at 1090 cm^{-1} and strong band at 625 cm^{-1}, indicating the presence of ionic perchlorate [37]. The former band is assignable to v$_3$(ClO$_4$) and unsplit band at 625 cm^{-1} assignable to v$_4$(ClO$_4$). These indicate that ClO$_4$ species is not coordinated (T_d). The other bands at 938 and 467 cm^{-1}, assignable to v$_1$ and v$_2$ of ClO$_4$, are very week.

Table 3.3. IR spectral features of thiosemicarbazones and their Ni(II) complexes.

Compds.	v(C=^{1}N)	v(^{2}N=C)	v(N–N)	v(C=S)/ v(C–S)	v(C–H)	v(Ni–N$_{azo}$), v(Ni–S), v(Ni–N$_{py/qu}$)
HL^7	1580	---	1102	1282	2970, 2870	
5	1561	---	1110	1278	2969, 2870	459, 352, 240
HL^8	1630		1118	1342		
6	1553	1590	1145	1337, 1283	2964, 2876	430, 354, 251
7	1537	1594	1150	1296	2969, 2876	433, 351, 270
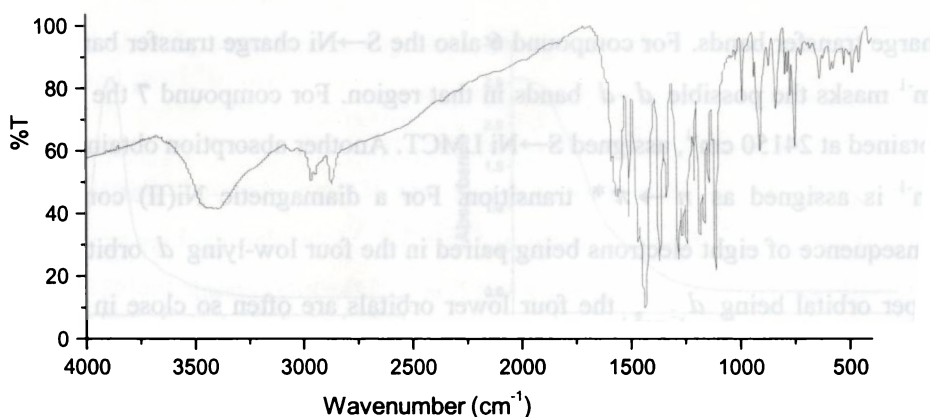
Fig. 3.16. IR spectrum of Ni(II) thiosemicarbazone complex [Ni(HL^7)$_2$]Cl$_2$ (**5**).
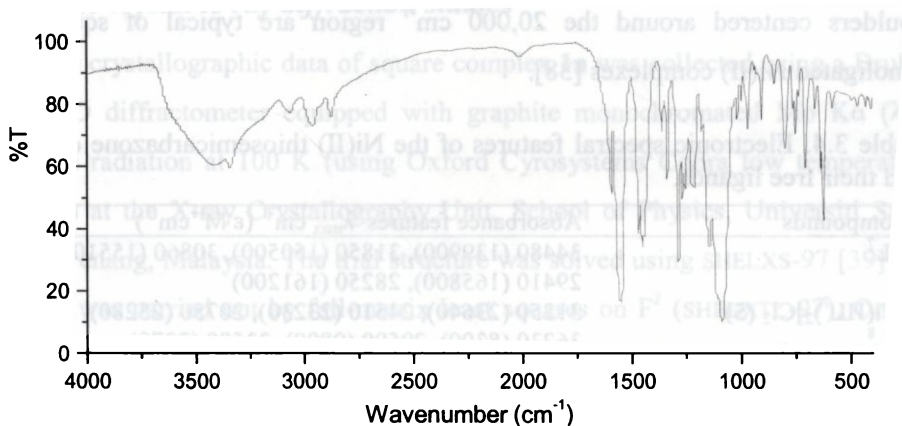
Fig. 3.17. IR spectrum of complex [Ni(HL^8)L^8]ClO$_4$· 7H$_2$O (**6**).

The electronic spectral data of thiosemicarbazones and their Ni(II) complexes in DMF solution are summarized in Table 3.4 and the spectra are given in Figs 3.18 and 3.19. The intraligand electronic transitions of HL^7 suffered considerable shift on coordination as evidenced by the absorptions obtained for **5**. The band with the highest molar absorptivity at 20750 cm^{-1} is assigned as S→Ni LMCT transition. The spin allowed transitions $^3T_{2g}(F) \leftarrow ^3A_{2g}(F)$ (v_1), $^3T_{1g}(F) \leftarrow ^3A_{2g}(F)$ (v_2) and $^3T_{1g}(P) \leftarrow ^3A_{2g}(F)$ (v_3) could not be located, probably due to masking by the high-intensity

95

charge transfer bands. For compound **6** also the S→Ni charge transfer band at 22470 cm^{-1} masks the possible d-d bands in that region. For compound **7** the CT band is obtained at 24150 cm^{-1}, assigned S→Ni LMCT. Another absorption obtained at 31250 cm^{-1} is assigned as $n \rightarrow \pi *$ transition. For a diamagnetic Ni(II) complex, as a consequence of eight electrons being paired in the four low-lying d orbitals with the upper orbital being $d_{x^2-y^2}$, the four lower orbitals are often so close in energy that individual transitions from them to the upper d level cannot be distinguished resulting in a single absorption band. The shoulder band obtained at 19380 cm^{-1} for **7** is attributed to the d-d band of this type. The d-d bands appearing as weak shoulders centered around the 20,000 cm^{-1} region are typical of square planar monoligated Ni(II) complexes [38].

Table 3.4. Electronic spectral features of the Ni(II) thiosemicarbazone complexes and their free ligands.

Compounds	Absorbance features λ_{max} cm^{-1} (ε M^{-1}cm^{-1})
HL^7	34480 (139900), 31850 (150500), 30860 (155100), 29410 (165800), 28250 (161200)
[Ni(HL^7)$_2$]Cl$_2$ (**5**)	31250 (23640), 24510 (23230), 20750 (25280)
HL^8	36230 (8300), 29590 (9800), 23580 (2270)
[Ni(HL^8)L^8]ClO$_4$· 7H$_2$O (**6**)	30030 (16550), 26530 (18080), 22470 (21200)
[NiL^{8}Cl]· ½H$_2$O (**7**).	31250 (7770), 24150 (12960), 19380 (1870)

5 in 10^{-4} M DMF   6 in 10^{-4} M DMF
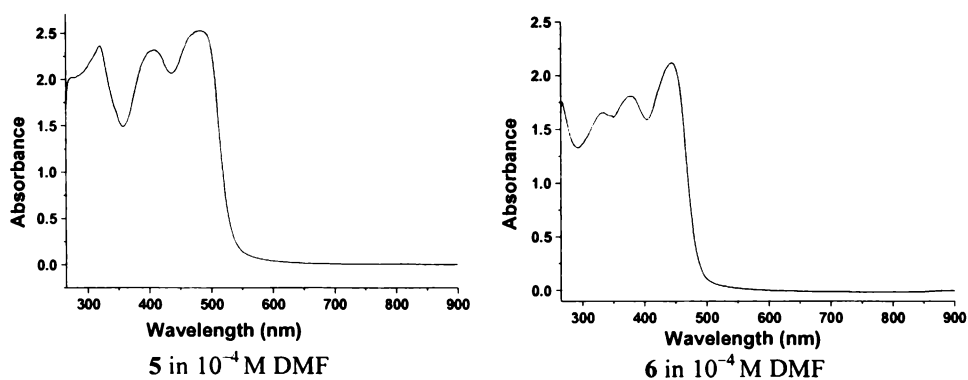
Fig. 3.18. Electronic spectra of Ni(II) thiosemicarbazone complexes.

7 in 10^{-4} M DMF   7 in 10^{-3} M DMF
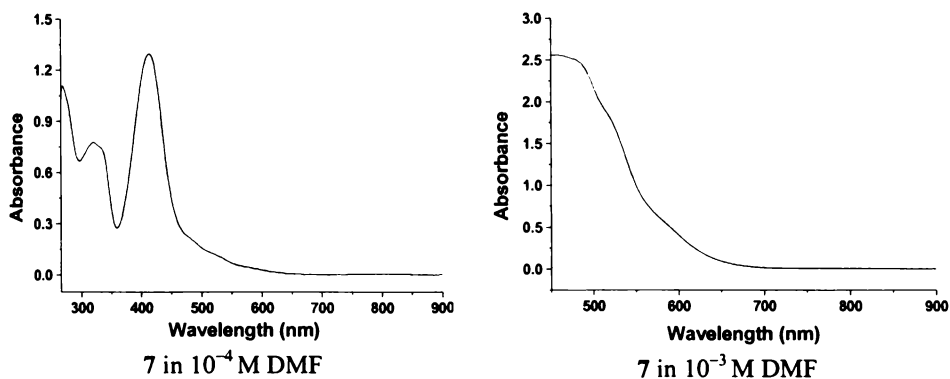
Fig. 3.19. Electronic spectra of Ni(II) thiosemicarbazone complex **7**.

3.3.3. Single crystal X-ray diffraction studies

The crystallographic data of square complex **1a** was collected using a Bruker APEX2 CCD diffractometer equipped with graphite monochromated Mo Kα (λ = 0.71073 Å) radiation at 100 K (using Oxford Cyrosystems Cobra low temperature attachment) at the X-ray Crystallography Unit, School of Physics, Universiti Sains Malaysia, Penang, Malaysia. The trial structure was solved using SHELXS-97 [39] and refinement was carried out by full-matrix least squares on F^2 (SHELXTL-97). One of the pyridyl groups is disordered over two sites and the rings have been constrained to be regular hexagons. H atoms were placed at calculated positions and allowed to ride on their parent atoms.

The data of single crystals of suitable dimension of **5**· 2½H$_2$O and **6a** were collected using a CrysAlis CCD, Oxford Diffraction Ltd. with graphite monochromated Mo Kα (λ = 0.71073 Å) radiation at 150(2) K at the National Single Crystal X-ray Diffraction Facility, IIT, Bombay. Both the crystals were found to be monoclinic. The trial structure was solved using SHELXS-97 [39] and refinement was carried out by full-matrix least squares on F^2 (SHELXTL-97). One of the pyrrolidine groups is disordered over C(15) and C(16) in complex **6a**. All nonhydrogen atoms

were refined anisotropically, while the hydrogen atoms were placed at calculated positions and allowed to ride on their parent atoms.

The crystallographic data and structure refinement parameters for the compound **1a** are given in Table 3.5 and that of the compounds [Ni(HL^7)$_2$]Cl$_2$ (**5**· 2½H$_2$O) and [Ni(L^8)$_2$] (**6a**) are given in Table 3.6. Molecular graphics employed were ORTEP-III [40] PLATON [41] MERCURY [42] and DIAMOND version 3.0 [43].

Table 3.5. Crystal data and structural refinement parameters of compound **1a**.

Parameters	[Ni(HL^1)]$_4$(PF$_6$)$_4$· ½CH$_3$CH$_2$OH· 2.8H$_2$O
Empirical Formula	C$_{93}$H$_{76.6}$F$_{24}$N$_{32}$Ni$_4$O$_{3.3}$P$_4$S$_4$
Formula weight (M)	2638.22
Color, shape	Black, Plate
Temperature (T) K	100.0(2)
Wavelength (Mo Kα) (Å)	0.71073
Crystal system	*Triclinic*
Space group	*P$\bar{1}$*
Lattice constants	
a (Å)	14.9345(8)
b (Å)	15.4023(8)
c (Å)	24.6220(13)
α (°)	98.950(3)
β (°)	96.098(3)
γ (°)	101.434(3)
Volume V (Å^3)	5428.5(5)
Z, D$_{calc}$ (*ρ*) (g cm^{-3})	2, 1.614
Absorption coefficient, *μ* (mm^{-1})	0.926
F(000)	2674
Crystal size (mm^3)	0.37× 0.15× 0.04
θ Range for data collection	0.85 to 20.00
Limiting Indices	$-14 \leq h \leq 14$,
	$-14 \leq k \leq 14$,
	$-23 \leq l \leq 23$
T$_{max}$ and T$_{min}$	0.964 and 0.846
Reflections collected	56387
Independent Reflections	10136 [R(int) = 0.1051]
Refinement method	Full-matrix least-squares on F^2
Data / restraints / parameters	10136 / 0 / 1387
Goodness-of-fit on *F^2*	1.043
Final *R* indices [I > 2σ (I)]	R$_1$ =0.0849, wR$_2$ = 0.2282
R indices (all data)	R$_1$ = 0.1296, wR$_2$ =0.2809
Largest difference peak and hole (e Å^{-3})	1.427 and -1.317

Table 3.6. Crystal data and structural refinement parameters of compounds 5· 2½H₂O and [Ni(L⁸)₂] (**6a**).

Parameters	$[Ni(HL^7)_2]Cl_2 \cdot 2\frac{1}{2}H_2O$	$[Ni(L^8)_2]$
Empirical Formula	$C_{30}H_{32}Cl_2N_8NiS_2O_{2.50}$	$C_{34}H_{34}N_8NiS_2$
Formula weight (M)	738.37	677.52
Color, shape	Brown, plate	Brown, block
Temperature (T) K	150(2)	150(2)
Wavelength (Mo Kα) (Å)	0.71073	0.71073
Crystal system	*Monoclinic*	*Monoclinic*
Space group	*P 21/n*	*P 21/c*
Lattice constants		
a (Å)	9.3866(5)	10.684(2)
b (Å)	27.0204(10)	20.229(4)
c (Å)	13.8731(8)	14.7177(18)
α (°)	90.00	90.00
β (°)	108.385(6)	96.762(13)
γ (°)	90.00	90.00
Volume V (Å³)	3339.0(3)	3158.8(9)
Z	4	4
D_{calc} (ρ) (Mg m⁻³)	1.469	1.425
Absorption coefficient, μ (mm⁻¹)	0.910	0.785
F(000)	1528	1416
Crystal size (mm³)	0.35× 0.18× 0.13	0.21× 0.10× 0.10
θ Range for data collection	3.02 to 25.00	2.96 to 25.00
Limiting Indices	-11≤ h ≤11, -32≤ k ≤32, -16≤ l ≤15	-12≤ h ≤12, -22≤ k ≤24, -17≤ l ≤17
T_{max} and T_{min}	0.888 and 0.822	0.925 and 0.910
Reflections collected	30854	16787
Independent Reflections	5857 [R(int) = 0.0694]	5521 [R(int) = 0.0685]
Refinement method	Full-matrix least-squares on F²	Full-matrix least-squares on F²
Data / restraints / parameters	5857/0/412	5521/21/425
Goodness-of-fit on F^2	1.087	1.089
Final R indices [I > 2σ (I)]	R₁ =0.0693, wR₂ = 0.1942	R₁ = 0.0652, wR₂ = 0.1656
R indices (all data)	R₁ = 0.1087, wR₂ =0.2218	R₁ = 0.1099, wR₂ = 0.2325
Largest difference peak and hole (e Å⁻³)	1.157 and -0.722	1.160 and -1.936

3.3.3.1. *Crystal structure of [Ni(HL¹)]₄(PF₆)₄· ½CH₃CH₂OH· 2.8H₂O (1a)*

The molecular structure of square grid complex (**1a**) is given in Fig. 3.20 and the coordination core about the Ni(II) centers with the atom numbering scheme is given in Fig. 3.21. Selected bond lengths and bond angles are summarized in Table 3.7. The $[Ni(HL^1)]_4^{4+}$ cation has four Ni(II) centers, organized by four monodeprotonated ligands H_2L^1, as a molecular square. Each metal center is octahedrally coordinated by making use of atoms like one of the pyridyl nitrogen, it's nearby azomethine nitrogen and thiolate sulfur atoms of two perpendicular $(HL^1)^-$ ligands. These two $(HL^1)^-$ ligands bind to Ni(II) in the *mer* configuration, with pairs of sulfur atoms and pyridyl N atoms each bearing a *cis* relationship and the azomethine N atoms keep a *trans* configuration, as found in related octahedral Ni(II) thiocarbohydrazone [8,16] and mononuclear thiosemicarbazone complexes [25,44]. As a result four fused five membered chelate rings share each metal center. The sulfur atoms share a position of adjacent Ni(II) octahedra (Fig. 3.21) and thus connect the centers to build a symmetrical molecular square (Fig. 3.22). The adjacent Ni⋯Ni distances are ~4.7 Å {they vary from 4.679(2) Å for Ni(1)⋯Ni(2) to 4.797(2) Å for Ni(2)⋯Ni(3)} and the angles subtended at the sulfur atoms Ni–S–Ni varies from 165.30(17)° for Ni(3)–S(4)–N(4) to 168.71(17)° for Ni(1)–S(3)–Ni(4). The Ni⋯Ni distances across the diagonals of the square are 6.749(2) Å for Ni(1)⋯Ni(3) and 6.692(2) Å for Ni(2)⋯Ni(4) and the Ni–Ni–Ni angles are ~90° {these vary from 88.73(4)° for Ni(2)–Ni(3)–Ni(4) to 90.82(4)° for Ni(1)–Ni(2)–Ni(3)}. The four Ni atoms are in a plane with a maximum mean plane deviation of 0.0525(17) Å for Ni(1). The sulfur atoms S(2) and S(4) are above and S(1) and S(3) are below this plane by ~0.2 Å.
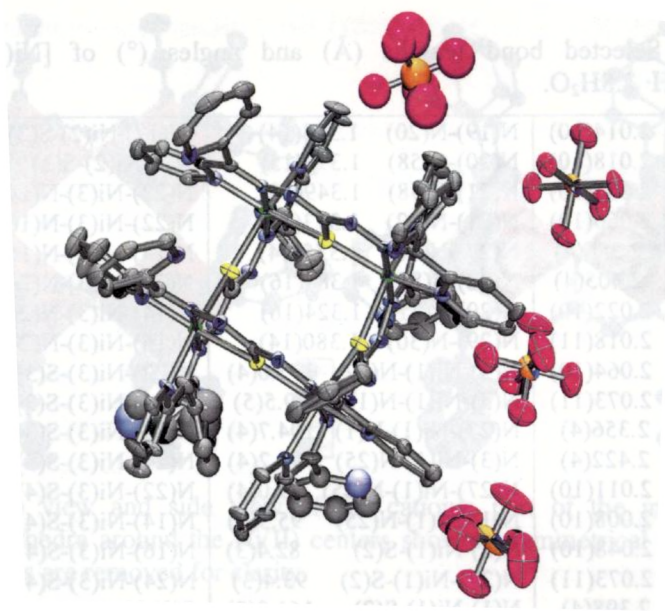
Fig. 3.20. ORTEP diagram for the compound **1a** with 50% probability ellipsoids. Hydrogen atoms, ethanol and lattice water molecules are omitted for clarity.
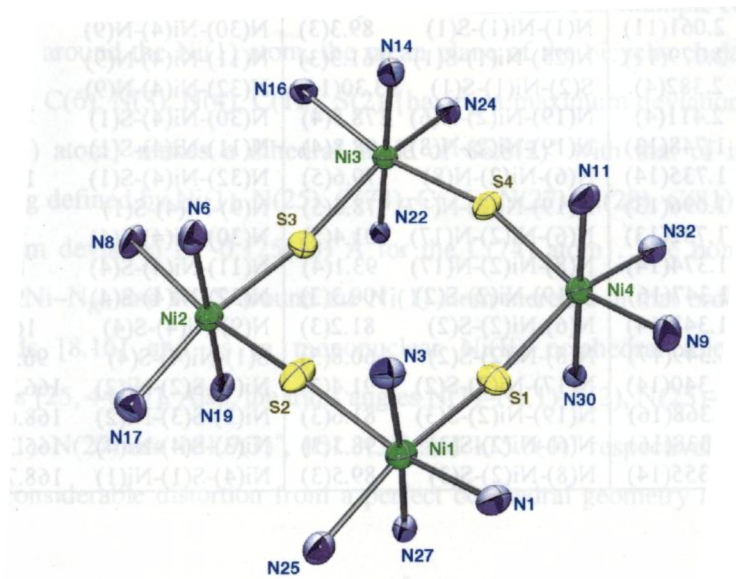
Fig. 3.21. The coordination core about Ni(II) centers of **1a** with the numbering scheme showing the octahedral centers of Ni(II) connected by sulfur bridges.

Table 3.7. Selected bond lengths (Å) and angles (°) of [Ni(HL¹)]₄(PF₆)₄·
½CH₃CH₂OH· 2.8H₂O.

Ni(1)-N(3)	2.014(10)	N(19)-N(20)	1.338(14)	N(17)-Ni(2)-S(3)	160.2(4)
Ni(1)-N(27)	2.018(10)	N(20)-C(58)	1.379(15)	S(2)-Ni(2)-S(3)	92.53(13)
Ni(1)-N(1)	2.055(10)	N(21)-C(58)	1.349(15)	N(22)-Ni(3)-N(14)	177.5(4)
Ni(1)-N(25)	2.066(10)	N(21)-N(22)	1.373(14)	N(22)-Ni(3)-N(16)	98.9(4)
Ni(1)-S(2)	2.356(4)	N(27)-N(28)	1.355(14)	N(14)-Ni(3)-N(16)	79.9(4)
Ni(1)-S(1)	2.405(4)	N(28)-C(81)	1.384(16)	N(22)-Ni(3)-N(24)	79.6(4)
Ni(2)-N(19)	2.022(10)	N(29)-C(81)	1.324(16)	N(14)-Ni(3)-N(24)	98.2(4)
Ni(2)-N(6)	2.018(11)	N(29)-N(30)	1.380(14)	N(16)-Ni(3)-N(24)	91.9(4)
Ni(2)-N(8)	2.064(10)	N(3)-Ni(1)-N(27)	175.0(4)	N(22)-Ni(3)-S(3)	82.1(3)
Ni(2)-N(17)	2.073(11)	N(3)-Ni(1)-N(1)	79.5(5)	N(14)-Ni(3)-S(3)	100.1(3)
Ni(2)-(S2)	2.356(4)	N(27)-Ni(1)-N(1)	104.7(4)	N(16)-Ni(3)-S(3)	89.5(3)
Ni(2)-S(3)	2.422(4)	N(3)-Ni(1)-N(25)	98.2(4)	N(24)-Ni(3)-S(3)	161.6(3)
Ni(3)-N(22)	2.011(10)	N(27)-Ni(1)-N(25)	79.0(4)	N(22)-Ni(3)-S(4)	99.9(3)
Ni(3)-N(14)	2.008(10)	N(1)-Ni(1)-N(25)	95.3(4)	N(14)-Ni(3)-S(4)	81.4(3)
Ni(3)-N(16)	2.048(10)	N(3)-Ni(1)-S(2)	82.4(3)	N(16)-Ni(3)-S(4)	161.3(3)
Ni(3)-N(24)	2.073(11)	N(27)-Ni(1)-S(2)	93.4(3)	N(24)-Ni(3)-S(4)	91.1(3)
Ni(3)-S(3)	2.398(4)	N(1)-Ni(1)-S(2)	161.9(3)	S(3)-Ni(3)-S(4)	93.51(13)
Ni(3)-S(4)	2.403(4)	N(25)-Ni(1)-S(2)	87.9(3)	N(30)-Ni(4)-N(11)	179.3(4)
Ni(4)-N(30)	2.023(10)	N(3)-Ni(1)-S(1)	100.5(3)	N(30)-Ni(4)-N(32)	78.7(5)
Ni(4)-N(11)	2.033(10)	N(27)-Ni(1)-S(1)	82.3(3)	N(11)-Ni(4)-N(32)	101.3(4)
Ni(4)-N(32)	2.061(11)	N(1)-Ni(1)-S(1)	89.3(3)	N(30)-Ni(4)-N(9)	100.5(4)
Ni(4)-N(9)	2.079(11)	N(25)-Ni(1)-S(1)	161.3(3)	N(11)-Ni(4)-N(9)	78.8(5)
Ni(4)-S(1)	2.382(4)	S(2)-Ni(1)-S(1)	93.30(14)	N(32)-Ni(4)-N(9)	91.8(4)
Ni(4)-S(4)	2.411(4)	N(19)-Ni(2)-N(6)	178.5(4)	N(30)-Ni(4)-S(1)	82.4(3)
S(1)-C(81)	1.748(13)	N(19)-Ni(2)-N(8)	98.8(4)	N(11)-Ni(4)-S(1)	97.6(3)
S(2)-C(12)	1.735(14)	N(6)-Ni(2)-N(8)	79.6(5)	N(32)-Ni(4)-S(1)	160.7(3)
S(3)-C(58)	1.696(13)	N(19)-Ni(2)-N(17)	78.6(5)	N(9)-Ni(4)-S(1)	88.1(3)
S(4)-C(35)	1.732(13)	N(6)-Ni(2)-N(17)	101.4(5)	N(30)-Ni(4)-S(4)	98.6(3)
N(3)-N(4)	1.374(14)	N(8)-Ni(2)-N(17)	93.1(4)	N(11)-Ni(4)-S(4)	82.1(3)
N(4)-C(12)	1.347(16)	N(19)-Ni(2)-S(2)	100.3(3)	N(32)-Ni(4)-S(4)	90.3(3)
N(5)-N(6)	1.343(14)	N(6)-Ni(2)-S(2)	81.2(3)	N(9)-Ni(4)-S(4)	160.8(3)
N(5)-C(12)	1.349(17)	N(8)-Ni(2)-S(2)	160.8(3)	S(1)-Ni(4)-S(4)	96.17(13)
N(11)-N(12)	1.340(14)	N(17)-Ni(2)-S(2)	91.4(3)	Ni(1)-S(2)-Ni(2)	166.30(18)
N(12)-C(35)	1.368(16)	N(19)-Ni(2)-S(3)	81.6(3)	Ni(3)-S(3)-Ni(2)	168.68(16)
N(13)-C(35)	1.338(16)	N(6)-Ni(2)-S(3)	98.3(3)	Ni(3)-S(4)-Ni(4)	165.30(17)
N(13)-N(14)	1.355(14)	N(8)-Ni(2)-S(3)	89.5(3)	Ni(4)-S(1)-Ni(1)	168.71(17)
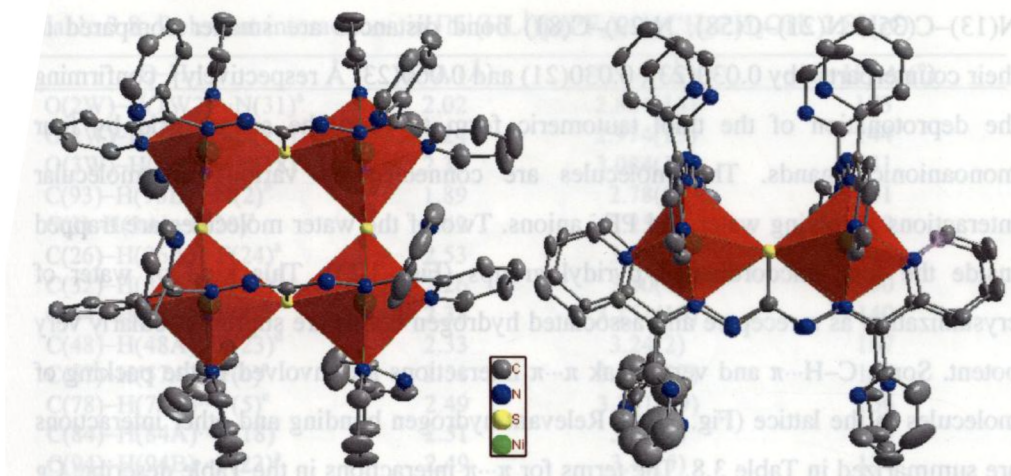
Fig. 3.22. Top view and side view of the cationic part of the molecule with octahedral polyhedra around the Ni(II) centers showing symmetrical nature of **1a**. Hydrogen atoms are removed for clarity.

The bond parameters (Table 3.7) show that the geometry around Ni(II) centers are distorted significantly from perfect octahedra. For example considering the octahedron around the Ni(1) atom, the mean plane of the bicyclic chelate ring Ni(1), N(1), C(5), C(6), N(3), N(4), C(12), S(2) {having a maximum deviation of 0.020(11) Å for N(1) atom} makes a dihedral angle of 86.8(2)° with that of its counterpart chelate ring defined by Ni(1), N(25), C(74), C(75), N(27), N(28), C(81), S(1) {having a maximum deviation of -0.125(13) Å for the C(74) atom}. The bond lengths Ni–N$_{azomethine}$, Ni–N$_{py}$, and Ni–S around the Ni(1) atom increase in that order as in similar compounds [8,16] and as in mononuclear Ni(II) octahedral thiosemicarbazone complexes [25, 44-47]. Also, the trans angles N(1)–Ni(1)–S(2), N(25)–Ni(1)–S(1) and N(3)–Ni(1)–N(27) are 161.9(3)°, 161.3(3)° and 175.0(4)° respectively. These factors suggest considerable distortion from a perfect octahedral geometry around the Ni(1) center.

The C–S bond lengths of ~1.73 Å are within the normal ranges of a C–S single bond. The hydrogen atoms were located at N(5), N(12), N(20) and N(28). The

103

N(13)–C(35), N(21)–C(58), N(29)–C(81) bond distances are smaller compared to their counterparts {by 0.030(23), 0.030(21) and 0.060(23) Å respectively}, confirming the deprotonation of the thiol tautomeric form to form the square grid by four monoanionic ligands. The molecules are connected by various intermolecular interactions involving water and PF_6^- anions. Two of the water molecules are trapped inside the four uncoordinated pyridyl groups (Fig. 3.23). This kind of water of crystallization as a receptee and associated hydrogen bonds are supramolecularly very potent. Some C–H···π and very weak π···π interactions are involved in the packing of molecules in the lattice (Fig. 3.24). Relevant hydrogen bonding and other interactions are summarized in Table 3.8. The terms for π···π interactions in the Table describe: Cg =Centroid, α =dihedral angles between planes I and J, β =angle Cg(I)···Cg(J). Only hydrogen bonding of angles <140 are excluded in the Table, except for intramolecular interactions.
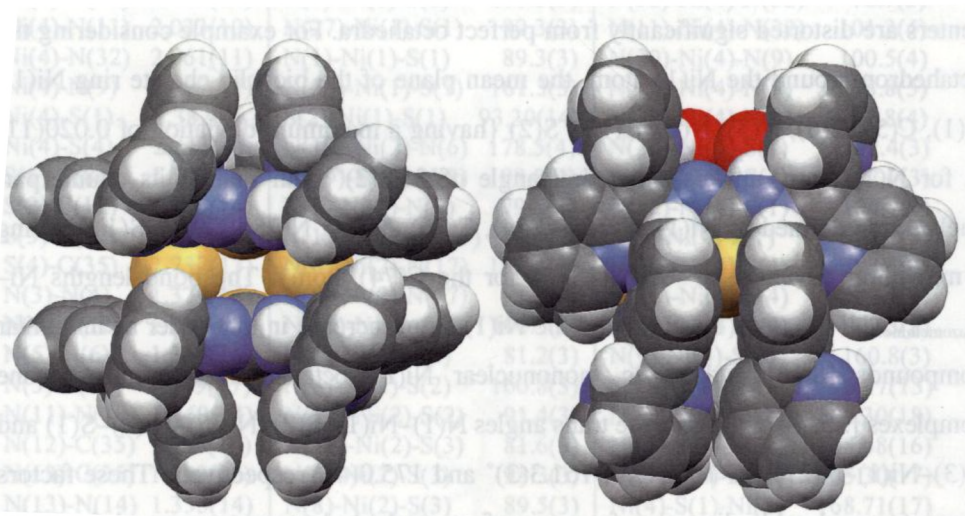
Fig. 3.23. Spacefill models showing the cavity inside the square grid $[Ni(HL^1)]_4^{4+}$ of the complex **1a** (left, top view) and side view showing the trapped water molecules inside four uncoordinated pyridyl groups of it (right).

Table 3.8. Relevant interactions in [Ni(HL^1)]$_4$(PF$_6$)$_4$· ½CH$_3$CH$_2$OH· 2.8H$_2$O.

D–H⋯A	H⋯A (Å)	D⋯A (Å)	D–H⋯A (°)
O(2W)–H(1W2)⋯N(31)[a]	2.02	2.864(14)	173
O(2W)–H(1W2)⋯N(21)[a]	2.24	2.974(13)	144
O(3W)–H(1W3)⋯N(18)[a]	2.38	3.084(14)	141
C(93)–H(93B)⋯N(2)[b]	1.89	2.78(3)	151
C(3)–H(3A)⋯F(20)[a]	2.42	3.25(2)	149
C(26)–H(26A)⋯F(24)[a]	2.53	3.35(3)	148
C(32)–H(32A)⋯F(22)[c]	2.26	3.10(4)	150
C(44)–H(44A)⋯F(8)[d]	2.38	3.151(19)	140
C(48)–H(48A)⋯F(23)[d]	2.33	3.24(2)	167
C(57)–H(57A)⋯F(6)[e]	2.51	3.388(17)	157
C(78)–H(78A)⋯F(5)[e]	2.49	3.361(19)	156
C(84)–H(84A)⋯F(18)[f]	2.51	3.30(2)	143
C(94)–H(94B)⋯F(23)[a]	2.49	3.44(5)	170
N(12)–H(12A)⋯N(10)	2.26	2.825(19)	123
N(20)–H(20B)⋯N(18)	2.30	2.888(15)	125
C(66)–H(66A)⋯N(23)	2.52	3.103(18)	121
C(73)–H(73A)⋯N(26)	2.56	3.136(19)	120

D–H⋯π	H⋯Cg (Å)	D⋯Cg (Å)	D–H⋯Cg (°)
C(8)–H(8A) ⋯Cg(23)[b]	2.75	3.38(2)	126
C(22)–H(22A)⋯Cg(32)[d]	2.87	3.690(16)	148
C(23)–H(23A)⋯Cg(6)[a]	2.96	3.254(14)	100
C(23)–H(23A)⋯Cg(8)[a]	2.98	3.298(15)	102
C(34)–H(34A)⋯Cg(18)[b]	2.94	3.71(2)	141
C(46)–H(46A)⋯Cg(9)[a]	2.89	3.240(14)	104
C(47)–H(47A)⋯Cg(5)[a]	2.96	3.316(17)	105
O(3W)–H(1W3)⋯Cg(30)[a]	2.96	3.132(11)	94
P(1)–F(1)⋯Cg(26)[g]	3.300(11)	4.668(7)	141.2(5)
P(1)–F(3)⋯Cg(9)[g]	3.963(10)	5.163(6)	131.0(5)

π⋯π interactions			
Cg(I)⋯Cg(J)	Cg⋯Cg (Å)	α (°)	β (°)
Cg(2)⋯Cg(29)[a]	3.962(7)	75.58	33.12
Cg(20)⋯Cg(21)[d]	3.719(9)	5.94	18.33
Cg(21)⋯Cg(20)[g]	3.719(9)	5.94	13.08

D=donor, A=acceptor; Equivalent position codes: a = x, y, z; b = 1-x,1-y,1-z ;
C = 2-x, 1-y, 1-z; d= -1+x, y, z ; e = 1-x, -y, -z; f= 1-x,1-y, -z; g= 1+x, y, z.
Cg(2)= Ni(1), S(2), C(12), N(4), N(3); Cg(5)= Ni(2), S(2), C(12), N(5), N(6);
Cg(6)= Ni(2), S(3), C(58), N(20), N(19); Cg(8)= Ni(2), N(17), C(51), C(52), N(19);
Cg(9)= Ni(3), S(3), C(58), N(21), N(22); Cg(18)= N(2), C(7), C(11), C(10), C(9), C(8);
Cg(20)= N(8), C(19), C(20), C(21), C(22), C(23); Cg(21)= N(9), C(24), C(25), C(26), (27),
C(28); Cg(23)= N(15), C(37), C(41), C(40), C(39), C(38); Cg(26)= N(18), (53), C(54),
C(55), C(56), C(57); Cg(29)= N(25), C(70), C(71), C(72), C(73), C(74); Cg(30)= N(26),
C(76), C(80), C(79), C(78), C(77); Cg(32)= N(32),C(88), C(89), C(90), C(91), C(92).
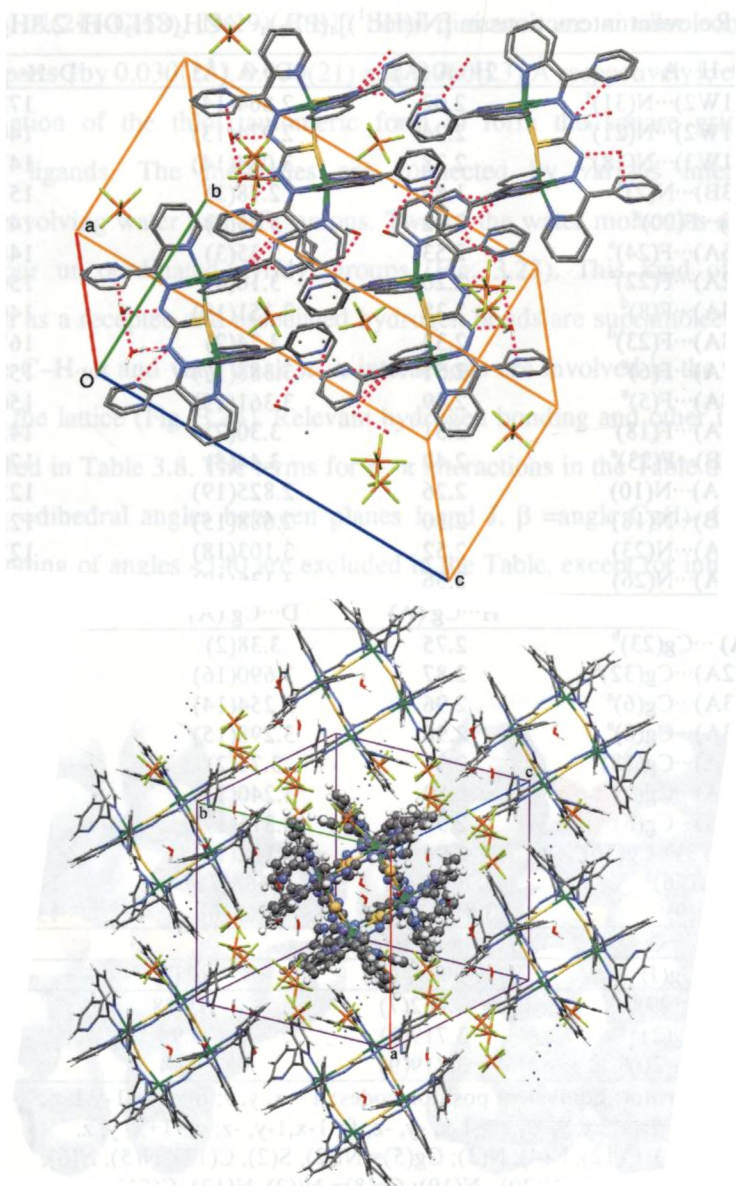
Fig. 3.24. A view of the packing diagram of the compound **1a**, showing relevant hydrogen bonding interactions. Hydrogen atoms not involved in HB interactions are removed for clarity (top). Another view of the packing is shown at the bottom.

3.3.3.2. *Crystal structures of [Ni(HL^7)$_2$]Cl$_2$· 2½H$_2$O and [Ni(L^8)$_2$]*

The X-ray structure determination of both the Ni(II) thiosemicarbazone complexes shows octahedral geometries around nickel centers and therefore a comparative description is given here. The octahedral geometry around the Ni(II) center in [Ni(HL^7)$_2$]Cl$_2$· 2½H$_2$O (**5**· 2½H$_2$O) is formed by the coordination of two neutral ligands HL^7, while by the two mono deprotonated form of the ligand HL^8 form the same in [Ni(L^8)$_2$] (**6a**). The molecular structures of **5**· 2½H$_2$O and **6a** along with the atom numbering schemes are depicted in Figs. 3.25 and 3.26 respectively. The relevant bond lengths and bond angles of **5**· 2½H$_2$O and [Ni(L^8)$_2$] (**6a**) are listed in Tables 3.9 and 3.10.
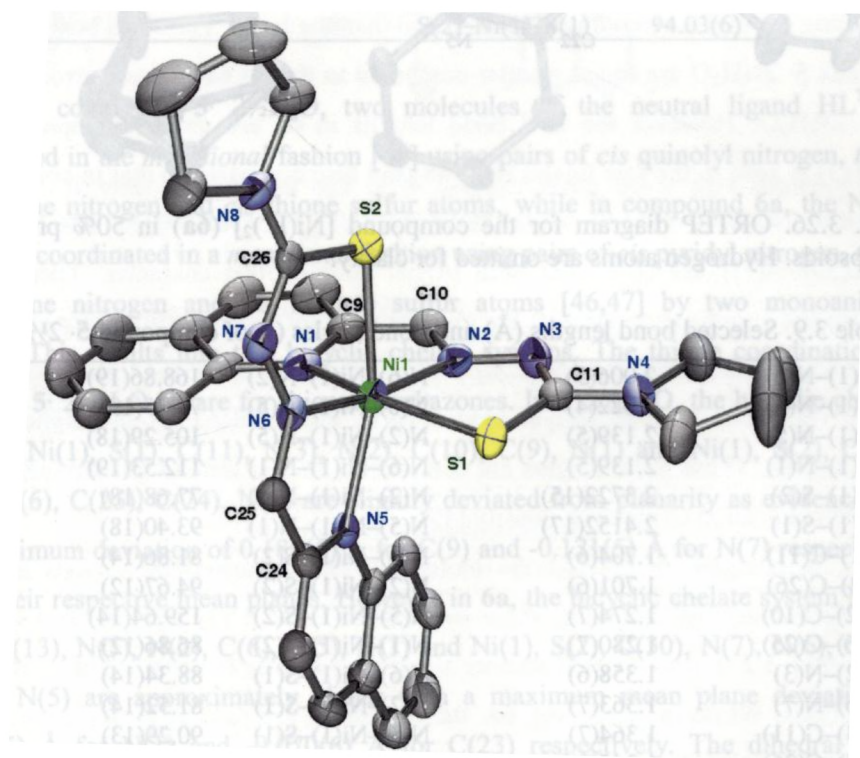
Fig. 3.25. ORTEP diagram of [Ni(HL^7)$_2$]Cl$_2$· 2½H$_2$O (**5**· 2½H$_2$O) in 50% probability ellipsoids. Hydrogen atoms, chloride ions and water molecules are omitted for clarity.
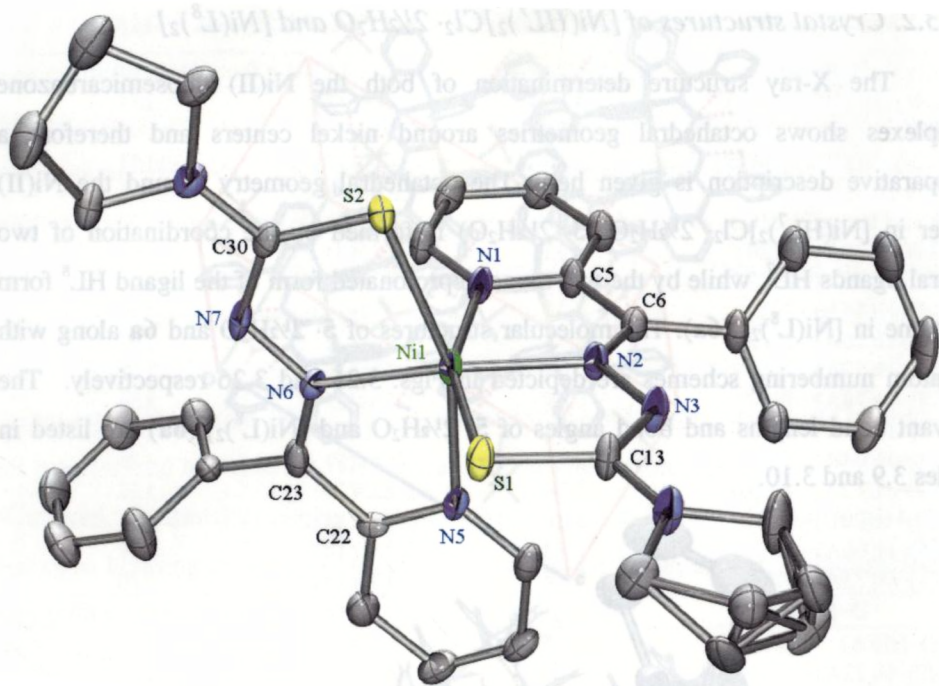
Fig. 3.26. ORTEP diagram for the compound [Ni(L^8)$_2$] (**6a**) in 50% probability ellipsoids. Hydrogen atoms are omitted for clarity.

Table 3.9. Selected bond lengths (Å) and bond angles (°) of compound **5**· 2½H$_2$O.

Ni(1)–N(6)	2.006(5)	N(6)–Ni(1)–N(2)	168.86(19)
Ni(1)–N(2)	2.022(4)	N(6)–Ni(1)–N(5)	79.25(19)
Ni(1)–N(5)	2.139(5)	N(2)–Ni(1)–N(5)	105.29(18)
Ni(1)–N(1)	2.139(5)	N(6)–Ni(1)–N(1)	112.53(19)
Ni(1)–S(2)	2.3722(15)	N(2)–Ni(1)–N(1)	77.68(18)
Ni(1)–S(1)	2.4152(17)	N(5)–Ni(1)–N(1)	93.40(18)
S(1)–C(11)	1.704(6)	N(6)–Ni(1)–S(2)	81.86(14)
S(2)–C(26)	1.701(6)	N(2)–Ni(1)–S(2)	94.67(12)
N(2)–C(10)	1.274(7)	N(5)–Ni(1)–S(2)	159.64(14)
N(6)–C(25)	1.280(7)	N(1)–Ni(1)–S(2)	86.86(12)
N(2)–N(3)	1.358(6)	N(6)–Ni(1)–S(1)	88.34(14)
N(6)–N(7)	1.363(7)	N(2)–Ni(1)–S(1)	81.52(14)
N(3)–C(11)	1.364(7)	N(5)–Ni(1)–S(1)	90.29(13)
N(7)–C(26)	1.345(8)	N(1)–Ni(1)–S(1)	159.12(13)
N(4)–C(11)	1.307(7)	S(2)–Ni(1)–S(1)	96.71(6)
N(8)–C(26)	1.357(7)		

Table 3.10. Selected bond lengths (Å) and bond angles (°) of [Ni(L^8)$_2$] (6a).

Ni(1)–N(6)	2.030(5)	N(6)–Ni(1)–N(2)	165.8(2)
Ni(1)–N(2)	2.035(5)	N(6)–Ni(1)–N(1)	92.40(19)
Ni(1)–N(1)	2.123(5)	N(2)–Ni(1)–N(1)	78.12 (19)
Ni(1)–N(5)	2.135(6)	N(6)–Ni(1)–N(5)	78.86(19)
Ni(1)–S(2)	2.4229(18)	N(2)–Ni(1)–N(5)	90.7(2)
Ni(1)–S(1)	2.4349(18)	N(1)–Ni(1)–N(5)	91.1(2)
S(1)–C(13)	1.729(6)	N(6)–Ni(1)–S(2)	79.96(14)
S(2)–C(30)	1.713(6)	N(2)–Ni(1)–S(2)	110.38(17)
C(6)–N(2)	1.301(8)	N(1)–Ni(1)–S(2)	90.76(15)
C(23)–N(6)	1.331(8)	N(5)–Ni(1)–S(2)	158.79(14)
N(2)–N(3)	1.353(7)	N(6)–Ni(1)–S(1)	109.03(14)
N(6)–N(7)	1.344(7)	N(2)–Ni(1)–S(1)	80.60(15)
N(3)–C(13)	1.334(8)	N(1)–Ni(1)–S(1)	158.54(14)
N(7)–C(30)	1.371(8)	N(5)–Ni(1)–S(1)	91.96(15)
		S(2)–Ni(1)–S(1)	94.03(6)

In compound **5·** 2½H$_2$O, two molecules of the neutral ligand HL^7 are coordinated in the *meridional* fashion [45] using pairs of *cis* quinolyl nitrogen, *trans* azomethine nitrogen and *cis* thione sulfur atoms, while in compound **6a**, the Ni(II) center is coordinated in a *meridional* fashion using pairs of *cis* pyridyl nitrogen, *trans* azomethine nitrogen and *cis* thiolate sulfur atoms [46,47] by two monoanionic ligands. This results into two bicyclic chelate systems. The thione coordination as found in **5·** 2½H$_2$O is rare for thiosemicarbazones. In **5·** 2½H$_2$O, the bicyclic chelate systems Ni(1), S(1), C(11), N(3), N(2), C(10), C(9), N(1) and Ni(1), S(2), C(26), N(7), N(6), C(25), C(24), N(5) are slightly deviated from planarity as evidenced by the maximum deviation of 0.183(6) Å for C(9) and -0.121(5) Å for N(7) respectively from their respective mean planes. However in **6a**, the bicyclic chelate system Ni(1), S(1), C(13), N(3), N(2), C(6), C(5), N(1) and Ni(1), S(2), C(30), N(7), N(6), C(23), C(22), N(5) are approximately planar with a maximum mean plane deviation of 0.100(5) Å for N(1) and -0.070(6) Å for C(23) respectively. The dihedral angle formed by the mean planes of the bicyclic chelate systems of each of the ligands is 83.50(10)° in **5·** 2½H$_2$O and 86.98(11)° in **6a**. In compound **5·** 2½H$_2$O, the trans

angles N(1)–Ni(1)–S(1), N(5)–Ni(1)–S(2) and N(2)–Ni(1)–N(6) are 159.12(13), 159.64(14) and 168.86(19)° respectively, while in compound **6a** these angles N(1)–Ni(1)–S(1), N(5)–Ni(1)–S(2) and N(2)–Ni(1)–N(6) are 158.54(14), 158.79(14) and 165.8(2)° respectively. These factors suggest considerable distortion from an octahedral geometry around Ni(II) center in both the complexes.

The bond lengths Ni–N$_{azo}$, Ni–N$_{py}$, and Ni–S in **6a** increase in that order as in similar compounds [44-47]. A similar increase is seen in the quinoline substituted compound **5**· 2½H$_2$O. The Ni–N$_{qu}$ bonds are of the same strength as both show 2.139(5) Å and weaker compared to Ni–N$_{py}$ bonds in compound **6a**. The Ni–N$_{azo}$ bond lengths are smaller compared to that of Ni–N$_{py/qu}$ in complexes **5**· 2½H$_2$O and **6a**, indicating the higher strength of former bond than the latter. The Ni–S bond lengths in complex **5**· 2½H$_2$O are found smaller compared to that in **6a** indicate stronger bonds in **5**· 2½H$_2$O. However the C–S bond lengths in **6a** are greater compared to the 1.681(3) Å seen in the free ligand HL^8 [48] and also compared to that in compound **5**· 2½H$_2$O. Also the C–N bond lengths in **6a** {1.334(8) Å for N(3)–C(13) and 1.371(8) Å for C(30)–N(7)} are consistent with partial double bond character. These factors confirm the coordination through the thiolate form by deprotonation after enolization of ligand HL^8 in compound [Ni(L^8)$_2$] (**6a**). However in **5**· 2½H$_2$O, the coordination occurs via thione form of HL^7 as evidenced by the smaller C–S and higher C–N$_{azo}$ bond lengths. These bond lengths are comparable to that seen in thiosemicarbazones with delocalization of electron density [49].

In complex **5**· 2½H$_2$O the molecules are connected by various hydrogen bonding interactions including water molecules (Table 3.11) and are packed in the lattice (Fig. 3.27) in an ordered manner along the *c* axis by making use of C–H···π ring interactions. While in compound **6a**, the molecules are packed in the same manner along the *a* axis as seen in Fig. 3.28, as a result of one intermolecular hydrogen bonding interaction and diverse C–H···π ring interactions (Table 3.12). However, no

significant $\pi\cdots\pi$ interactions are found in the packing of both compounds. We have reported these results recently [50].
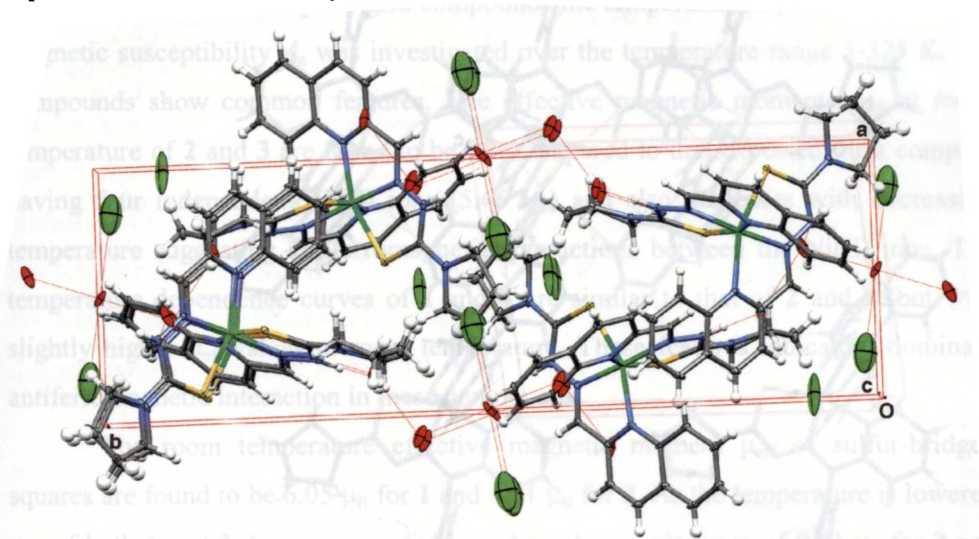
Fig. 3.27. A view of the unit cell of **5**· 2½H₂O along the *c* axis showing the molecules are packed along the *c* axis (left part) and connected through hydrogen bonding interactions involving chloride and water molecules.

Table 3.11. Interaction parameters of [Ni(HL⁷)₂]Cl₂· 2½H₂O.

C–H···π interactions			
X–H(I) Res(I)···Cg(J)	H···Cg (Å)	X···Cg (Å)	X–H···Cg (°)
C(2)–H(2) [1]...Cg(4)[a]	2.55	3.3546(67)	145
C(13)–H(13A) [1]...Cg(9)[b]	2.95	3.6529(91)	130
Cg(4)= Ni(1), N(5), C(24), C(25), N(6); Cg(9)= C(1), C(2), C(3), C(4), C(5), C(6).			
Hydrogen bonding interactions			
Residue	D–H···A	D–H (Å)	H···A (Å)	D···A (Å)	D–H···A (°)
1	N(3)–H(3)···O(w2)	0.86	1.88	2.702(8)	158
1	N(7)–H(7)···O(w1)[c]	0.86	2.51	2.911(9)	110
1	C(10)–H(10)···O(w2)	0.93	2.54	3.209(8)	129
1	C(17)–H(17)···N(2)	0.93	2.44	3.231(8)	143
1	C(23)–H(23)···Cl(1)	0.93	2.60	3.496(10)	163

D= donor, A= acceptor. Eqivalent position codes: a = x, y, z; b = 1/2+x, 1/2-y, -1/2+z; c = 1/2+x,1/2-y,1/2+z.
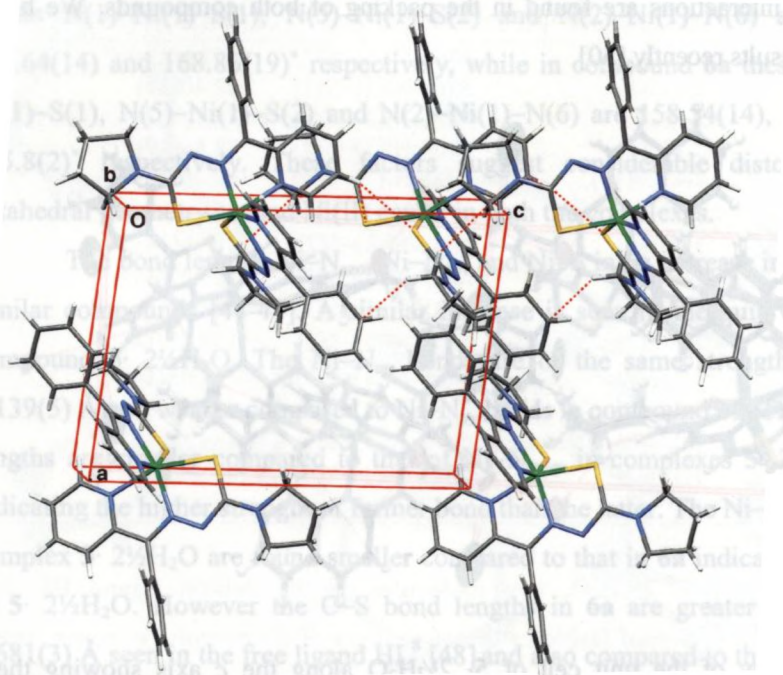
Fig. 3.28. Unit cell of the molecule [Ni(L⁸)₂] (**6a**) along the *b* axis showing molecules are packed along the *c* axis (bottom part) and connected through intermolecular hydrogen bonding interactions with molecules of the nearby layer (top part).

Table 3.12. Interaction parameters of [Ni(L⁸)₂].

C–H···π interactions				
X–H(I) Res(1)...Cg(J)		H···Cg (Å)	X···Cg (Å)	X–H···Cg (°)
C(1)–H(1)	[1]···Cg(15)ᵃ	2.73	3.160(6)	109
C(18)–H(18)	[1]···Cg(14)ᵃ	2.69	3.113(7)	108
C(19)–H(19)	[1]···Cg(15)ᵇ	2.55	3.310(6)	139

Cg(14)= Ni(1), S(1), C(13), N(3), N(2); Cg(15)= Ni(1), S(2), C(30), N(7), N(6).

Hydrogen bonding interaction					
Residue	D–H···A	D–H (Å)	H···A (Å)	D···A (Å)	D–H···A (°)
1	C(27)–H(27)···S(2)ᶜ	0.93	2.79	3.510(8)	135

D= donor, A= acceptor. Equivalent position codes: a = x, y, z; b = x, 1/2-y, 1/2+z, c = -1+x, y, z.

3.3.4. Magnetochemistry of the molecular square grids

For all the four square grid compounds the temperature dependence of molar magnetic susceptibility χ_m was investigated over the temperature range 5-325 K. All compounds show common features. The effective magnetic moments μ_{eff} at room temperature of **2** and **3** are found to be low compared to that expected for a complex having four independent Ni(II) ions (5.66 μ_B) and also decreases with decreasing temperature suggesting antiferromagnetic interactions between the Ni(II) ions. The temperature dependence curves of **1** and **4** are similar to that of **2** and **3**, but with slightly higher μ_{eff} values at room temperature. These features indicate a dominant antiferromagnetic interaction in these compounds.

The room temperature effective magnetic moment μ_{eff} of sulfur-bridged squares are found to be 6.05 μ_B for **1** and 4.01 μ_B for **2**. As the temperature is lowered μ_{eff} of both **1** and **2** decreases gradually and reaches a minimum of 0.51 μ_B for **2** and 0.45 μ_B for **1** at 5 K. The variable temperature magnetic behaviour of both compounds are indicative of antiferromagnetic coupling between the Ni(II) ions and this is greater in **2**. The room temperature μ_{eff} of 4.50 μ_B shown by complex **3** is low compared to its sulfur bridged counterpart compound **1**. The thermal dependence curve of **3** implies strong antiferromagnetic interactions between Ni(II) centers. The μ_{eff} values show a regular decrease upon decreasing the temperature and reach a minimum value of 0.66 μ_B at 5 K. The antiferromagnetic coupling in complex **4** is found to be low compared to that of **3**, as evidenced by the room temperature magnetic moment of 5.80 μ_B. On cooling, μ_{eff} decreases and reaches a minimum value of 0.83 μ_B at 5 K.

To fit and interpret the magnetic susceptibility data of complexes, first it is necessary to find all possible magnetic pathways in the complicated but regular structures. In a general case a square (D_{4h}) or distorted square (D_{2d}) [2 × 2] grid can be described by an exchange coupling scheme involving three exchange integrals ($J1, J2$ and $J3$) according to the appropriate Heisenberg exchange Hamiltonian [51], eqn (1).

$$\hat{H}_{ex} = -2J1\{\hat{S}_2 \cdot \hat{S}_3 + \hat{S}_1 \cdot \hat{S}_4\} - 2J2\{\hat{S}_1 \cdot \hat{S}_2 + \hat{S}_3 \cdot \hat{S}_4\} - 2J3\{\hat{S}_1 \cdot \hat{S}_3 + \hat{S}_2 \cdot \hat{S}_4\} \quad (1)$$

For compounds **1** to **4** *J3* is assumed to be zero, because there is no cross-coupling connection, and it is reasonable to assume that $J = J1 = J2$ by the approximation of similar M–X–M angles within each square grid. Assuming all the four Ni(II)–X–Ni(II) couplings are equal, i.e. using a single coupling constant J that takes into account all the exchange pathways to be equal (Scheme 3.2), is a reasonable assumption in the light of the X-ray crystallographic study of **1a** which reveals a similar nature of M–S–M angles (~167°), there is probably a super exchange mechanism through the intervening sulfur atoms. Therefore, for a square arrangement of four metal centers, D_{4h} [2 × 2] grid, eqn. (1) reduces to eqn. (2) [26],

$$\hat{H} = -2J(\hat{S}_1 \cdot \hat{S}_2 + \hat{S}_2 \cdot \hat{S}_3 + \hat{S}_3 \cdot \hat{S}_4 + \hat{S}_1 \cdot \hat{S}_4) \quad (2)$$
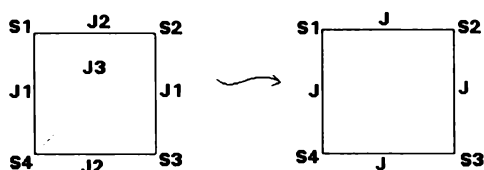
Scheme 3.2. Magnetic exchange models, showing the general case (left) and approximation used for **1** to **4** (right).

Here, the values of the spin angular momentum operator $\hat{S}_i$ ($i = 1 - 4$) are the same, and using the conventional spin-vector coupling model [52,53] the corresponding eigenvalues can be obtained analytically and are given by eqn. (3) [51],

$$E(S', S_{13}, S_{24}) = -J[S'(S'+1) - S_{13}(S_{13}+1) - S_{24}(S_{24}+1)] \quad (3)$$

where $\hat{S}_{13} = \hat{S}_1 + \hat{S}_3$; $\hat{S}_{24} = \hat{S}_2 + \hat{S}_4$; $\hat{S}' = \hat{S}_1 + \hat{S}_2 + \hat{S}_3 + \hat{S}_4$. For Ni(II) molecular squares $S_1, S_2, S_3, S_4 = 1$. There are nineteen spin states as given below.

S'	4	3	2	1	0
No. of spin states	1	3	6	6	3

The allowed values are then substituted in to the modified van Vleck equation, eqn. (4),

$$\chi_M = \frac{N\beta^2 g^2}{3k(T-\Theta)} \frac{\sum S'(S'+1)(2S'+1)e^{-E(S')/kT}}{\sum(2S'+1)e^{-E(S')/kT}}(1-\rho) + \frac{N\beta^2 g^2 S(S+1)\rho}{3kT} + TIP$$

(4)

Where χ_M is the molar magnetic susceptibility, ρ is the fraction of paramagnetic impurity, TIP is the temperature independent paramagnetism, Θ is a Weiss-like temperature correction and $E(S')$ refers to the energy of each spin state defined by S'.

The procedure of generating exchange equation for such large systems presents a somewhat daunting task, [particularly in the case of Mn(II) (S = 5/2)] and so we used MAGMUN4.1 [54] software package for calculation of the spin state energy spectrum for a cluster, and substitution into the van Vleck equation. Then, fitting of variable temperature magnetic data were done to an exchange expression, expanded form of eqn. (4), using the same program MAGMUN4.1. For complex 1, poor magnetic data collection (Fig. 3.29) made it difficult the fitting.

The temperature dependence curve of effective magnetic moment μ_{eff} for complexes 2 and 3 with their best fits obtained are given in Figs. 3.30 and 3.31. The best fit for 2 were obtained with $g = 2.047\pm 0.067$, $J = -126.24\pm 8.88$ cm^{-1}, $\Theta = -0.0385$ K, $\rho = 0.0405$, $R = 4.57\times10^{-2}$. Similarly for 3, the best fit were obtained with $g = 2.221\pm 0.064$, $J = -113.85\pm 7.57$ cm^{-1}, $\Theta = -0.016$ K, $\rho = 0.05$, $R = 4.90\times10^{-2}$. TIP was assumed as 6×10^{-4} emu mol^{-1} for fitting of both compounds, a typical value for Ni$_4$ complexes [22]. Where R is the agreement factor calculated as $R = [\sum(\chi_{obs.} - \chi_{calc.})^2 / \sum \chi_{obs.}^2]^{1/2}$. The coupling constant J obtained for both 2 and 3 are consistent with intramolecular antiferromagnetic interactions between the Ni(II) electron spins. Relatively high J (negative) values are suggestive of strong

115

antiferromagnetic coupling. For complex **4** (the temperature dependence curves of χ_m and μ_{eff} are shown in Fig. 3.32), however, we could not get a reasonable fit, may be associated with zero-field splitting (D) especially at lower temperatures and/or due to slight variations in M–X–M angles, so that more J values need to be considered. The M–O–M arrangement at 180° is known as an ideal structure for strong antiferromagnetism [55]. This linearity as the origin of strong AF coupling is in accordance with VB [56-58] and MO [59] studies. Logically, Kahn also explained this feature in his book [60]. The temperature dependence of effective magnetic moment curves for complexes **1** and **4** are also consistent with these results, though lacks reasonable fits. We have reported these results recently [61]. The field dependence of magnetic susceptibility for these compounds (Fig. 3. 33) not showed any indication of ferromagnetic component and is in agreement with overall antiferromagnetism.
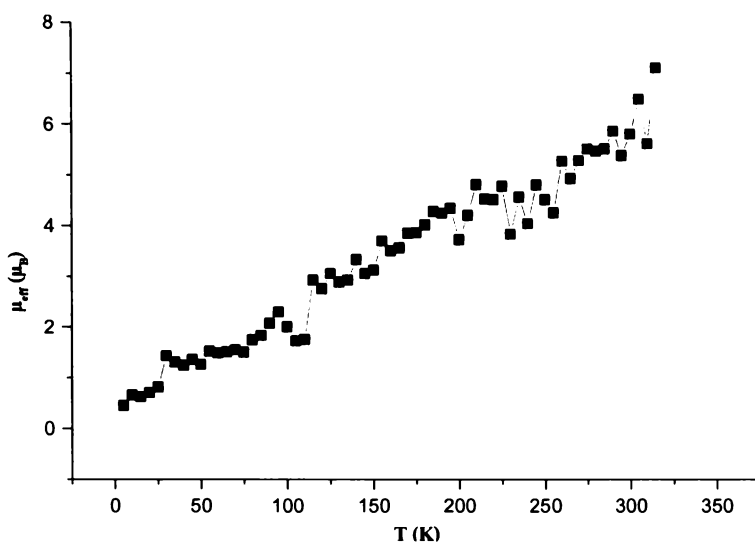
Fig. 3.29. Temperature dependence of effective magnetic moment μ_{eff} (■) for the complex **1** (the variations are due to poor data collection).
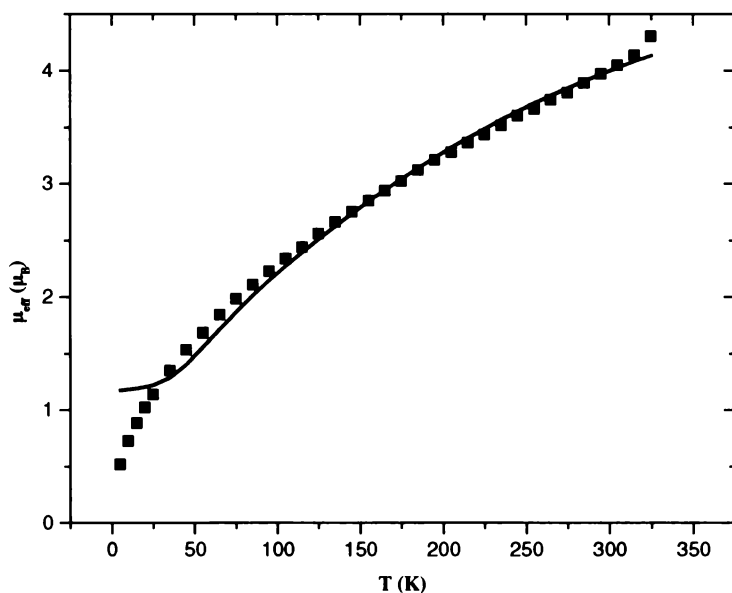
Fig. 3.30. Temperature dependence of effective magnetic moment μ_{eff} (■) for **2**. The solid line represents the best fit obtained (details in text).
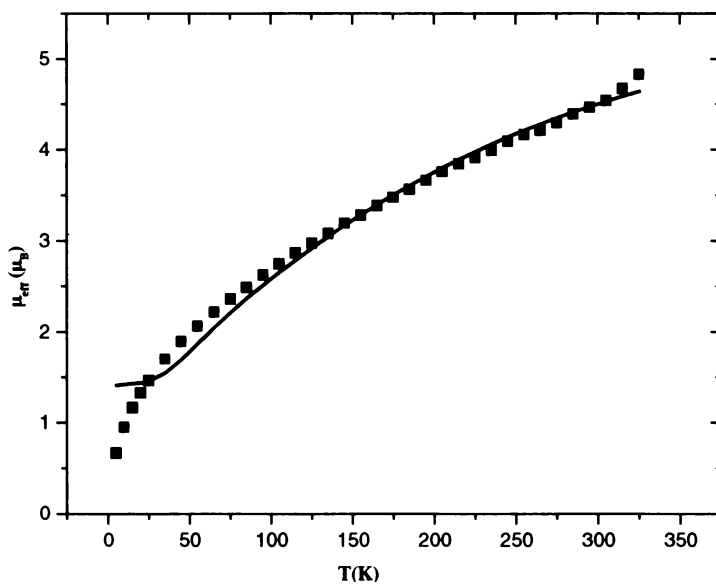
Fig. 3.31. Temperature dependence of effective magnetic moment μ_{eff} (■) for **3**. The solid line represents the best fit obtained (details in text).

117
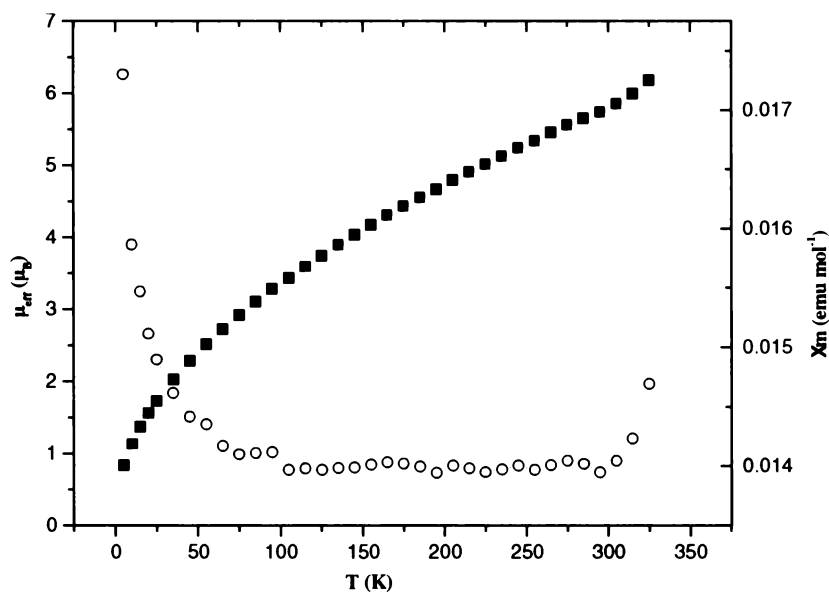
Fig. 3.32. Temperature dependence of effective magnetic moment μ_{eff} ($\blacksquare$) and molar magnetic susceptibility χ_m ($\circ$) of the complex **4**.
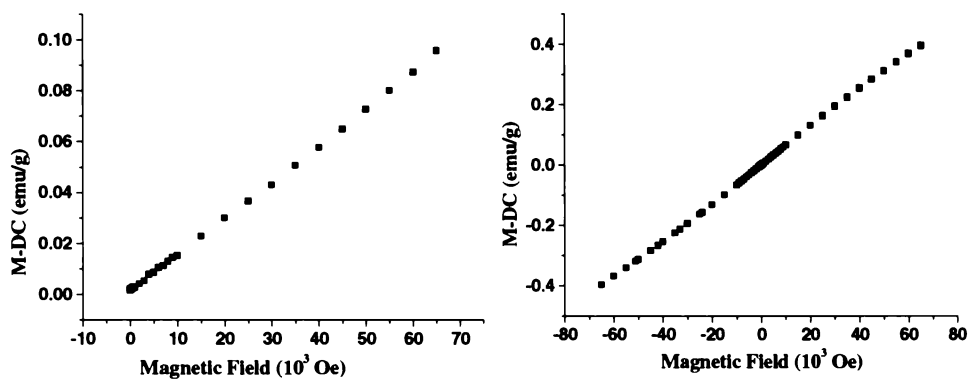
Fig. 3.33. Field dependence of magnetization for complex **1** at 300 K (left) and **4** (right) at 5K.

3.4. Concluding remarks

Four novel molecular square grids, of which three having a general formula [Ni(HL)]$_4$[PF$_6$]$_4$· nH$_2$O (1, 3 and 4) and one [Ni$_2$(HL^3)L^3]$_2$(PF$_6$)$_2$· 7H$_2$O (2) were achieved by self-assembly using two thiocarbohydrazone (H$_2$L^1 and H$_2$L^3) and two carbohydrazone (H$_2$L^4 and H$_2$L^5) ligands as building blocks. Carbohydrazones by making use of the bridging mode of oxygen are reported as novel potential building blocks for metallosupramolecular square grid complexes through self-assembly.

In addition, three new mononuclear nickel(II) complexes of ligands HL^7 and HL^8, were synthesized and physico-chemically characterized by means of partial elemental analyses, molar conductance measurements, magnetic measurements, electronic and infrared spectral studies. The three complexes were given the formulae as [Ni(HL^7)$_2$]Cl$_2$ (5), [Ni(HL^8)L^8]ClO$_4$· 7H$_2$O (6) and [NiL^{8}Cl]· ½H$_2$O (7). The compound 6 on crystallization deprotonated to form another new complex [Ni(L^8)$_2$] (6a). The structures of the compounds 5· 2½H$_2$O and 6a have been solved by single crystal X-ray crystallography and are found to be distorted octahedral geometries. In compound 5, the HL^7 coordinate the metal in thione form while in compound 7, HL^8 coordinates through its deprotonated thiolate form.

The MALDI MS spectra of compounds 1, 2, 3 and 4 reveal the formation of tetranuclear molecular squares. Theoretical simulations of isotropic distribution patterns of all main peaks could be achieved well and is found that the MALDI MS spectroscopy is very useful technique for the characterization of stable framework complexes. The square grid of Ni(II) centers in complexes 1, 3 and 4 were organized by respective monodeprotonated ligands, while in 2 coordination found to be occurred through mono and dideprotonation of H$_2$L^3. Interestingly, the complex 1a, got crystallized from a solution of complex 1, is found to possess two trapped water molecules inside the four uncoordinated pyridyl groups. The water of crystallization as a receptee and associated hydrogen bonds are supramolecularly very potent though

it is small, as water can play a crucial role in molecular association and aggregation and is almost a philosophical abstraction. Single crystal X-ray study of **1a** reveal octahedral geometries around the Ni(II) centers. Variable temperature magnetic susceptibility of all the Ni(II) square grids **1, 2, 3** and **4** were investigated. Magnetic data have been rationalized successfully on the basis of expected square grid structures, as supported by single crystal X-ray study and MALDI MS spectra. The magnetostructural correlation study reveals intramolecular antiferromagnetic coupling between the Ni(II) electrons by a super exchange mechanism through the intervening sulfur/oxygen atoms, consistent with the bridging structural arrangement. The field dependence of magnetic susceptibility curves also were found to be consistent with antiferromagnetic nature for all the square grid complexes.

References

1. R.S. Nyholm, Chem. Rev. 53 (1953) 263.

2. H.E. Shook Jr, J.B. Thompson, U.S. Patent (1975) 3903120.

3. M.A. Halcrow, G. Christou, Chem. Rev. 94 (1994) 2421.

4. S. Chandra, L.K. Gupta, Spectrochim. Acta Part A 62 (2005) 1089.

5. Z. Afrasiabi, E. Sinn, W. Lin, Y. Ma, C. Campana, S. Padhye, J. Inorg. Biochem. 99 (2005) 1526.

6. M.B. Ferrari, S. Capacchi, G. Reffo, G. Pelosi, P. Tarasconi, R. Albertini, S. Pinelli, P. Lunghi, J. Inorg. Biochem. 81 (2000) 89.

7. H.G. Petering, G.J. Van Giessen, Biochem. Copper. Proc. Symp. (1966) 197.

8. C. He, C.-y. Duan, C.-j. Fang, Y.-j. Liu, Q.-j. Meng, J. Chem. Soc., Dalton Trans. (2000) 1207.

9. L.K. Thompson, L. Zhao, Z. Xu, D.O. Miller, W.M. Reiff, Inorg. Chem. 42 (2003) 128.

10. T.K. Paine, E. Rentschler, T. Weyhermuller, P. Chaudhuri, Eur. J. Inorg.

Chem. (2003) 3167.

11. G.R. Burns, Inorg. Chem. 7 (1968) 277.

12. Z.H. Chohan, H. Pervez, K.M. Khan, C.T. Supuran, J. Enzym. Inhib. Med. Chem. 20 (2005) 81.

13. Z.H. Chohan, K.M. Khan, C.T. Supuran, Appl. Organometal. Chem. 18 (2004) 305.

14. D.P. Singh, R. Kumar, P. Tyagi, Trans. Met. Chem. 31 (2006) 970.

15. A.A.A. Abu-Hussen, A.A.A. Emara, J. Coord. Chem. 57 (2004) 973.

16. G. Han, D. Guo, C.-y. Duan, H. Mo, Q.-j. Meng, New J. Chem. 26 (2002) 1371.

17. M. Bell, A.J. Edwards, B.F. Hoskins, E.H. Kachab, R. Robson, J. Am. Chem. Soc. 111 (1989) 3603.

18. K.K. Nanda, K. Venkatsubramanian, D. Majumdar, K. Nag, Inorg. Chem. 33 (1994) 1581.

19. S. Mohanta, K.K. Nanda, R. Werner, W. Haase, A.K. Mukherjee, S.K. Dutta, K. Nag, Inorg. Chem. 36 (1997) 4656.

20. A.J. Edwards, B.F. Hoskins, E.H. Kachab, A. Markiewicz, K.S. Murray, R. Robson, Inorg. Chem. 31 (1992) 3585.

21. C.J. Matthews, K. Avery, Z. Xu, L.K. Thompson, L. Zhao, D.O. Miller, K. Biradha, K. Poirier, M.J. Zaworotko, C. Wilson, A.E. Goeta, J.A.K. Howard, Inorg. Chem. 38 (1999) 5266.

22. M. Fondo, N. Ocampo, A.M. Garcya-Deibe, R. Vicente, M. Corbella, M.R. Bermejo, J. Sanmartin, Inorg. Chem. 45 (2006) 255.

23. Z. Xu, L.K. Thompson, V.A. Milway, L. Zhao, T. Kelly, D.O. Miller, Inorg. Chem. 42 (2003) 2950.

24. D.S. Cati, J. Ribas, J. Ribas-Arino, H. Stoeckli-Evans, Inorg. Chem. 43 (2004) 1021.

25. V. Suni, M.R.P. Kurup, M. Nethaji, Polyhedron 26 (2007) 3097.

26. W.J. Geary, Coord. Chem. Rev. 7 (1971) 81.

27. P. Souza, A.I. Matesanz, V. Fernandez, J. Chem. Soc., Dalton Trans. (1996) 3011.

28. C. Bustos, O. Burckhardt, R. Schrebler, D. Carrillo, A.M. Arif, A.H. Cowley. C.M. Nunn, Inorg. Chem. 29 (1990) 3996.

29. M.A. Ali, A.H. Mirza, M.H.S.A. Hamid, F.H. Bujang, P.V. Bernhardt, Polyhedron 23 (2004) 2405.

30. R.M. Silverstein, G.C. Bassler, T.C. Morrill, Spectrometric Identification of Organic Compounds, 4th ed., John Wiley & Sons, New York (1981).

31. A.B.P. Lever, Inorganic Electronic Spectroscopy, 2nd ed., Elsevier, Amsterdam (1984).

32. A. Sreekanth, M.R.P. Kurup, Polyhedron 22 (2003) 3321.

33. M.B. Ferrari, F. Bisceglie, G. Pelosi, M. Sassi, P. Tarasconi, M. Cornia, S. Capacchi, R. Albertini, S. Pinelli, J. Inorg. Biochem. 90 (2002) 113.

34. G. Devoto, M. Massacesi, R. Pinna,, G. Ponticelli, Spectrochim. Acta Part A 38 (1982) 725.

35. R. Roy, M. Chaudhuri, S.K. Mondal, K. Nag, J. Chem. Soc., Dalton Trans. (1984) 1681.

36. V. Philip, V. Suni, M.R.P. Kurup, M. Nethaji, Polyhedron 23 (2004) 1225.

37. B.S. Garg, M.R.P. Kurup, S.K. Jain, Y.K. Bhoon, Transit. Met. Chem. 13 (1988) 309.

38. M.A. Ali, S.M.G. Hossain, S.M.M.H. Majumder, M. Nazimuddin, M.T.H. Tazafder, Polyhedron 6 (1987) 1653.

39. G.M. Sheldrick, SHELXTL Version 5.1, Software Reference Manual, Bruker AXS Inc., Madison, Wisconsin, USA (1997).

40. L.J. Farrugia, J. Appl. Cryst. 30 (1997) 565.

41. A.L. Spek, J. Appl. Cryst. 36 (2003) 7.

42. C.F. Macrae, P.R. Edgington, P. McCabe, E. Pidcock, G.P. Shields, R. Taylor, M. Towler, J. van de Streek, J. Appl. Cryst. 39 (2006) 453.

43. K. Brandenburg, H. Putz, DIAMOND version 3.0, Crystal Impact, GbR, Postfach 1251, D-53002 Bonn, Germany (2004).

44. A. Sreekanth, S. Sivakumar, M. R. P. Kurup, J. Mol. Struct. 655 (2003) 47.

45. I. Garcya, E. Bermejo, A K. El Sawaf, A. Castineiras, D.X. West, Polyhedron 21 (2002) 729.

46. K.A. Ketcham, I. Garcia, E. Bermejo, J.K. Swearingen, A K. El Sawaf, E. Bermejo, A. Castineiras, D.X. West, Polyhedron 21 (2002) 859.

47. N.C. Kasuga, K. Sekino, C. Koumo, N. Shimada, M. Ishikawa, K. Nomiya, J. Inorg. Biochem. 84 (2001) 55.

48. A. Sreekanth, M.R.P. Kurup, Polyhedron 23 (2004) 969.

49. L. Latheef, E. Manoj, M.R.P. Kurup, Acta Cryst. C61 (2006) o16.

50. E. Manoj, M.R.P. Kurup, Polyhedron, DOI: 10.1016/j.poly.2007.09.023

51. L.N. Dawe, T.S.M. Abedin, T.L. Kelly, L.K. Thompson, D.O. Miller, L. Zhao, C. Wilson, M.A. Leech, J.A.K. Howard, J. Mater. Chem. 16 (2006) 2645.

52. K. Kambe, J. Phys. Soc. Jpn. 5 (1950) 48.

53. R.L. Martin, in New Pathways in Inorganic Chemistry, ed. E.A.V. Ebsworth, A.G. Maddock and A.G. Sharpe, Cambridge University Press, Cambridge (1978) ch. 9.

54. http://www.ucs.mun.ca/~lthomp/magmun. MAGMUN has been developed by Dr Zhiqiang Xu (Memorial University), and OW01.exe by Dr O. Waldmann.

55. Y.-B. Jiang, H.-Z. Kou, R.-J. Wang, A.-L. Cui, J. Ribas, Inorg. Chem. 44 (2005) 709.

56. J.B. Goodenough, Phys. Rev. 100 (1955) 565.

57.   J.B. Goodenough, J. Phys. Chem. Solids 6 (1958) 287.

58.   J. Kanamori, J. Phys. Chem. Solids 10 (1959) 87.

59.   P.J. Hay, J.C. Thibeault, R. Hoffmann, J. Am. Chem. Soc. 97 (1975) 4884.

60.   O. Kahn, Molecular Magnetism, VCH Publishers, New York (1993).

61.   E. Manoj, M.R.P. Kurup, H.-K. Fun, A. Punnoose, Polyhedron 26 (2007) 4451.

****

Cu(II) complexes of carbohydrazone and thiocarbohydrazone ligands: Spectral, magnetic and anticancer studies

4.1. Introduction

The copper(II) ion is a typical transition metal ion in respect of the formation of coordination complexes, but less typical in its reluctance to take up a regular octahedral or tetrahedral stereochemistry [1]. Cu(II) is the most stable oxidation state of copper, though Cu(I) and Cu(III) are also relevant. The Cu(II) ion with $3\,d^{9}$ outer electron configuration lacks cubic symmetry and hence exhibits distorted forms of the basic stereochemistries such as tetrahedral, square planar, square pyramidal and octahedral. Jahn Teller effect plays a major role in deciding the distortion effect of stereochemistries of Cu(II) complexes. The typical distortion involved in octahedral geometry is elongated structures with the odd electron residing in the $d_{x^2-y^2}$ orbital resulting in four short Cu–L bonds and two trans long bonds, which are usually more energetically favorable than the compressed structures, consistent with their more frequent occurrence. The coordination numbers of four, five and six predominate, but variations of each structure occur through bond-length or bond-angle distortions [1]. The Cu(II) complexes are magnetic and EPR active and have been attracted the eyes of various research groups. Depending on the coupling between Cu(II) centers in multinuclear complexes, the EPR and magnetic features are interesting and their coordination chemistry have a distinct role in the progress of inorganic chemistry. Copper(I) [2×2] grid complexes [2] are known. For Cu(II) grid structures of [2×2] or [3×3], both ferromagnetic and antiferromagnetic intramolecular couplings were

observed [3]. Conversely, copper is an important bioelement and an active site in several metalloenzymes and proteins. The chemistry of copper proteins involves Cu(I), Cu(II) and Cu(III) species and also systems with more than one type of Cu is present. The Cu atom switches between the Cu(I) and Cu(II) states [4,5] in redox reactions involving copper containing enzymes and is an essential factor for many of the properties of these enzymes.

One of the most striking aspect of copper(II) coordination complexes is their biological activity, which is of great interest in pharmacology. Cu(II) complexes of many Schiff bases like hydrazones, semicarbazones, thiosemicarbazones, etc have been reported to have a great variety of biological activity. Of these, thiosemicarbazones present activities ranging from fungicide [6], bactericide [7], antitumoral [8,9] anti-inflammatory [10], etc and are explored well by various research groups. In most cases, the metal complexes show more activity compared to their metal free chelating ligands. The present series of ligands can be considered as an extension of these types of compounds with an additional binding site. Several mono- and bis- carbohydrazone and thiocarbohydrazone ligands and some Cu(II) complexes have been synthesized and studied along with their antimicrobial and anti-mutagenic activity [11]. Thiocarbohydrazones on complexation with Cu(II) are proposed as anticancer drug analogues [12,13] like thiosemicarbazones and their Cu(II) complexes [14,15]. Hence we considered it worthwhile to synthesize and characterize Cu(II) complexes of thiocarbohydrazones and their oxygen analogues carbohydrazone complexes with a view to study their anticancer properties.

The present ligands of carbohydrazones and thiocarbohydrazones with mainly two coordination pockets are expected to form complexes of interesting magnetic properties. Also, it is found that the temperature dependence of magnetic susceptibility with multinuclear Cu(II) complexes of carbohydrazones and thiocarbohydrazones and their EPR characteristics are least studied. There is only one such work reported for thiocarbohydrazone [12] and is of a dimeric dicopper(II)

126

complex of bis(pyridine-2-aldehyde) thiocarbohydrazone, along with its crystal structure. The dinuclear symmetric dicopper(II) complex of bis(phenyl(2-pyridyl)methanone) thiocarbohydrazone (H_2L^2) [16] describes the X-ray structure and lacks EPR and magnetic studies. For carbohydrazones, similarly, there is only single report [17] of magnetic and EPR features discussed along with its dinuclear X-ray crystal structure. The EPR characteristic of this complex is described with only a powder spectrum broad single g value and magnetochemistry is confirmed with antiferromagnetic coupling between Cu(II) electrons. Therefore, an investigation including temperature dependence of magnetic susceptibility and EPR characteristics appeared interesting, which prompted this study and is the initial step towards this spectrum of wide scope.

4.2. Experimental

4.2.1. Materials

Cu(OAc)$_2$· H$_2$O (Qualigens), CuSO$_4$· 5H$_2$O (Merck), CuBr$_2$ (Merck), CuCl$_2$· 2H$_2$O (Merck), Cu(ClO$_4$)$_2$· 6H$_2$O (Aldrich), NaN$_3$ (Reidel-De Haen) were used as received and solvents methanol (Rankem), chloroform (S.D. Fine), DMF (S.D. Fine), etc were used as received.

Caution! Perchlorate and azide complexes of metals with organic ligands are potentially explosive and should be handled with care.

4.2.2. Synthesis of copper(II) complexes

[Cu₃(HL¹)L¹Cl₃]· 3H₂O (8)

To a hot methanolic solution of H$_2$L^1 (0.330 g, 0.75 mmol) was added an equimolar amount of CuCl$_2$· 2H$_2$O (0.132 g) dissolved in 10 ml hot methanol. The brown colored mixture was refluxed for 10 minutes and allowed to stand at room temperature to get brown solid product. The compound precipitated was filtered,

washed with methanol and ether and dried *in vacuo* over P_4O_{10}. Yield: 0.286 g (93.4%). Elemental Anal. Found (Calc.): C, 45.48 (45.10); H, 3.78 (3.21); N, 18.28 (18.29); S, 5.35 (5.24)%.

$[Cu_4L^2{}_2]\cdot 2H_2O](ClO_4)_4$ *(9)*

A solution of $CuClO_4\cdot 6H_2O$ (0.378 g, 1 mmol) in 10 ml of methanol was added to a solution of H_2L^2 (0.220 g, 0.5 mmol) in 10 ml chloroform and refluxed for ½ h and allowed to stand at room temperature. Brown product separated out was filtered, washed with methanol followed by ether and dried over P_4O_{10} *in vacuo*. Yield: 0.326 g (83.7%). Elemental Anal. Found (Calc.): C, 38.38 (38.57); H, 2.92 (2.59); N, 10.45 (10.79); S, 4.16 (4.12)%. Molar conductivity (Λ_M, 10^{-4} M DMF): 5 Ω^{-1} cm^2 mol^{-1}.

$[Cu_2(HL^2)Br_2]Br\cdot H_2O$ *(10)*

A solution of $CuBr_2$ (0.226 g, 1 mmol) in 10 ml of methanol was added to a solution of H_2L^2 (0.220 g, 0.5 mmol) in 10 ml chloroform and refluxed for ½ h and allowed to stand at room temperature. Brown product separated out was filtered, washed with methanol followed by ether and dried over P_4O_{10} *in vacuo*. Yield: 0.313 g (76.3%). Elemental Anal. Found (Calc.): C, 36.00 (36.60); H, 2.14 (2.58); N, 9.96 (10.24); S, 3.66 (3.91)%. Molar conductivity (Λ_M, 10^{-3} M DMF): 88 Ω^{-1} cm^2 mol^{-1}.

$[Cu_2(HL^3)Cl_3]\cdot 2H_2O$ *(11)*

A solution of $CuCl_2\cdot 2H_2O$ (0.265 g, 1.5 mmol) in 10 ml of methanol was added to a solution of H_2L^3 (0.291 g, 0.75 mmol) in 40 ml boiling methanol and refluxed for 10 minutes and the reddish solution allowed to stand at room temperature. Brown product separated out was filtered, washed with methanol followed by ether and dried over P_4O_{10} *in vacuo*. Yield: 0.435 g (88.8%). Elemental Anal. Found

(Calc.): C, 39.16 (38.63); H, 3.24 (2.93); N, 12.89 (12.87); S, 5.04 (4.91)%. Molar conductivity (Λ_M, 10^{-3} M DMF): 49 Ω^{-1} cm^2 mol^{-1}.

[Cu₂(HL3)Br₂]Br· H₂O (12)

A solution of CuBr₂ (0.338 g, 1.5 mmol) in 10 ml of methanol was added to a solution of H₂L³ (0.291 g, 0.75 mmol) in 40 ml methanol and refluxed for 20 minutes and allowed to stand at room temperature. Brown product separated out was filtered, washed with methanol followed by ether and dried over P₄O₁₀ *in vacuo*. Yield: 0.536 g (93.1%). Elemental Anal. Found (Calc.): C, 33.12 (32.83); H, 2.60 (2.23); N, 11.10 (10.94); S, 4.21 (4.17)%. Molar conductivity (Λ_M, 10^{-3} M DMF): 76 Ω^{-1} cm^2 mol^{-1}.

[Cu₃(HL⁴)Cl₂]Cl₃· 2H₂O (13)

A solution of CuCl₂· 2H₂O (0.344 g, 2 mmol) in 10 ml of methanol was added to a solution of H₂L⁴ (0.427 g, 1 mmol) in 40 ml boiling methanol and refluxed for 20 minutes and the green colored solution allowed to stand at room temperature. Dark colored product separated out was filtered, washed with methanol followed by ether and dried over P₄O₁₀ *in vacuo*. Yield: 0.379 g (68.9%). Elemental Anal. Found (Calc.): C, 33.68 (33.47); H, 2.91 (2.56); N, 13.59 (13.58)%. Molar conductivity (Λ_M, 10^{-3} M DMF): 214 Ω^{-1} cm^2 mol^{-1}.

[Cu₂(HL⁴)(HSO₄)· H₂O]SO₄· 6H₂O (14)

To a solution of H₂L⁴ (0.422 g, 1 mmol) in hot methanol (40 ml), CuSO₄· 5H₂O (0.500 g, 2 mmol) in hot methanol were added and refluxed the solution for 20 minutes. The solution was kept for precipitation; the dark brown precipitate was then filtered and washed with absolute ethanol and diethyl ether, and dried over P₄O₁₀ *in vacuo*. Yield: 0.721 g (83.1%). Elemental Anal. Found (Calc.): C, 31.88 (31.83); H, 3.88 (3.72); N, 12.90 (12.91)%. Molar conductivity (Λ_M, 10^{-3} M methanol): 81 Ω^{-1} cm^2 mol^{-1}.

[Cu₂(HL⁴)Br₂]Br· 3H₂O (15)

A solution of CuBr₂ (0.338 g, 1.5 mmol) in 20 ml of ethanol was added to a solution of H₂L⁴ (0.320 g, 0.75 mmol) in 40 ml boiling ethanol and refluxed for 20 minutes and allowed to stand at room temperature. Dark colored product separated out was filtered, washed with methanol followed by ether and dried over P₄O₁₀ *in vacuo*. Yield: 0.320 g (50.6%). Elemental Anal. Found (Calc.): C, 32.44 (32.80); H, 2.45 (2.75); N, 13.37 (13.30)%. Molar conductivity (Λ_M, 10^{-3} M DMF): 93 Ω^{-1} cm² mol⁻¹.

[Cu₂(L⁴)· 2H₂O](ClO₄)₂· 2H₂O (16)

A solution of CuClO₄· 6H₂O (0.378 g, 1 mmol) in 10 ml of methanol was added to a solution of H₂L⁴ (0.214 g, 0.5 mmol) in 40 ml boiling methanol and refluxed for ½ h and allowed to stand at room temperature. Dark product separated out was filtered, washed with methanol and ether and dried over P₄O₁₀ *in vacuo*. Yield: 0.390 g (95.3%). Elemental Anal. Found (Calc.): C, 33.86 (33.75); H, 2.57 (2.96); N, 13.78 (13.69)%. Molar conductivity (Λ_M, 10^{-3} M DMF): 164 Ω^{-1} cm² mol⁻¹.

[Cu₂L⁴(N₃)₂]· CH₃OH (17)

To a boiling solution of H₂L⁴ (0.320 g, 0.75 mmol) in 40 ml boiling ethanol Cu(CH₃COO)₂· H₂O (0.302 g, 1.5 mmol) in 10 ml of ethanol was added followed by NaN₃ (0.098 g, 1.5 mmol) in hot ethanol and refluxed for 1 h and allowed to stand at room temperature. Dark colored product separated out was filtered, washed with methanol, hot water and ether and dried over P₄O₁₀ *in vacuo*. Yield: 0.194 g (38.9%). Elemental Anal. Found (Calc.): C, 43.31 (43.44); H, 2.99 (3.04); N, 29.50 (29.55)%. Molar conductivity (Λ_M, 10^{-3} M DMF): 12 Ω^{-1} cm² mol⁻¹.

[Cu₂(HL⁶)Cl₃]· H₂O (18)

A solution of CuCl₂· 2H₂O (0.206 g, 1.2 mmol) in 10 ml of methanol was added to a solution of H₂L⁶ (0.291 g, 0.6 mmol) in 70 ml boiling methanol and

refluxed for 1 h and allowed to stand at room temperature. Dull brown colored mass separated out was filtered, washed with methanol and ether and dried over P_4O_{10} _in vacuo_. Yield: 0.260 g (56.0%). Elemental Anal. Found (Calc.): C, 40.90 (40.76); H, 3.23 (2.77); N, 13.37 (13.58)%. Molar conductivity (Λ_M, 10^{-3} M DMF): 28 Ω^{-1} cm^2 mol^{-1}.

$[Cu_2(HL^6)Br_2]Br$ _(19)_

A solution of CuBr$_2$ (0.271 g, 1.2 mmol) in 10 ml of methanol was added to a solution of H$_2$L^6 (0.291 g, 0.6 mmol) in 70 ml boiling methanol and refluxed for ½ h and allowed to stand at room temperature. Yellow brown colored solid separated out was filtered, washed with methanol and ether and dried over P_4O_{10} _in vacuo_. Yield: 0.269 g (48.9%). Elemental Anal. Found (Calc.): C, 34.94 (34.35); H, 2.24 (2.06); N, 11.60 (11.45)%. Molar conductivity (Λ_M, 10^{-3} M DMF): 63 Ω^{-1} cm^2 mol^{-1}.

4.3. Results and discussion

All the copper complexes, except **8**, were synthesized by the reaction between 1:2 ratios of corresponding ligand to metal salts under neutral conditions. All the complexes, except **8, 9** and **13**, are found to be bimetallic within the coordination pockets of respective ligands. For all complexes the respective ligands coordinate either by monodeprotonated or by dideprotonated forms. The solvents used were methanol, ethanol or methanol chloroform mixture mainly with a view to dinuclear complexes [17]. So far and in the present study, the Cu(II) species are found reluctant to form molecular squares with carbohydrazones and thiocarbohydrazones. According to the thermodynamic analysis of self-assembly macrocyclization, desired macrocyclic products exist as major species only within a limited range of concentration under certain reaction conditions. In order to accomplish self-assembly already at low concentration, the coordinative bonds should exhibit considerable

thermodynamic stability. To achieve this, the binding constant (and the related Gibbs free energy) for the respective monotopic model building blocks should be high and also the square macrocycles should be free of strain [18]. Jahn Teller distortions of octahedral geometry, rigidity of carbohydrazones and thiocarbohydrazones, etc may also be behind the reluctance of Cu(II) towards self-assembly.

Maubaraki *et al.* [11] have reported the synthesis of binuclear Cu(II) compounds of bis(pyridine-2-aldehyde) thiocarbohydrazone in acid medium by stirring and their selective elimination of N, N, N coordinated copper in appropriate ethanolic mineral acids to form mononuclear complexes. In our study, the dibasic ligands are found to be deprotonated under neutral conditions itself, and resulted in metal complexes with ligand to metal ratio 1:2, coordinating first Cu(II) through thiolate sulfur (or enolate oxygen for carbohydrazones), azomethine N and pyridyl or quinolyl N. The binding atoms to second metal involve the azomethine N and pyridyl or quinolyl N of the remaining half of ligands: usually, the imine nitrogen of the first half of ligand acts as the third coordinating atom. The second copper can be coordinated by the NNS/ NNO mode also to form symmetric dicopper complex through sulfur/oxygen bridging. However, for the present complexes the spectroscopic data are more consistent with asymmetric dicopper complexes, as would be expected primarily. Unfortunately, we could not get any X-ray quality single crystals of any of the copper complexes for confirming the exact coordination. The coordination mode towards Cu(II) is flexible, and thus, the final assemblies are less predictable. In the majority of cases the NNS/NNO and NNN coordination modes of (thio)carbohydrazones are seen, and the only one crystal study of a Cu(II) carbohydrazone [17] agree with NNO and NNN coordination.

The complexes prepared were either green or dark brown in color. All the complexes were found to be soluble in DMF and DMSO, but only partially soluble in other organic solvents such as CHCl₃, ethanol, methanol etc. The variable temperature magnetic susceptibility measurements of all complexes show antiferromagnetic

interactions between the Cu(II) centers. The room temperature magnetic moment and antiferromagnetic interactions rule out the possibility of tetranuclear grid formation, as there is such a possibility also for the complexes. For example, the possibility of molecular formula of **9** as $[CuH_2L^2]_4(ClO_4)_8 \cdot 3CHCl_3 \cdot 4H_2O$ will lead to a room temperature magnetic moment of 5.2 μ_B, which is unreasonably high to the expected spin only magnetic moment of $(\sum 4Si(Si+1))^{\frac{1}{2}} = 3.46$ μ_B for a system having four independent Cu(II) species. Complex **9** was assigned with four Cu(II) atoms coordinated within the coordination pockets of two doubly deprotonated thiocarbohydrazone ligands H_2L^2. The complex **8** was synthesized by equimolar reaction between H_2L^1 and metal salt in methanol solution, but resulted into a product of 3:2 metal ligand ratio. The formation of carbohydrazone complex **13** was found to be distinctive as there is a report for similar reaction conditions for H_2L^5 with $CuCl_2$ resulted a degradation of -CO- group and cyclization to form a copper complex of 3-phenyltriazolo[1,5-a]-pyridine [11]. However we could synthesize the chloride complex of H_2L^4, compound **13**, and found to undergo degradation only in solutions at lower concentration on exposure to air. Instead of an expected bimetallic complex, the compound **13** was formed with three Cu(II) centers. The complex **17** was synthesized by metathetical displacement of acetate ions of the metal salt with azide ions.

The molecular formula of all the Cu(II) complexes were tentatively assigned by considering spectral, magnetic and conductance studies with agreeing elemental analysis results. The existence of other possibilities, however, was not excluded for all compounds on characterization. The TGA data of complex **14** shows a loss of six water molecules (12.4%) within the temperature range 40-112 °C and then the loss of one molecule of water (2%) in the range 112-210 °C. However at 247 °C the complex had undergone an outburst. The TGA studies of other compounds are therefore not carried out, to locate the water molecules, and so the positions of water molecules were tentatively assigned. Molar conductance studies are found useful to assign the

exact position of anions [19]. The tentative structures of complexes are shown in Schemes 4.1. to 4.5.
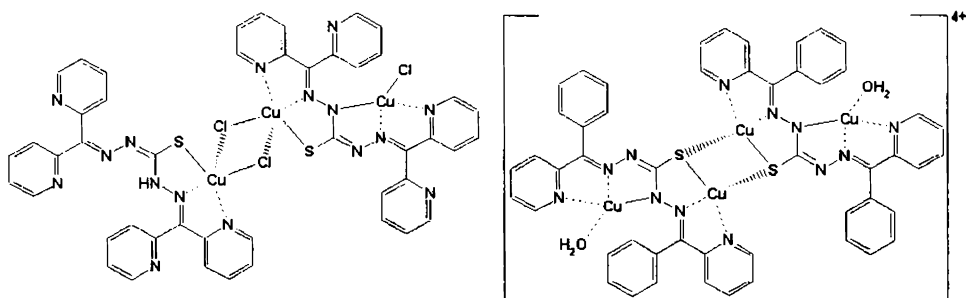
Scheme 4.1. The tentative structures of complexes **8** (left) and **9** (right).
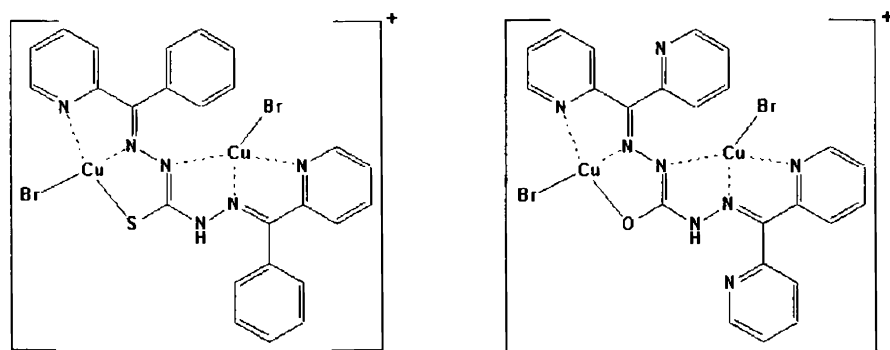
Scheme 4.2. The tentative structures of Cu(II) complexes **10** (left) and **15** (right).
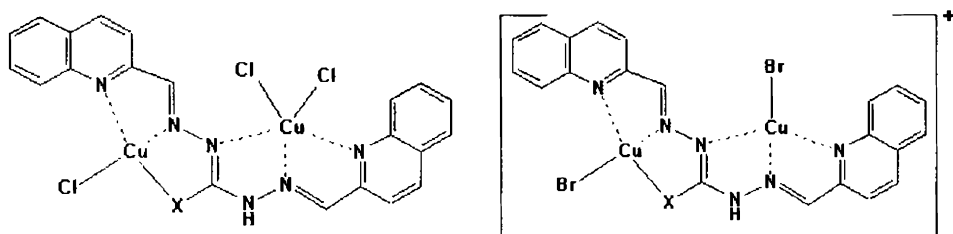
Scheme 4.3. The tentative structures of Cu(II) complexes **11** and **18** (left) and **12** and **19** (right). X= S for **11** and **12**. X= O for **18** and **19**.
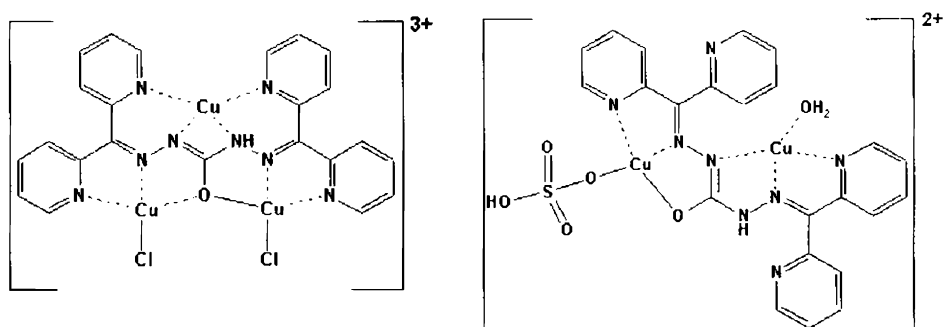
Scheme 4.4. The tentative structures of Cu(II) carbohydrazone complexes **13** (left) and **14** (right).
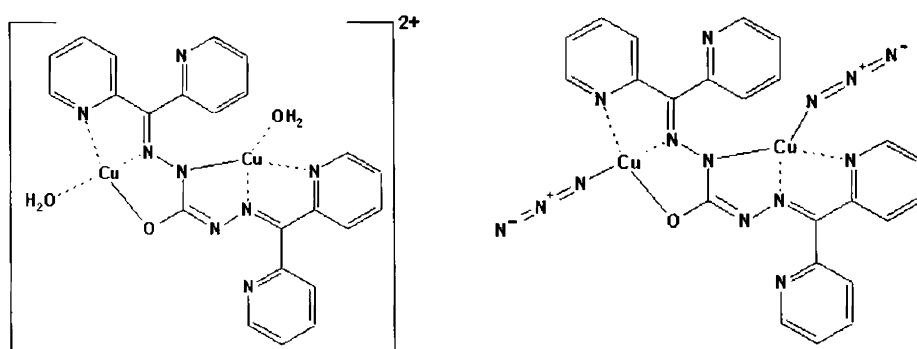
Scheme 4.5. The tentative structures of Cu(II) carbohydrazone complexes **16** (left) and **17** (right).

4.3.1. MALDI MS spectral features

The MALDI MS spectra of Cu(II) complexes show some similar features and are different from stable molecular square grid complexes. Though molecular ions could not be observed for all compounds, sensible fragments were observed. This was not surprising as the structure and stability of coordination complexes under ionization conditions are dependent on various factors like the ligand itself, metal ions, counter ions, solvent, temperature, concentration, etc. However, the [Cu(HL)]⁺ fragment was readily observed in all cases. MALDI mass spectra of all the complexes were taken in CH₂Cl₂ as DCTB mix on positive ion mode. The application of MALDI to cluster

compounds has been very limited as aggregation process may arise from ion-molecule reactions in the gas phase to complicate the spectra sometimes [20].

The complex **8** exhibits peaks centered at m/z 501.1, 467.1, 445.2, 405.2, etc (Fig. 4.1.). The peak at 501.1 assigned as $[Cu(HL^1)]^+$ (calc. 500) and at 467.1 as $[Cu(HL^1)-SH]^+$ (calc. 468) agreeing with calculated isotropic distribution patterns.
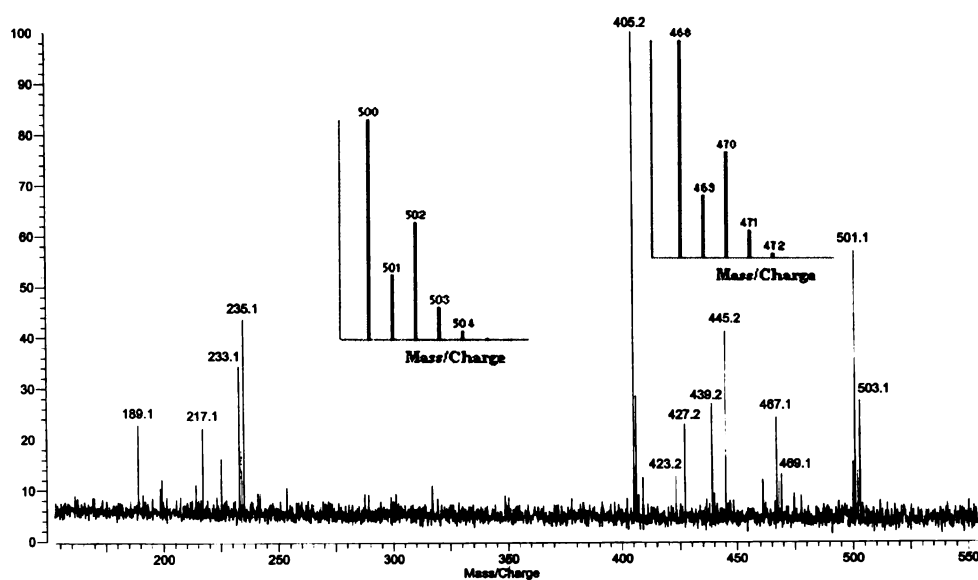
Fig. 4.1. MALDI MS spectrum of **8**. Insets are calculated isotropic patterns.

The compound **9** shows peaks centered at m/z 1219, 1123, 1061, 998, 935, 561, 499, etc (Fig. 4.2). The very low intense peak at 1219 may be of the species $[Cu_4L^2_2(ClO_4)-2H^+]^+$ (calc. 1220). Other major peaks are assigned as $[Cu_2L^2(HL^2) \cdot CH_3OH \cdot H_2O]^+$ (calc. 1061), $[Cu_2L^2(HL^2)]^+$ (calc. 997), $[Cu(H_2L^2)HL^2]^+$ (calc. 934), $[Cu_2L^2-H^+]^+$ (calc. 559). The base peak corresponds to $[Cu(HL^2)]^+$ (calc. 498). All these are in well agreement with simulation (Fig. 4.3) and are characteristic peaks for the compound which assigned as molecular formula $[Cu_4L^2_2 \cdot 2H_2O](ClO_4)_4$.
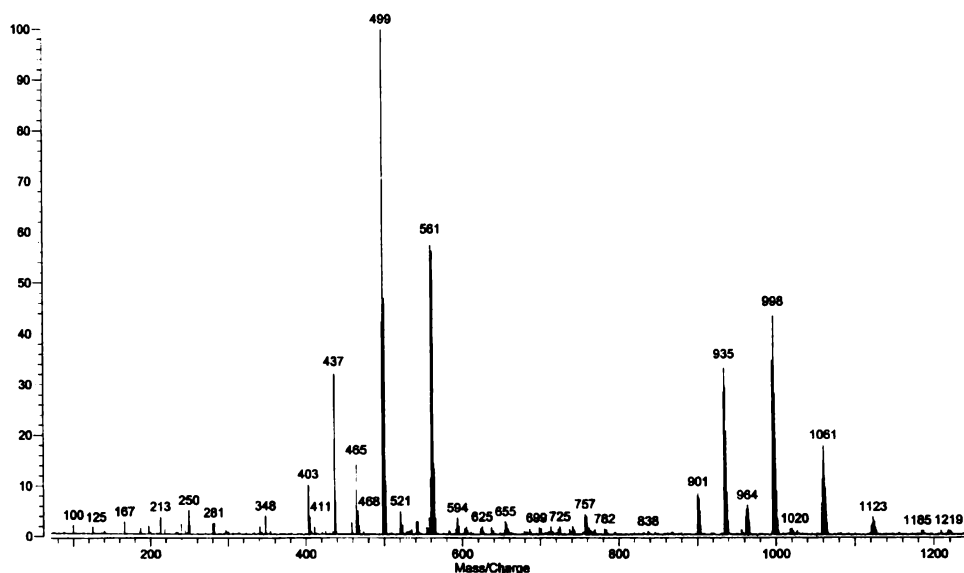
Fig. 4.2. The MALDI MS spectrum of tetranuclear copper(II) compound **9**.
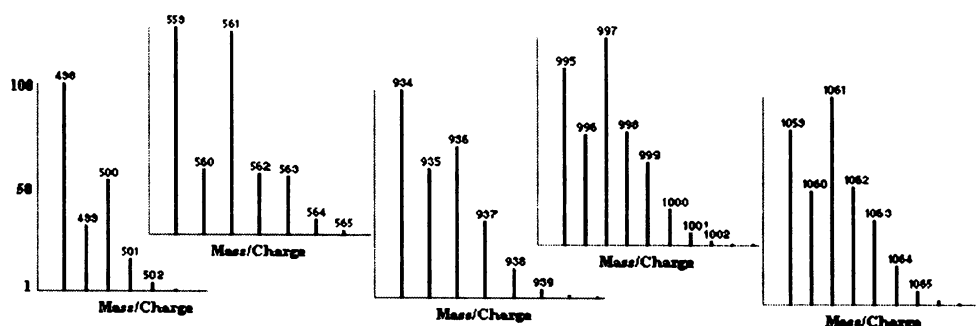
Fig. 4.3. Calculated agreeing distribution patterns of main mass peaks of **9**.

The mass spectrum of **10** is given in Fig. 4.4. The peaks centered at m/z 641.8, 560.9 and base peak 498 are assigned as $[Cu_2L^2Br]^+$ (calc. 641), $[Cu_2L^2-H^+]^+$ (calc. 559) and $[Cu(HL^2)]^+$ (calc. 498) are in well agreement with simulation. Of the other weaker peaks, m/z 785.6 corresponds to $[Cu_3L^2Br_2-H^+]^+$ (calc. 784) may be formed under ionization condition by the coordination of one copper to the species $[Cu_2L^2Br]^+$.

137
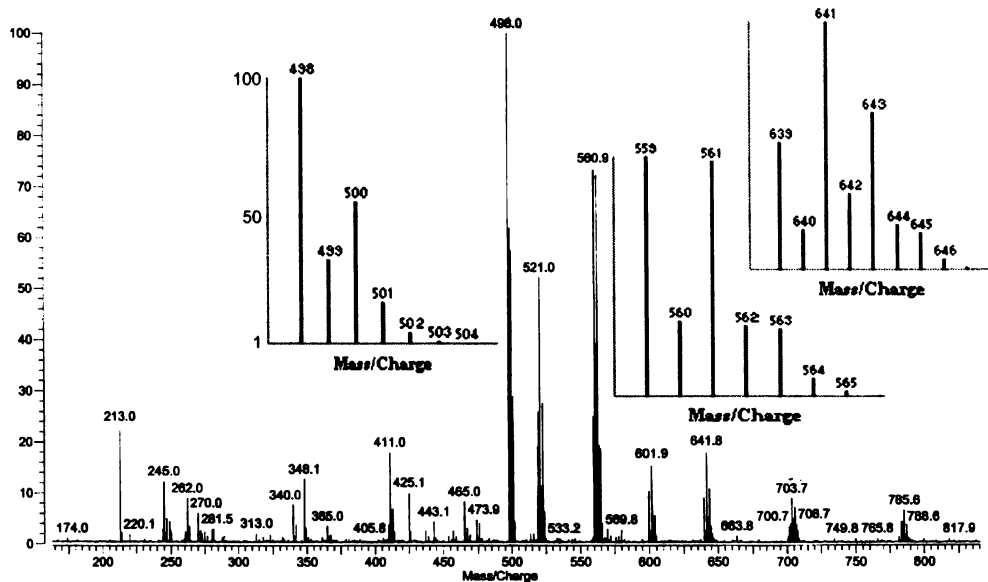
Fig. 4.4. MALDI MS spectrum of complex **10**. Insets are calculated isotropic distribution patterns of main peaks.

The spectrum of Cu(II) thiocarbohydrazone complex **11** exhibits peaks centered at m/z 831, 447, 385, etc. The peak at 447 corresponds to $[Cu(HL^3)]^+$ (calc. 446) and is in agreement with calculated isotropic distribution (Fig. 4.5). The base peak at 385 is of the free ligand H_2L^3 and weaker peak at 831 is assigned as $[Cu(HL^3)(H_2L^3)]^+$ (calc. 830), may be formed under MALDI conditions. The spectrum of **12** shows m/z 447 as base peak, which corresponds to $[Cu(HL^3)]^+$ (calc. 446) and the peak at 413 corresponds to $[Cu(HL^3)-SH]^+$ (calc. 414), both are in agreement with calculated isotropic patterns. The spectrum of complex **12** with calculated isotropic patterns are given in Fig. 4.6.
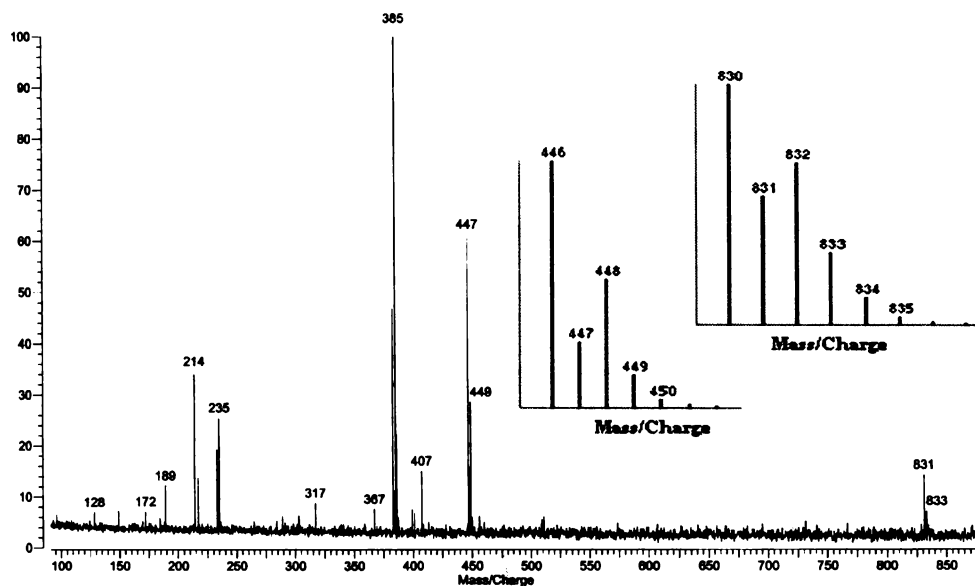
Fig. 4.5. MALDI MS spectrum of compound **11**. Insets are calculated isotropic distribution patterns.
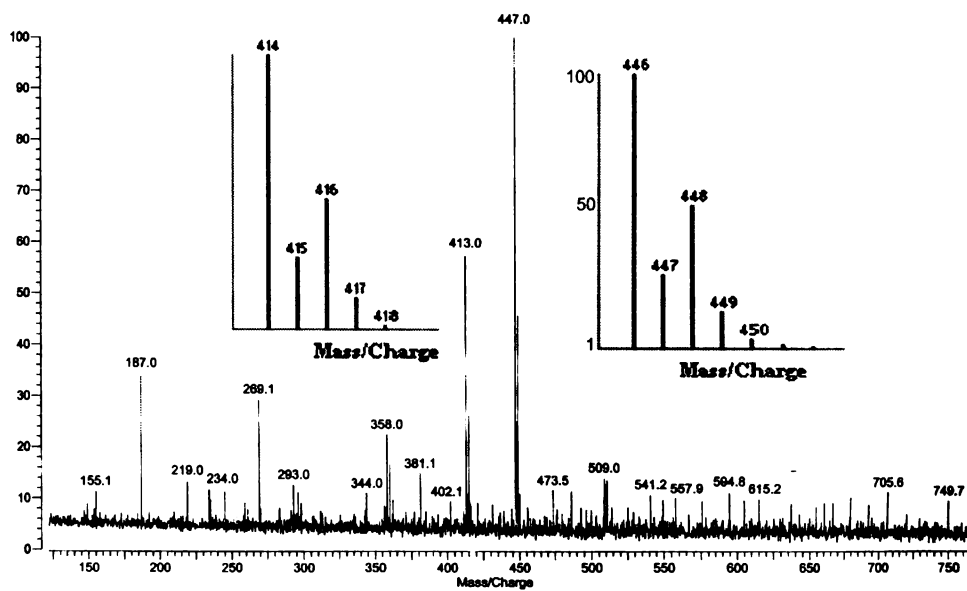
Fig. 4.6. MALDI MS spectrum of **12**. Insets are calculated isotropic patterns of main peaks.

The spectrum of Cu(II) carbohydrazone complex **13** is as shown in Fig. 4.7. The base peak centered at m/z 485 is assigned as $[Cu(HL^4)]^+$ (calc. 484) and another major peak at 423 is assigned as that of the free ligand and their coordinated species, may be formed under MALDI ionization condition, is seen as a weaker peak at 907 corresponding $[Cu(HL^4)(H_2L^4)]^+$ (calc. 906).
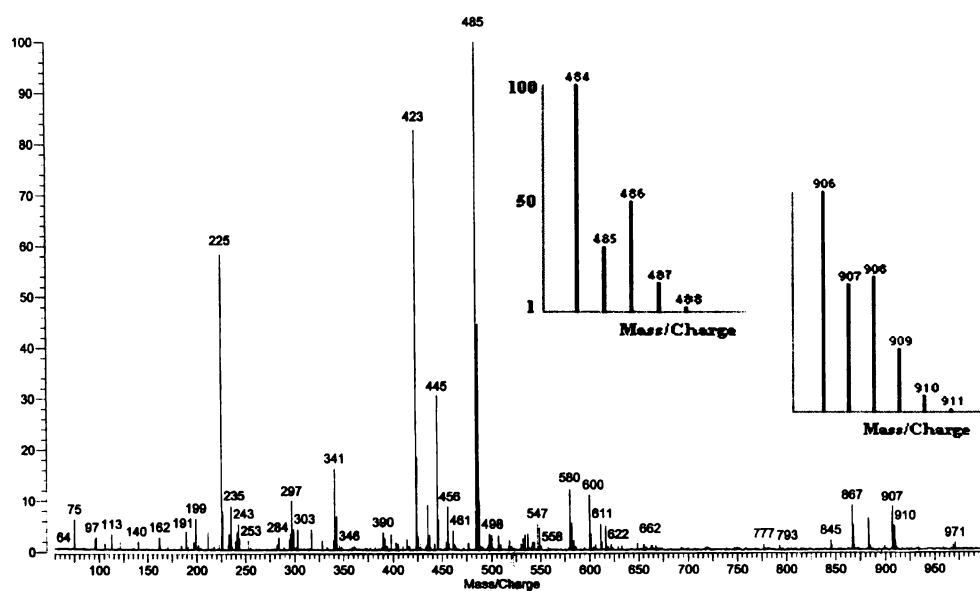
Fig. 4.7. MALDI MS spectrum of compound **13**. Insets are calculated isotropic distribution patterns.

The spectra of complexes **14** to **17** are found not good enough to get characteristic peaks. This is attributed to the less stability of these carbohydrazone copper complexes in solution and/or under the condition of MALDI. A very weak peak centered at 567 is assigned to $[Cu(H_2L^4)Br]^+$ (calc. 566) for compound **15** (Fig. 4.8).

The base peak of **18** and **19** at m/z 369 are of the free ligand H_2L^6. The spectrum of **18** (Fig. 4.9) exhibits a characteristic peak at 431 $[Cu(HL^6)]^+$ (calc. 430) and a new coordinated species at 799 $[Cu(HL^6)(H_2L^6)]^+$ (calc. 798) as weaker peak.
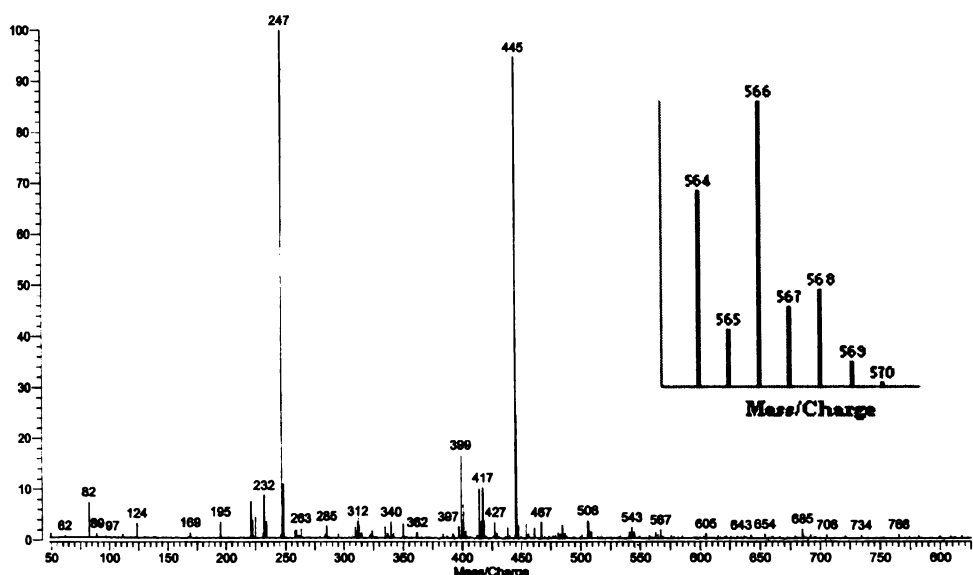
Fig. 4.8. MALDI MS spectrum of Cu(II) complex **15**. Inset is calculated isotropic distribution pattern of weak peak centered at 567.
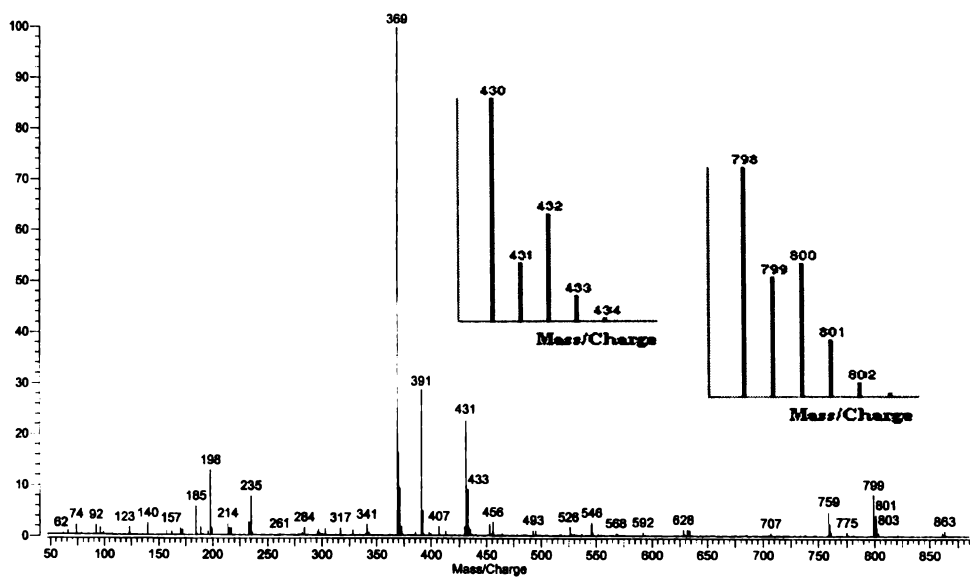
Fig. 4.9. MALDI MS spectrum of complex **18**. Insets are calculated isotropic distribution patterns.

4.3.2. IR spectral studies

IR spectral study, very useful for mononuclear or dinuclear metal complexes, are found useful to assign various coordination modes of flexible ligands viz carbohydrazones and thiocarbohydrazones towards copper centers to some extend. It was found that some significant changes and differences in mixing patterns of common group frequencies of complexes compared to their respective metal free ligands, and are attributed to the coordination to metal centers. Though the spectra in the IR and far IR region is rich with bands, tentative assignments of bands of Cu(II) complexes were made and are listed in Tables 4.1 and 4.2.

Most of the compounds reveal a band at ~3200 cm^{-1}, along with a broad band at ~3400 cm^{-1} corresponding to the lattice water, attributed to free N–H vibrations and confirm the coordination still leaves one free –NH group. For the carbohydrazone complexes absence of bands at ~1700 cm^{-1} and new v(C–O) bands at ~1300 cm^{-1} indicate the coordination through enolate form after deprotonation. This is similar to the frequency shifts seen with the thiocarbohydrazone copper complexes **8** to **12**, where new v(C–S) bands are seen in the range 1100 to 1148 cm^{-1}. Absence of bands at ~2600 cm^{-1} for thiocarbohydrazone complexes are indicative of absence of thiol tautomers in free or coordinated form in these complexes [16]. The sulfur coordination is supported by the evidences of strong bands seen in the range 320 to 349 cm^{-1} of v(Cu–S) for complexes **8** to **12**, while oxygen coordination is clear as the presence of strong bands in the range 344 to 390 cm^{-1} assigned v(Cu–O) [21] for complexes **13** to **19**. The differences in mixing patterns of C–N and N–N groups of complexes compared to their respective metal free ligands may be attributed to possible azomethine coordination. Also, the bands in the range 408-425 cm^{-1}, assigned to the v(Cu–N$_{azo}$) band [22] also support the azomethine nitrogen coordination in all complexes. The pyridyl or quinolyl coordination is supported by the bands in the range 255-298 cm^{-1}, consistent with the v(Cu-N$_{py}$) [23]. However it is not possible to

confirm the position of coordination explicitly from IR results alone. Single crystal X-ray studies can only confirm the exact coordination for these kinds of complexes.

The perchlorate complex **9** shows strong bands at 1100 and 626 cm^{-1}, while complex **16** show broad bands at 1060-1140 and strong bands at 623 cm^{-1} indicating the presence of ionic perchlorate. The bands at ~1100 cm^{-1} are assignable to $v_3(ClO_4)$ and the unsplit bands at ~625 cm^{-1} assigned to $v_4(ClO_4)$. For both the compounds, very weak bands at 938 cm^{-1} may be due to $v_1(ClO_4)$ suggesting that ionic perchlorate is distorted from tetrahedral symmetry due to lattice effects or hydrogen bonding by the NH functions of the coordinated ligand [24]. This along with unsplit v_3 and v_4 bands show exclusive presence of non-coordinated perchlorate group [25]. For sulphato complex **14** very strong bands seen at 1110-1145 and 616 cm^{-1} are assigned v_3 and $v_4(SO_4)$, and a medium band at 976 cm^{-1} $v_1(SO_4)$ are indicative of the presence of T_d sulphate ions [22]. For the azido complex **17**, a broad band at 2051 is assigned as asymmetric stretching of coordinated azido group [22]. The broadness may be due to the presence of second azide group. A strong band at 1240 cm^{-1} may be attributed to symmetric stretching band of coordinated azido groups. Also the weak band at 640 cm^{-1} may be of $\delta(NNN)$. The far IR spectrum also supports this assignment as the $v(Cu-N_{azide})$ vibration is seen at 420 cm^{-1}.

The far IR spectra of complexes are found interesting and worth to support the metal ligand coordination modes. The spectrum of compound **8** shows strong bands at 320 and 161 cm^{-1}, $v(Cu-Cl)$ terminal and bridging modes [25-27], indicating bridging character in the Cu–Cl bond. However for the other chloro compounds **11**, **13** and **18** only terminal $v(Cu-Cl)$ band is observed at 304, 304 and 329 cm^{-1} respectively. Also no bands at ~160 cm^{-1} corresponding to the bridging $v(Cu-Cl)$ are found for these complexes. The $v(Cu-Br)$ frequency of **12**, **15** and **19** are observed at 240 cm^{-1}, while that of **10** is seen at 238 cm^{-1}, consistent with the terminal bromo ligand [22,26,27]. Selected IR and far IR spectra are given in Figs. 4.10 to 4.15.

Table 4.1. IR spectral assignments of Cu(II) complexes (cm⁻¹).

c.	νH₂O	νN-H	νC-H	νC=N+νC=C	νC-N/ νHeterocyclic	νC-S	νC-O	νN-N
8	3409br	3229sh	3054w	1583m, 1488s, 1455vs, 1422vs	1385s, 1282s	1100s		1236m, 1153m
9	3424br		3057m	1593s, 1493m, 1467s, 1407vs	1318s, 1296s	1142s		1207s
10	3338m	3581m	3062m	1591s, 1561vs, 1529s, 1466s, 1438s, 1410m	1330m, 1300s	1100s		1200m, 1152m
11	3440br	3205sh	3029w, 2965w	1585m, 1550m, 1510m, 1470m	1377m, 1315vs, 1251s	1148vs		1218vs, 1088s
12	3436br		3053m, 2920m	1618m, 1591m, 1552m, 1464s, 1413vs	1332vs, 1251m	1148vs		1215s, 1083s
13	3415br	3222sh	3052m	1562m, 1516s, 1480s, 1423s	1366s, 1274s, 1246s		1303vs	1172m, 1124vs
14	3408br	3220sh	3083sh	1597vs, 1562m, 1515m, 1473m, 1425m	1366m		1310s	1235s
15	3412br	3252sh	3062m	1602vs, 1567s, 1511s, 1474s, 1427s	1361s, 1237s		1307vs	1174m, 1124s
16	3421br		3070m	1597s, 1564s, 1514vs, 1464s	1371s, 1270s		1311vs	1240s
17			3058m	1593s, 1561s, 1498s, 1450s	1357m, 1336m		1285s	1172m, 1126s
18	3414br	3207sh	3048m, 2915m	1615m, 1583s, 1547m, 1512s, 1483s, 1448m	1385vs, 1345m		1296s	1245m, 1140vs
19	3432br	3212sh	3050m, 2926m	1605m, 1585vs, 1540m, 1515s, 1476s, 1445m	1378vs, 1355m		1294s	1240s, 1142vs

c. = compounds, br = broad, sh = shoulder, s = strong, vs = very strong, m = medium, w = weak.

Table 4.2. IR and far IR spectral assignments of Cu(II) complexes (cm⁻¹).

c.	vCu–Nazo	vCu–Npy/qu	vCu–S	vCu–O	vCu–X	δC–H	py/qu
8	409s	267s	337s		320s, 161s	990m, 973m, 871m, 791m, 738s	645s, 613m, 558m
9	415s	270s	320s			972m, 787m, 740m, 708s	652m, 476w, 413w
10	410s	270s	340m		238s	1024m, 973m, 794s, 743m, 710s	655m, 470m
11	408m	264m	349s		304m	886m, 824s, 784m, 751s	630w, 610m, 486m
12	411m	298s	349s		240s	989m, 949m, 886m, 814s, 784m, 754s	610m, 562w, 489m
13	413s	281s		384m	304s	1018m, 973m, 790s, 750s	674m, 626m, 518w
14	414s	275s		350s		790, 748m	610s, 570w
15	417s	274s		344s	240s	974m, 784vs, 744s	687s, 627s, 527m
16	415m	280m		379m		974m, 790s, 747s	671m, 624s, 504m
17	403s	259s		370s		967m, 790m, 743s,	676m, 620m, 509m, 484w
18	405m	255m		380m	329m	1040m, 986m, 938m, 878m, 829m, 772m, 742s	637m, 519m, 495m, 430m
19	425s	275s		390s	240s	1042m, 986m, 938m, 827m, 776m, 743s	635m, 517m, 494s, 431m

c. = compounds, br = broad, s = strong, vs = very strong, m = medium, w = weak. X = Cl for **8, 11, 13** and **18**. X = Br for **10, 12, 15** and **19**.
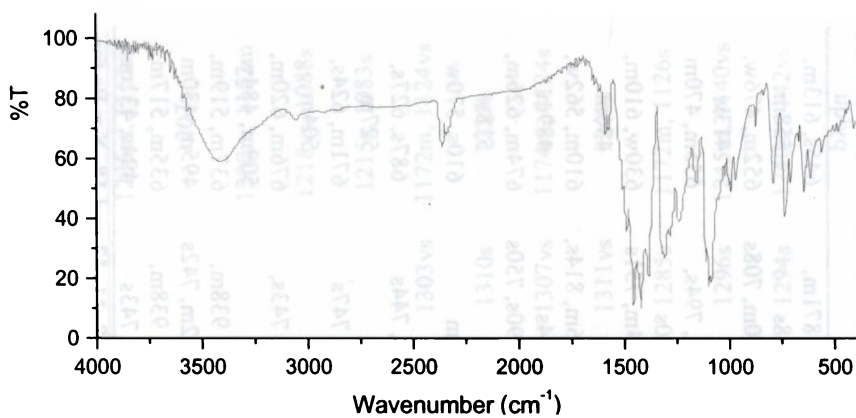
Fig. 4.10. IR spectrum of thiocarbohydrazone Cu(II) complex **8**.
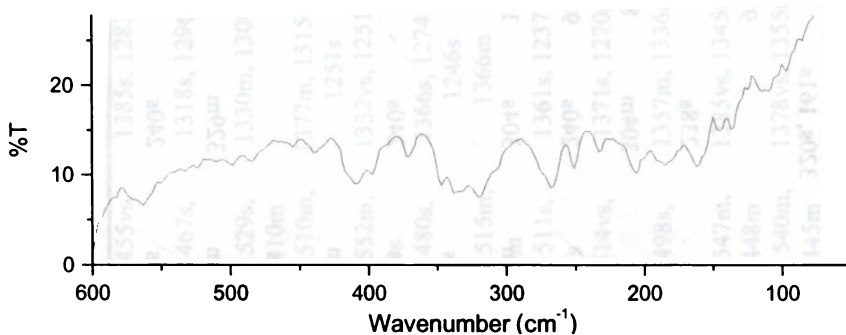
Fig. 4.11. Far IR spectrum of thiocarbohydrazone Cu(II) complex **8**.
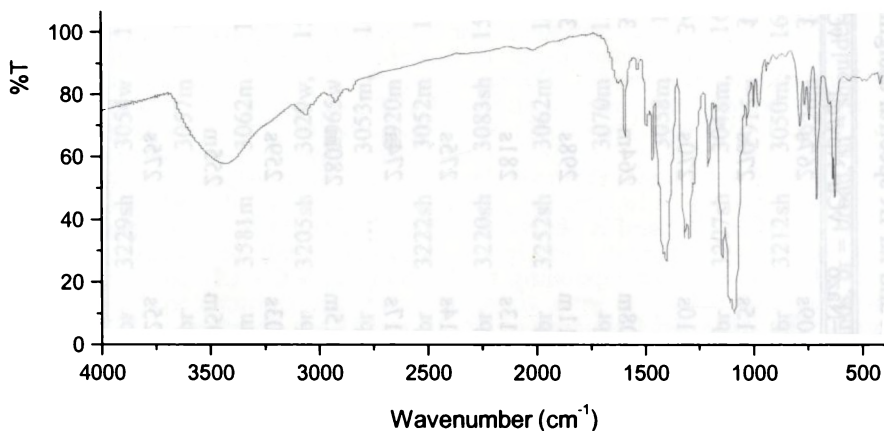
Fig. 4.12. IR spectrum of thiocarbohydrazone Cu(II) complex **9**.
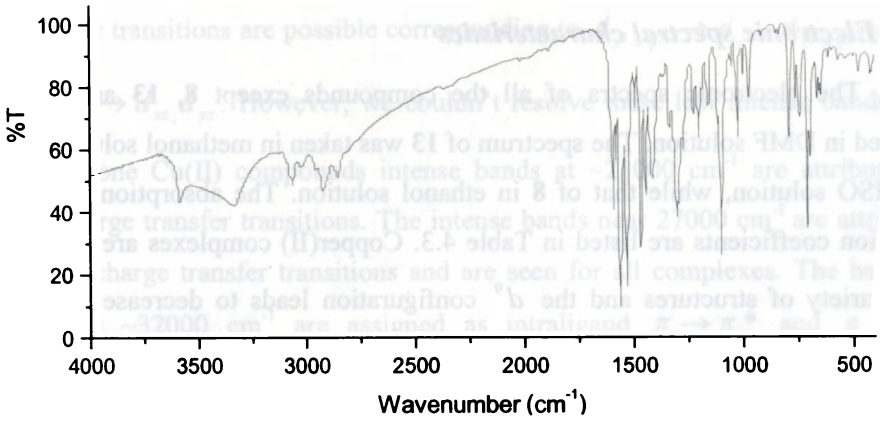
Fig. 4.13. IR spectrum of thiocarbohydrazone Cu(II) complex **10**.
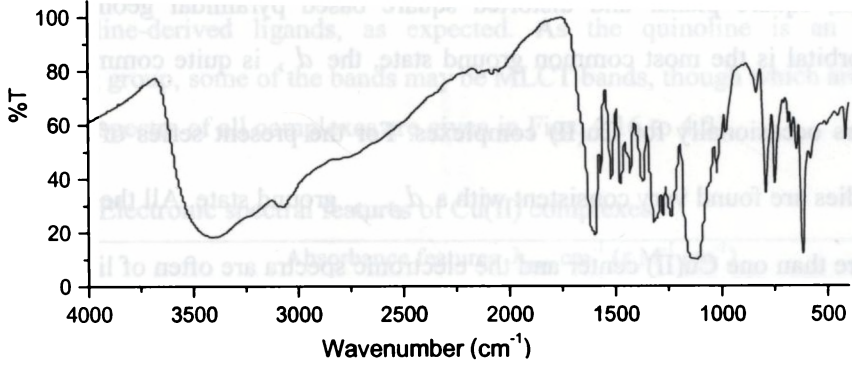
Fig. 4.14. IR spectrum of carbohydrazone Cu(II) complex **14**.
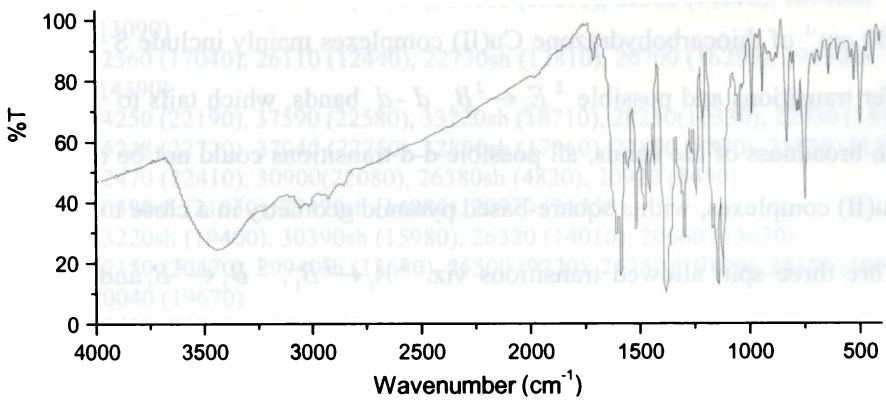
Fig. 4.15. IR spectrum of carbohydrazone Cu(II) complex **19**.

4.3.3. Electronic spectral characteristics

The electronic spectra of all the compounds except **8**, **13** and **14** were recorded in DMF solution. The spectrum of **13** was taken in methanol solution and **14** in DMSO solution, while that of **8** in ethanol solution. The absorption bands with extinction coefficients are listed in Table 4.3. Copper(II) complexes are known in a wide variety of structures and the d^9 configuration leads to decrease from cubic symmetries of environments around the Cu(II) ion and extensive Jahn Teller distortion results to more splitting in energy levels compared to that in typical coordination geometries. However, the expecting possibilities include tetragonal distorted octahedral, square planar and distorted square based pyramidal geometries. The $d_{x^2-y^2}$ orbital is the most common ground state, the d_{z^2} is quite common, and the d_{xy} occurs occasionally for Cu(II) complexes. For the present series of complexes, EPR studies are found very consistent with a $d_{x^2-y^2}$ ground state. All the compounds have more than one Cu(II) center and the electronic spectra are often of little value in structural assignment making difficult for identifying the geometry.

The electronic absorptions of carbohydrazone Cu(II) complexes (**13** to **19**) differ considerably from thiocarbohydrazone Cu(II) complexes. The intense bands at ~20000 cm^{-1} of thiocarbohydrazone Cu(II) complexes mainly include S $\rightarrow$ Cu charge transfer transitions and possible $^2E_1 \leftarrow ^2B_1$ d-d bands, which tails to ~17000 cm^{-1}. Due to broadness of the bands, all possible d-d transitions could not be resolved. For the Cu(II) complexes, with a square-based pyramid geometry in a close to C_{4v} group, there are three spin allowed transitions viz. $^2A_1 \leftarrow ^2B_1$, $^2B_2 \leftarrow ^2B_1$ and $^2E_1 \leftarrow ^2B_1$, usually very difficult to resolve them into separate bands due to the very low energy difference between these bands. For a square planar geometry with $d_{x^2-y^2}$ ground

state, similar transitions are possible corresponding to $d_{x^2-y^2} \rightarrow d_{z^2}$, $d_{x^2-y^2} \rightarrow d_{xy}$

and $d_{x^2-y^2} \rightarrow d_{xz}, d_{yz}$. However, we couldn't resolve these low intense bands. For

carbohydrazone Cu(II) compounds intense bands at ~21000 cm^{-1} are attributed to

O$\rightarrow$Cu charge transfer transitions. The intense bands near 27000 cm^{-1} are attributed

to N$\rightarrow$Cu charge transfer transitions and are seen for all complexes. The bands at

~44000 and ~32000 cm^{-1} are assigned as intraligand $\pi \rightarrow \pi^*$ and $n \rightarrow \pi^*$

transitions of complexes, suffered marginal shift from that of their corresponding free

ligands. However some charge transfer bands may also be present in this region for

Cu(II) complexes [28]. Also, many intraligand transitions are observed in complexes

with quinoline-derived ligands, as expected. As the quinoline is an electron

delocalizing group, some of the bands may be MLCT bands, though which are hard to

assign. The spectra of all complexes are given in Figs. 4.16 to 4.21.

Table 4.3. Electronic spectral features of Cu(II) complexes.

Compds	Absorbance features λ_{max} cm^{-1} (ε M^{-1} cm^{-1})
8	45660, 37170, 30770, 24690sh, 22075, 19010sh
9	36500 (8900), 29760 (6560), 21830sh (8100), 18940 (10760)
10	35970 (18370), 29070 (15500), 27100sh (13090), 20640sh (21120), 18730 (24930)
11	33560sh (14950), 31850 (15010), 26180 (13270), 20580 (14970), 18940sh (13090)
12	32360 (17040), 26110 (12440), 22730sh (13810), 20700 (16280), 19050sh (14390)
13	44250 (22190), 37590 (22580), 33220sh (18710), 28250(10330), 22030 (15160)
14	45248 (22720), 37040 (22750), 32890sh (17360), 27850 (8870), 21830 (11590).
15	32470 (22410), 30900(22080), 26380sh (4820), 20920 (8450)
16	30390sh (21050), 27470sh (14880), 20920 (21550)
17	33220sh (19400), 30390sh (15980), 26320 (14010), 20660 (13620)
18	32150 (20470), 29940sh (13640), 26500 (9720), 25250 (10190), 24150 (10600), 20040 (19670)
19	32890 (23230), 29940sh (16630), 26670 (13470), 25250 (13910), 23810sh (14180), 21100 (20940), 20040sh (18580)
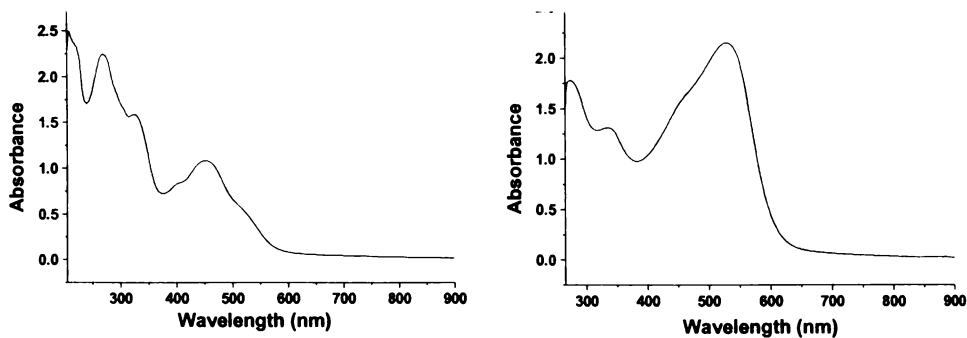
Fig. 4.16. Electronic spectra of Cu(II) thiocarbohydrazone complexes **8** in ethanol (left) and **9** in 2×10^{-4} M DMF (right).
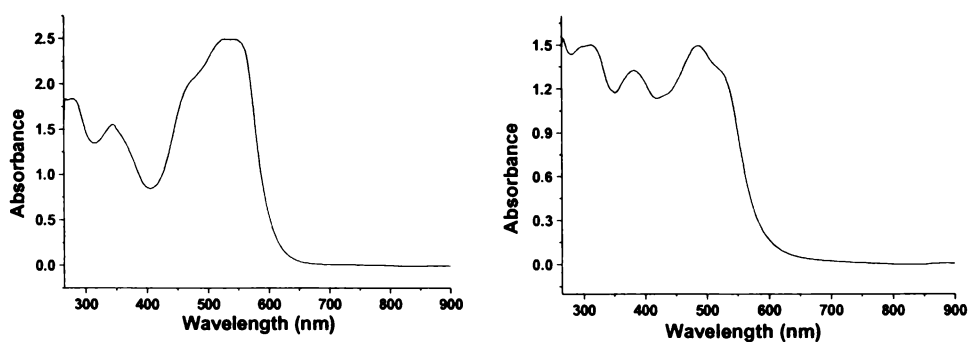
Fig. 4.17. Electronic spectra of Cu(II) thiocarbohydrazone complexes **10** (left) and **11** (right) in 10^{-4} M DMF.
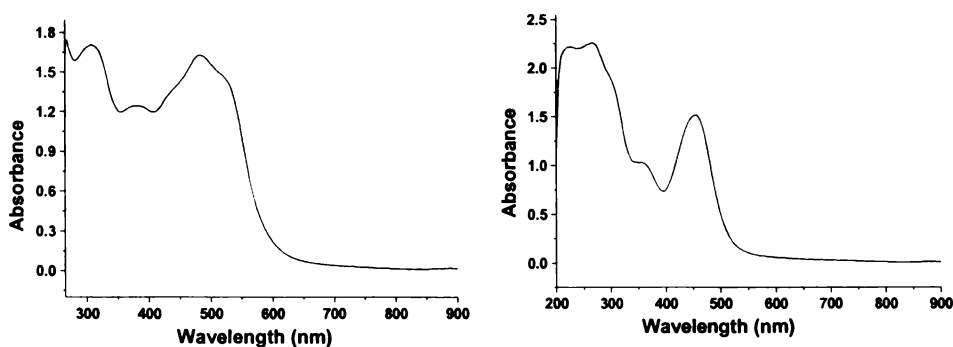
Fig. 4.18. Electronic spectra of complexes **12** in 10^{-4} M DMF (left) and **13** in 10^{-4} M methanol (right).
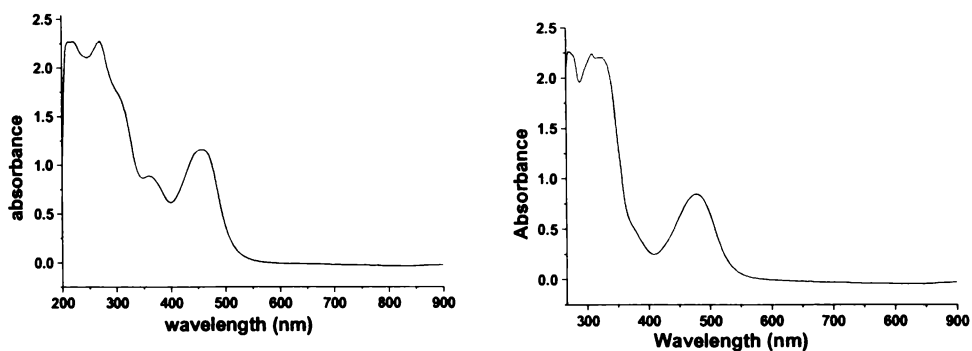
Fig. 4.19. Electronic spectra of Cu(II) carbohydrazone complexes **14** in 10⁻⁴ M DMSO (left) **15** in 10⁻⁴ M DMF (right).
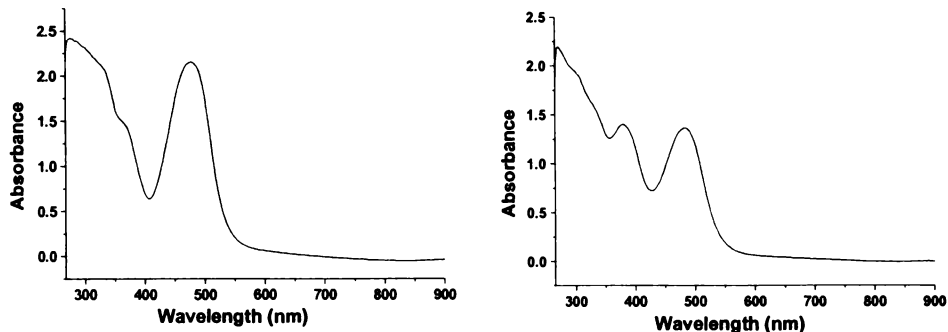
Fig. 4.20. Electronic spectra of Cu(II) carbohydrazone complexes **16** (left) and **17** in 10⁻⁴ M DMF (right).
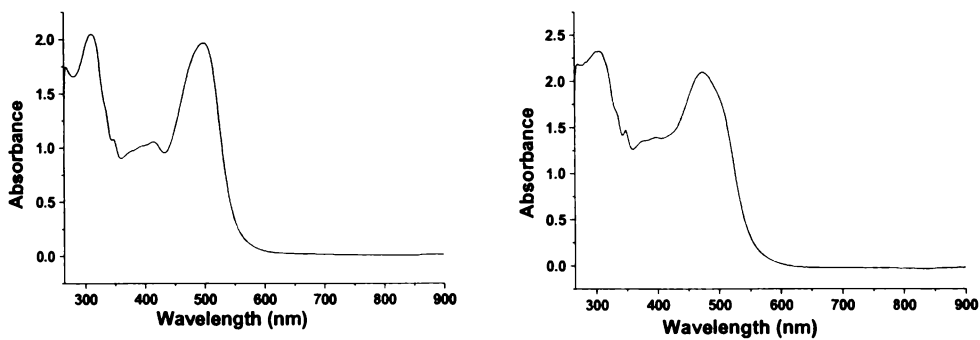
Fig. 4.21. Electronic spectra of Cu(II) carbohydrazone complexes **18** (left) and **19** in 10⁻⁴ M DMF (right).

151

4.3.4. EPR spectral studies

The EPR spectra of all the complexes in frozen DMF solutions at 77 K were recorded in the X-band using a cw EPR spectrometer. All compounds under the investigation condition exhibit signals characteristics of uncoupled Cu(II) species at ~3300 G and not showed signals typical for coupled binuclear complexes. The binuclear complex is connected with the antiferromagnetic coupling of two Cu(II) ions, leading to a singlet ground state and an excited spin triplet state. For a coupled system of two Cu(II) species equally distributed seven hyperfine features (2nI+1; n=2 and I=3/2) are expected. However none of the frozen solution spectra show this feature and half field signals, and the computer simulation of most of the compounds is in good agreement with the presence of two uncoupled Cu(II) species. This frozen DMF features are in contradiction with the solid-state magnetic studies, is attributed to the possible fragmentation in DMF at low concentrations. Absence of any half-field signals in solution for all the compounds may be due to the absence of any considerable Cu–Cu interactions, and might be due to the absence of enough intensity. Another possibility is the dissociation of dinuclear to mononuclear copper compounds and presence of an equilibrium mixture with greater monomer percentage. The EPR spectra of binuclear compounds are reported to dissociate to yield a series of mononuclear species, depending upon concentration [29].

The copper (II) ion, with a $3d^9$ configuration, has an effective spin of S = ½ and is associated with a spin angular momentum, m_s = ±½, leading to a doubly degenerate spin state in the absence of a magnetic field. In a magnetic field the degeneracy is lifted between these states and the energy difference between them is given by $E = h\nu = g\beta B$, where h is Planck's constant, ν is the frequency, g is the Lande splitting factor (equal to 2.0023 for a free electron), β is the Bohr magneton and B is the magnetic field. The appropriate axially symmetric spin Hamiltonian [30,31] is then given by,

$$\hat{H} = g_{\parallel}\beta B_z S_z + g_{\perp}\beta(B_x S_x + B_y S_y) + A_{\parallel}S_z I_z + A_{\perp}(S_x I_x + S_y I_y) \quad (1)$$

The formation of a binuclear complex is connected with the antiferromagnetic coupling of two Cu(II) ions, leading to a singlet ground state and an excited spin triplet state. The energy difference, $2J$, between these states depends on the strength of the interaction. If the triplet state is thermally accessible ($2J \sim kT \sim 200\text{--}400$ cm^{-1}), paramagnetism is observed and the EPR spectra could be satisfactorily described using the interactive spin Hamiltonian [32] for isolated Cu(II) dimer (S =1),

$$\hat{H} = g\beta BS + DS_z^2 + E(S_x^2 - S_y^2) - \tfrac{2D}{3} \quad (2)$$

Where D and E are the zero field splitting parameters.

However, the present spectra all indicate the presence of two different Cu(II) species and there are no characteristic features of transfer of any coupling between the two Cu(II) centers by the bridging moiety connecting them in frozen DMF. So the spectra were simulated by considering with the presence of two noninteracting Cu(II) d^9 groups using EasySpin [33] written in MATLAB to get accurate values of various EPR parameters $g_{\parallel}$, $g_{\perp}$, $A_{\parallel}$ (Cu), $A_{\perp}$ (Cu). The systems with the presence of two Cu(II) species, each species described by eqn. (3) [34], were considered; as the spectra all not showed typical coupled binuclear nature but show two monomeric axial species.

$$\hat{H}_0 = \beta_e \widetilde{B}_0 gS + \widetilde{S}A^{Cu}I \quad (3)$$

Where the first term is the electron Zeeman interaction with the external magnetic field vector B_0 and the second term represents the hyperfine interaction between the electron spin S and the nuclear spin I of the copper nucleus. The g and A matrices in eqn. (3) are assumed to be axially symmetric and coaxial, so that eqn. (3) is similar to eqn. (1). The various magnetic interaction parameters obtained by simulations are summarized in Table 4.4 for compounds **8** to **19**.

Table 4.4. EPR spectral parameters of the copper(II) complexes in frozen DMF solutions.

Compds.	Species	$g_\parallel$	$g_\perp$	$A_\parallel$ (Cu) cm^{-1} (10^{-4})	$A_\perp$ (Cu) cm^{-1} (10^{-4})	G	Species g_{av}	$g_{av.}$	α^2	f
8	A	2.226	2.049	175.12	20.01	4.79	2.108	2.1	0.7702	127.11
	B	2.186	2.045	166.78	18.35	4.30	2.092		0.7052	131.07
9	A	2.185	2.061	191.79	25.01	3.11	2.102	2.145	0.7806	113.93
	B	2.391	2.085	135.09	13.34	4.70	2.187		0.8394	176.99
10	A	2.392	2.085	133.43	10.01	4.71	2.183	2.185	0.8358	179.27
	B	2.392	2.078	133.43	10.01	5.14	2.187		0.8328	179.27
11	A	2.392	2.080	133.43	10.01	5.01	2.184	2.144	0.8336	179.27
	B	2.147	2.082	120.08	10.01	1.81	2.104		0.5524	178.79
12	A	2.391	2.080	133.43	10.01	5.00	2.184	2.137	0.8326	179.19
	B	2.123	2.074	113.41	8.34	1.68	2.090		0.5066	187.19
13		2.078								
14	A	2.244	2.051	186.68	20.01	4.96	2.115	2.129	0.8211	120.21
	B	2.296	2.066	175.12	13.34	4.61	2.143		0.8474	131.11
15	A	2.310	2.075	163.45	16.68	4.23	2.153	2.142	0.8329	141.33
	B	2.254	2.070	176.79	20.01	3.72	2.131		0.8117	127.49
16		2.0955								
17	A	2.257	2.054	145.1	16.68	4.93	2.122	2.121	0.7199	155.55
	B	2.244	2.050	173.45	26.68	5.07	2.119		0.7839	129.37
18	A	2.392	2.0801	133.43	10.01	5.01	2.184	2.175	0.8337	179.27
	B	2.352	2.0711	146.77	13.34	5.08	2.165		0.8269	160.25
19	A	2.391	2.0845	135.09	6.67	4.73	2.187	2.179	0.8391	176.99
	B	2.352	2.0803	146.77	8.34	4.48	2.171		0.8308	160.25

The spectrum of an uncoupled Cu(II) species is expected to show clearly four well resolved hyperfine lines, due to the interaction of the electron spin with the copper nuclear spin (^{65}Cu, I=3/2) corresponding to M_I = -3/2, - 1/2, 1/2, 3/2 transitions (ΔM_s = ±1), need not show well resolved lines if another Cu(II) species is present, eventhough there are no interactions taking place. The spectrum of such a sample is expected to show a resultant combination depending on the g values and their intensities of each species.

In the dissolved frozen state at 77 K in a suitable solvent, usually, the intermolecular interactions are reduced, and the EPR spectrum normally is expected to exhibit appreciable hyperfine interactions for a Cu(II) center. The hyperfine splitting, $A_{\perp}$ arising from the nuclear magnetic moment of the Cu(II) at $g_{\perp}$ is usually very small so that this feature of the spectrum often shows no splitting. On the other hand, $A_{\parallel}$ the nuclear hyperfine splitting at $g_{\parallel}$ is usually much larger and the four features at $g_{\parallel}$ are often resolved. It is the magnitude of $A_{\parallel}$ and $g_{\parallel}$ which are dependent, among other things, on the nature of the ligands of Cu(II), and these values can often be used to assign structure. It has been suggested that the smaller value of $A_{\parallel}$ arises from a distortion of a copper site away from planarity [35]. The hyperfine spacing are more or less twice than that for dimers indicating the complex under investigation behaves like localized electrons [36] in each copper(II) centers.

The spectra of all the compounds, except **13** and **16**, exhibit some common features as evidenced by the nature of spectra. The spectra of **13** and **16** are broad but not isotropic in nature and don't give much information, but may be consistent with antiferromagnetic interaction between Cu(II) centers, as it is expected. This can be attributed to concentration difference of solutions taken for recording the spectra. The experimental and simulated best fits of EPR spectra of all complexes are given in Figs. 4.22 to 4.34. All of these spectra are found axial in nature and $g_{\parallel} > g_{\perp} > 2.0023$

155

for both species considered, which points towards a $d_{x^2-y^2}$ ground state [36]. Generally, the variation in the g values indicate that the geometry around Cu(II) centers are affected by the nature of the coordinating anions.

The geometric parameters G, empirical factor f and in-plane sigma bonding parameter α^2 values of all simulated spectra are calculated. G is a measure of the exchange interaction between the copper centers, is calculated for each species using the equation: $G = (g_{\parallel} - 2.0023)/(g_{\perp} - 2.0023)$ for all axial spectra. If $G > 4$, exchange interaction is negligible and if it is less than 4, considerable exchange interaction is indicated in the solid complex [1]. Though, the two Cu(II) centers are not coupled enough the possibility of presence of other Cu(II) centers of a second molecule may cause considerable exchange interactions, which is usually less possible in solution. Most of the G values calculated are greater than four and the exchange interaction of that complexes are negligible. The value of in plane sigma bonding parameter α^2 was estimated for each species, from the expression,

$$\alpha^2 = -A_{\parallel}/0.036+(g_{\parallel}-2.0023)+3/7(g_{\perp}-2.0023)+0.04$$

The empirical factor f, an index of tetragonal distortion, is calculated as $f = \dfrac{g_{\parallel}}{A_{\parallel}}$.

The value of $A_{\parallel} < 0.0140$ cm^{-1} rules out the possibility of square planar nature for such Cu(II) centers as such values are not reported for any complexes even with four sulfur ligands [37]. The empirical factor f is an index of tetragonal distortion and its value may vary from 105 to 135 for small to extreme distortion in square planar complexes, and that depends on the nature of the coordinated atom [38]. The f values of the complexes are indicating significant distortion from planarity. The value of f increases markedly on the introduction of tetrahedral distortion to the chromophore. The tetrahedral distortion of a square planar chromophore with any of

the biomimetic (N, O or S) donors reduces $A_{\parallel}$ and increases $g_{\parallel}$, shifting the f

values [37]. The factor α^2 is a covalency parameter, which describes the in-plane

sigma bonding, arises from the dipole-dipole interaction between magnetic moments

associated with the spin motion of the electron and the nucleus and its value decreases

with increasing covalency [39]. The stronger covalency should result in smaller

hyperfine interaction. Since, α^2 values obtained lies above 0.5 and below 1.0, which

is expected for 100% ionic character of the bonds and become smaller with increasing

covalent bonding, it is inferred that the complexes have some covalent character in the

ligand environment. The values of α^2 indicate that approximately 80% of the spin

population is in the copper $d_{x^2-y^2}$ orbitals of most of the Cu(II) species concerned.
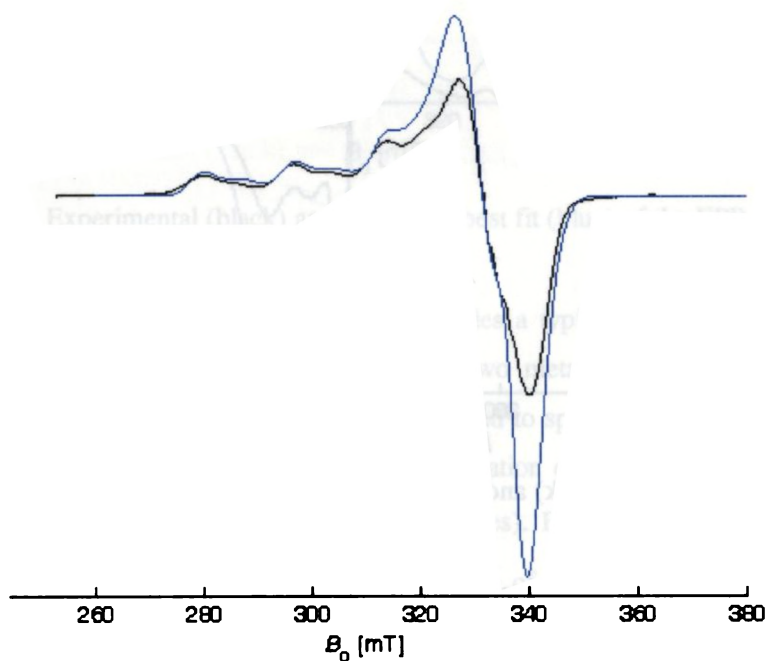
Fig. 4.22. Experimental (black) and simulated best fit (blue) of the EPR spectrum of complex **8** in DMF at 77 K.

The spectrum of compound **8** shows an axial nature with the indication of a second species as evidenced in the spectrum, there was hardly any indications of a third species. Both two species of the complex **8** show typical axial behavior with different $g_{\parallel}$ and $g_{\perp}$ values. $g_{\parallel} > g_{\perp} > 2.0023$ are consistent with a $d_{x^2-y^2}$ ground state in a square planar or square pyramidal geometry. The f values obtained are nearly the same as reported for similar chloro-bridged copper(II) dimers [40].
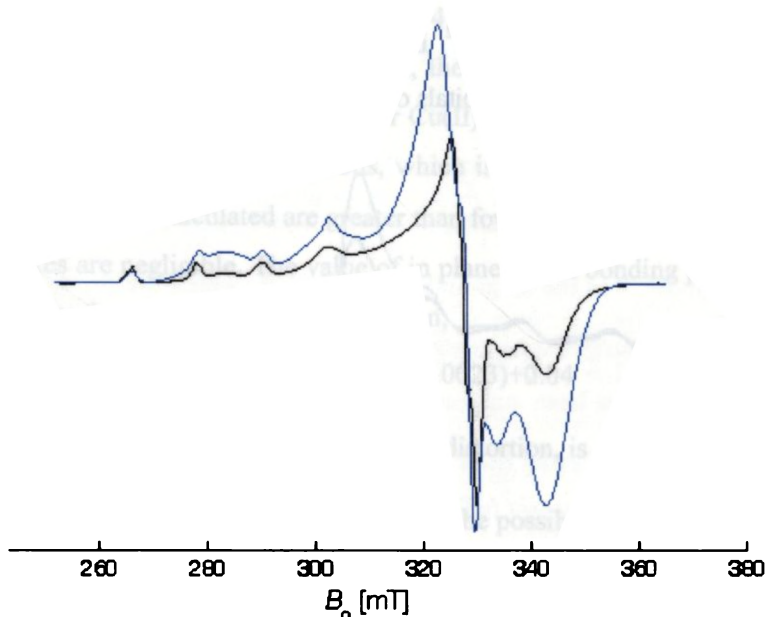
Fig. 4.23. Experimental (black) and simulated best fit (blue) of the EPR spectrum of complex **9** in DMF at 77 K.

The spectrum of the compound **9** is found to be more of an axial type. The simulation was done by considering two uncoupled axial Cu(II) species, though the second Cu(II) species might be of rhombic features. There may be more than two

different species also. However, the simulation is found in good agreement with two axial Cu(II) species.
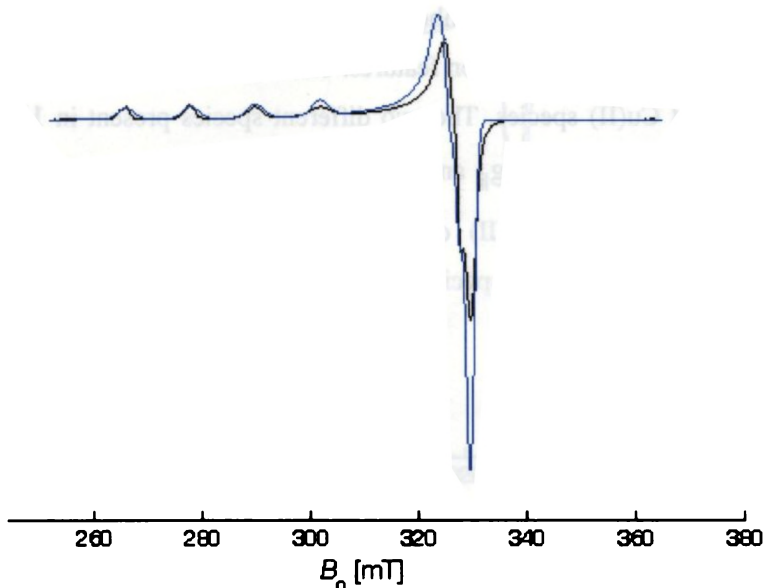
Fig. 4.24. Experimental (black) and simulated best fit (blue) of the EPR spectrum of complex **10** in DMF at 77 K.

The spectrum of compound **10** resembles a typical axial Cu(II) monomeric species. However, as the complex is having two metal centers, the possibility of similar environment around metal centers can lead to spectra like this, the simulation was done by considering so. However, fragmentation due to lower stability in DMF can also lead to spectra like this (high $g_{\parallel}$ values). But, the EPR of the copper is governed by the chemical nature and charge state of the close-lying ligand atoms to the metal atom and is not directly correlated with thermodynamic parameters, which govern stability of metal-ligand complexes [35]. For example, various polyamines bind to copper with first dissociation constants ranging over 16 orders of magnitude [35,41] while the EPR parameters do not vary significantly. Thus, arguments based on

159

stability alone could not be used to make the type of assignment [35]. Also it is reported that, on the whole, EPR studies even of frozen solutions of a wide range of copper(II) systems, do not show any evidence of pair formation, though EPR triplet spectra had been observed in a number of copper compounds [42]. The spectra of compounds **11** and **12** show common features. The axial spectra show the presence of second uncoupled Cu(II) species. The two different species present in **11** resembles that in **12** as evidenced by the $g_{\parallel}$ and $g_{\perp}$ values of the two species A and B. Both complexes have a similar Cu(II) center as evidenced by an exactly matching parameters of one of their Cu(II) species (species A).
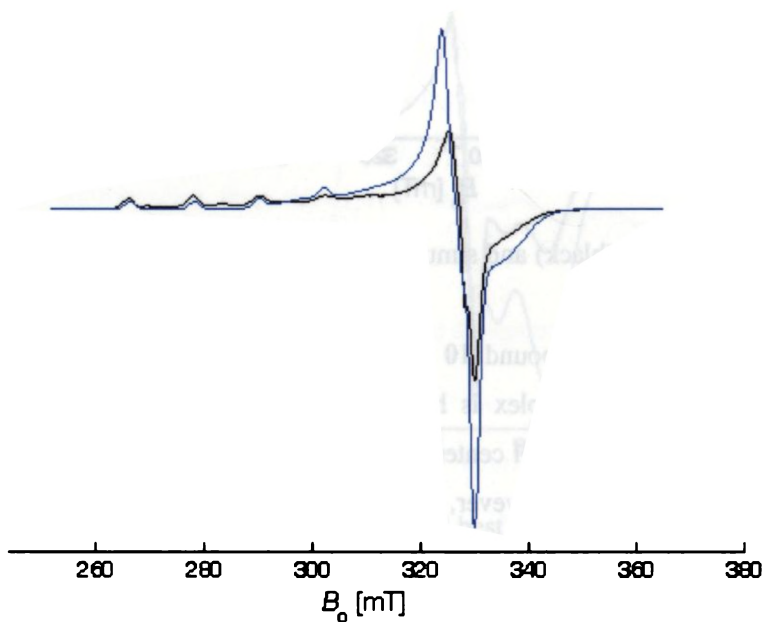
Fig. 4.25. Experimental (black) and simulated best fit (blue) of the EPR spectrum of complex **11** in DMF at 77 K.

160
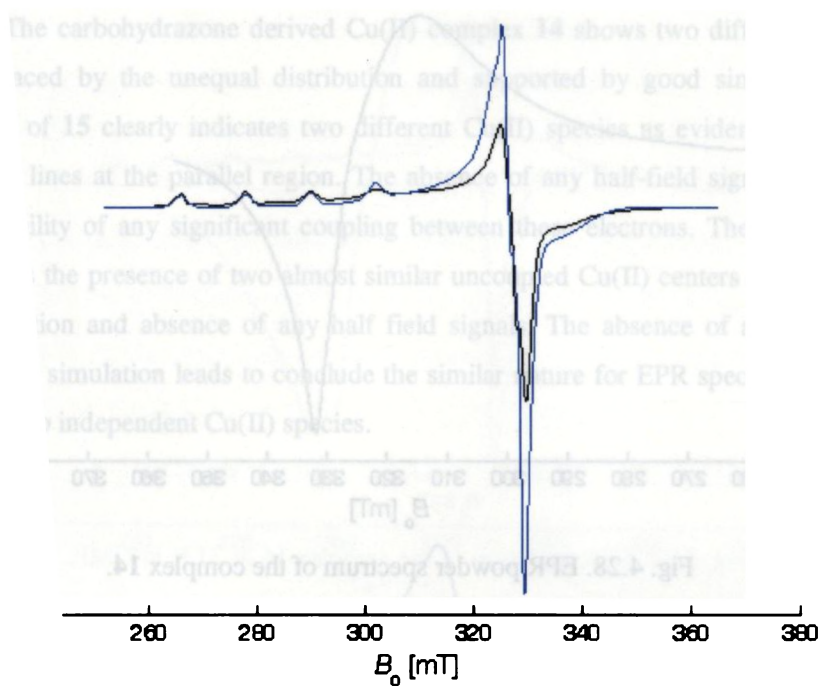
Fig. 4.26. Experimental (black) and simulated best fit (blue) of the EPR spectrum of complex **12** in DMF at 77 K.
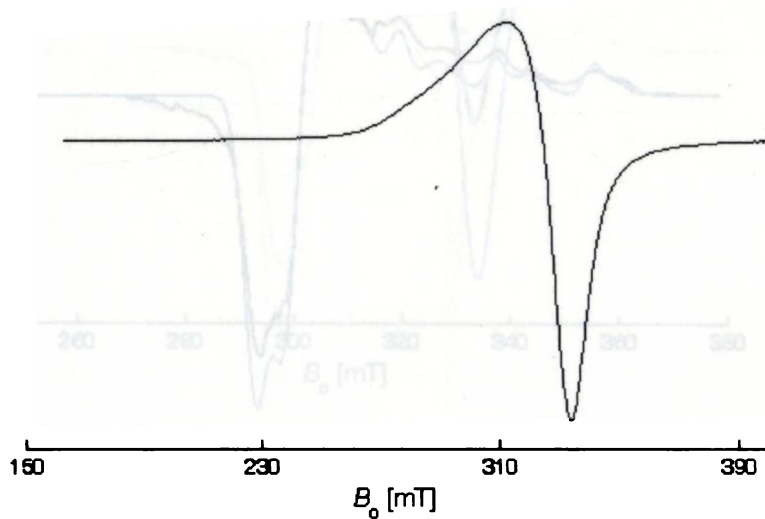
Fig. 4.27. Experimental EPR spectrum of the complex **13** in DMF at 77 K.
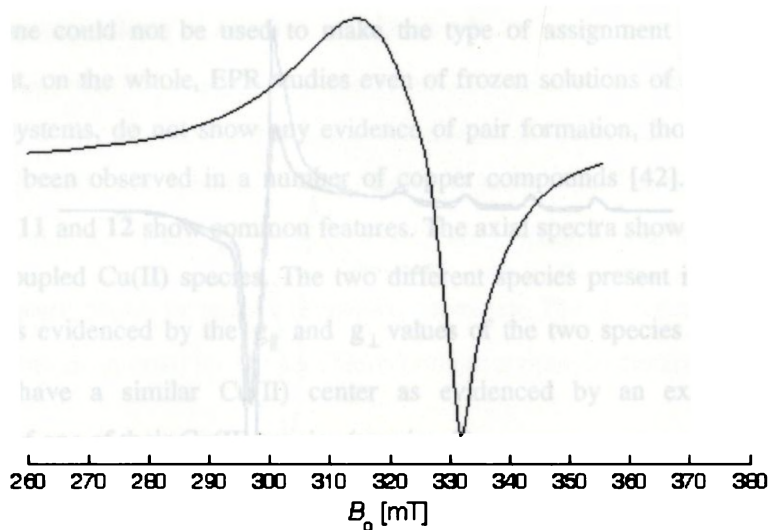
Fig. 4.28. EPR powder spectrum of the complex **14**.
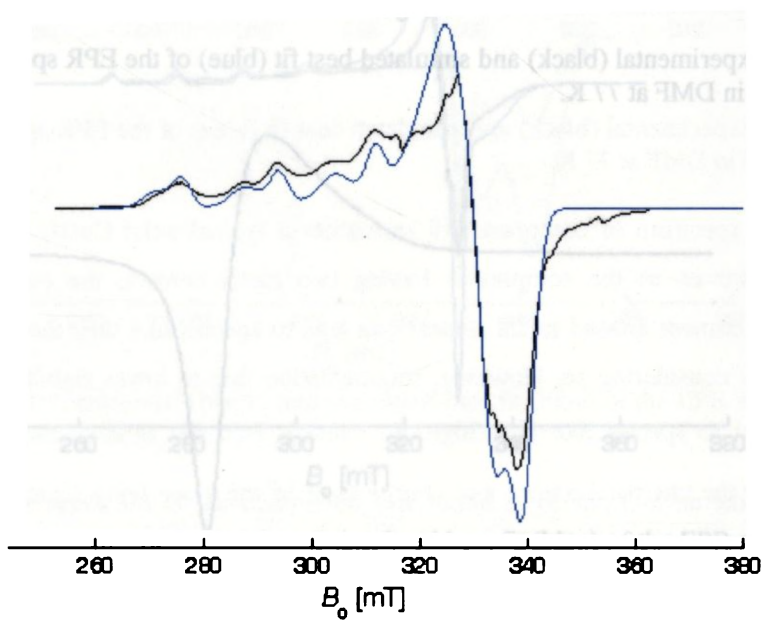
Fig. 4.29. Experimental (black) and simulated best fit (blue) of the EPR spectrum of complex **14** in DMF at 77 K.

The carbohydrazone derived Cu(II) complex **14** shows two different species as evidenced by the unequal distribution and supported by good simulation. The spectrum of **15** clearly indicates two different Cu(II) species as evidenced by eight hyperfine lines at the parallel region. The absence of any half-field signals rules out the possibility of any significant coupling between these electrons. The complex **17** also shows the presence of two almost similar uncoupled Cu(II) centers supported by the simulation and absence of any half field signals. The absence of any half field signals and simulation leads to conclude the similar nature for EPR spectra of **18** and **19**, with two independent Cu(II) species.
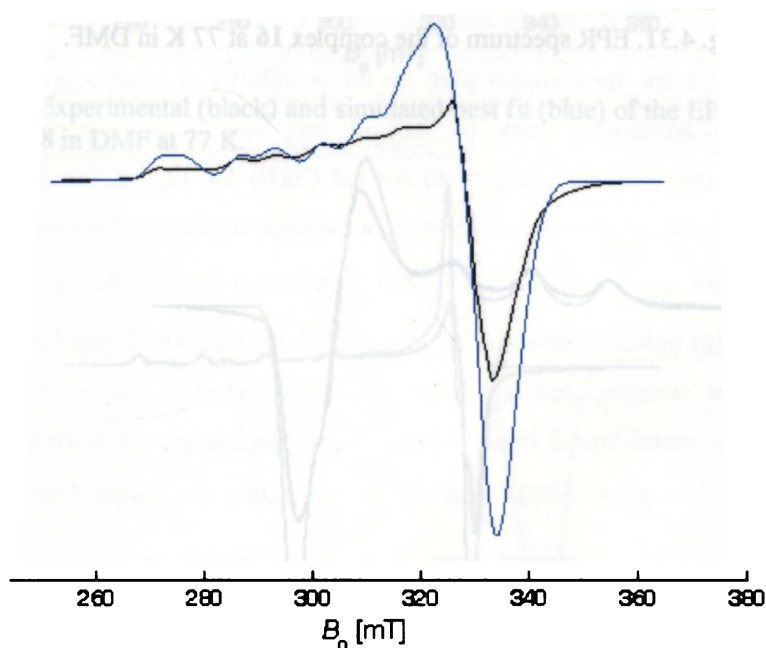
Fig. 4.30. Experimental (black) and simulated best fit (blue) of the EPR spectrum of complex **15** in DMF at 77 K.
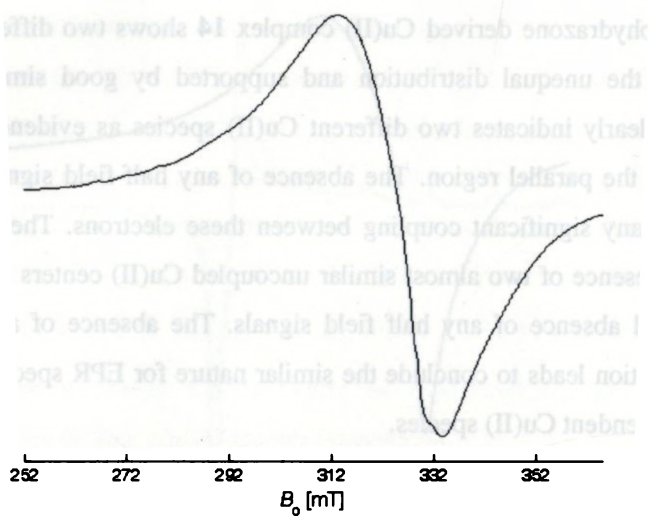
Fig. 4.31. EPR spectrum of the complex **16** at 77 K in DMF.
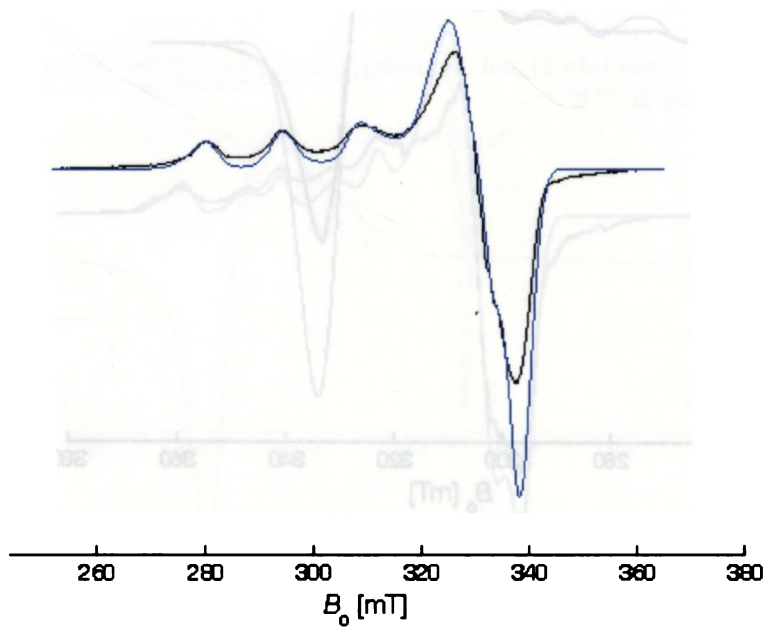
Fig. 4.32. Experimental (black) and simulated best fit (blue) of the EPR spectrum of complex **17** in DMF at 77 K.
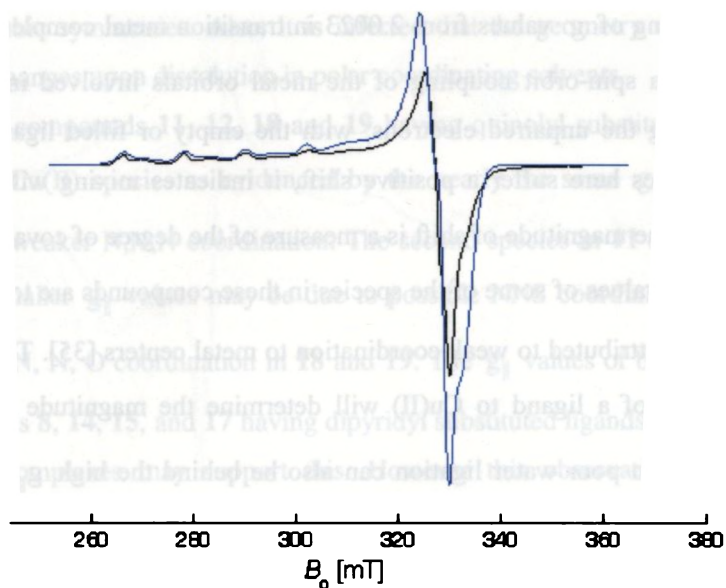
Fig. 4.33. Experimental (black) and simulated best fit (blue) of the EPR spectrum of complex **18** in DMF at 77 K.
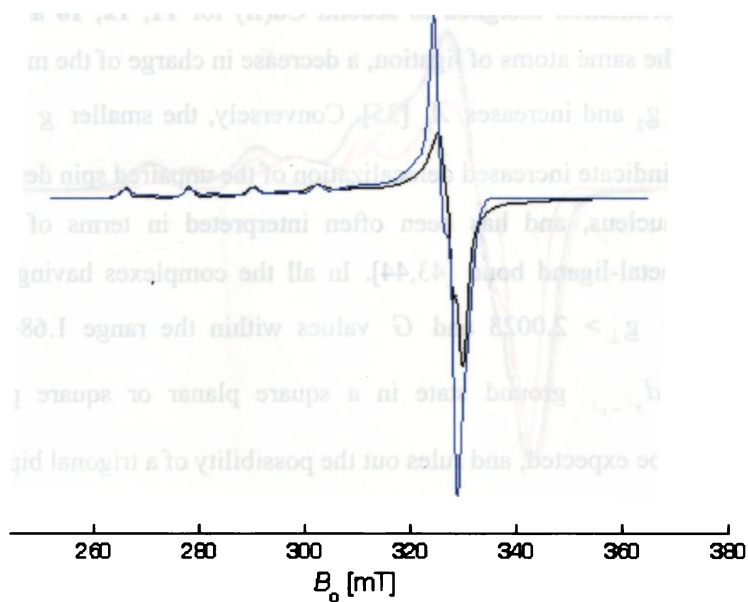
Fig. 4.34. Experimental (black) and simulated best fit (blue) of the EPR spectrum of complex **19** in DMF at 77 K.

The shifting of g values from 2.0023 in transition metal complexes are due to the mixing, via spin-orbit coupling of the metal orbitals involved in molecular orbitals containing the unpaired electrons, with the empty or filled ligand orbitals. Since the g values here suffer a positive shift, it indicates mixing with the filled ligand orbitals. The magnitude of shift is a measure of the degree of covalency of the complex. The $g_{\parallel}$ values of some of the species in these compounds are too high than expected, may be attributed to weak coordination to metal centers [35]. The electron-donating capacity of a ligand to Cu(II) will determine the magnitude of $g_{\parallel}$. The presence of electron poor water ligation can also be behind the high $g_{\parallel}$ values, for example. The very low $A_{\parallel}$ values also support this. These high $g_{\parallel}$ values expect a positive net charge for the complex part. So the possibility of ionic copper at NNN centers and its weakening may be behind this and is in accordance with thiolato/enolato coordination assigned to second Cu(II) for **11**, **12**, **18** and **19**. For complexes having the same atoms of ligation, a decrease in charge of the metal-ligand complex decreases $g_{\parallel}$ and increases $A_{\parallel}$ [35]. Conversely, the smaller g values for some other species indicate increased delocalization of the unpaired spin density away from the copper nucleus, and has been often interpreted in terms of increased covalency in the metal-ligand bond [43,44]. In all the complexes having different Cu(II) species $g_{\parallel} > g_{\perp} > 2.0023$ and G values within the range 1.68–5.14 are consistent with a $d_{x^2-y^2}$ ground state in a square planar or square pyramidal geometry, as would be expected, and rules out the possibility of a trigonal bipyramidal structure which would be expected to have $g_{\perp} > g_{\parallel}$. Octahedral geometry is rarely sustained in Cu(II) complexes as they are most prone to Jahn Teller distortion giving

rise to rhombic symmetries. Also, it is inferred that the geometry of the compound undergoes changes upon dissolution in polar coordinating solvents.

The compounds **11**, **12**, **18** and **19** having quinolyl substituted ligands have one similar Cu(II) species as evidenced by the nearly the same $g_{\parallel}$ values, may be indicating a weaker N,N,N coordination. The second species in **11** and **12** are almost same and smaller $g_{\parallel}$ values may be due to possible NNS coordination compared to the possible N, N, O coordination in **18** and **19**. The $g_{\parallel}$ values of both Cu(II) species in compounds **8**, **14**, **15**, and **17** having dipyridyl substituted ligands are different from the above complexes may support this. However this observation is ambiguous, especially without confirming the exact nature of the complexes in solution and in the absence of any crystal structure to support the coordinations. The simulated spectra of two different Cu(II) species designated, A and B, in the spectral simulation of selected copper complexes are shown in Figs. 4.35 to 4.39.
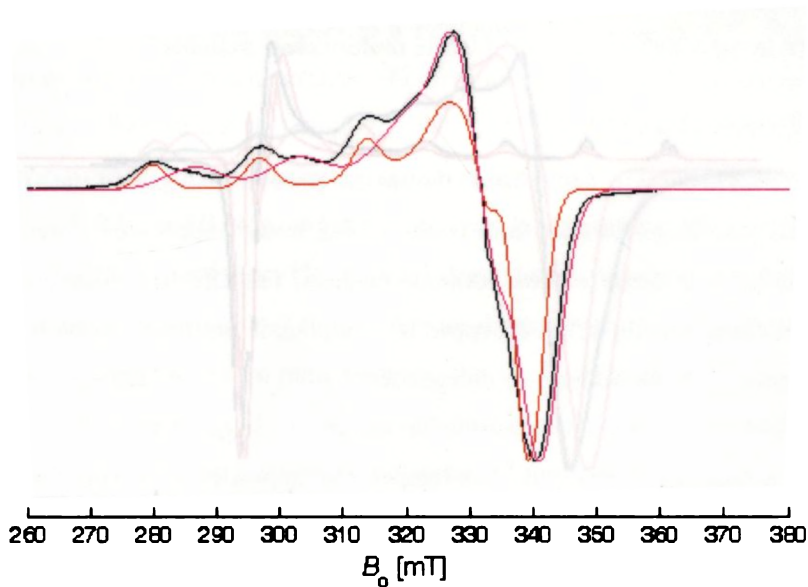
Fig. 4.35. The two simulated spectra of species A (red) and B (magenta) for the complex **8**, with its experimental EPR spectrum (black) (Please see Fig. 4.22 also).

167
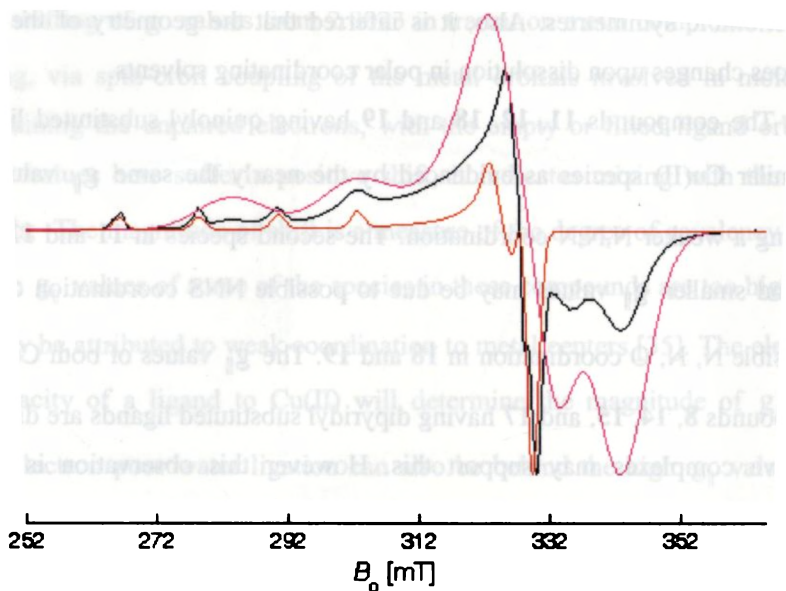
Fig. 4.36. The two simulated spectra of species A (magenta) and B (red) for the complex **9**, with its experimental EPR spectrum (black) (Please see Fig. 4.23 also).
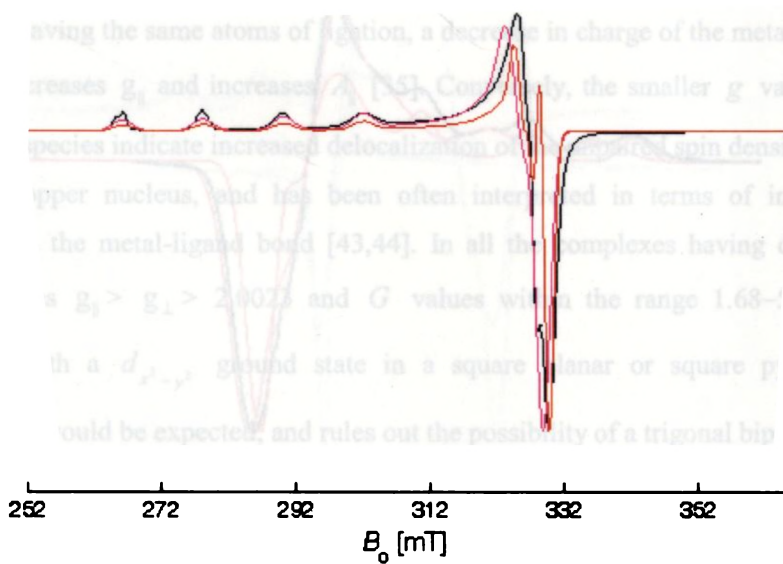
Fig. 4.37. The two simulated spectra of species A (magenta) and B (red) for the complex **10**, with its experimental EPR spectrum (black) (Please see Fig. 4.24 also).

168
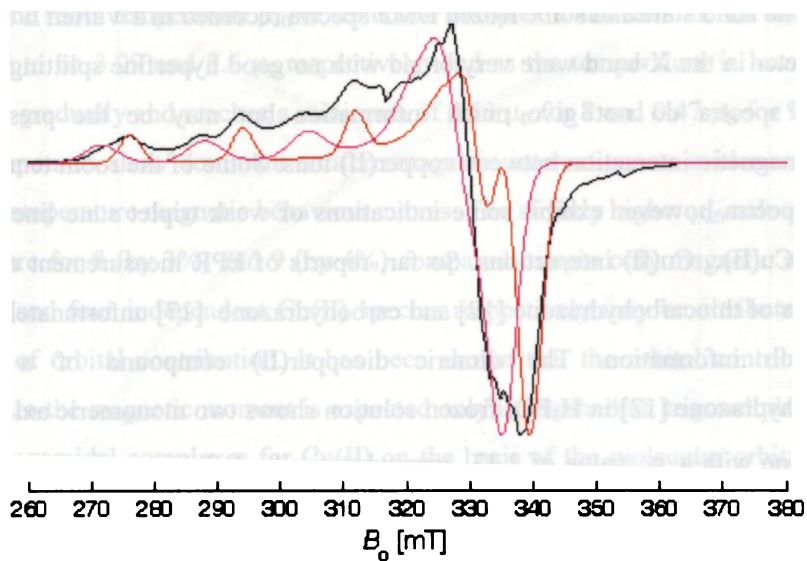
Fig. 4.38. The two simulated spectra of species A (red) and B (magenta) for the complex **14**, with its experimental EPR spectrum (black) (Please see Fig. 4.29 also).
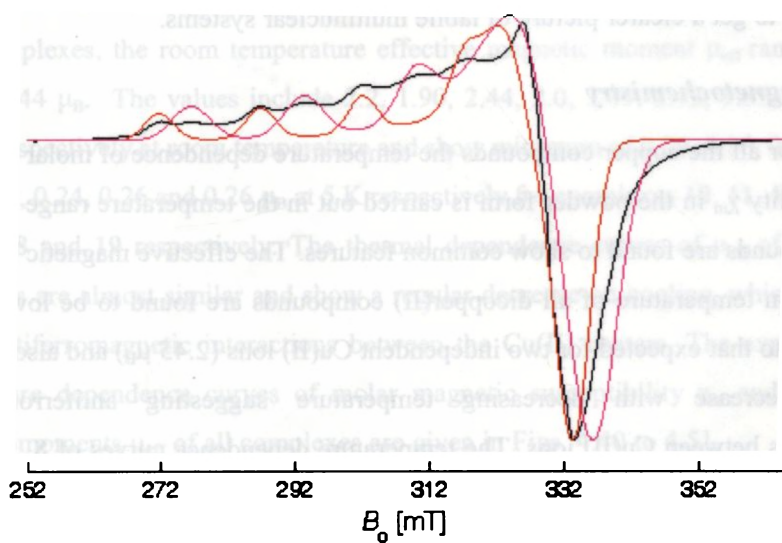
Fig. 4.39. The two simulated spectra of species A (red) and B (magenta) for the complex **15**, with its experimental EPR spectrum (black) (Please see Fig. 4.30 also).

169

The solid state and some frozen DMF spectra recorded in a Varien E 112 EPR spectrometer in the X-band were very broad with no good hyperfine splittings. These kinds of spectra do not give much information but may be the presence of antiferromagnetic interaction between copper(II) ions. Some of the room temperature powder spectra however exhibit some indications of weak triplet state lines at half fields of Cu(II)...Cu(II) interactions. So far, reports of EPR measurement of Cu(II) complexes of thiocarbohydrazone [12] and carbohydrazone [17] unfortunately do not give much information. The dimeric dicopper(II) compound of a similar thiocarbohydrazone [12] in H_3PO_4 frozen solution shows two monomeric axial Cu(II) species, one with a $g_{\parallel}$ value of 2.33, somewhat similar behaviour of our study. The absence of any detailed EPR studies of similar multinuclear carbohydrazone or thiocarbohydrazone Cu(II) complexes with single crystal X-ray results for molecular structural corroborative studies still leaves the matter for further research. A detailed analysis of the EPR behavior by varying concentration in different solvents is found obligatory to get a clearer picture of labile multinuclear systems.

4.3.5. Magnetochemistry

For all the copper compounds the temperature dependence of molar magnetic susceptibility χ_m in the powder form is carried out in the temperature range 5-325 K. All compounds are found to show common features. The effective magnetic moments μ_{eff} at room temperature of all dicopper(II) compounds are found to be low or near compared to that expected for two independent Cu(II) ions (2.45 μ_B) and also shows a regular decrease with decreasing temperature suggesting antiferromagnetic interactions between Cu(II) ions. The temperature dependence curves of **8**, **9** and **13** also show similar nature. These features indicate a dominant antiferromagnetic interaction in these compounds. Also it is found that Curie law is not obeyed by all systems, in agreement with the exchange coupling.

The room temperature μ_{eff} of trinuclear complex **8** and tetranuclear complex **9** are found to be 3.09 and 3.6 μ_B respectively, and as the temperature is lowered μ_{eff} decreases gradually and reaches a minimum of 0.53 μ_B for **8** and 0.47 μ_B for **9** at 5 K. Both compounds show dominant antiferromagnetic interactions as evidenced by the variable temperature magnetic behaviour curves. The slightly higher μ_{eff} value at room temperature for **8** (by 3%) and **9** (by 4%) compared to spin only magnetic moments for three and four independent Cu(II) species respectively may be attributed to the presence of orbital contribution. It has been shown that the orbital contribution of electrons to the magnetic moment is expected only in tetrahedral, trigonal planar, and trigonal pyramidal complexes for Cu(II) on the basis of the molecular orbital theory [45]. The effective magnetic moment of tetrahedral monomeric Cu(II) complexes has been estimated to be about 2.2 μ_B at room temperature and that of tri-coordinated Cu(II) complexes to be higher than the spin-only value [45].

For the trinuclear copper(II) complex **13**, μ_{eff} at room temperature is 2.19 μ_B and decreases on cooling and reaches to a minimum of 0.31 μ_B at 5 K. For all the other complexes, the room temperature effective magnetic moment μ_{eff} ranges from 1.83 to 2.44 μ_B. The values include 2.2, 1.90, 2.44, 2.0, 2.09, 2.13, 1.83, 2.03 and 1.98 μ_B respectively at room temperature and show minimum of 0.29, 0.30, 0.31, 0.29, 0.40, 0.28, 0.24, 0.26 and 0.26 μ_B at 5 K respectively for complexes **10**, **11**, **12**, **14**, **15**, **16**, **17**, **18** and **19** respectively. The thermal dependence curves of μ_{eff} of all these complexes are almost similar and show a regular decrease on cooling, which suggest strong antiferromagnetic interactions between the Cu(II) centers. The experimental temperature dependence curves of molar magnetic susceptibility χ_m and effective magnetic moments μ_{eff} of all complexes are given in Figs. 4.40 to 4.51.
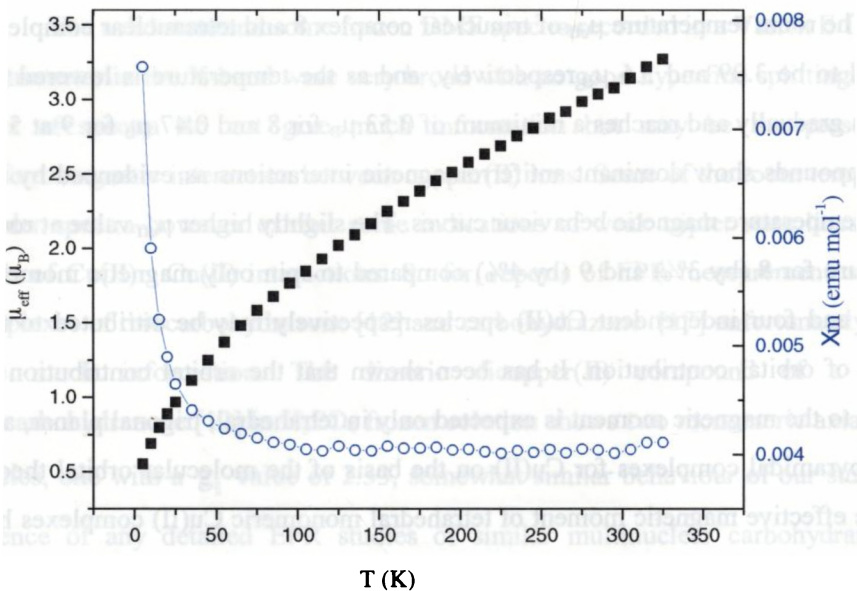
Fig. 4.40. Temperature dependence of effective magnetic moment μ_{eff} (■) and of molar magnetic susceptibility χ_m (○) of **8**.
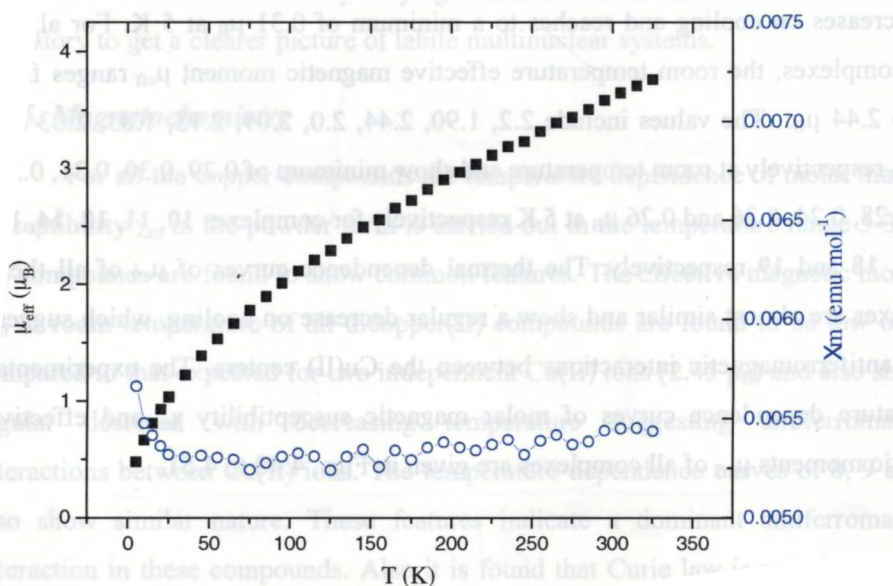
Fig. 4.41. Effective magnetic moment μ_{eff} (■) and molar magnetic susceptibility χ_m (○) data as a function of temperature for **9**.
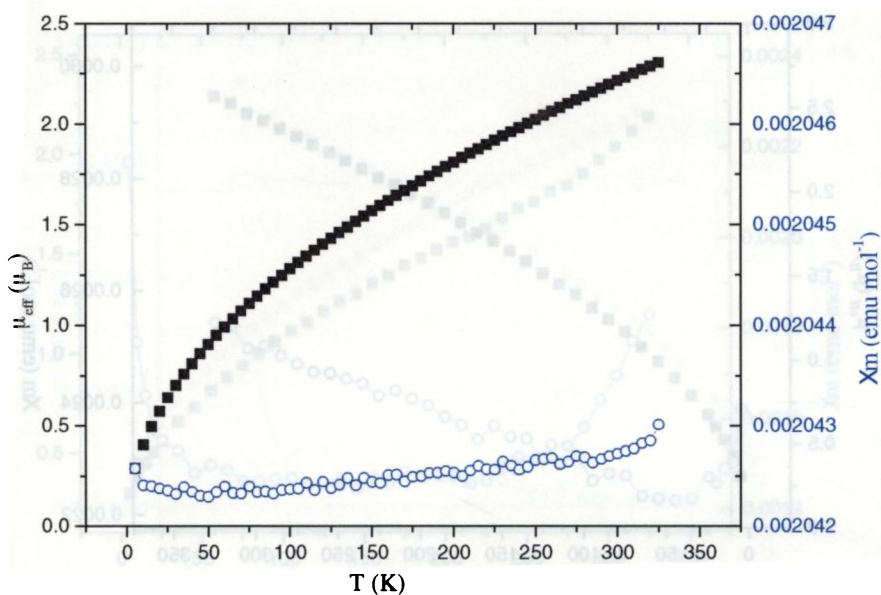
Fig. 4.42. Effective magnetic moment μ_{eff} (■) and molar magnetic susceptibility χ_m (○) data as a function of temperature for **10**.
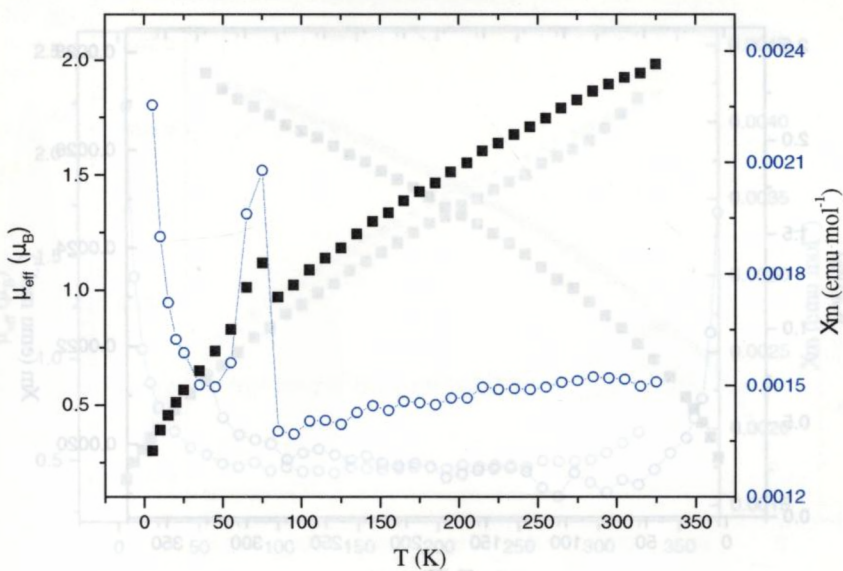
Fig. 4.43. Temperature dependence of effective magnetic moment μ_{eff} (■) and of molar magnetic susceptibility χ_m (○) of complex **11**.

173
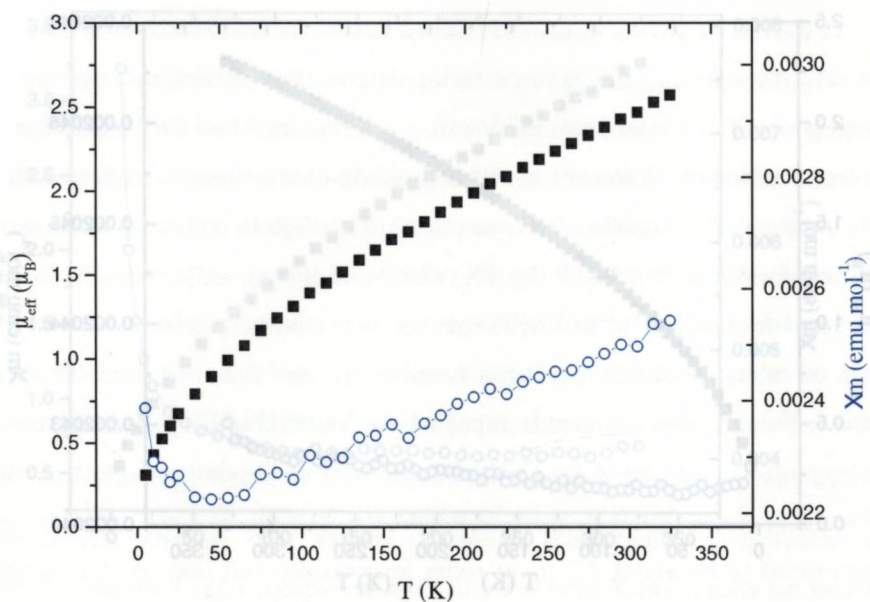
Fig. 4.44. Effective magnetic moment μ_{eff} (■) and molar magnetic susceptibility χ_m (○) data as a function of temperature for complex **12**.
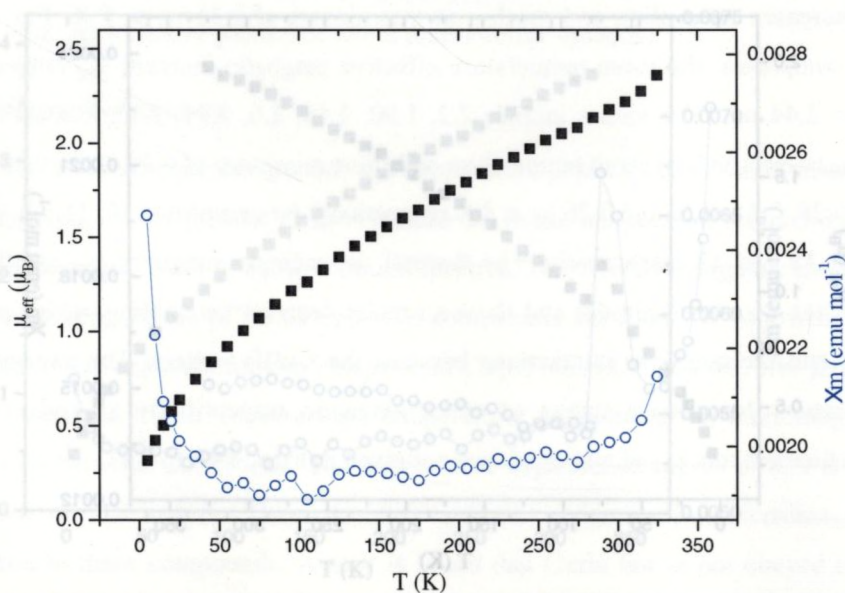
Fig. 4.45. Temperature dependence of effective magnetic moment μ_{eff} (■) and of molar magnetic susceptibility χ_m (○) of complex **13**.
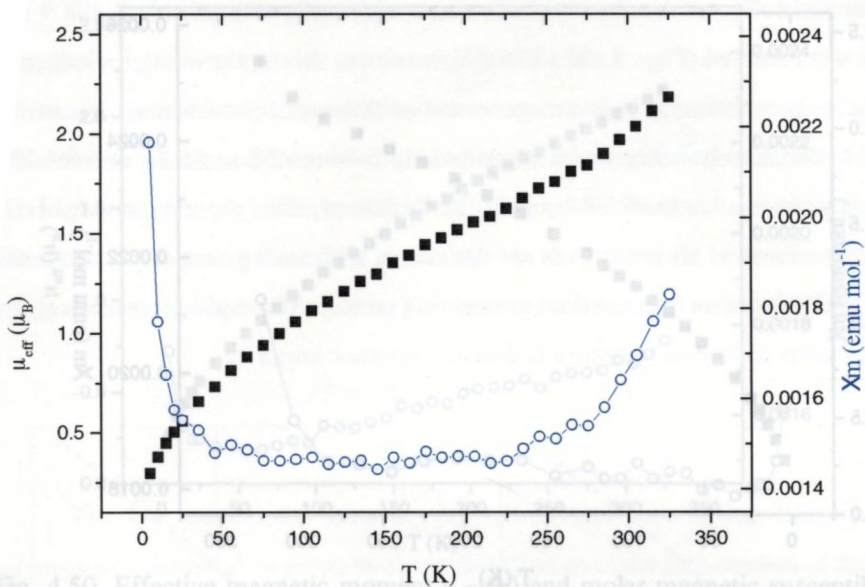
Fig. 4.46. Effective magnetic moment μ_{eff} (■) and molar magnetic susceptibility χ_m (○) data as a function of temperature for complex **14**.
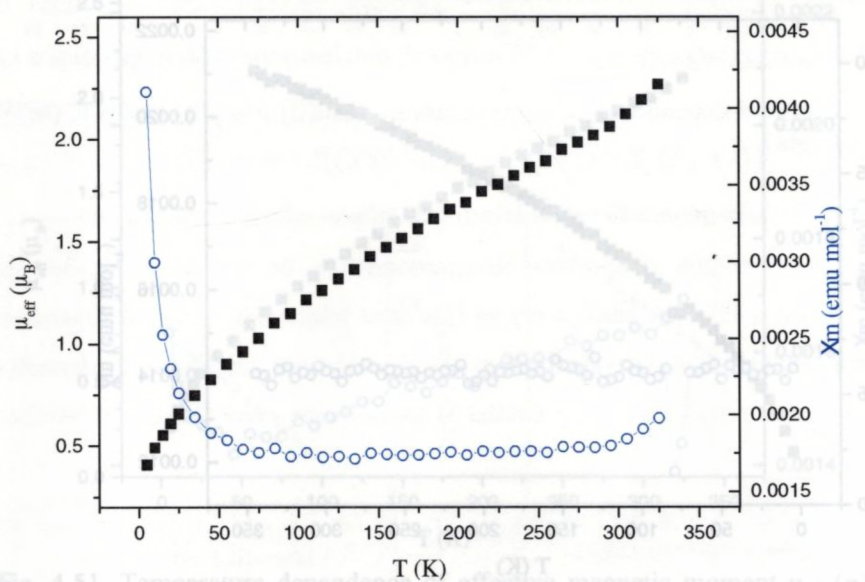
Fig. 4.47. Effective magnetic moment μ_{eff} (■) and molar magnetic susceptibility χ_m (○) data as a function of temperature for complex **15**.
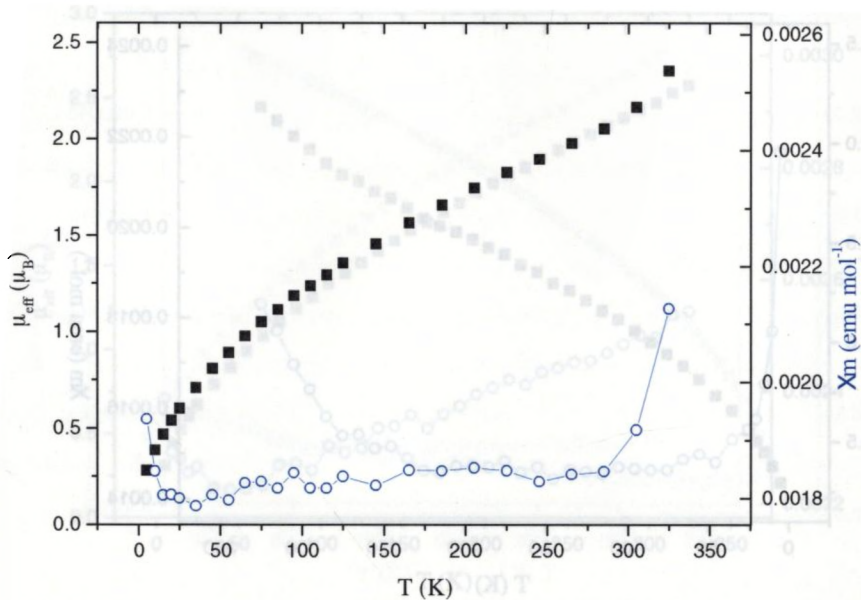
Fig. 4.48. Temperature dependence of effective magnetic moment μ_{eff} (■) and of molar magnetic susceptibility χ_m (○) of complex **16**.
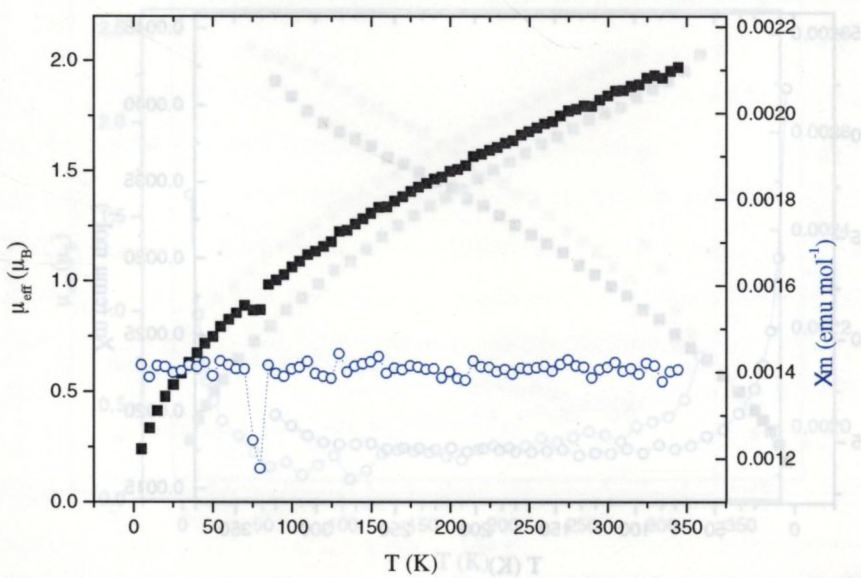
Fig. 4.49. Effective magnetic moment μ_{eff} (■) and molar magnetic susceptibility χ_m (○) data as a function of temperature for complex **17**.
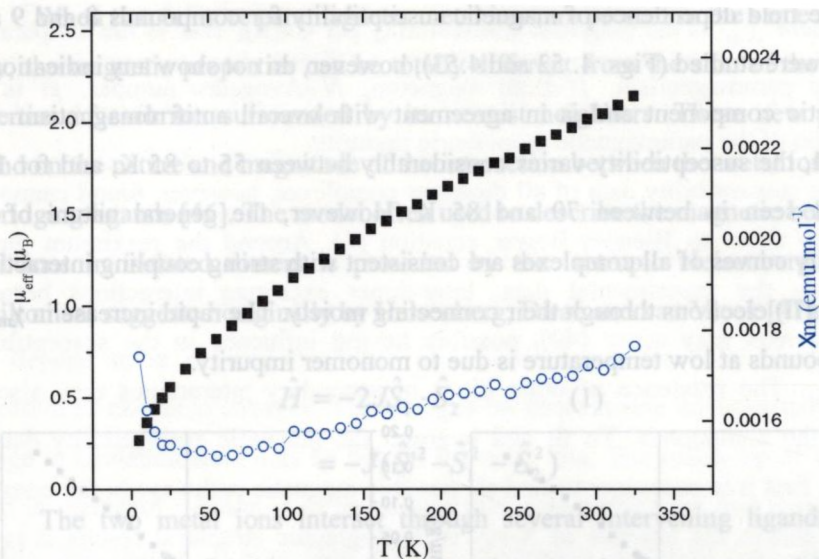
Fig. 4.50. Effective magnetic moment μ_{eff} (■) and molar magnetic susceptibility χ_m (○) data as a function of temperature for complex **18**.
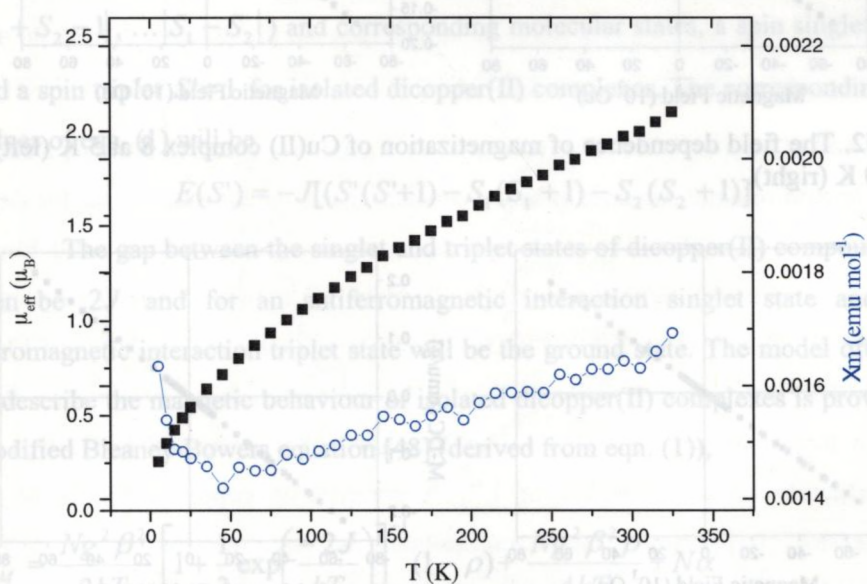
Fig. 4.51. Temperature dependence of effective magnetic moment μ_{eff} (■) and of molar magnetic susceptibility χ_m (○) of complex **19**.

177

The field dependence of magnetic susceptibility for compounds **8** and **9** at 5 and 300 K were studied (Figs. 4. 52 and 4.53), however, do not show any indication of ferromagnetic component and is in agreement with overall antifrromagnetism. For complex **11**, the susceptibility varies considerably between 55 to 85 K, and for **17** a variation is seen in between 70 and 85 K. However, the general nature of the susceptibility curves of all complexes are consistent with strong coupling interactions between Cu(II) electrons through their connecting moiety. The rapid increase in χ_m for some compounds at low temperature is due to monomer impurity.
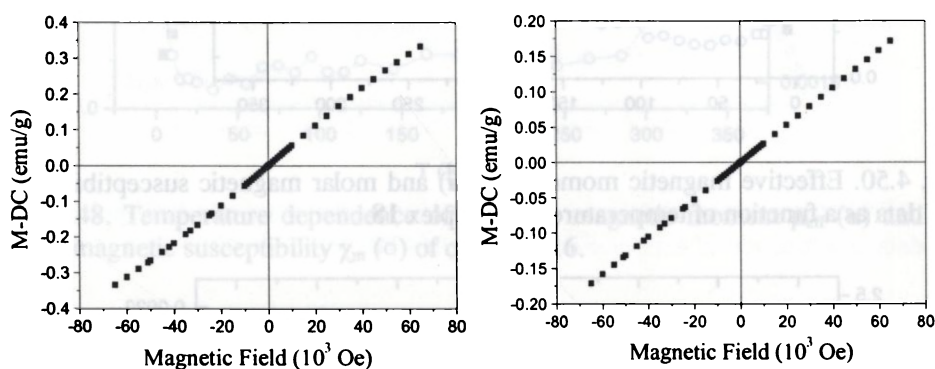
Fig. 4.52. The field dependence of magnetization of Cu(II) complex **8** at 5 K (left) and 300 K (right).
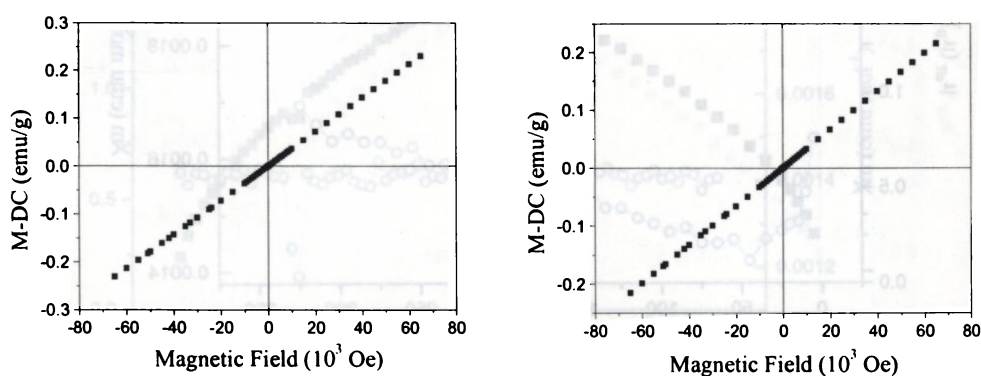
Fig. 4.53. The field dependence of magnetization of Cu(II) complex **9** at 5 K (left) and 300 K (right).

When two or more paramagnetic metal ions are present in the same molecular entity, the magnetic properties can be totally different from the sum of the magnetic properties of each ion surrounded by its nearest neighbors. These new properties depend on the nature and magnitude of the interaction between the metal ions through the bridging ligands [46]. The model often used to describe the magnetic behaviour of metal ions in isolated dimers is provided by the isotropic Heisenberg exchange Hamiltonian, suggested originally by Heisenberg, Dirac and van Vleck [47]

$$\hat{H} = -2J\hat{S}_1 \cdot \hat{S}_2 \qquad (1)$$

$$= -J(\hat{S}'^2 - \hat{S}_1^2 - \hat{S}_2^2)$$

The two metal ions interact through several intervening ligands and the exchange interaction J is given by the summation over the two centers of the dimeric molecule. These interactions lead to new quantum numbers ($S' = |S_1 + S_2|$, $|S_1 + S_2 - 1|$, ... $|S_1 - S_2|$) and corresponding molecular states, a spin singlet $S' = 0$ and a spin triplet $S' = 1$ for isolated dicopper(II) complexes. The corresponding eigen values of eqn. (1) will be

$$E(S') = -J[(S'(S'+1) - S_1(S_1 + 1) - S_2(S_2 + 1)]$$

The gap between the singlet and triplet states of dicopper(II) compounds will then be $2J$ and for an antiferromagnetic interaction singlet state and for a ferromagnetic interaction triplet state will be the ground state. The model often used to describe the magnetic behaviour of isolated dicopper(II) complexes is provided by modified Bleaney-Bowers equation [48] (derived from eqn. (1)),

$$\chi_M = \frac{Ng^2\beta^2}{3kT} \left[1 + \frac{1}{3}\exp\left(\frac{-2J}{kT}\right) \right]^{-1} (1 - \rho) + \frac{Ng^2\beta^2\rho}{4kT} + N\alpha \qquad (2)$$

Where χ_M is the magnetic susceptibility per Cu(II), $N\alpha$ is the temperature independent paramagnetism. β-Bohr magneton, N-Avogadro number. ρ is the mole fraction of the paramagnetic monomeric impurity.

The susceptibility data of all dicopper complexes, however, found cannot be satisfactorily fitted to Bleaney-Bower equation (2). Around the maximum the fit departs from the experimental data. Inter-dimer exchange interactions between neighboring ions may occur [40], possibly having influence in the susceptibility around T_{max}. The existence of other kinds of secondary interactions may also be present in the compounds. To fit and interpret the magnetic susceptibility data of complexes, first it is necessary to find all possible magnetic pathways in the complex structures, and in the absence of X-ray crystallographic structural results it is not possible to use any magnetic interacting models as that may lead to erroneous conclusions. Single crystal study is mandatory for a magneto structural correlation study also.

4.3.6. Characterization of an unusual complex

The Cu(II) complexes of carbohydrazone ligands are found to undergo a color loss in common organic solvents in lower concentrations on exposure to air for days attributed to possible dissociation, though they are very stable in their solid form. Fortunately, we could isolate the single crystals of a new copper compound $[Cu(L^{4a})_2Cl_2]\cdot CH_3OH\cdot H_2O\cdot H_3O^+Cl^-$ (13a) by slow evaporation of a solution of 13 in methanol in air after a month. Where L^{4a} is 3-(2-pyridyl)triazolo[1,5-a]-pyridine. It is found that the compound 13 suffered degradation of -CO- group and cyclization to form a chloride copper complex of L^{4a}. A comparable copper complex of 3-phenyltriazolo[1,5-a]-pyridine has been isolated by the reaction of 1,5-bis(2-benzoylpyridine) carbohydrazone (H_2L^5) with $CuCl_2$ [11], resulted with a degradation of -CO- group and cyclization. Also, somewhat similar kind of ligand N', N'^2-

bis[(1E)-1-(2-pyridyl)ethylidene] ethanedihydrazide having two N,N,O coordination pockets on reaction with $Fe(ClO_4)_3 \cdot 6H_2O$ have been reported to undergone an oxidative degradation of the side chain (-CO-CO-) and a reduction of Fe^{III} to Fe^{II} to form a complex, with crystallographic evidence [49].

The transition metal complexes may be very stable, or very reactive; and the stabilities of transition metal complexes may be thermodynamic or kinetic in origin. As the metal compounds are frequently colored and the color of a particular metal ion will depend upon its oxidation state and environment, the color change can be indicative of chemical changes. The changes on coordination environment or even a change in oxidation state may be behind the color loss. The follow up of UV spectra of **13** in methanol solution at different intervals were carried out and found useful to identify this change. It was seen that the absorption at 22030 cm^{-1}, attributed to O→Cu(II) charge transfer transition, gradually losses its intensity. However the band at 28250 cm^{-1} assigned to Cl→Cu(II) charge transfer transition retains its identity. Therefore it is attributed to the degradation of –CO– group of complex **13** in methanol solution on exposure to air. The UV spectra follow up is given in Fig. 4.54.
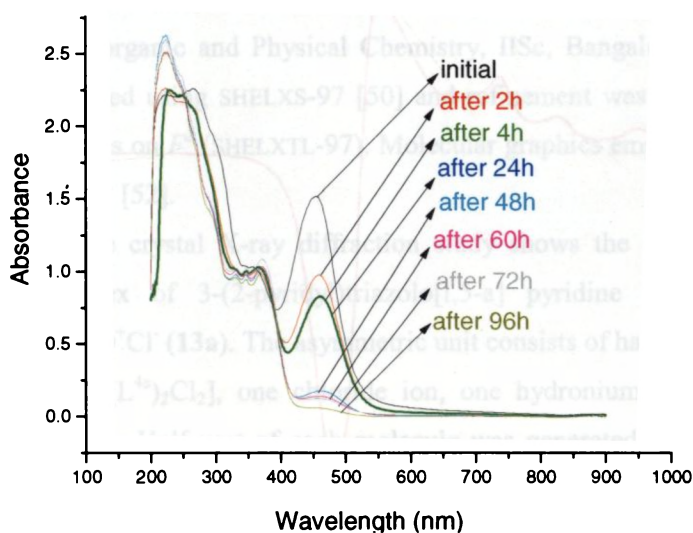
Fig. 4.54. The Electronic spectra follow up of complex **13** in 10^{-4} M methanol.

The powder and frozen DMF solution EPR spectra recorded in a Varien E 112 EPR spectrometer in the X-band (Figs. 4.55 and 4.56) of compound **13a** suggest the presence of a Cu(II) $3d^9$ species with typical axial nature.
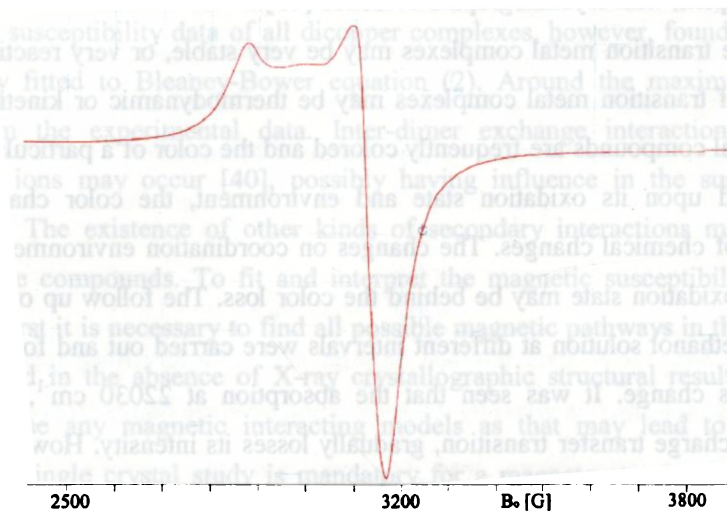
Fig. 4.55. EPR spectrum of the complex **13a** at 298 K in polycrystalline state.
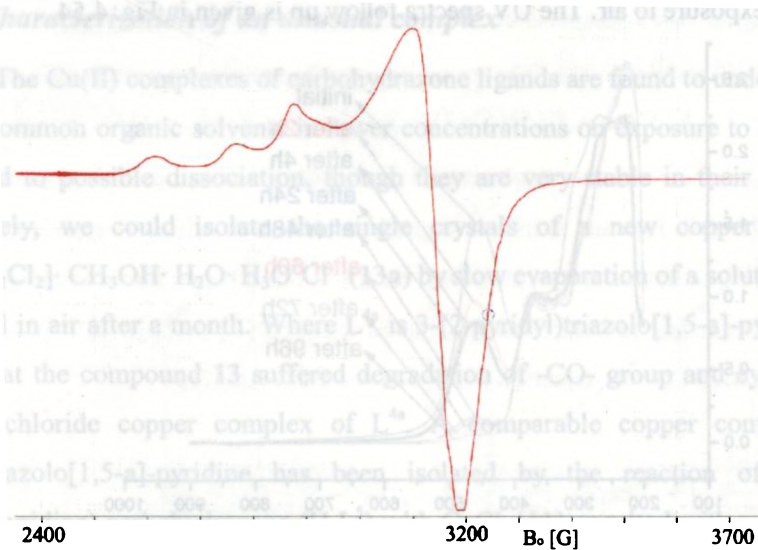
Fig. 4.56. The EPR spectrum of the complex **13a** in DMF at 77 K.

The powder spectrum exhibits a $g_\parallel$ value of 2.257 and $g_\perp$ value of 2.073. The frozen DMF spectrum also exhibits similar values as evidenced by $g_\parallel$ = 2.063 (with $A_\parallel$ = 196 G) and $g_\perp$ = 2.237. $g_\parallel > g_\perp > 2.0023$ and G value of 3.60 at 298 K in powder state and 3.87 at 77 K in DMF are consistent with a $d_{x^2-y^2}$ ground state. The $g_\parallel$ values obtained indicate a significant degree of covalency in the metal-ligand bonds and the G values indicate some exchange interaction. However there was no half-field signal. The α^2 value of 0.7256 indicates that 72% electron density is in the copper $d_{x^2-y^2}$ orbital.

4.3.6.1. Crystal structure of $[Cu(L^{4a})_2Cl_2] \cdot CH_3OH \cdot H_2O \cdot H_3O^+Cl^-$ (13a)

The crystallographic data and structure refinement parameters for the compounds are given in Table 4.5. The data of single crystals of suitable dimension of **13a** was collected with Bruker SMART APEX CCD diffractometer using graphite monochromated Mo Kα (λ = 0.71073 Å) radiation at temperature 293(2) K at the Department of Inorganic and Physical Chemistry, IISc, Bangalore, India. The trial structure was solved using SHELXS-97 [50] and refinement was carried out by full-matrix least squares on F^2 (SHELXTL-97). Molecular graphics employed were PLATON [51] and MERCURY [52].

The single crystal X-ray diffraction study shows the presence of a novel copper(II) complex of 3-(2-pyridyl)triazolo[1,5-a] pyridine (L^{4a}), $[Cu(L^{4a})_2Cl_2]\cdot$ $CH_3OH\cdot H_2O\cdot H_3O^+Cl^-$ (**13a**). The asymmetric unit consists of half of two independant molecules of $[Cu(L^{4a})_2Cl_2]$, one chloride ion, one hydronium ion, a water and a methanol molecule. Half part of each molecule was generated. However, hydrogen atoms of water or hydronium ion could not be located by using difference Fourier maps; and the assignment of hydronium ion was done by taking in consideration of

various aspects like bond lengths, planarity of triazolo group and earlier reports. A CSD search shows one report of a related Cu(II) complex with the same topology (octahedral coordination by four nitrogens and two chloride ions) [53] and is having hydronium ion and perchlorate anion. The EPR spectra of **13a** also agrees a Cu(II) species and rules out the possibility of a Cu(III) species, which is rare.

The crystal structure of the ligand L[4a] has been reported elsewhere [54]. The Cu(II) centers in both molecules are in an octahedral coordination and the difference between the molecules is slight variations in bond parameters. The Cu(1A) is coordinated by triazolo nitrogen N(1A) and pyridyl nitrogen N(4A) of two neutral ligands L[4a], to form the basal plane and the apical positions are occupied by chloride ions to form the octahedral geometry. The molecular structure of **13a** along with atom numbering scheme is given in Fig. 4.57 and the bond parameters are given in Table 4.6. The bond lengths in the ligand moieties of **13a** are comparable with its related Cu complex [54].

Each of the ligand moiety in both molecules is in a plane, with maximum mean plane deviation of 0.036(3) Å for C(10A) and for molecule B this deviation is 0.038(2) Å for C(4B). And the molecule itself except the apical chlorides are in an approximate plane with maximum deviations of -0.95(2) Å for N(2A) and 0.95(2) Å for N(2A') for molecule A. In molecule B these maximum deviations are -0.96(2) Å for N(2B) and 0.96(2) Å for N(2B'). The bicyclic chelate ring N(1A)–C(6A)–C(7A)–N(4A)–Cu(1A)–N(1A')–C(6A')–C(7A')–N(4A') formed by the coordination is in a plane with a maximum mean plane deviations of -0.033(2) Å for N(1A) and 0.033(2) Å for N(1A') and is likewise in molecule B also. This along with the angles around Cu(II) centers are indicative of the deviation from a perfect octahedron is least.

The Cu(1A)–N(1A) and Cu(1B)–N(1B) bond lengths are less than that seen in related Cu(II) complexes [54,55], where Cu-N$_{triazolo}$ bond lengths are 2.017(3) Å and 2.018(3) Å, and rules out the possibility of Cu(III). The unit cell packing of the molecules is given in Fig. 4.58.

184
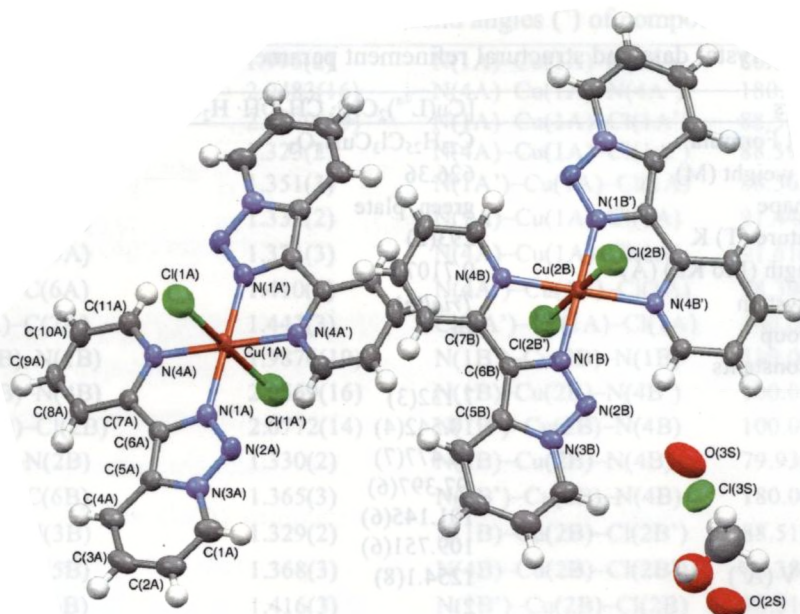
Fig. 4.57. The molecular structures of the two molecules of **13a** in the asymmetric unit. The hydrogen atoms on O(2S) and O(3S) are not shown.
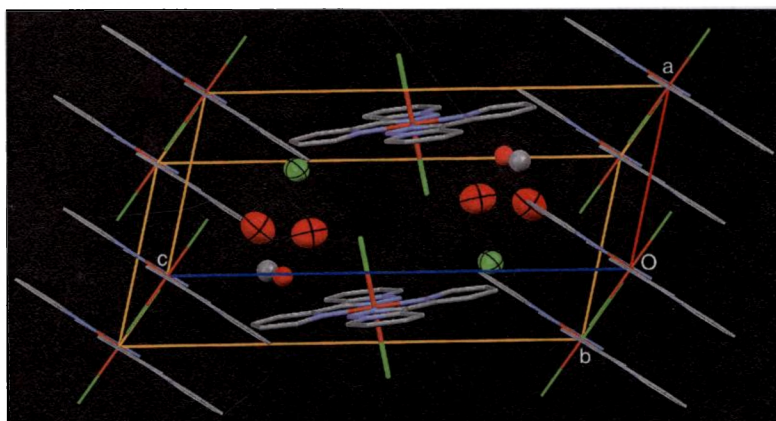
Fig. 4.58. The unit cell packing of the complex **13a**. Eight occupied corners (wireframe) contribute one molecule and two occupied face centers (stick) contribute the second molecule. The charges of the two free chloride ions (green, 70% ellipsoid) are balanced by two hydronium ions of four oxygen atoms shown (red, 70% ellipsoid). Methanol molecules are shown by ball model. Hydrogen atoms all are omitted for clarity.

Table 4.5. Crystal data and structural refinement parameters of compound **13a**.

Parameters	$[Cu(L^{4a})_2Cl_2]\cdot CH_3OH\cdot H_2O\cdot H_3O^+Cl^-$
Empirical Formula	$C_{23}H_{25}Cl_3CuN_8O_3$
Formula weight (M)	626.36
Color, shape	green, plate
Temperature (T) K	293(2)
Wavelength (Mo Kα) (Å)	0.71073
Crystal system	*Triclinic*
Space group	$P\bar{1}$
Lattice constants	
a (Å)	7.132(3)
b (Å)	10.542(4)
c (Å)	18.477(7)
α (°)	97.397(6)
β (°)	101.145(6)
γ (°)	109.751(6)
Volume V (Å^3)	1254.1(8)
Z	2
$D_{calc.}$ (ρ) (Mg m^{-3})	1.659
Absorption coefficient, μ (mm^{-1})	1.235
F(000)	636
θ Range for data collection	1.15 to 27.44
Limiting Indices	$-9 \le h \le 8,$
	$-13 \le k \le 13,$
	$0 \le l \le 23$
Reflections collected	5735
Independent Reflections	5735 [R(int) = 0.0000]
Refinement method	Full-matrix least-squares on F^2
Data / restraints / parameters	5735/1/348
Goodness-of-fit on *F^2*	1.161
Final *R* indices [I > 2σ (I)]	R$_1$ =0.0404, wR$_2$ = 0.1547
R indices (all data)	R$_1$ = 0.0405, wR$_2$ =0.1548
Largest difference peak and hole (e Å^{-3})	0.317 and -0.880

Table 4.6. Selected bond lengths (Å) and bond angles (°) of compound **13a**.

Cu(1A)–N(1A)	1.996(2)	N(1A)–Cu(1A)–N(4A)	80.04(7)
Cu(1A)–N(4A)	2.0483(16)	N(4A)–Cu(1A)–N(4A')	180.000(1)
Cu(1A)–Cl(1A)	2.6770(13)	N(1A)–Cu(1A)–Cl(1A')	88.56(6)
N(1A)–N(2A)	1.323(2)	N(4A)–Cu(1A)–Cl(1A')	88.39(6)
N(1A)–C(6A)	1.351(3)	N(1A')–Cu(1A)–Cl(1A)	88.56(6)
N(2A)–N(3A)	1.333(2)	N(1A)–Cu(1A)–Cl(1A)	91.44(6)
N(3A)–C(5A)	1.371(3)	N(4A)–Cu(1A)–Cl(1A)	91.61(6)
C(5A)–C(6A)	1.410(3)	N(4A')–Cu(1A)–Cl(1A)	88.39(6)
C(6A)–C(7A)	1.443(3)	Cl(1A')–Cu(1A)–Cl(1A)	180.000(1)
Cu(2B)–N(1B)	1.9876(19)	N(1B')–Cu(2B)–N(1B)	180.00(11)
Cu(2B)–N(4B)	2.0559(16)	N(1B)–Cu(2B)–N(4B')	100.07(7)
Cu(2B)–Cl(2B)	2.6772(14)	N(1B')–Cu(2B)–N(4B)	100.07(7)
N(1B)–N(2B)	1.330(2)	N(1B)–Cu(2B)–N(4B)	79.93(7)
N(1B)–C(6B)	1.365(3)	N(4B')–Cu(2B)–N(4B)	180.000(1)
N(2B)–N(3B)	1.329(2)	N(1B)–Cu(2B)–Cl(2B')	88.51(6)
N(3B)–C(5B)	1.368(3)	N(4B)–Cu(2B)–Cl(2B')	88.38(5)
C(5B)–C(6B)	1.416(3)	N(1B')–Cu(2B)–Cl(2B)	88.51(6)
C(6B)–C(7B)	1.431(3)	N(1B)–Cu(2B)–Cl(2B)	91.49(6)
N(1A')–Cu(1A)–N(1A)	180.000(1)	N(4B')–Cu(2B)–Cl(2B)	88.38(5)
N(1A')–Cu(1A)–N(4A)	99.96(7)	N(4B)–Cu(2B)–Cl(2B)	91.62(5)
		Cl(2B')–Cu(2B)–Cl(2B)	180.0

4.4. Anticancer properties

Anticancer activity (*in vitro*) of selected Cu(II) complexes was analyzed by standard growth inhibitory assays. Mechanism of action is analyzed in MCF-7 cell lines and is one of the three cell line panel recommended by NCI (National Cancer Institute) for anticancer drug screening (NCI developmental therapeutic program). Determination of the Effectiveness of the compounds was achieved by MTT Cell Proliferation Assay. The procedures are as reported in Chapter 2. The cell survival of various compounds in different concentration is summarized in Table 4.7.

Table 4.7. Cell survival shown by complexes at different concentration.

Conc.	Cell survival shown by					
	11	**13**	**15**	**16**	**17**	**18**
10 µM	51.8	90	68.28	86.25	94.2	66.07
50 µM	69.38	88.43	84.14	80.31	83.56	76.79
100 µM	89.79	76.875	94.71	79.68	72.67	89.57

A graph plotted taking the concentration of the compound (X-axis) against the percentage viability (Y-axis) is given in Fig 4. 59.
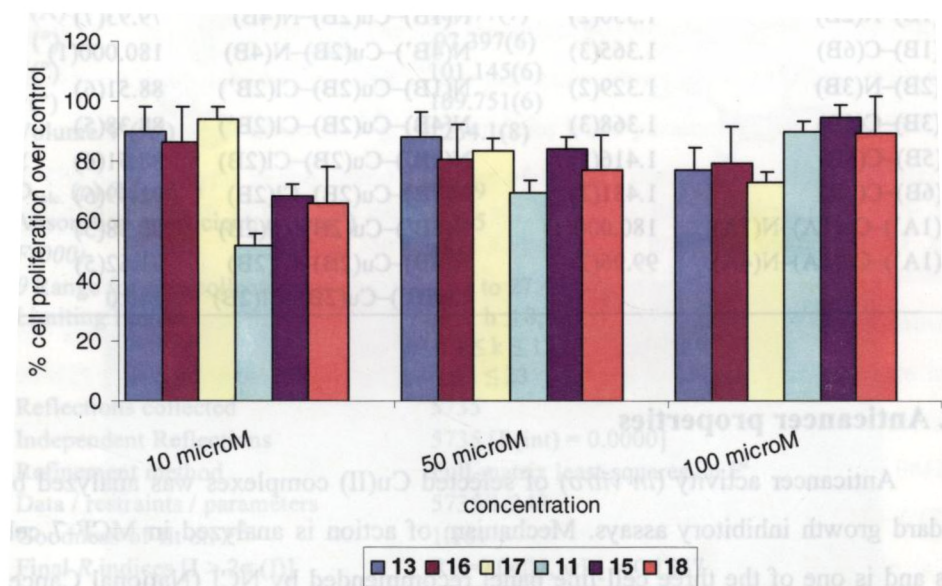
Fig. 4.59. Cell proliferation over control of selected compounds at different concentrations.

LD$_{50}$ value (lethal dose of drug for killing 50% of cells) of a drug is used to indicate the effectiveness of the compounds used; the lesser the value, the more effective the compounds are. It is found that complexes such as **13**, **16** and **17** showed reduced proliferation of MCF-7 cells as the concentration of the compounds increased

from 10 μM to 100 μM. The above complexes attain a LD_{50} at a higher concentration, which was found to be above 100 μM. But complexes such as **11, 15** and **18** not showed a promising anti cancer effect. This makes us to suggest **13, 16** and **17** as superior anticancer gadgets against breast cancer.

4.5. Concluding remarks

This chapter presents syntheses and physico-chemical characterizations of twelve novel di/polynuclear Cu(II) coordination compounds. Nine of these complexes are assigned as dicopper(II) complexes of carbohydrazones or thiocarbohydrazones, two are assigned as trinuclear while one is assigned as a tetranuclear complex of copper(II). All the Cu(II) complexes were organized by mono or dideprotonated carbohydrazone or thiocarbohydrazone ligands under neutral reaction conditions. The Cu(II) compounds are found very reluctant to form molecular grids by self-assembly with present series of carbohydrazone and thiocarbohydrazone ligands possessing mainly two coordination pockets, consistent with their reluctance to take up a regular octahedral geometry. The structures of the complexes were assigned tentatively, in the absence of single crystal X-ray studies, and are consistent with other spectral and magnetic studies.

In the literature survey, it is found that coordination studies of carbohydrazone and thiocarbohydrazone are more with copper compared to other transition metals. The EPR and magnetic features of all copper complexes are discussed. The spectra are generally found to exhibit two uncoupled Cu(II) species in DMF solutions recorded at 77 K. Spectral simulations of all these species, under the investigation conditions, are obtained well and the EPR parameters are reported. Variable temperature magnetic studies of all the Cu(II) complexes are found to exhibit strong antiferromagnetic coupling between metal centers. It is found that EPR solution behaviour of most of the Cu(II) complexes contradicts with the solid powder form

magnetic studies. This is attributed to the labiality of carbohydrazone and thiocarbohydrazone copper complexes in DMF at low concentrations. The MALDI MS spectra also reveal that the compounds are not very stable in solution or under ionization conditions of MALDI. However a detailed study in connection with EPR and magnetism of carbohydrazone and thiocarbohydrazone derived Cu(II) complexes is still to come and is open for further research.

An unusual complex $[Cu(L^{4a})_2Cl_2] \cdot CH_3OH \cdot H_2O \cdot H_3O^+Cl^-$ (**13a**) isolated from a solution of **13** in methanol on exposure to air and characterized with single crystal X-ray diffraction study. It is found to be formed by degradation of –CO– group and cyclization of ligand unit of **13**. Based on the UV spectral follow up as a function of time, intensity loss of bands corresponding to O→Cu(II) charge transfer is confirmed for complex **13**. This is attributed to the degradation of –CO– group. The complex **13a** is found to be having an octahedral Cu(II) center.

As a preliminary application study we have screened selected Cu(II) complexes for *in vitro* anticancer activity in MCF-7 cell lines. The activities of complexes are found different from their corresponding free ligands. Three complexes **13**, **16** and **17** are reported as anticancer gadgets against breast cancer. The complexes show antiproliferation effect, though their corresponding free ligands showed cell proliferation. The Cu(II) complexes derived from a carbohydrazone ligand 1,5-bis(di-2-pyridyl ketone) carbohydrazone H_2L^4 are found to exhibit better activities. The present chapter is thus reported as a beginning to explore novel anticancer compounds of potential class of carbohydrazone ligands.

References

1.   B.J. Hathaway, D.E. Billing, Coord. Chem. Rev. 5 (1970) 143.

2.   M.-T. Youinou, N. Rahmouni, J. Fischer, J. A. Osborn, Angew. Chem. Int.

Ed. Engl. 31 (1992) 733.

3. D.S. Cati, J. Ribas, J. Ribas-Arino, H. Stoeckli-Evans, Inorg. Chem. 43 (2004) 1021 and refs therein.

4. I. Solomon, L.B. La Croix, D.W. Randall, Pure Appl. Chem. 70 (1998) 799.

5. K. Pierloot, J.O.A. De Kerpel, U. Ryde, M.H.M. Olsson, B.O. Roos, J. Am. Chem. Soc. 120 (1998) 13156.

6. S.P. Mittal, R.K. Sharma, R.V. Singh, J.P. Tandon, Curr. Sci. 50 (1981) 483.

7. A.S. Dobeck, D.I. Klayman, E.J. Dickson, J.P. Scovill, E.C. Tramont, Antimicrob. Agents Chemother. 18 (1980) 27.

8. I.H. Hall, K.G. Rajendran, D.X. West, A.E. Liberta, Anticancer Drugs 4 (1993) 231.

9. D.X. West, A.E. Liberta, K.G. Rajendran, I.H. Hall, Anticancer Drugs 4 (1993) 241.

10. K. Raman, H.K. Singh, S.K. Salman, S.S. Parmar, J. Pharm. Sci. 82 (1993) 167.

11. A. Bacchi, M. Carcelli, P. Pelagatti, C. Pelizzi, G. Pelizzi, F. Zani, J. Inorg. Biochem. 75 (1999) 123.

12. B. Moubaraki, K.S. Murray, J.D. Ranford, X. Wang, Y. Xu, Chem. Commun. (1998) 353.

13. B. Moubaraki, K.S. Murray, J.D. Ranford, J.J. Vittal, X. Wang, Y. Xu, J. Chem. Soc., Dalton Trans. (1999) 3573.

14. L.A. Saryan, E. Ankel, C. Krishnamurti, D.H. Petering, H. Elford, J. Med. Chem. 22 (1979) 1218.

15. R.C. DeConti, B.R Toftness, K.C. Agarwal, R. Tomchick, J.A. Mead, J.R. Bertino, A.C. Sartorelly, W.A. Creasey, Cancer Res. 32 (1972) 1455.

16. C. He, C.-y. Duan, C.-j. Fang, Y.-j. Liu,Q.-j. Meng, J. Chem. Soc., Dalton Trans. (2000) 1207.

17. A. Bacchi, A. Bonini, M. Carcelli, F.J. Farraro, J. Chem. Soc., Dalton Trans. (1996) 2699.

18. F. Wurthner, C.-C. You, R. Saha-Moller, Chem. Soc. Rev. 33 (2004) 133 and refs therein.

19. W.J. Geary, Coord. Chem. Rev. 7 (1971) 81.

20. B.F.G. Johnson, J.S. McIndoe, Coord. Chem. Rev. 200-202 (2000) 901.

21. U.L. Kala, S. Suma, M.R.P. Kurup, S. Krishnan, R.P. John, Polyhedron 26 (2007) 1427.

22. K. Nakamoto, Infrared and Raman spectra of Inorganic and Coordination Compounds, 5th ed., Wiley, New York (1997).

23. R.J. Clark, C.S. Williams, Inorg. Chem. 4 (1965) 350.

24. A.M. Bond, R.L. Martin, Coord. Chem. Rev. 54 (1984) 23.

25. P.F. Rapheal, E. Manoj, M.R.P. Kurup, Polyhedron 26 (2007) 818.

26. A. Sreekanth, M.R.P. Kurup, Polyhedron 22 (2003) 3321.

27. M. Joseph, M. Kuriakose, M.R.P. Kurup, E. Suresh, A. Kishore, S.G. Bhat, Polyhedron 25 (2006) 61.

28. A.B.P. Lever, Inorganic Electronic Spectroscopy, 2nd ed., Elsevier, Science Publishing Company, Amsterdam (1984).

29. B. Viossat, F.T. Greenaway, G. Morgant, J.-C. Daran, N.-H. Dung, J.R.J. Sorenson, J. Inorg. Biochem. 99 (2005) 355.

30. D. Kivelson, R. Neiman, J. Chem. Phys. 35 (1961) 149.

31. A.L. van den Brenk, J.D.A. Tyndall, R.M. Cusack, A. Jones, D.P. Fairlie, L.R. Gahan, G.R. Hanson, J. Inorg. Biochem. 98 (2004) 1857,

32. R. Cejudo, G. Alzuet, M. Gonzalez-Alvarez, J.L. Garcia-Gimenez, J. Borras, M. Liu-Gonzalez, J. Inorg. Biochem. 100 (2006) 70.

33. S. Stoll, A. Schweiger, J. Mag. Res. 178 (2006) 42.

34. C. Finazzo, C. Calle, S. Stoll, S. Van Doorslaer, A. Schweiger, Phys. Chem.

Chem. Phys. 8 (2006) 1942.

35. P. Peisach, W.E. Blumberg, Arch. Biochem. Biophys. 165 (1974) 691.

36. V. Uma, M. Kanthimathi, J. Subramanian, B.U. Nair, Biochim. Biophys. Acta 1760 (2006) 814.

37. U. Sakaguchi, A.W. Addison, J. Chem. Soc., Dalton Trans. (1979) 600.

38. R. Pogni, M.C. Bartto, A. Diaz, R. Basosi, J. Inorg. Biochem. 79 (2000) 333.

39. A. Rockenbauer, J. Magn. Res. 35 (1979) 429.

40. W.A. Alves, R.H. A. Santos, A. Paduan-Filho, C.C. Becerra, A.C. Borin, A.M.D.C. Ferreira, Inorg. Chim. Acta 357 (2004) 2269.

41. Stability Constants, Special Publication 17, The Chemical Society, London (1964).

42. T.D. Smith, J.R. Pilbrow, Coord. Chem. Rev. 13 (1974) 173.

43. B.J. Hathaway, in: G. Wilkinson, R.D. Gillard, J.A. McCleverty (eds.), Comprehensive Coordination Chemistry II, vol. 5, Pergamon, Oxford (1987) 533.

44. A.H. Maki, B.R. McGravey, J. Chem. Phys. 28 (1958) 35.

45. K. Ito, T. Ito, Aust. J. Chem. 11 (1958) 406.

46. O. Kahn, Angew. Chem. Int. Ed. Engl. 24 (1985) 834.

47. P.J. Hay, J.C. Thibeault, R. Hoffmann, J. Am. Chem. Soc. 97 (1975) 4884.

48. B.Bleaney, K.Bowers, Proc. R. Soc. London, Sect. A 214 (1952) 451.

49. K. Andelkovic, D. Sladic, A. Bacchi, G. Pelizzi, N. Filipovic, M. Rajkovic, Trans. Met. Chem. 30 (2005) 243.

50. G.M. Sheldrick, SHELXTL Version 5.1, Software Reference Manual, Bruker AXS Inc., Madison, Wisconsin, USA (1997).

51. A.L. Spek, J. Appl. Cryst. 36 (2003) 7.

52. C.F. Macrae, P.R. Edgington, P. McCabe, E. Pidcock, G.P. Shields, R. Taylor, M. Towler, J. van de Streek, J. Appl. Cryst. 39 (2006) 453.

53. Y.D. Lampeka, I.M. Maloshtan, P. Lightfoot, R.W. Hay Teor. Eksp. Khim. (Russ.) (Theoret. Exp. Chem.) 34 (1998) 355.

54. L.P. Battaglia, M. Carcelli, F. Ferraro, L. Mavilla, C. Pelizzi, G. Pelizzi, J. Chem. Soc., Dalton Trans. (1994) 2651.

55. E. Amadei, M. Carcelli, S. Lanelli, P. Cozzini, P. Pelagatti, C. Pelizzi, J. Chem. Soc., Dalton Trans. (1998) 1025.

****

Spectral and magnetic studies of Mn(II) molecular frameworks of carbohydrazone and thiocarbohydrazone ligands

5.1. Introduction

Manganese, an essential trace nutrient in all forms of life, shows oxidation states ranging from -3 to +7 [1], however the most common oxidation states being +2 to +7. The +2 state is the most common and Mn^{2+} ions exist in the solid, in solution and as complexes. The coordination chemistry of manganese with N and/or O containing ligands has recently been receiving much attention, because of the variable structures of manganese complexes, the wide occurrence of manganese enzymes in plants and bacteria [2,3], the possibility of magnetic coupling interactions [4] and the application of manganese compounds in industrial catalysis [3]. High spin Mn(II) complexes are characterized by the absence of ligand field stabilization energy and this has two main consequences: (i) the possibility to obtain various coordination geometries and (ii) a lower stability of Mn(II) complexes compared with those of other divalent 3d metals. With regard to second point, there are lesser number of reports for Mn(II) complexes compared to complexes of Ni(II), Cu(II), Zn(II), etc.

The name manganese originates from the Latin word 'magnes' meaning magnet. The magnetochemistry of manganese complexes has been the subject of interest from their very beginning. The synthesis and magnetic properties of discrete polynuclear molecules of manganese are of considerable interest to the field of molecular magnetism, as the first single-molecule magnet was an Mn_{12} complex [5]. Polynuclear manganese clusters have received attention in recent years as potential precursors to molecular magnetic materials or as single-molecule magnets. The

magnetism of polynuclear complexes containing magnetic metal ions, often called molecular nano magnets, has captured the imagination of chemists and physicists alike. Synthesis and structural characterization of novel materials are of special interest in the chemical arena. One of the characteristic features of molecular magnetism is its deeply interdisciplinary character, bringing together organic, organometallic and inorganic synthetic chemists as well as theoreticians from both the chemistry and physics communities, and materials and life-science specialists [6]. Another important impetus for investigating polynuclear manganese clusters lies in their biological relevance. It has become accepted that the water-oxidizing complex of photosystem II contains a tetranuclear manganese aggregate [7,8]. The role of manganese in biological systems is related to its ability to yield polynuclear complexes where various oxidation levels, involving single atom oxidation states in the range II-IV, are accessible [9]. In the design of nanoscale materials, grid structures are of special interest because a two-dimensional, precise grid like configuration of metal centers suggests applications in information storage and processing technology. Moreover, depending on the packing such assemblages of grids have the potential to exhibit either long-range order or single molecule magnetic behavior.

Manganese complexes of thiosemicarbazones are infrequently reported [10-16]. Ferromagnetic and antiferromagnetic cubane like Mn(II) complexes of di-2-pyridyl ketone in the gem-diol form are reported [17]. Self-assembled [3x3] Mn(II) grid complexes are reported to exhibit well defined electrochemical and magnetic properties, and solution studies indicate that groups of metal ions within the grid can be selectively oxidized from Mn(II) to Mn(III) [18] and possible to isolate mixed valence complexes, molecular devices. A self-assembled Mn(II) square grid $[Mn_4L_4](ClO_4)_8$ where L is a bis-tridentate (two N, N, N pockets) ligand is reported as having four octahedral coordination centers [19], this complex decomposes completely in DMF. Compared to other transition metal molecular square grids there are only few reports for Mn(II). There was no previous report of self-assembled

compounds of manganese with thiocarbohydrazones or with carbohydrazones. However, a very closely related Mn(II) tetranuclear complex, [Mn(2-OHpicpn)]$_4$· (ClO$_4$)$_4$, is reported [20] with its catalytic disproportionation of hydrogen peroxide, showing the possibility of formation of Mn(II) squares. Also, there are reports of mono and binuclear carbohydrazide Mn(II) complexes as energetic materials [21-24]. Coordination number and configuration of [Mn(carbohydrazide)$_3$](ClO$_4$)$_2$ are six and octahedron respectively, and for the other three binuclear complexes of Mn(II) are seven and pentagonal bipyramid configuration [21]. Simultaneously, the first example of a seven-coordinate Mn(II) complex with a monodentate organic ligand N,N'-dimethylurea have been reported [25]. The Mn(II) complex of bis(2-hydroxyacetophenone) thiocarbohydrazone and that of bis(5-chlorosalicylaldehyde) thiocarbohydrazone are assigned to mononuclear with octahedral geometry [26]. The aim of the present work is the synthesis and characterization of novel coordination frameworks of magnetically coupled Mn(II) complexes.

5.2. Experimental

5.2.1. Materials

MnCl$_2$· 4H$_2$O (Fluka), Mn(CH$_3$COO)$_2$· 4H$_2$O (Merck), Mn(ClO$_4$)$_2$· 6H$_2$O (Aldrich), NaN$_3$ (Reidel-De Haen), HClO$_4$, HCl, etc were used as received and solvents were purified by standard procedures before use.

Caution! Perchlorate and azide complexes of metals with organic ligands are potentially explosive and should be handled with care.

5.2.2. Synthesis of Mn(II) complexes

[Mn$_2$(HL^2)L^2]$_2$Cl$_2$· CHCl$_3$· 9H$_2$O (19)

A solution of MnCl$_2$· 4H$_2$O (0.199 g, 1 mmol) in 10 ml of methanol was added to a solution of H$_2$L^2 (0.440 g, 1 mmol) in 10 ml chloroform and refluxed for 1 h and allowed to stand at room temperature. Orange colored product separated out

after three days was filtered, washed with methanol followed by ether and dried over P_4O_{10} *in vacuo*. Yield: 0.364 g (63%). Elemental Anal. Found (Calc.): C, 52.54 (52.46); H, 3.69 (4.05); N, 14.75 (14.54); S, 5.45 (5.55)%.

[Mn₂(HL³)L³(N₃)· 2H₂O]· 2H₂O (20)

[Mn₂(HL³)L³(N₃)· 2H₂O]· 2H₂O (20)
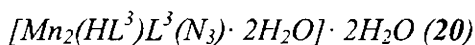
To a boiling solution of H_2L^3 (0.388 g, 1 mmol) in 60 ml methanol, $Mn(CH_3COO)_2$· $4H_2O$ (0.247 g, 1 mmol) in 10 ml of methanol was added with a drop of dil HCl and refluxed for 5 minutes. It was then added NaN_3 (0.131 g, 2 mmol) in boiling methanol and refluxed for 1 h and allowed to stand at room temperature. Orange brown product separated out was filtered, washed with methanol, hot water and ether and dried over P_4O_{10} *in vacuo*. Yield: 0.335 g (68%). Elemental Anal. Found (Calc.): C, 50.50 (50.96); H, 3.55 (3.77); N, 21.53 (21.23); S, 6.57 (6.48)%.

[Mn₂(H₂L⁴)HL⁴]₂(ClO₄)₆·10H₂O (21)
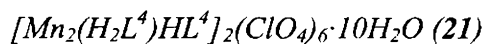
To a boiling solution of H_2L^4 (0.212 g, 0.5 mmol) in 20 ml methanol, $Mn(ClO_4)_2$· $6H_2O$ (0.365 g, 1 mmol) in 10 ml of methanol was added with a drop of $HClO_4$ and refluxed for 1 h and allowed to stand at room temperature. The orange white powder precipitated was filtered, washed with methanol and ether and dried *in vacuo* over P_4O_{10}. Yield: 0.290 g (86%). Elemental Anal. Found (Calc.): C, 41.09 (41.16); H, 3.98 (3.38); N, 17.23 (16.70)%.

[Mn₂(H₂L⁵)HL⁵]₂(ClO₄)₆· 13H₂O (22)
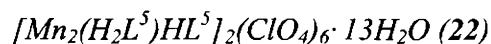
To a boiling solution of H_2L^5 (0.169 g, 0.4 mmol) in 20 ml methanol, $Mn(ClO_4)_2$· $6H_2O$ (0.292 g, 0.8 mmol) in 10 ml of methanol was added with a drop of $HClO_4$ and refluxed for 1 h and allowed to stand at room temperature. White yellow product separated out was filtered, washed with methanol, followed by ether and dried over P_4O_{10} *in vacuo*. Yield: 0.160 g (59%). Elemental Anal. Found (Calc.): C, 44.13 (43.99); H, 4.24 (3.84); N, 12.37 (12.31)%.

[Mn₂(H₂L⁶)HL⁶]₂(ClO₄)₆· 3H₂O (23)

Mn(ClO₄)₂· 6H₂O (0.256 g, 0.70 mmol) in 10 ml of methanol was added to a boiling solution of H₂L⁶ (0.169 g, 0.35 mmol) in 20 ml methanol with a drop of HClO₄ and refluxed for 1 h and allowed to stand at room temperature. The yellow powder precipitated was filtered, washed with methanol and ether and dried *in vacuo* over P₄O₁₀. Yield: 0.180 g (88%). Elemental Anal. Found (Calc.): C, 43.36 (43.08); H, 3.14 (2.93); N, 14.43 (14.35)%.

5.3. Results and discussion

The carbohydrazones and thiocarbohydrazones having well defined and appropriately separated two coordination pockets, using the bridging mode of sulfur or oxygen, in principle have a better chance of control over the outcome of a self-assembly process to produce the predefined square grids of metals. The synthesis of complex **19** was done in neutral medium, while the others were carried out in acidic medium. The formation of these kind of materials are hard to prove with common physico-chemical techniques as the formation of multinuclear manganese complexes of thiocarbohydrazones and carbohydrazones are not reported previously, and especially when the Mn(II) complexes lacks stability compared with those of other divalent 3d metals. Unfortunately, all attempts to crystallize any of the complexes went in vain. The MALDI MS spectra revealed sensible fragmentation peaks of the formation of tetranuclear structures for all complexes except **20**, which was assigned to be a dinuclear complex. This can be attributed to the formation of thermodynamically controlled single product and the square grids **19, 21, 22** and **23** have a sufficient thermodynamic advantage over the other possible species under the reaction conditions. The complexes **21, 22** and **23** were formed in the 1:1 ratios even though we used a 1:2 ratios of respective ligand to metal salt for syntheses. The structure and stability of coordination complexes under ionization conditions are dependent on various factors like the ligand itself, metal ions, counter ions, solvent,

199

temperature, concentration etc. It is seen that most of the complexes fragmented extensively and is more for carbohydrazones derived Mn(II) complexes. The [Mn(HL)]⁻ fragment was readily observed in all cases, with the presence of characteristic dinuclear and trinuclear fragments of assigned square structures. The electronic spectra of all complexes are consistent with Mn(II) centers. The variable temperature magnetic studies are in agreement with antiferromagnetic couplings among Mn(II) centers, with the possible tetranuclear Mn(II) complexes. The X-band EPR spectra in frozen DMF solution show many features for **19** and **20**, is in accordance with the presence of more than one metal centers. The features of EPR spectra of other complexes **21** and **22** are close to indicate mononuclear octahedral Mn(II), attributed to fragmentation in DMF solution. This is attributed to the concentration of taken solution; for example a very closely related complex [20] in acetonitrile remains as tetramer only above 25 µM. An ESI MS study show peaks corresponding to tetrameric species only at higher concentrations. Also, the same complex shows different EPR characteristics on varying the concentration; a $g = 2$ resonance with nearly 2200 G in width at 77 K in acetonitrile/dichloromethane and EPR silent at 5 K. So for a highly coupled Mn(II) cluster a resonance at $g = 2$ with high width is expected; however the fragmentation in DMF is clear in the spectra of complexes **19, 21** and **22** under the investigation conditions. The EPR spectrum recorded for complex **23** in DMF at 77 K lacks any signal. However, it is not possible to get a complete characterization between mononuclear and multinuclear Mn(II) complexes by X-band EPR spectra alone. The MALDI mass spectrum of **23** also didn't show any characteristic peaks attributed to lack of enough concentration or due to complete fragmentation in solution. Molar conductivity measurement in 10^{-3} M DMF solution of complex **19** shows a 2:1 electrolyte (121 $\Omega^{-1}cm^2mol^{-1}$) [27] and complex **20** exhibits nonelectrolytic nature (9 $\Omega^{-1}cm^2mol^{-1}$). For Mn(II) carbohydrazone complexes, the conductance values obtained were 68, 62 and 61 Ω^-

^{1}cm^{2}mol^{-1} in10^{-4} M DMF solutions respectively for **21, 22** and **23**, which is found comparable to the behaviour of molecular squares of other metals. The complex **19** is assigned to a molecular square grid of formula [Mn$_2$(HL^2)L^2]$_2$Cl$_2$· CHCl$_3$· 9H$_2$O, while **20** to be a dinuclear complex [Mn$_2$(HL^3)L^3· 2H$_2$O]· 2H$_2$O. The other three complexes **21, 22** and **23** are assigned to a general formula [Mn$_2$(H$_2$L)HL]$_2$(ClO$_4$)$_6$· nH$_2$O. The tentative structures of these complexes are shown in Schemes 5.1 and 5.2.
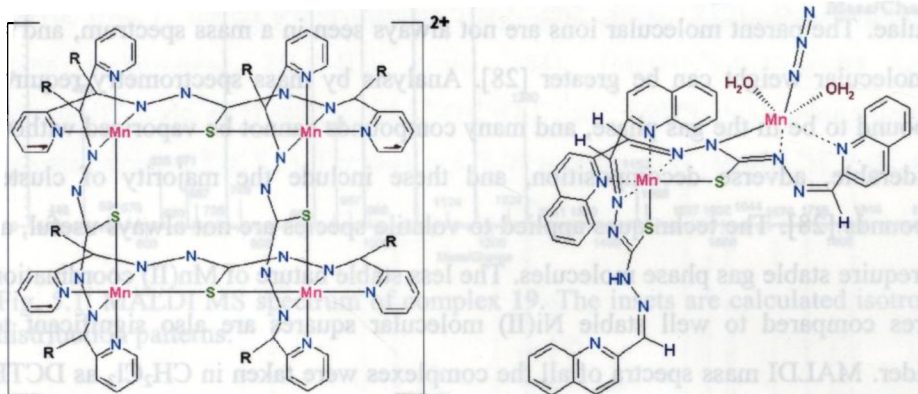
Scheme 5.1. The tentative structural skeleton of complex **19** (left) and structure of **20** (right). R= phenyl. The exact position of six –NH hydrogens in **19** are uncertain and are not shown. Most of the C–N bonds in **19** are double bonds, also not shown.
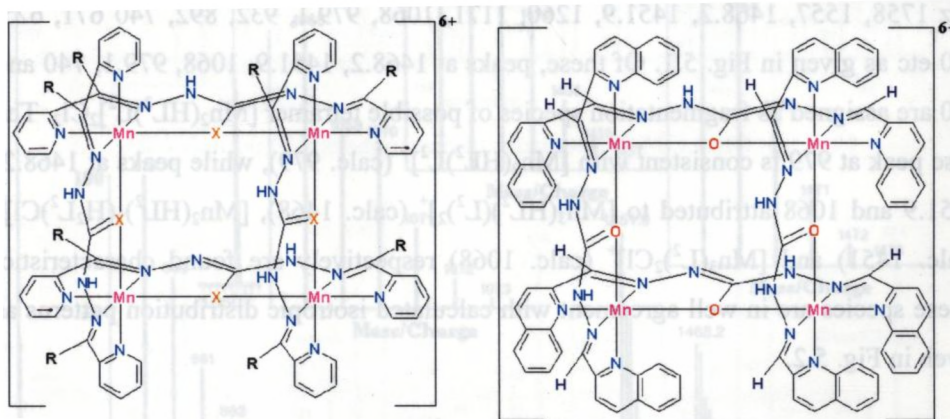
Scheme 5.2. Tentative structures of complexes **21** and **22** (left) and **23** (right). X= O. R= pyridyl for **21** and phenyl for **22**. The exact positions of –NH hydrogens shown in these three complexes are uncertain.

5.3.1. MALDI MS spectral studies

For revealing the formation of rigid tetranuclear molecular structures of Ni(II), MALDI MS spectra were found very successful. Mn(II) complexes are found to be not so stable, however formation of molecular square complexes are indicative by significant fragmentation species. Theoretical simulations of isotropic distribution patterns of fragmentation peaks are found useful to confirm expected structural formulae. The parent molecular ions are not always seen in a mass spectrum, and so the molecular weight can be greater [28]. Analysis by mass spectrometry requires compound to be in the gas phase, and many compounds cannot be vaporized without considerable, adverse decomposition, and these include the majority of cluster compounds [28]. The techniques applied to volatile species are not always useful, as they require stable gas phase molecules. The less stable nature of Mn(II) coordination squares compared to well stable Ni(II) molecular squares are also significant to consider. MALDI mass spectra of all the complexes were taken in CH_2Cl_2 as DCTB mix on positive ion mode.

The complex **19** exhibits peaks of well defined isotropic patterns centered at m/z 1758, 1557, 1468.2, 1451.9, 1260, 1171, 1068, 979.1, 932, 892, 740 671, 625, 490 etc as given in Fig. 5.1. Of these, peaks at 1468.2, 1451.9, 1068, 979.1, 740 and 490 are assigned as fragmentation species of possible tetramer $[Mn_2(HL^2)L^2]_2Cl_2$. The base peak at 979 is consistent with $[Mn_2(HL^2)L^2]^+$ (calc. 979), while peaks at 1468.2, 1451.9 and 1068 attributed to $[Mn_3(HL^2)(L^2)_2]^+$ (calc. 1468), $[Mn_2(HL^2)_2(H_2L^2)Cl]^+$ (calc. 1451) and $[Mn_3(L^2)_2Cl]^+$ (calc. 1068) respectively are found characteristic. These species are in well agreement with calculated isotropic distribution patterns as given in Fig. 5.2.
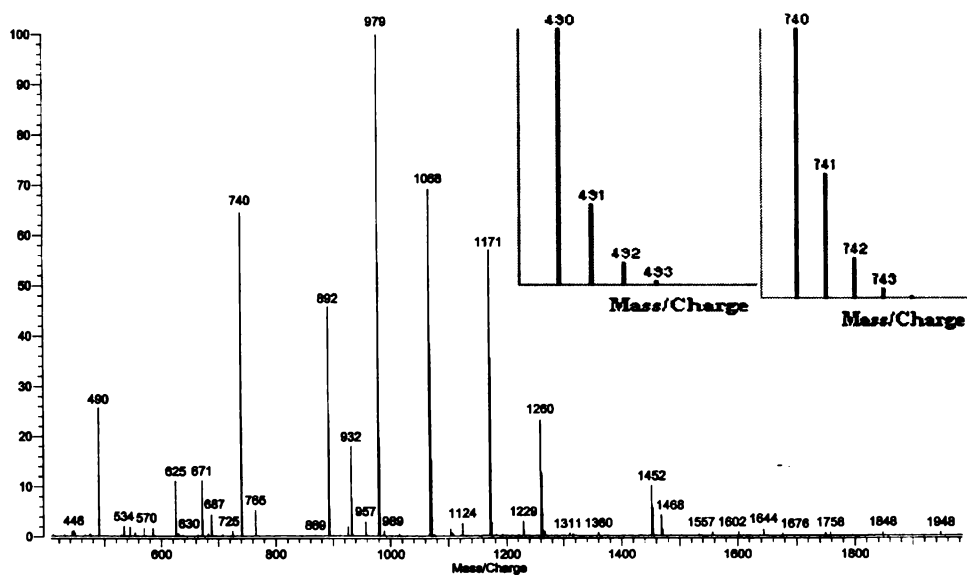
Fig. 5.1. MALDI MS spectrum of complex **19**. The insets are calculated isotropic distribution patterns.
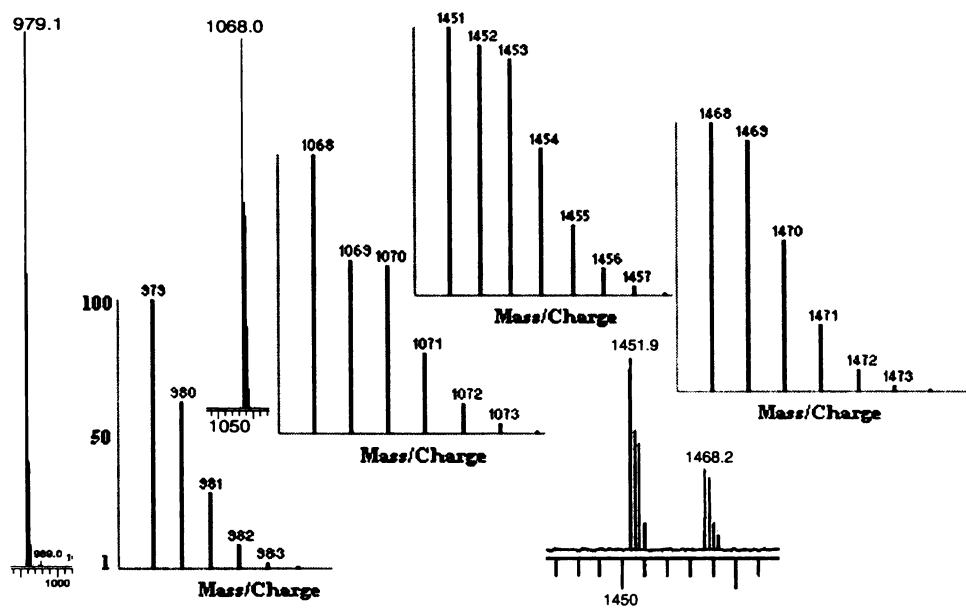
Fig. 5.2. Isotropic distribution patterns of peaks of **19** with their calculated patterns.

The spectrum of **20** shows many peaks (Fig. 5.3). The peak at 438 is assigned as $[Mn(HL^3)]^+$ (calc. 438) with matching isotropic distribution pattern. The small peak at 913 may be of $[Mn_2(HL^3)L^3 \cdot 2H_2O]^+$ (calc. 912), which lacks isotropic pattern due to very low intensity. The peak at 875 is assigned as $[Mn_2(HL^3)L^3]^+$ (calc. 875), 822 as $[Mn(HL^3)H_2L^3]^+$ (calc. 822), 651 as $[Mn(H_2L^3)N_3+\text{quinoline-2-aldehyde hydrazone}]^+$ (calc. 651) and 609 as $[Mn(HL^3)+\text{quinoline-2-aldehyde hydrazone}]^+$ (calc. 609) with agreeing calculated isotropic patterns (Fig. 5.4).
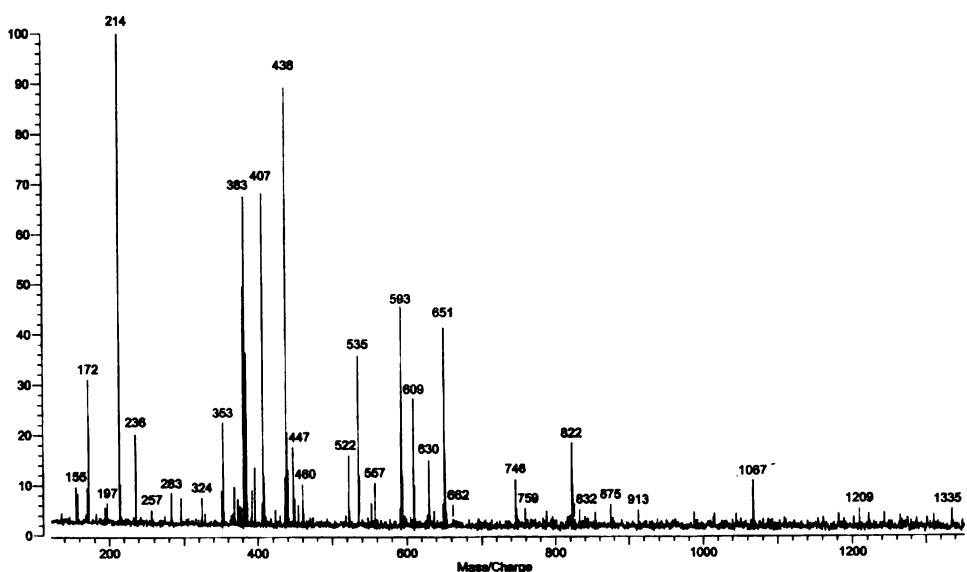
Fig. 5.3. MALDI MS spectrum of dimanganese(II) complex **20**.
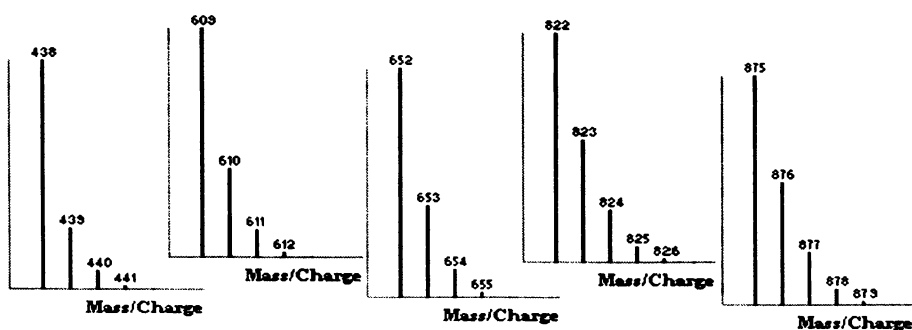
Fig. 5.4. Calculated agreeing isotropic distribution patterns of main peaks of **20**.

MALDI MS spectra of the carbohydrazone complexes are found to be fragmented extensively under ionization conditions compared to thiocarbohydrazone complexes. The complex **21** shows peaks centered at m/z 1021.1843, 983.2309, 898.2527, 883.2750, 785.1430, 685.1847, 674.1828, 561.0714, 476.0900, 445.1490, etc. The peaks at 983.2309, 898.2527, 883.2750, 685.1847, 674.1828 and 561.0714 are found characteristic and assigned as $[Mn_2(HL^4)L^4 \cdot CH_3OH]^+$ (calc. 983), $[Mn(HL^4)H_2L^4]^+$ (calc. 898), $[Mn(HL^4)(H_2L^4-O)]^+$ (calc. 882), [Mn(di-2-pyridyl ketone hydrazone)$_3 \cdot 2H_2O-H^+]^+$ (calc. 684), $[Mn(HL^4)(\text{di-2-pyridyl ketone hydrazone})]^+$ (calc. 674) and $[Mn(H_2L^4-O)ClO_4]^+$ (calc. 560) with agreeing calculated isotropic patterns (Fig. 5.5). The peak at 476.09 is assigned as $[Mn(HL^4)]^+$ (calc. 476).
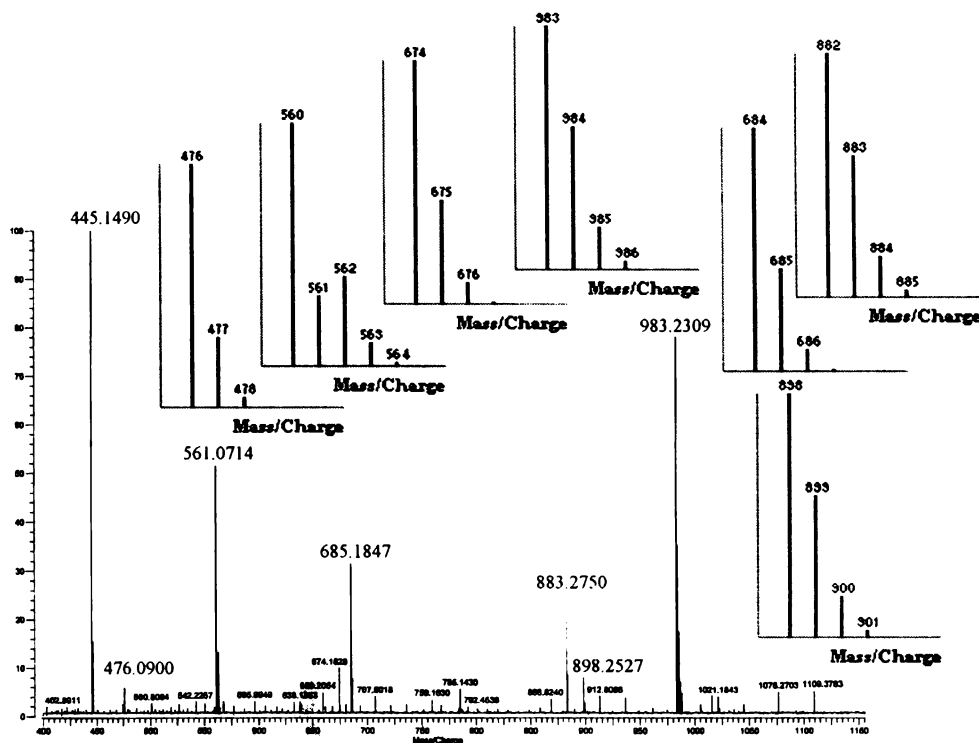
Fig. 5.5. MALDI MS spectrum of complex **21**. The insets are calculated isotropic patterns of relevant peaks.

The peaks of complex **22** are seen centered at m/z 979.2559, 894.2743, 824.0774, 809.1023, 671.1977, 574.0566, 559.0818, 474.0995, etc. These characteristic peaks are assigned as $[Mn_2(HL^5)L^5 \cdot CH_3OH]^+$ (calc. 979), $[Mn(H_2L^5)HL^5]^+$ (calc. 894), $[Mn(HL^5)(di-2-benzoylpyridine\ hydrazone)]^+$ (calc. 671), $[Mn(H_2L^5)ClO_4]^+$ (calc. 574), $[Mn(H_2L^5-O)ClO_4]^+$ (calc. 558) and base peak $[Mn(HL^5)]^+$ (calc. 474) with well agreeing calculated isotropic patterns (Fig. 5.6). The Mn(II) complex **23** exhibits many peaks, but none of the peaks match well with simulation because of the absence of isotropic patterns, may be due to absence of enough concentrated solution for measurement under the investigation condition or due to extensive fragmentation along with coordination with DCTB under ionization condition.
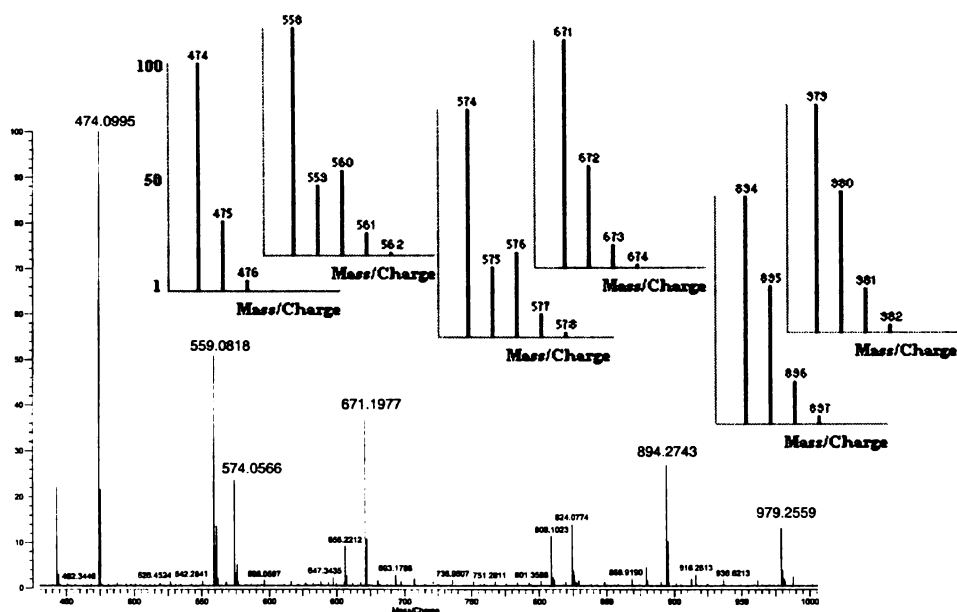
Fig. 5.6. MALDI MS spectrum of **22**. The insets are calculated agreeing distribution patterns of main peaks.

5.3.2. EPR spectral studies

High spin Mn(II) ion with five unpaired electrons (S=5/2) have an orbitally non-degenerate $^6A_1$ ground state. Also, all the excited states are far removed and hence the spin-orbit coupling is expected to be very small or unimportant and the zero field splitting should be rather small. Due to this remoteness of excited states, the g factors of Mn(II) species lie very close to the free electron g value.

The static spin Hamiltonian used to describe the energies of states of a paramagnetic species in the ground state with an effective electron spin S and m nuclei with nuclear spins I is given [29] by,

$$\hat{H}_0 = \hat{H}_{EZ} + \hat{H}_{ZFS} + \hat{H}_{HF} + \hat{H}_{NZ} + \hat{H}_{NQ}$$

$$= \beta_e \widetilde{B}_0 g S + \widetilde{S} D S + \sum_{k=1}^{m} \widetilde{S} A_k I_k - \beta_n \sum_{k=1}^{m} g_{n,k} \widetilde{B}_0 I_k + \sum_{I>\frac{1}{2}} \widetilde{I}_k P_k K_k \quad (1)$$

$\hat{H}_0$ is called the spin Hamiltonian since it contains only phenomenological constants and spin coordinates described by the electron spin vector operator $\widetilde{S} = [\hat{S}_x, \hat{S}_y, \hat{S}_z]$ and the nuclear spin operators $\widetilde{I}_k = [\hat{I}_{x,k}, \hat{I}_{y,k}, \hat{I}_{z,k}]$. The terms describe; $\hat{H}_{EZ}$ - electron Zeeman interaction, $\hat{H}_{ZFS}$ - zero-field splitting; $\hat{H}_{HF}$ - hyperfine interactions between the electron spins and the m nuclear spins, $\hat{H}_{NZ}$ - nuclear Zeeman interactions and $\hat{H}_{NQ}$ - nuclear quadrupole interactions for $I > \frac{1}{2}$. In the case of Mn(II) the zerofield splitting, term become relevant, which is given by

$$\widetilde{S} D S = D[S_z^2 - S(S+1)/3] + E(S_x^2 - S_y^2)$$

B_0 is a vector describing the direction and strength of the permanent magnetic field. The transpose is denoted with $^{\sim}$. The zero-field splitting term here ignores second-order contributions, which are only different from zero for symmetries

207

lower than cubic. However, in eqn. (1) we can ignore the terms of the spin-spin interactions, NZ interaction and the quadrupole interactions between pairs of nuclear spins, since their magnitudes are very small compared to the other terms and the usual linewidths observed in paramagnetic complexes. Therefore the Hamiltonian takes the form,

$$\hat{H}_0 = \beta_e \widetilde{B}_0 gS + D[S_z^2 - S(S+1)/3] + E(S_x^2 - S_y^2) + \sum_{k=1}^{m} \widetilde{S}A_k I_k \quad (2)$$

The construction of a proper model for the simulation is very hard, especially in the lack of X-ray crystal structure data and fragmentation in DMF. However, the Mn(II) systems were simulated by considering eqn. (2), as the taken spectra resembles a possible fragmentation of all complexes to monomeric species, to get the magnetic parameters.

In the zero field splitting terms, D is the axial zero field splitting term and E is the rhombic zero field splitting parameter. If D and E are very small compared to *electron Zeeman term*, five ESR transitions corresponding to $\Delta m_s = \pm 1$ are expected. But if D is very large, then only transition between $\left| + \frac{1}{2} \right\rangle \leftrightarrow \left| - \frac{1}{2} \right\rangle$ with a g value of ~2 will be observed. However, for the case where D or E is very large, the lowest doublet has effective g values of $g_{\parallel}$~2, $g_{\perp}$~6 for $D \neq 0$ and $E=0$, but for $D=0$ and $E \neq 0$ the middle Kramer's doublet has an isotropic g value of 4.29 [30, 31]. Depending upon the values of D and A, the number of lines appear in the spectra will be 30 or 24 or six [32].

In the present study, X-band EPR spectra of all the complexes in DMF at 77 K were recorded in a cw EPR spectrometer. The numerical data of these frozen solution spectra were calculated by using EasySpin [33,34] written in MATLAB, and allows fitting of the experimental spectra by simulations by variation of the independent parameters including g, hyperfine coupling constant A, ZFS parameters

D and E, etc. The g values other than that at ~2 of **19** and **20** were calculated from the spectra without simulations. For all complexes, EPR spectral simulation was done by considering them as mononuclear Mn(II) systems, i.e. under the investigation conditions. The simulations of **19** (Fig. 5.7) and **20** (Fig. 5.8) are not matching well with mononuclear Mn(II) models, as they doesn't show g values other than at ~2; however, the simulation at the hyperfine sextet could yield precise values of g and A, though the D-term might be unreliable, due to wrong model usage. However, the simulations of **21** (Fig. 5.9) and **22** (Fig. 5.10) are in well agreement with experimental spectra and suggesting the possible decomposition of these complexes in DMF.

All manganese complexes, except **23**, exhibit a resonance at $g \approx 2$, show a six line hyperfine structure, which is due to the interaction of electron spin of manganese ions with its own nuclear spin $I=5/2$. The g value for the hyperfine splitting is indicative of the nature of bonding in the matrix. The strength of the hyperfine splitting depends on the matrix into which the ion is dissolved and is mainly determined by the electronegativety of the neighbors. This means a qualitative measure of the covalency of the bonding in the matrix that can be determined from the value of A; the smaller the splitting, the more covalent the bonding of the anion. In the spectra of all the complexes additional forbidden lines are observed in between each of the two lines of the central hyperfine sextet. These lines are arising by the violation of $\Delta m_I = \pm 0$ of allowed transitions ($\Delta m_s = \pm 1$, $\Delta m_I = \pm 0$).

The EPR spectrum of **19** exhibits a well-defined hyperfine sextet at $g = 1.995$. Several additional features can be observed including five other ESR resonances at $g = 7.161$, $g = 4.002$, $g = 3.239$, $g = 2.473$ and $g = 1.582$ as small disturbances. A similar, but along with two sets of eleven lines are reported for a dinuclear Mn(II) system in X-band frozen solution spectrum [35]. The hyperfine coupling constant

value of 265 MHz (94.9 G) at $g = 1.995$ is consistent with octahedral coordination [36]. The average separation of the forbidden hyperfine lines lying between each of the two main hyperfine lines in the spectrum is approximately 55.8 MHz (20 G). A D value of 460 MHz (1.5344×10^{-2} cm^{-1}, 164.74 G) was used for simulation.
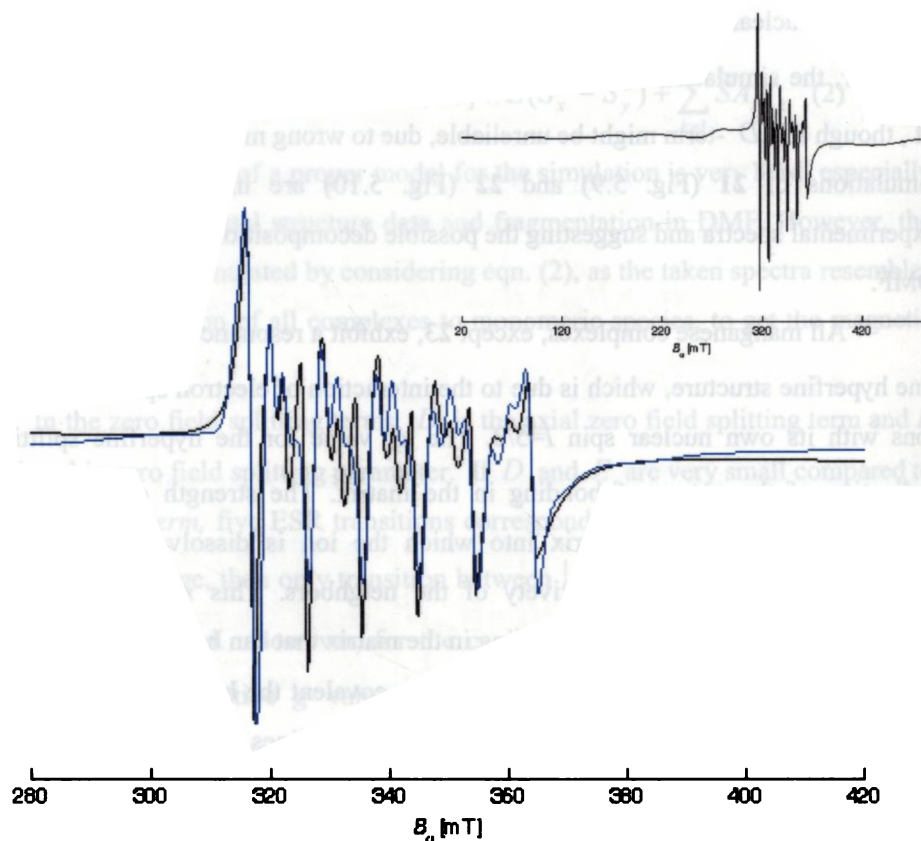
Fig. 5.7. The sextet part at $g = 1.995$ of EPR spectrum of **19** (black) and its simulation (blue). The inset shows the full spectrum.

The EPR spectrum of **20** also shows some features including a well-defined sextet pattern at $g = 1.995$. Another g value at 5.074 is also clear in the spectrum. For a dinuclear coupled Mn(II) system an eleven-line hyperfine pattern [2nI+1=4(5/2)+1=11] with additional features are expected. However, the origin of

210

the pattern is uncertain and it is not observed for all dinuclear Mn(II) centers [37]. Spectra have been identified as arising from dimer systems by their dissimilarity to the spectra of monomeric analogues, their similarity to other dimer spectra, or more definitively, by their characteristic eleven-line hyperfine pattern with a splitting of 4.0-4.7mT [37]. The sextet pattern at $g = 1.995$ of **20** is typical for octahedral manganese(II) environment. The magnitude of the hyperfine splitting, 263 MHz (94.2 G), is consistent with octahedral coordination [36]. For simulation, a D value of 500 MHz (1.6678×10^{-2} cm^{-1}, 179.07 G) was used.
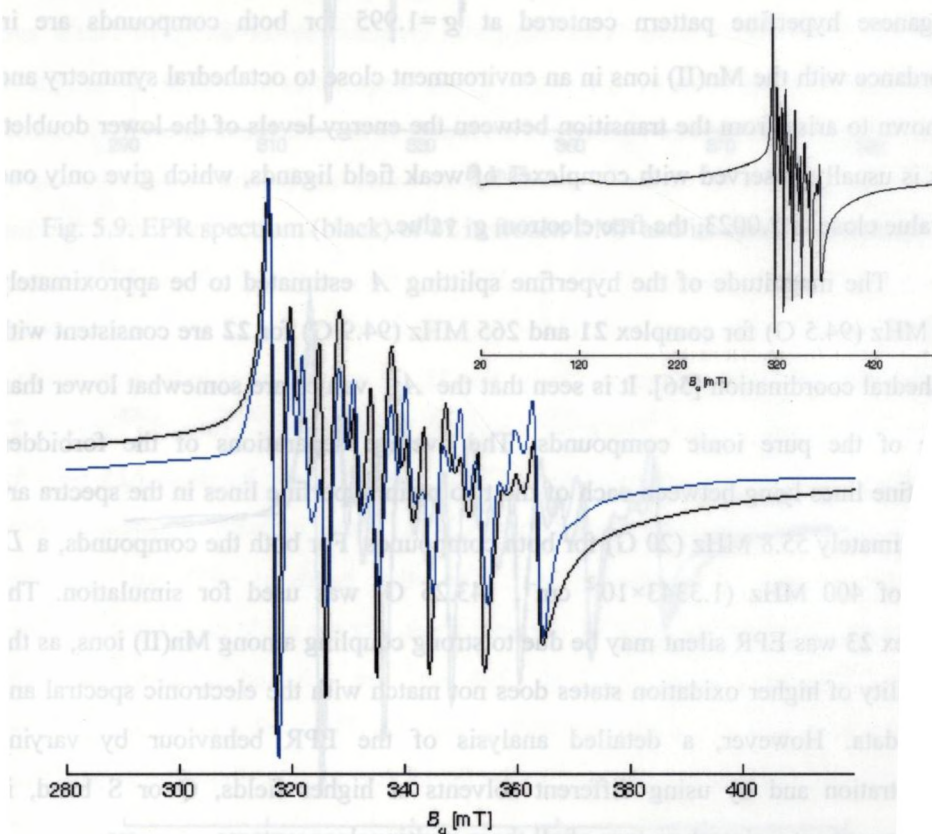
Fig. 5.8. The sextet part at $g = 1.995$ of EPR spectrum of **20** (black) and its simulation (blue). The inset shows the full spectrum.

Broad signals above $g=2$, due to the $S=5/2$ ZFS has been reported for distorted mononuclear octahedral Mn(II) [38] and dimanganese(II) complexes [39]. So, here the presence of dinuclear species is hard to prove, as the same broad EPR features may also arise from ZFS of mononuclear species [3]. Alternatively, partial decomposition of the dimer to mononuclear species by the coordinating solvent may give same result [3].

The spectra of **21** and **22** are more close to Mn(II) monomeric species, due to possible decomposition to monomeric units, and similar to each other. The six line manganese hyperfine pattern centered at $g=1.995$ for both compounds are in accordance with the Mn(II) ions in an environment close to octahedral symmetry and is known to arise from the transition between the energy levels of the lower doublet. This is usually observed with complexes of weak field ligands, which give only one g value close to 2.0023, the free electron g value.

The magnitude of the hyperfine splitting A estimated to be approximately 264 MHz (94.5 G) for complex **21** and 265 MHz (94.9 G) for **22** are consistent with octahedral coordination [36]. It is seen that the A_{iso} values are somewhat lower than those of the pure ionic compounds. The average separations of the forbidden hyperfine lines lying between each of the two main hyperfine lines in the spectra are approximately 55.8 MHz (20 G) for both compounds. For both the compounds, a D value of 400 MHz (1.3343×10^{-2} cm^{-1}, 143.25 G) was used for simulation. The complex **23** was EPR silent may be due to strong coupling among Mn(II) ions, as the possibility of higher oxidation states does not match with the electronic spectral and other data. However, a detailed analysis of the EPR behaviour by varying concentration and by using different solvents at higher fields, Q or S band, is obligatory to get a clearer picture of all these multinuclear systems.
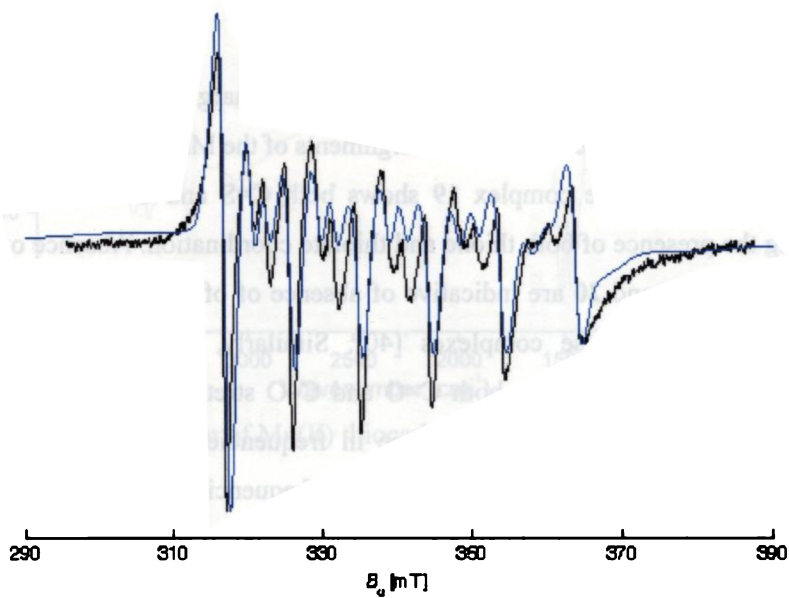
Fig. 5.9. EPR spectrum (black) of **21** in frozen DMF and its simulation (blue).
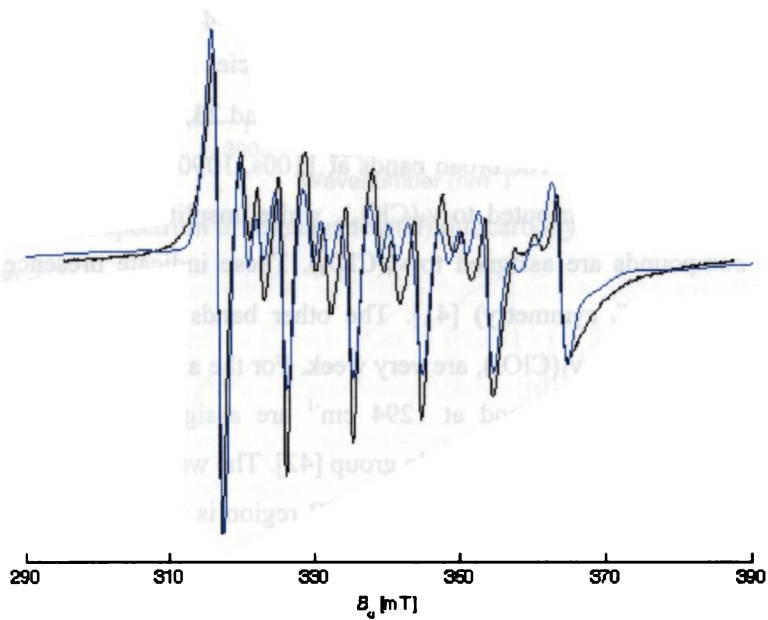
Fig. 5.10. EPR spectrum (black) of **22** in frozen DMF and its simulation (blue).

5.3.3. IR and electronic spectral studies

The IR spectra of manganese complexes show marginal differences from their corresponding ligands. The IR spectral assignments of the Mn(II) complexes are listed in Table 5.1. The square complex **19** shows both C=S and C–S stretching bands suggesting the presence of both thione and thiolate coordination. Absence of bands at ~ 2600 cm^{-1} for **19** and **20** are indicative of absence of of thiol tautomers in free or coordinated form in these complexes [40]. Similarly, the carbohydrazone grid complexes **21**, **22** and **23** show both C=O and C–O stretching bands. These are in agreement with other results. The change in frequencies for assigned bands and differences in mixing patterns of common group frequencies of complexes compared to their respective metal free ligands are attributed to the coordination to metal center. The spectra in the far IR region is also rich with bands attributable to coordination of pyridyl N, azomethine N and sulfur/oxygen to Mn(II). The sulfur metal coordination is supported by strong bands at 350 and 354 cm^{-1} for complexes **19** and **20**, assigned to ν(Mn-S). The ν(Mn-N$_{azo}$) and ν(Mn-N$_{py/qu}$) frequencies for all the complexes are seen at ~420 and ~280 cm^{-1} respectively. For **21**, **22** and **23**, clear indication of ionic form of perchlorate is seen. The broad bands at 1100s, 1090s, 1100s cm^{-1} for **21**, **22** and **23** respectively are attributed to ν_3(ClO$_4$), while unsplit bands at 625 cm^{-1} for these three compounds are assigned to ν_4(ClO$_4$). These indicate presence of ionic perchlorate species (T_d symmetry) [41]. The other bands at ~935 cm^{-1} for these compounds, assignable to ν_1(ClO$_4$), are very week. For the azido complex **20**, a sharp band at 2058 and a strong band at 1294 cm^{-1} are assigned as asymmetric and symmetric stretching of coordinated azido group [42]. The weak band at 630 cm^{-1} may be of δ(NNN). The band at 324 cm^{-1} in the far IR region is attributed to ν(Mn-N$_{azide}$) [42], also supporting the azide coordination to metal. Selected IR and far IR spectra are given in Figs. 5.11 to 5.15.
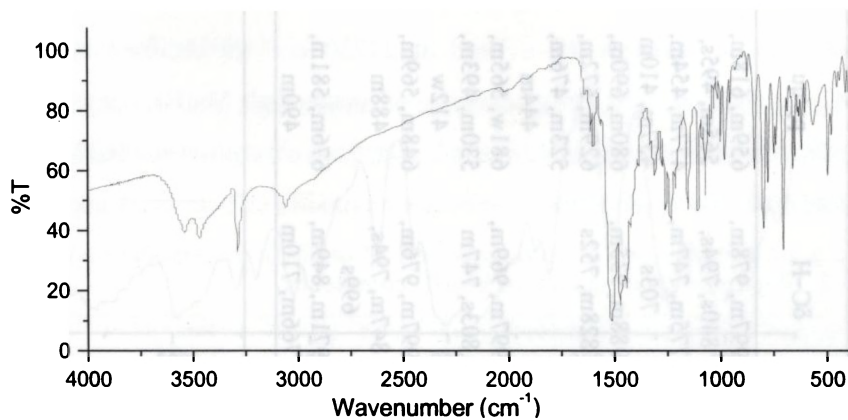
Fig. 5.11. IR spectrum of Mn(II) thiocarbohydrazone square complex **19**.
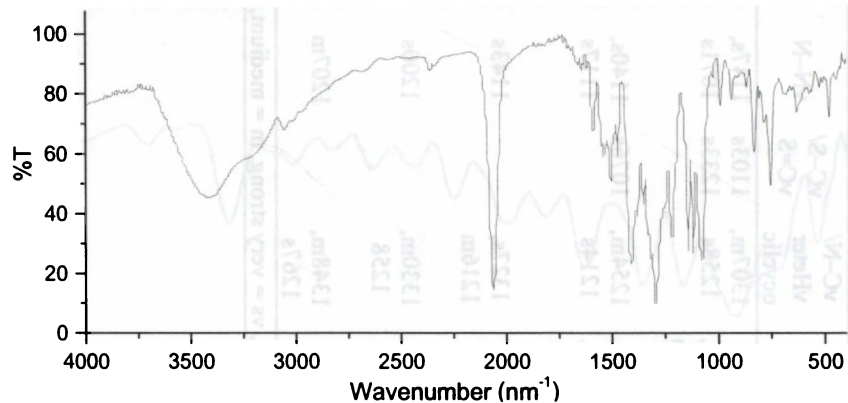
Fig. 5.12. IR spectrum of dimanganese(II) thiocarbohydrazone complex **20**.
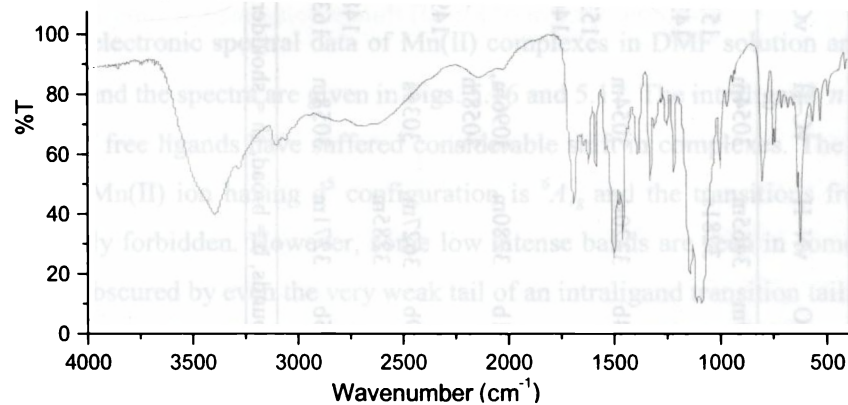
Fig. 5.13. IR spectrum of Mn(II) carbohydrazone square complex **21**.

Table 5.1. IR spectral assignments of Mn(II) complexes (cm^{-1}).

c.	νH_2O	$\nu N-H$	$\nu C-H$	$\nu C=N+ \nu C=C$	$\nu C-N/$ νHeterocyclic	$\nu C-S/$ $\nu C=S$	$\nu N-N$	$\nu C=O/$ $\nu C-O$	$\delta C-H$	py/qu
19	3539m	3465m, 3281s	3054m	1595m, 1513vs, 1468s, 1439m, 1422m	1307m, 1258s	1103s 1233s	1147s, 1071s		997m, 978m, 840s, 794s, 775m, 747m, 703s	659m, 618m, 565m, 495s, 477m, 454m, 437m, 410m
20	3414b	3220sh	3054m	1584m, 1535m, 1501s, 1468m, 1406s	1254m, 1214s	1076s	1140s, 1117s		988m, 935m, 828m, 752s	680m, 690m, 629m, 572m, 523m, 476m, 444m
21	3391b	3280m	3096m, 3058m	1620m, 1580m, 1498vs, 1459s	1327s, 1216m	1143s		1690s, 1385m	997m, 969m, 803s, 747m	681w, 565m, 530m, 493m, 412w
22	3469b	3627m, 3285m	3035s	1618m, 1552vs, 1487m, 1459s	1330m, 1258	1200s		1707s, 1389s	997m, 976m, 847m, 794s, 699s	648m, 569m, 488m
23	3405b	3271m	3058m	1634m, 1581s, 1457m	1348m, 1267s	1207m		1713s, 1383s	971m, 849m, 766m, 710m	676m, 581m, 490m

c. = compounds, b = broad, sh = shoulder, s = strong, vs = very strong, m = medium, w =weak.
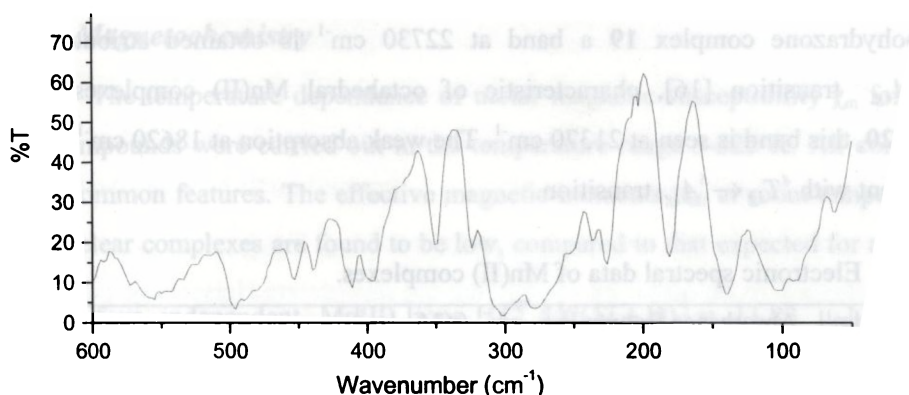
Fig. 5.14. Far IR spectrum of Mn(II) thiocarbohydrazone square complex **19**.
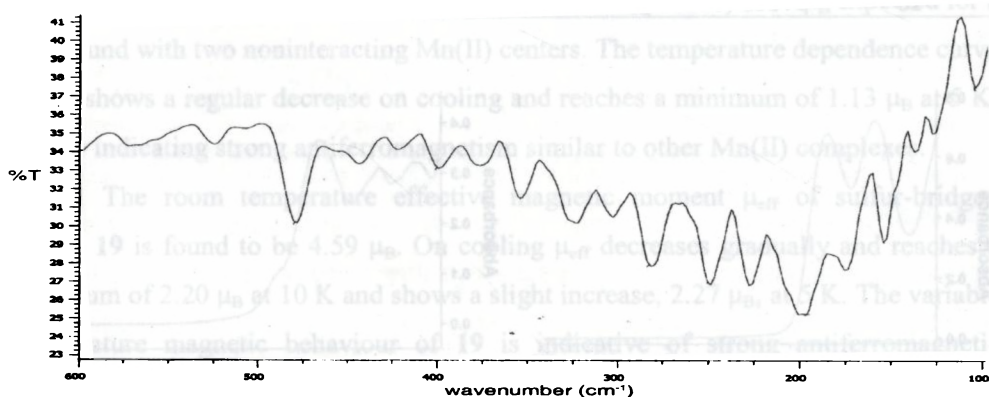
Fig. 5.15. Far IR spectrum of dimanganese(II) thiocarbohydrazone **20**.

The electronic spectral data of Mn(II) complexes in DMF solution are listed in Table 5.2 and the spectra are given in Figs. 5.16 and 5.17. The intraligand $n \rightarrow \pi*$ transitions of free ligands have suffered considerable shift in complexes. The ground state for an Mn(II) ion having d^5 configuration is $^6A_{1g}$ and the transitions from this state is doubly forbidden. However, some low intense bands are seen in some cases, but may be obscured by even the very weak tail of an intraligand transition tailing into the visible region [43]. For the light colored complexes **21**, **22** and **23** the possible fragmentation makes the absorbance values nonreliable. However, for the

thiocarbohydrazone complex **19** a band at 22730 cm^{-1} is obtained atributed to $^4T_{2g} \leftarrow {}^6A_{1g}$ transition [16], characteristic of octahedral Mn(II) complexes. For complex **20**, this band is seen at 21370 cm^{-1}. The weak absorption at 18620 cm^{-1} of **20** is consistent with $^4T_{1g} \leftarrow {}^6A_{1g}$ transition.

Table 5.2. Electronic spectral data of Mn(II) complexes.

Compounds	Absorbance features λ_{max} cm^{-1} (ε M^{-1} cm^{-1})
19	27470 (72100), 22730 (67700)
20	32050 (16050), 27170 (15500), 21370 (18250), 18620 (4770)
21	36360 (104100), 29850 (105400)
22	35590 (78880), 32050 (133900)
23	37310 (148800), 31550 (188600), 29940 (196800), 28740 (167900)

19 in 10^{-5} M DMF   20 in 2×10^{-5} M DMF
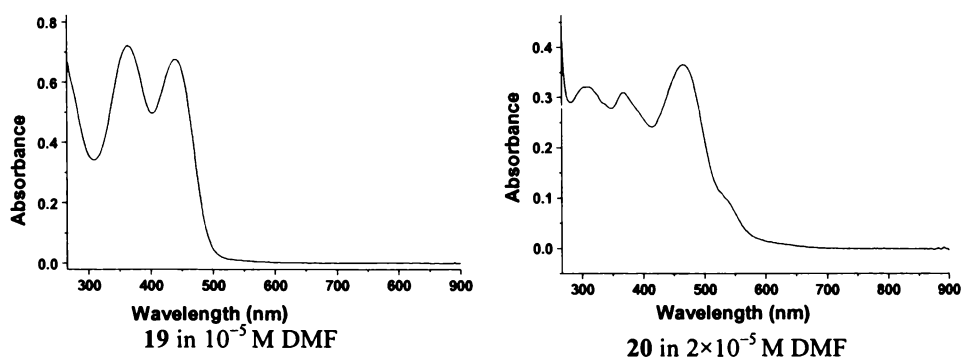
Fig. 5.16. Electronic spectra of Mn(II) thiocarbohydrazone complexes.

21 in 10^{-5} M DMF   23 in 10^{-5} M DMF
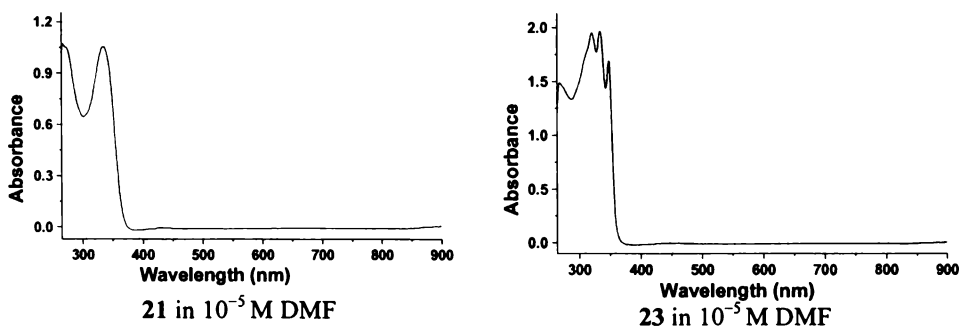
Fig. 5.17. Electronic spectra of Mn(II) carbohydrazone complexes.

5.3.4. Magnetochemistry

The temperature dependence of molar magnetic susceptibility χ_m for all the five compounds were carried out in the temperature range 5-325 K. All compounds show common features. The effective magnetic moments μ_{eff} at room temperature of tetranuclear complexes are found to be low, compared to that expected for a complex having four independent Mn(II) ions $\{(\sum 4Si(Si+1))^{\frac{1}{2}} = 11.83\ \mu_B\}$, and also decreases regularly with decreasing temperature suggesting antiferromagnetic interactions between Mn(II) ions. The room temperature effective magnetic moment μ_{eff} of dinuclear compound **20**, 2.95 μ_B, is very low compared to 8.37 μ_B expected for a compound with two noninteracting Mn(II) centers. The temperature dependence curve of μ_{eff} shows a regular decrease on cooling and reaches a minimum of 1.13 μ_B at 5 K, clearly indicating strong antiferromagnetism similar to other Mn(II) complexes.

The room temperature effective magnetic moment μ_{eff} of sulfur-bridged square **19** is found to be 4.59 μ_B. On cooling μ_{eff} decreases gradually and reaches a minimum of 2.20 μ_B at 10 K and shows a slight increase, 2.27 μ_B, at 5 K. The variable temperature magnetic behaviour of **19** is indicative of strong antiferromagnetic coupling between Mn(II) ions. The sharp increase in the χ_m values at lower temperature is attributed to the presence of monomeric impurity. The carbohydrazone Mn(II) complexes **21, 22** and **23** show common features. The room temperature μ_{eff} of 4.08 μ_B shown by complex **22** is low compared to that of the sulfur bridged compound **19**. The μ_{eff} values show a regular decrease upon decreasing the temperature and reach a minimum of 0.53 μ_B at 5 K. Similarly, the compounds **21** and **23** show magnetic moments of 4.24 and 4.18 μ_B at room temperature and undergo a regular decrease on cooling to reach a minimum value of 0.52 μ_B at 5 K for both complexes. The thermal dependence curve of all these Mn(II) square complexes implies a dominant strong antiferromagnetic interactions between Mn(II) centers. The results are as expected for the proposed structures of these complexes.

To fit and interpret the magnetic susceptibility data of complexes, first it is necessary to find all possible magnetic pathways in the structures. The complexes, except **20**, are expected to be molecular square grids, as would be expected, as in the case of Ni(II) square grids discussed in Chapter 3. So the Mn(II) compounds **19, 21, 22** and **23** are modeled, with a single coupling constant J that takes into account all exchange pathways to be equal, by considering the appropriate Heisenberg exchange Hamiltonian for D_{4h} [2 × 2] grid as,

$$\hat{H} = -2J(\hat{S}_1 \cdot \hat{S}_2 + \hat{S}_2 \cdot \hat{S}_3 + \hat{S}_3 \cdot \hat{S}_4 + \hat{S}_1 \cdot \hat{S}_4) \qquad (1)$$

The corresponding eigenvalues are then obtained using the conventional spin-vector coupling model [44] and are given [45] by,

$$E(S', S_{13}, S_{24}) = 2J[S'(S'+1) - S_{13}(S_{13} + 1) - S_{24}(S_{24} + 1)] \qquad (2)$$

For Mn(II) molecular squares $S_1, S_2, S_3, S_4 = \frac{5}{2}$. There are 146 spin states as given below,

S'	10	9	8	7	6	5	4	3	2	1	0
No. of spin states	1	3	6	10	15	21	24	24	21	15	6

The allowed values are then substituted in to the modified van Vleck equation,

$$\chi_M = \frac{N\beta^2 g^2}{3k(T-\Theta)} \frac{\sum S'(S'+1)(2S'+1)e^{-E(S')/kT}}{\sum (2S'+1)e^{-E(S')/kT}}(1-\rho) + \frac{N\beta^2 g^2 S(S+1)\rho}{3kT} + TIP$$

$$(4)$$

The procedure of generating the exchange equation for such large systems presents a somewhat daunting task in the case of Mn(II) ($S = 5/2$) and so we used MAGMUN4.1 [46] software package for calculation of the spin state energy spectrum for a cluster, and substitution into the van Vleck equation. Then, fitting of variable temperature magnetic data were done to an exchange expression, eqn. (4), using the same program MAGMUN4.1.

The best-fit results obtained for **19**, **21**, **22** and **23** are given in Figs. 5.18 to 5.21. Reasonably good fitting are obtained for all Mn(II) squares. The fitting parameters of Mn(II) thiocarbohydrazone square grid **19** are $g = 2.000\pm 0.017$, $J = -98.87\pm 2.22$ cm^{-1}, $\Theta = -0.08$ K, $\rho = 0.0403$ and $R = 1.93\times10^{-2}$. For complex **21**, the fitting parameters obtained are $g = 2.0008\pm 0.0325$, $J = -92.11\pm 2.25$ cm^{-1}, $\Theta = -2.5$ K, $\rho = 0.0065$ with $R = 2.51\times10^{-2}$. Similarly, for complex **22** the magnetic data were fitted to the van Vleck equation using the Hamiltonian (1) to get the parameters $g = 2.004\pm 0.064$, $J = -98.75\pm 5.27$ cm^{-1}, $\Theta = -1.5$ K, $\rho = 0.0072$ and $R = 3.13\times10^{-2}$. The fitting of magnetic data of **23** using the same model gave $g = 2.013\pm 0.059$, $J = -97.91\pm 4.92$ cm^{-1}, $\Theta = -0.4$ K, $\rho = 0.00736$ and $R = 2.09\times10^{-2}$. For all Mn(II) complexes, the *TIP* was assumed as 0 cm^{3} mol^{-1}, as there is no second order Zeeman perturbations. The exchange integral obtained for all Mn(II) squares are essentially similar and is in accordance with the similar nature of complexes. Relatively high values (negative) are consistent with strong intramolecular antiferromagnetic coupling interactions, result of sulfur/oxygen bridging between the Mn(II) centers in all these expected structures of complexes. The small −ve values of Weiss-like corrective term Θ account for weak intermolecular associations. The deviations at lower temperature in fitting for all complexes may be associated with zero-field splitting (D).

For complex **20**, however, we could not get a reasonable fit for the susceptibility data with the appropriate Heisenberg exchange Hamiltonian considered,

$$\hat{H} = -2J\hat{S}_1 \cdot \hat{S}_2.$$

And the corresponding eigenvalues given by,

$$E(S') = -J[(S'(S'+1) - S_1(S_1 +1) - S_2(S_2 +1)]$$

221
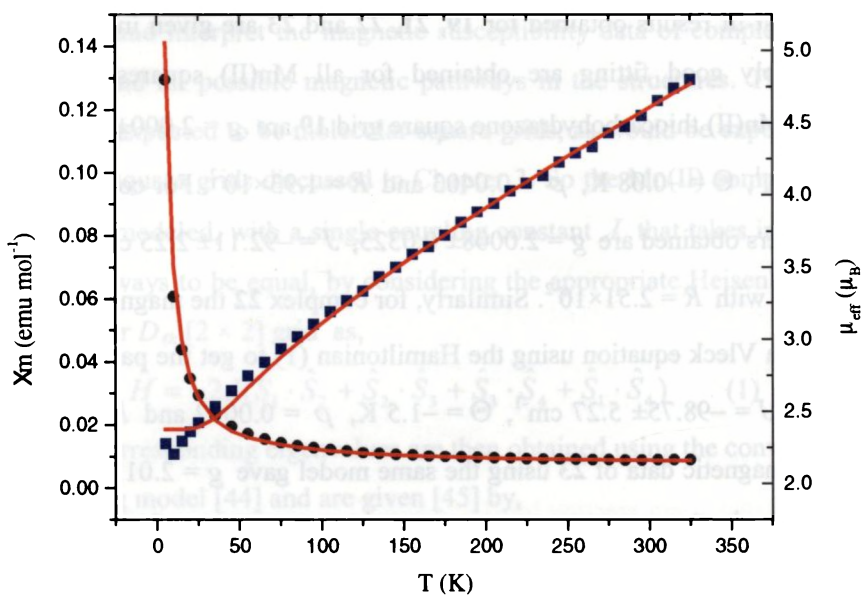
Fig. 5.18. Temperature dependence of molar magnetic susceptibility χ_m (●) and effective magnetic moment μ_{eff} (■) of **19**. The solid lines represent the best fit got.
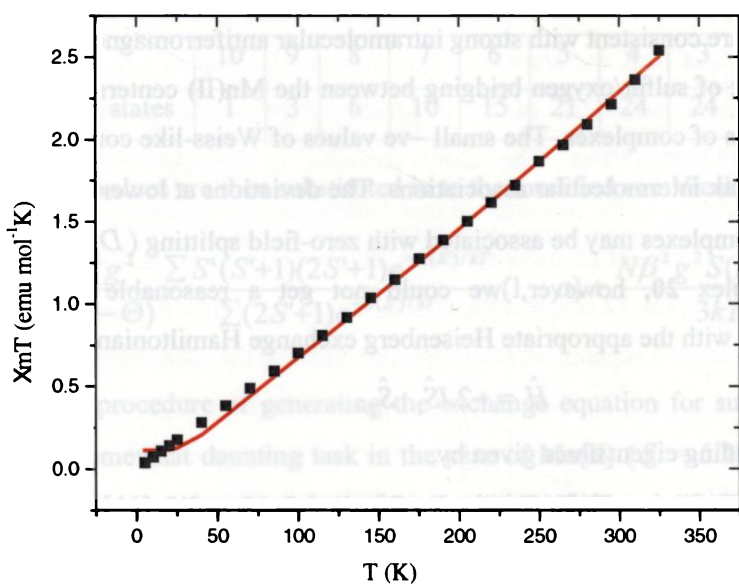
Fig. 5.19. $\chi_m T$ data (■) as a function of temperature for complex **21**. The solid line represents the best fit obtained.
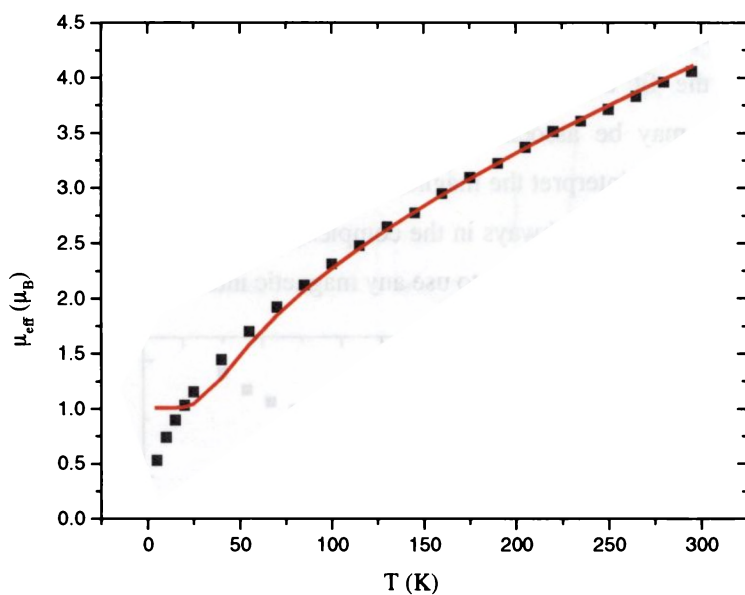
Fig. 5.20. Temperature dependence of effective magnetic moment μ_{eff} (■) for **22**. The solid line represents the best fit obtained.
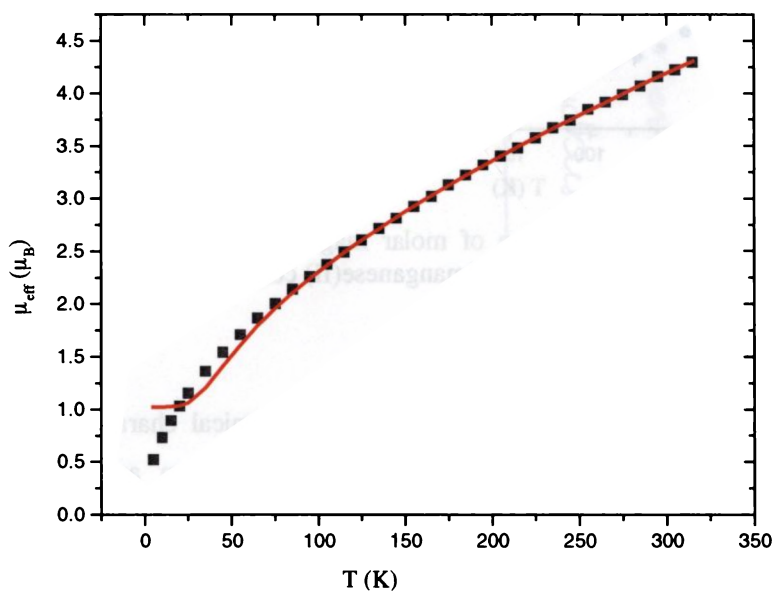
Fig. 5.21. Temperature dependence of effective magnetic moment μ_{eff} (■) for complex **23**. The solid line represents the best fit obtained.

The temperature dependence of χ_m and μ_{eff} curves of complex **20** is given in Fig. 5.22. It is found that the fit departs from the experimental data especially at lower temperatures. This may be associated with presence of other interactions in the compound **20**. To fit and interpret the magnetic susceptibility data, first it is necessary to find all possible magnetic pathways in the complex structure, and in the absence of X-ray structural result it is not possible to use any magnetic interacting models.
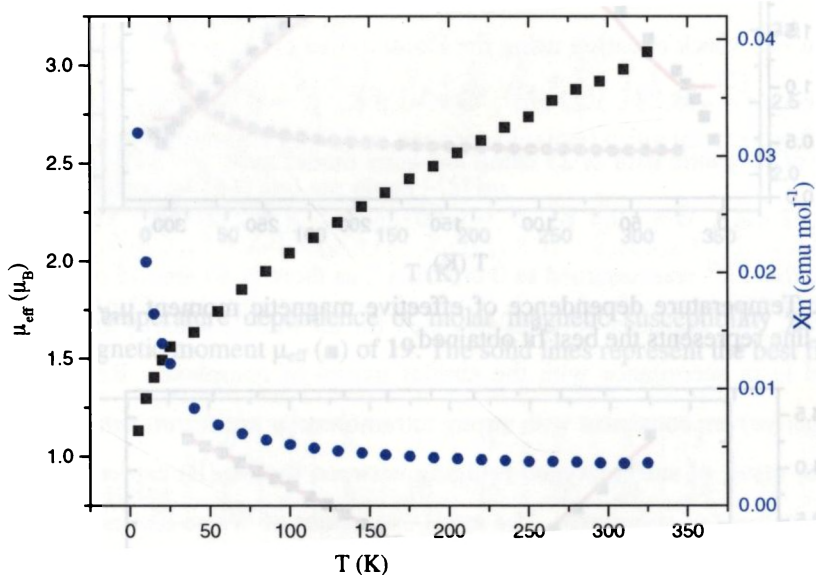
Fig. 5.22. Temperature dependence of molar magnetic susceptibility χ_m (●) and effective magnetic moment μ_{eff} (■) of dimanganese(II) complex **20**.

5.4. Concluding remarks

This chapter presents syntheses and physico-chemical characterizations of five novel manganese coordination compounds. Four of them are assigned as molecular square grids of Mn(II), of which three Mn(II) carbohydrazone complexes are with a general formula $[Mn_2(H_2L)HL]_2(ClO_4)_6 \cdot nH_2O$. The Mn(II) thiocarbohydrazone square complex is having a formula $[Mn_2(HL^2)L^2]_2Cl_2 \cdot CHCl_3 \cdot 9H_2O$. Mn(II) square complexes of carbohydrazones and thiocarbohydrazones are

224

reported for the first time. The MALDI MS spectra reveal sensible fragmentation peaks of tetranuclear molecular squares, and it is found that the Mn(II) squares are not so stable like their Ni(II) counterparts in solution or under ionization conditions of MALDI. The Mn(II) complexes were organized by mono and dideprotonated thiocarbohydrazones and by monodeprotonated and neutral carbohydrazones. Variable temperature magnetic studies of all the Mn(II) square grids exhibit intramolecular antiferromagnetic coupling between electrons, consistent with the expected bridging structural arrangement, by a super exchange mechanism through intervening sulfur/oxygen atoms. Magnetic data have been rationalized successfully on the basis of expected square grid structures, as supported by MALDI MS and other data, in the absence of single crystal X-ray studies. The theoretical simulations of isotropic patterns of characteristic fragmentation peaks were achieved well, confirm the proposed structural formulae and this is found inevitable in the absence of single crystal X-ray studies. The molar conductance, magnetic studies and elemental analyses along with other spectral studies differentiate the square grid frameworks from mononuclear metal complexes. However, the complex **20** was found to be a dimanganese(II) complex, may be due to the effect of concentration or the preference of azide ion to coordinate to metal center. The magnetic complexes, especially the colorless materials derived from carbohydrazones would find applications.

References

1. N.N. Greenwood, A. Earnshaw, Chemistry of the Elements, 2nd ed., Reed Educational and Professional, Oxford (1997).

2. T.G. Carrell, A.M. Tyryshkin, G.C. Dismukes, J. Biol. Inorg. Chem. 7 (2002) 2.

3. J.-Z. Wu, E. Bouwman, A.M. Mills, A.L. Spek, J. Reedijk, Inorg. Chim. Acta

357 (2004) 2694.

4. O. Khan, Molecular Magnetism, Wiley-VCH, New York (1993).

5. R. Sessoli, H.-L. Tsai, A.R. Schake, S. Wang, J.B. Vincent, K. Folting, D. Gatteschi, G. Christou, D.N. Hendrickson, J. Am. Chem. Soc. 115 (1993) 1804.

6. J.-P. Sauvage, C. Dietrich-Buchecker, Molecular Catenanes, Rotaxanes and Knots Wiley-VCH, New York (1999).

7. J. Nugent, Ed. Photosynthetic water oxidation. Biochim. Biophys. Acta. Bioenerg. Special dedicated issue. 1503 (2001) 1.

8. K.N. Ferreira, T.M. Iverson, K. Maghlaoui, J. Barber, S. Iwata, Science 303 (2004) 1831.

9. T. Glowiak, H. Kozlowski, L.S. Erre, G. Micera, Inorg. Chim. Acta 236 (1995) 149.

10. M.B. Ferrari, G.G. Fava, C. Pelizzi, P. Tarasconi, G. Tori, J. Chem. Soc., Dalton Trans. (1987) 227.

11. B.S. Garg, M.R.P. Kurup, S.K. Jain, Y.K. Bhoon, Trans. Met. Chem. 13 (1988) 92.

12. P. Bindu, M.R.P. Kurup, J.I. Bhat, J. Electrochem. Soc. Ind. 48 (1999) 154.

13. R.P. John, A. Sreekanth, H.-K. Fun, M.R.P. Kurup, Polyhedron 24 (2005) 601.

14. A. Usman, I.A. Razak, S. Chantrapromma, H.-K. Fun, A. Sreekanth, S. Sivakumar, M.R.P. Kurup, Acta. Cryst. C 58 (2002) m461.

15. H.A. Tang, L.F. Wang, R.D. Yang, Trans. Met. Chem. 28 (2003) 395.

16. V. Philip, V. Suni, M.R.P. Kurup, M. Nethaji, Spectrochim. Acta Part A 64 (2006) 171.

17. M.-L. Tong, S.-L. Zheng, J.-X. Shi, Y.-X. Tong, H.K. Lee, X.-M. Chen, J. Chem. Soc., Dalton Trans. (2002) 1727.

18. L.K. Thompson, T.L. Kelly, L.N. Dawe, H. Grove, M.T. Lemaire, J.A.K. Howard, E.C. Spencer, C.J. Matthews, S.T. Onions, S.J. Coles, P.N. Horton, M.B. Hursthouse, M.E. Light, Inorg. Chem. 43 (2004) 7605.

19. M. Ruben. E. Breuning, M. Barboiu, J.-P. Gisselbrecht, J.-M. Lehn, Chem. Eur. J. (2003) 291.

20. A. Gelasco, A. Askenas, V.L. Pecoraro, Inorg. Chem. 35 (1996) 1419.

21. H.-Y. Chen, T.L. Zhang, J.-G. Zhang, K.-B. Yu, Struct. Chem. (2005) 657.

22. C.H. Lu, T.L. Zhang, Z.R. Wei, R.J. Cai, K.B. Yu, Chin. J. Inorg. Chem. 15 (1999) 377.

23. T.L. Zhang, C.H. Lu, X.J. Qiao, R.J. Cai, K.B. Yu, Chin. J. Struct. Chem. 18 (1999) 432.

24. J.G. Zhang, T.L. Zhang, Z.R. Wei, K.B. Yu, Chem. J. Chin. Univ. 22 (2001) 895.

25. R. Keuleers, G.S. Papaefstathiou, C.P. Raptopoulou, V. Tangoulis, H.O. Desseyn, S.P. Perlepes, Inorg. Chem. Commun. 2 (1999) 472.

26. A.A.A. Abu-Hussen, A.A.A. Emara, J. Coord. Chem. 57 (2004) 973.

27. W.J. Geary, Coord. Chem. Rev. 7 (1971) 81.

28. B.F.G. Johnson, J.S. McIndoe, Coord. Chem. Rev. 200-202 (2000) 901.

29. C. Calle, A. Sreekanth, M.V. Fedin, J. Forrer, I. Garcia-Rubio, I.A. Gromov, D. Hinderberger, B. Kasumaj, P. Léger, B. Mancosu, G. Mitrikas, M.G. Santangelo, S. Stoll, A. Schweiger, R. Tschaggelar, J. Harmer, Helv. Chim. Acta 89 (2006) 2495.

30. K.B. Pandeya, R. Singh, P.K. Mathur, R.P. Singh, Trans. Met. Chem. 11 (1986) 347.

31. M.R.P. Kurup, Stereochemical investigations on transition metal complexes of biologically active substituted 2-acetylpyridine thiosemicarbazones, Ph. D. Thesis, University of Delhi, Delhi (1988).

32. S. Sivakumar, Structural, spectral, biological and electrochemical studies of some 3d transition metal complexes of O-N-S and N-N-S donor ligands, Ph. D. Thesis, CUSAT, Kochi (2003).

33. S. Stoll, A. Schweiger, J. Mag. Res, 178 (2006) 42.

34. http://www.easyspin.ethz.ch. EasySpin has been developed by Dr. S. Stoll.

35. T. Howard, J. Telser, V.J. DeRose, Inorg. Chem. 39 (2000) 3379.

36. R. Singh, I.S. Ahuja, C.L. Yadava, Polyhedron 1 (1981) 327.

37. A.P. Golombek, M.P. Hendrich, J. Mag. Res. 165 (2003) 33 and refs therein.

38. S.T. Warzeska, F. Micciche, M.C. Mimmi, E. Bouwman, H. Kooijman, A.L. Spek, J. Reedijk, J. Chem. Soc., Dalton Trans. (2001) 3507.

39. S.V. Khangulov, P.J. Pessiki, V.V. Barynin, D.E. Ash, G.C. Dismukes, Biochemistry 34 (1995) 2015.

40. C. He, C.-y. Duan, C.-j. Fang, Y.-j. Liu, Q.-j. Meng, J. Chem. Soc., Dalton Trans. (2000) 1207.

41. B.S. Garg, M.R.P. Kurup, S.K. Jain, Y.K. Bhoon, Trans. Met. Chem. 13 (1988) 309.

42. K. Nakamoto, Infrared and Raman Spectra of Inorganic and Coordination Compounds, 5th ed., Wiley-Interscience, New York (1997).

43. A.B.P. Lever, Inorganic Electronic Spectroscopy, 2nd ed., Elsevier, Amsterdam (1984).

44. K. Kambe, J. Phys. Soc. Jpn. 5 (1950) 48.

45. L.N. Dawe, T.S.M. Abedin, T.L. Kelly, L.K. Thompson, D.O. Miller, L. Zhao, C. Wilson, M.A. Leech, J.A.K. Howard, J. Mater. Chem. 16 (2006) 2645.

46. http://www.ucs.mun.ca/~lthomp/magmun. MAGMUN has been developed by Dr. Zhiqiang Xu (Memorial University) and OW01.exe by Dr. O. Waldmann.

****

Self-assembled Zn(II) and Cd(II) molecular frameworks: Structural and spectral properties

6.1. Introduction

Zn and Cd are not typical members of transition elements and they are stable with their only significant oxidation state of +2 with completely filled d shell. Their coordination chemistry, however, can be considered along with that of typical transition metals. Both metal ions form stable complexes with N, O or S donor ligands well. Cd(II) is a soft ion and preferred to bond to sulfur compared to nitrogen atoms. Stable complexes of Zn(II) and Cd(II) with NNS and NNO donor ligands like thiosemicarbazones [1-6] and semicarbazones [7,8] have been reported. However, there are only very few reports of Zn(II) and Cd(II) coordination compounds of carbohydrazones and thiocarbohydrazones [8-14]. Some theoretical and dipole moment studies of closely similar Zn(II) carbazone complexes have been reported by Siddalingaiah *et al.* [15-18]. The stereochemistry of Zn(II) complexes mainly depends on the nature of the coordinating ligands as the d^{10} configuration is well stable. Zn(II) usually favors tetrahedral coordination; in that respect one review cited over six hundred Zn(II) complexes which are predominantly tetrahedral [19]. Among the less common five coordinate complexes, trigonal bipyramidal geometry occurs more frequently than square pyramidal [20]. There are many reports of six coordinated octahedral complexes, normally with two tridentate ligands. Reports of tetranuclear Zn(II) complexes having six coordinated octahedral centers are also found but very rare [21]. There are few reports of 2×2 square grids of Zn(II) having two NNO tridentate binding units [22,23]. Comparing the number and stability of Zn(II) octahedral complexes, Cd(II) are capable of forming octahedral complexes readily as

the latter have larger size. The coordination number of Zn(II) complexes with semicarbazones and thiosemicarbazones (lower homologues) ranges from four to seven while that of Cd(II) complexes ranges from four to eight [24].

Zinc is an essential element, necessary for sustaining all forms of life. It is estimated that 3000 of the hundreds of thousands of proteins in the human body contain zinc prosthetic groups. In addition, there are over a dozen types of cells in the human body that secrete zinc ions, and the roles of these secreted zinc signals in medicine and health are now being actively studied [25]. Despite its critical importance in maintaining such basic functions as proliferation and cell growth, little is known about how zinc is acquired, stored, and utilized by the cell. Recent pioneering studies have started to uncover the mysteries of subcellular distribution and to some extend on the proteins that maintain it. Many zinc complexes serve as models of biologically active zinc systems [25]. In biological chemistry, zinc serves as an electrophilic catalyst; that is, it stabilizes negative charges encountered during an enzyme-catalyzed reaction. Thus, protein-zinc recognition and discrimination requires proper chemical composition and proper stereochemistry of the metal-ligand environment. The fact that zinc is not subject to any ligand field stabilization effects and the change from an octahedral to a tetrahedral ligand field is not energetically disfavored for Zn(II) also have to be considered in biological studies. Zinc(II) ion has been found to be of catalytic importance in enzymatic reactions [26]. The enhancement of antitumor activity of some thiosemicarbazones in the presence of zinc(II) ions has been reported [27]. Some zinc complexes of thiosemicarbazones have been shown to be active as anti-tumor agents, are as cytotoxic as cisplatin and are also effective against cisplatin resistant cell lines [28]. Recently, the *in vitro* antiproliferative activity of Zn(II) thiosemicarbazones against the cells of MCF-7 and T24 human cancer cell lines have been reported [29]. Although, zinc is an important element in biological systems, cadmium, similar to zinc chemically in many ways, apparently does not substitute or "stand in" for it. The toxicity of cadmium is

230

interpreted as being caused by the replacement of enzymatic zinc by these metals. Their complexes being more stable than those of zinc, they block the enzyme and slow down the exchange of substrates. Therefore the study of Zn(II) and Cd(II) complexation towards various environments have biological and pharmacological interest. Conversely, there are reports of nonlinear optical materials exhibiting efficient second harmonic generation (SHG) shown by Zn(II) thiosemicarbazone complexes [30], which are needed for many applications including high-density optical recording, laser printing and optical measurement systems. In the light of these kinds of applications in various fields including chemistry, biology and material sciences and growing interest of new classes of materials, synthesis and characterization of some novel Zn(II) and Cd(II) coordination compounds of carbohydrazones and thiocarbohydrazones by self-assembly are also found useful.

6.2. Experimental

6.2.1. Materials

$Zn(NO_3)_2 \cdot 6H_2O$ (Merck), $ZnBr_2$ (Reidel-De Haen), $Zn(BF_4)_2 \cdot 2H_2O$ (Aldrich), $Cd(NO_3)_2 \cdot 4H_2O$ (Merck) and absolute ethanol (S.D.fine) were used as received and solvents methanol (Ranchem), chloroform (S.D.fine), etc were purified by standard procedures before use.

6.2.2. Synthesis of Zn(II) complexes

[Zn(H₂L²)Br₂]₂·H₂O (24)

A solution of $ZnBr_2$ (0.229 g, 1 mmol) in 10 ml of methanol was added to a solution of H_2L^2 (0.220 g, 0.5 mmol) in 10 ml chloroform and refluxed for 1 h and allowed to stand at room temperature. Yellow product separated out was filtered, washed with methanol followed by ether and dried over P_4O_{10} *in vacuo*. Yield: 0.312

g (47%). Elemental Anal. Found (Calc.): C, 44.92 (44.77); H, 3.10 (3.16); N, 12.67 (12.53); S, 5.05 (4.78)%.

[Zn(HL^2)]$_4$(BF$_4$)$_4$· 7H$_2$O (25)

To a hot solution of H$_2$L^2 (0.220 g, 0.5 mmol) in 10 ml chloroform was added an equimolar amount of Zn(BF$_4$)$_2$· 2H$_2$O (0.120 g) dissolved in 10 ml hot methanol. The yellow colored solution was then refluxed for 2 h and allowed to stand at room temperature for slow evaporation. The yellow solid mass precipitated after evaporation was washed with methanol and ether and dried *in vacuo* over P$_4$O$_{10}$. Yield: 0.146 g (47%). Elemental Anal. Found (Calc.): C, 48.59 (48.49); H, 3.88 (3.66); N, 13.77 (13.57); S, 5.40 (5.18)%.

[Zn(H$_2$L^3)Br$_2$]$_2$· 6H$_2$O (26)

A solution of ZnBr$_2$ (0.229 g, 1 mmol) in 10 ml of methanol was added to a solution of H$_2$L^3 (0.398 g, 1 mmol) in 50 ml boiling methanol and refluxed for 1 h and allowed to stand at room temperature. Orange yellow powder separated out was filtered, washed with methanol followed by ether and dried over P$_4$O$_{10}$ *in vacuo*. Yield: 0.411 g (62%). Elemental Anal. Found (Calc.): C, 38.10 (38.00); H, 2.83 (3.34); N, 12.69 (12.66); S, 4.92 (4.83)%.

[Zn(HL^3)]$_4$(BF$_4$)$_4$· 2CH$_3$OH· 2H$_2$O (27)

To a hot solution of H$_2$L^3 (0.298 g, 0.75 mmol) in 50 ml methanol was added an equimolar amount of Zn(BF$_4$)$_2$· 2H$_2$O (0.180 g) dissolved in 10 ml hot methanol. The orange colored solution was then stirred for 3 h and allowed to stand at room temperature for slow evaporation. The orange powder precipitated after evaporation was washed with methanol and ether and dried *in vacuo* over P$_4$O$_{10}$. Yield: 0.326 g (77%). Elemental Anal. Found (Calc.): C, 46.18 (46.06); H, 3.72 (3.24); N, 15.35 (14.99); S, 5.93 (5.72)%.

[Zn(HL⁴)]₄(BF₄)₄· CH₃OH· 2H₂O (28)

To a hot solution of H_2L^4 (0.256 g, 0.6 mmol) in 40 ml methanol was added an equimolar amount of $Zn(BF_4)_2$· $2H_2O$ (0.144 g) dissolved in 10 ml hot methanol. The orange colored solution was then refluxed for 1 h and allowed to stand at room temperature for slow evaporation. The orange powder precipitated after evaporation was washed with methanol and ether and dried *in vacuo* over P_4O_{10}. Yield: 0. 194 g (54%). Elemental Anal. Found (Calc.): C, 48.97 (49.07); H, 3.52 (3.37); N, 19.92 (19.70)%.

[Zn(HL⁵)]₄(BF₄)₄· 10H₂O (29)

A solution of the H_2L^5 (0.215 g, 0.5 mmol) in 10 ml chloroform was added to a solution of $Zn(BF_4)_2$· $2H_2O$ (0.120 g, 0.5 mmol) in methanol (20 ml) and refluxed for 1 h. The yellow crystalline solid which formed after a week was filtered, washed with methanol and ether and dried *in vacuo* over P_4O_{10}. Yield: 0.180 g (58%). Elemental Anal. Found (Calc.): C, 48.87 (48.69); H, 4.12 (3.92); N, 13.60 (13.63)%.

Crystals suitable for X-ray structure determination were obtained from slow evaporation of a chloroform: methanol mixture solution of **29** in air.

6.2.3. Synthesis of Cd(II) complexes

[Cd(H₂L¹)]₄(NO₃)₈· 8H₂O (30)

To a hot methanolic solution of H_2L^1 (0.440 g, 1 mmol) was added an equimolar amount of $Cd(NO_3)_2$· $4H_2O$ (0.311 g) dissolved in 10 ml hot methanol. The orange colored solution was then boiled for 5 minutes and filtered. This was boiled for 45 minutes and allowed to stand at room temperature for slow evaporation. The orange transparent plates precipitated after evaporation was collected and washed with ether and dried *in vacuo* over P_4O_{10}. Yield: 0.600 g (84%). Elemental Anal. Found (Calc.): C, 38.37 (38.86); H, 3.29 (3.12); N, 19.69 (19.70); S, 4.87 (4.51)%.

[Cd(HL²)]₄(NO₃)₄· 9H₂O (31)

To a hot solution of H_2L^2 (0.330 g, 0.75 mmol) in 60 ml boiling absolute ethanol was added an equimolar amount of $Cd(NO_3)_2$· $4H_2O$ (0.234 g) dissolved in 10 ml hot ethanol. The orange colored solution was then boiled for 5 minutes and filtered. This was boiled for 45 minutes and allowed to stand at room temperature for slow evaporation. The yellow solid mass precipitated after evaporation was collected and washed with ethanol and ether and dried *in vacuo* over P_4O_{10}. Yield: 0.174 g (36%). Elemental Anal. Found (Calc.): C, 46.06 (46.16); H, 3.57 (3.64); N, 14.96 (15.07); S, 5.04 (4.93)%.

6.3. Results and discussion

The molecular 2×2 square grids of Zn(II) and Cd(II) were readily synthesized in solvents like methanol, methanol chloroform mixture and absolute ethanol. Mononuclear and binuclear compounds of Zn(II) with carbohydrazones [9-11] and thiocarbohydrazones [9-12] have been reported previously. The only report of formation of molecular square of Zn(II) with thiocarbohydrazone ligand is with bis(2-acetylpyridine) thiocarbohydrazone [13]. Also, recently one neutral molecular square of Cd(II) with bis(6-methyl-2-pyridyl-methylene) thiocarbohydrazone has been reported [14]. Remarkably, so far no reports of molecular square grids of Zn(II) or Cd(II) with any carbohydrazone ligands are available. Reaction with equimolar ratios of corresponding suitable ligands and metal salts with suitable reaction conditions and slow precipitation are found favored to get these classes of compounds.

In all Zn(II) complexes, except **24** and **26**, the ligands are coordinated in monodeprotonated form. For the bromide complexes **24** and **26**, the ligands are coordinated in the neutral form. These compounds are found to be dinuclear with IR and MALDI mass spectral evidences. The Cd(II) complex as nitrate with H_2L^1 in methanol resulted into the coordination of ligand through neutral form while with

234

H_2L^2 in absolute ethanol coordination is found to occur through monodeprotonated form. Ali *et al.* [14] have reported the formation of a neutral Cd(II) complex (by dideprotonated form of ligand) under the same condition and remarked the importance of nitrate anion over chloride in ethanol for consuming protons released upon complexation. The conductance measurements in DMF showed all the complexes except **24** and **26**, are electrolytes of 1:4 or higher ratio. The molar conductance study is found an important tool for assigning the formation of multinuclear complexes. The conductance values of **24** and **26**, as 12 and 20 $\Omega^{-1}cm^2mol^{-1}$ in 10^{-3} M DMF solutions respectively, are suggestive of non-electrolytic nature for these compounds [31]. However, all the other complexes show conductivity in 10^{-4} M DMF solutions as 40, 36 and 26 $\Omega^{-1}cm^2mol^{-1}$ for **25**, **27** and **29** respectively. The two thiocarbohydrazone Cd(II) complexes **30** and **31** show conductance values of 87 and 40 $\Omega^{-1}cm^2mol^{-1}$ in 10^{-4} M DMF solution, suggesting the conductance of **30** is almost twice as that of **31**. The proposed molecular formulae agree well with these results.

All the Zn(II) complexes and Cd(II) complex **31** prepared are yellow in color. All these complexes, except **28**, were found to be soluble in DMF, but only partially soluble in other organic solvents such as DMSO, CHCl₃, ethanol, methanol etc. The poor solubility of **28** made it difficult even to measure the conductivity with a known concentration. The Cd(II) complex **30** is with a red glassy appearance, readily soluble in all common organic solvents. The poor solubility of Zn(II) and Cd(II) complexes in DMSO-d_6 and CDCl₃ made it difficult to obtain good quality ^{1}H NMR spectra. Also, the assignments of protons are found difficult in the region 7 - 9 ppm as they are seen as multiplets and with low intensity. Peaks of NH protons are however present in the spectra of some complexes with low intensity, but their absence do not implies the loss of –NH protons especially with poorly low intensity spectra. Tentative structures of all Zn(II) and Cd(II) complexes are given in Schemes 6.1 to 6.3.
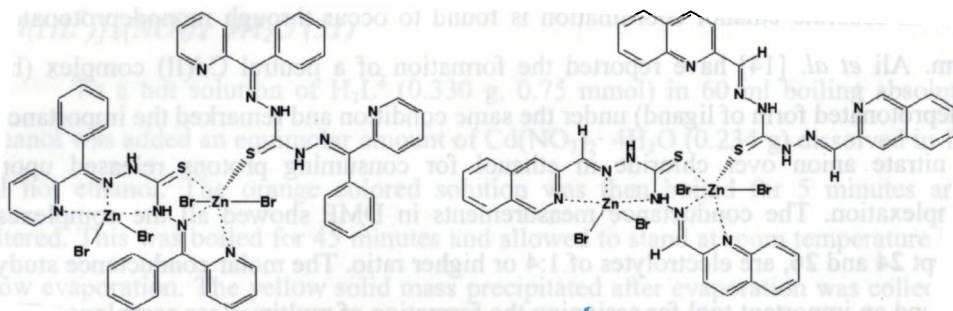
Scheme 6.1. Tentative structures of complexes **24** (left) and **26** (right).
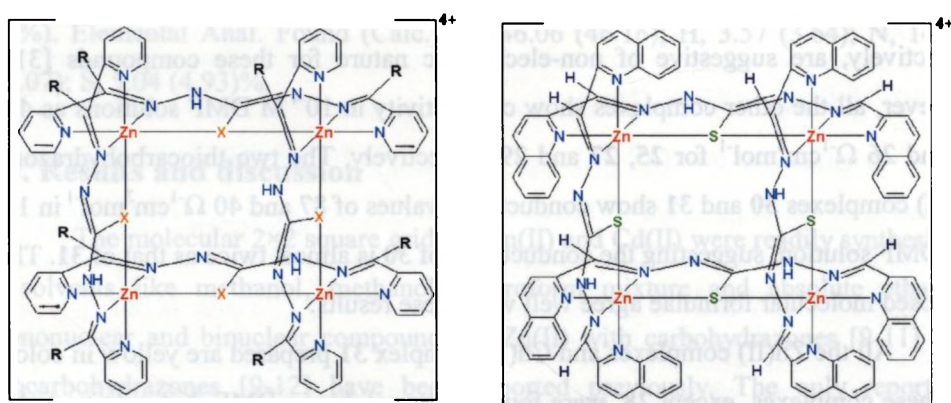
Scheme 6.2. General structures of complexes **25**, **28** and **29** (left). X=S, R=pyridyl for **25**, X=O, R=pyridyl for **28** and X=O, R=phenyl for **29**. Tentative structure of **27** (right). Exact positions of N bound hydrogen atoms are uncertain for **25**, **27** and **28**.
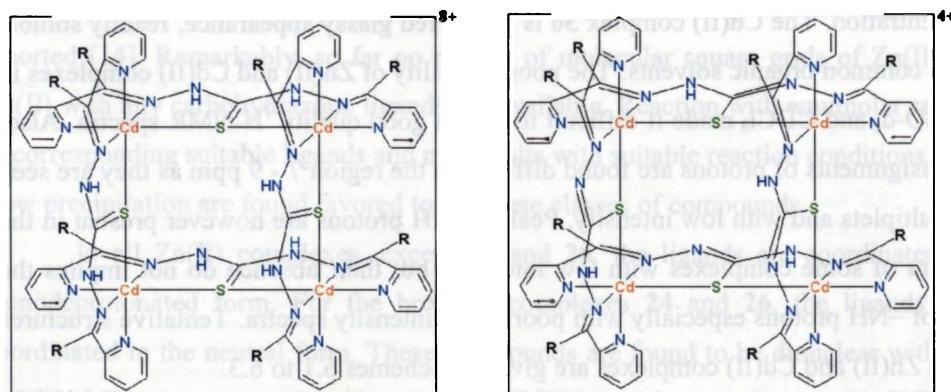
Scheme 6.3. Tentative structures of **30** (left) and **31** (right). R=pyridyl for **30** and R=phenyl for **31**. Exact positions of N bound hydrogen atoms are uncertain for **31**.

6.3.1. MALDI MS spectral studies

The MALDI MS spectroscopy is found very successful for rigid 2×2 square grids of Ni(II) complexes for revealing the formation of tetranuclear molecular structures. The structure and stability of coordination complexes under ionization conditions are dependent on various factors like the ligand itself, metal ions, counter ions, solvent, temperature, concentration etc. For Zn(II) and Cd(II) square grid complexes also MALDI MS spectra obtained are found quite useful. Excellent results were obtained with compounds **25, 27, 28, 29, 30** and **31** to establish the tetranuclear macrocyclic nature of complexes. The nature and fragmentation species exhibited by the complexes **24** and **26**, somewhat similar to the results obtained for Cu(II) complexes, however clearly indicate dinuclear structures. The theoretical simulation of isotropic distribution patterns of all molecular ion peaks and most of their fragmentation peaks could be achieved well, confirms the proposed structural formulae. MALDI mass spectra of all the complexes were taken in CH_2Cl_2 as DCTB mix on positive ion mode.

The spectrum of **24** show many peaks centered at m/z 1001, 935, 901, 762, 738, 725, 696, 662, 645, 581, 547, 499, 384 and 342. Of these, the base peak centered at 499 was assigned as $[Zn(HL^2)]^+$. Other peaks centered at 1001, 935, 761, 725, 645, 580 are assigned as fragmentation species. The peaks at 1001, assigned as $[Zn_2(HL^2)L^2]^+$ (calc. 1001) and at 935 correspond to $[Zn(HL^2)H_2L^2]^+$ (calc. 935) are found characteristic for fragmentation species of molecule with assigned formula $[Zn(H_2L^2)Br_2]_2 \cdot H_2O$. The other peaks are assigned to $[Zn_2(HL^2)Br_2 \cdot 2H_2O]^+$ (calc. 761), $[Zn_2(HL^2)Br_2]^+$ (calc. 725), $[Zn_2(L^2)Br]^+$ (calc. 645) and $[Zn_2(L^2) \cdot H_2O-H^+]^+$ (calc. 580) also support this assignment. The spectrum along with calculated isotropic distribution patterns of peaks are given in Fig. 6.1.
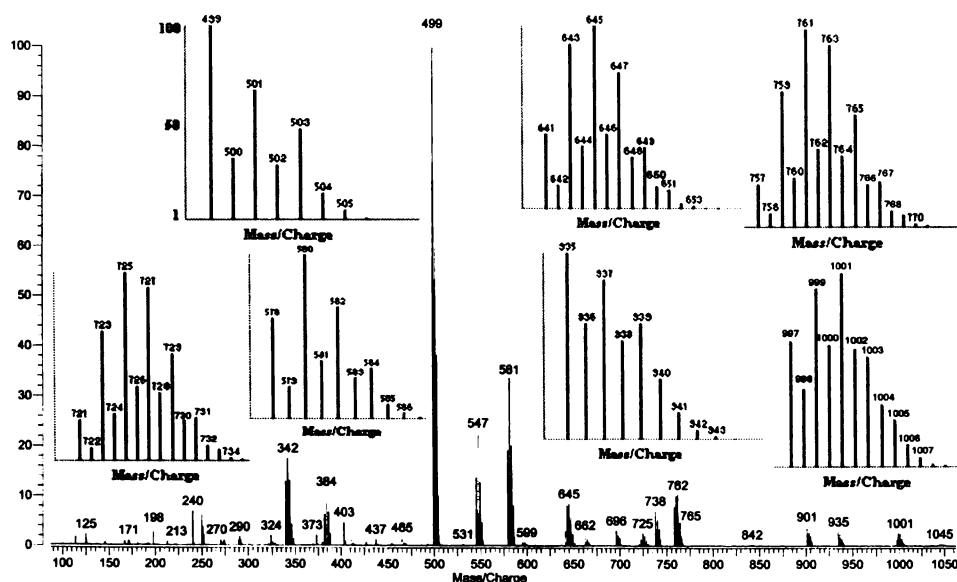
Fig. 6.1. The MALDI MS spectrum of complex **24**. The insets are calculated isotropic distribution patterns.

The complex **25** exhibits peaks centered at m/z 2498.9, 1999, 1760, 1499, 1357.9, 1260, 1096.9, 1001.1, 857.9, 762, etc. The base peak at 1999 assigned as $[Zn_4(HL^2)L^2_3]^+$ (calc. 1999) is characteristic. Interestingly, the molecular ion peak with well resolved isotropic pattern at 2498.9 attributed to the species $[Zn_4(HL^2)_4(BF_4)_4 \cdot 3CH_3OH \cdot 3H_2O+H^+]^+$ (calc. 2500) is found very rare for molecular square complexes. Both these isotropic distribution patterns and their simulation patterns are given in Fig. 6.2. The spectrum with other calculated distribution patterns of peaks are given in Fig. 6.3. Presence of methanol may be attributed to the usage of methanol dichloromethane mixture for MALDI measurement for complex **25**. Other species, found to be in well agreement with calculated isotropic distribution patterns, include $[Zn_4L^2_3-H^++benzoylpyridine\ ketone\ hydrazone]^+$ (calc. 1760), $[Zn_3(HL^2)L^2_2]^+$ (calc. 1499), $[Zn_3(HL^2)_2(BF_4)_3 \cdot CH_3OH]^+$ (calc. 1359), $[Zn_3L^2_2-H^++benzoylpyridine\ ketone\ hydrazone]^+$ (calc. 1260) and $[Zn_2(HL^2)L^2]^+$ (calc. 1001).
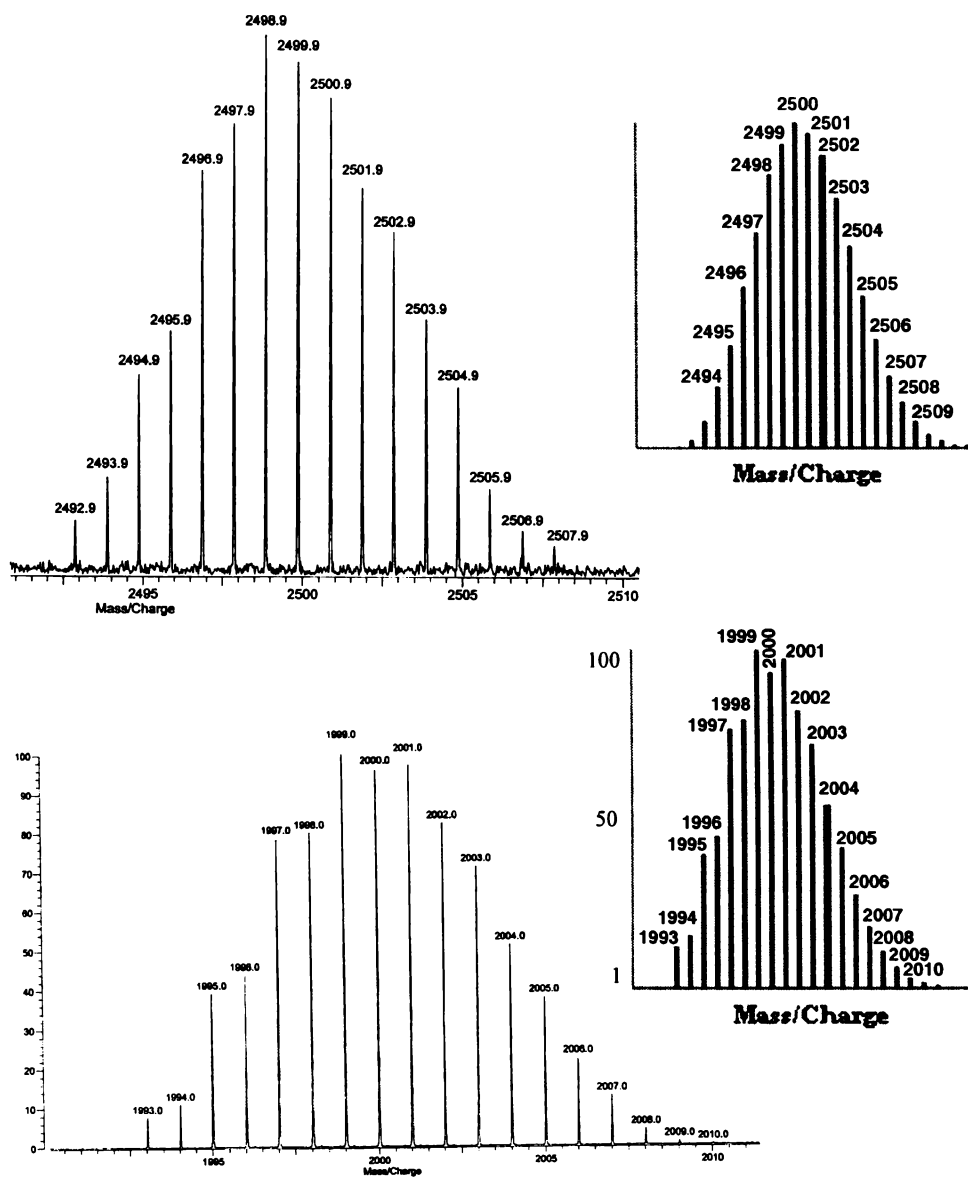
Fig. 6.2. Isotropic distribution peaks assigned for $[Zn_4(HL^2)_4(BF_4)_4 \cdot 3CH_3OH \cdot 3H_2O+H^+]^+$ (top) and $[Zn_4(HL^2)L^2_3]^+$ (bottom) of complex **25** with simulated isotropic distribution patterns on right sides.
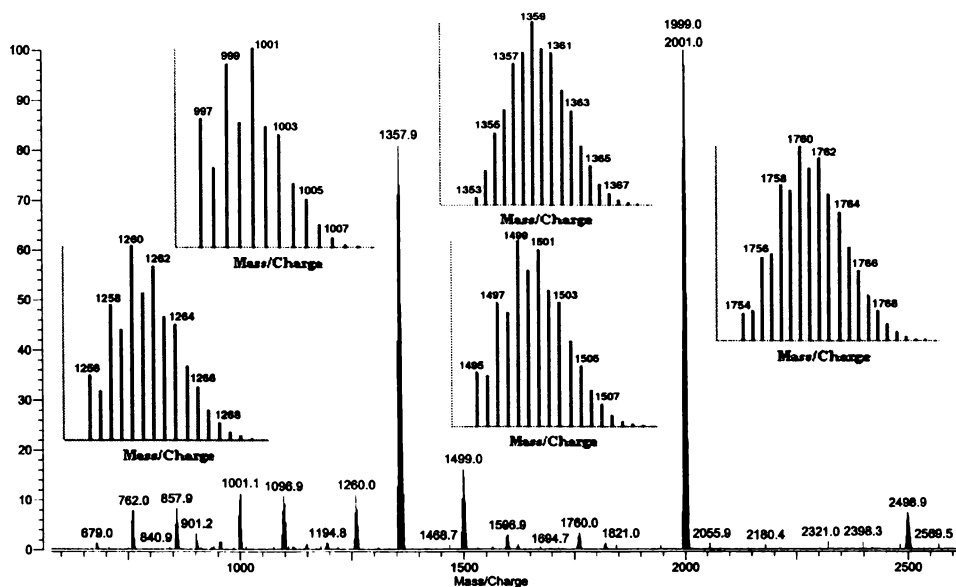
Fig. 6.3. The MALDI MS spectrum of **25**. The insets are calculated isotropic distribution patterns.

The compound **26** exhibits somewhat similar spectrum of **24** attributed to their similar nature under ionization condition since both complexes are formed by the neutral form of respective ligands. The peaks of **26** are seen centered at m/z 915, 835, 809, 754, 674, 660, 630, 608, 586, 551, 529, 469, 447, 407, etc. Two main peaks centered at 529 and 447 are assigned with well agreeing calculated isotropic distribution patterns as $[Zn(H_2L^3)Br]^+$ (calc. 529), $[Zn(HL^3)]^+$ (calc. 447). The base peak at 407 was assigned as a dissociated species $ZnC_{20}H_{19}N_6^+$ (calc. 407) with well agreeing calculated isotropic distribution pattern. The spectrum with simulation patterns is given in Fig. 6.4. The other main peaks are found to show in agreement with simulation pattern as $[Zn(H_2L^3)_2Br]^+$ (calc. 913), $[Zn_2(H_2L^3)Br_3]^+$ (calc. 755), $[Zn_2(HL^3)Br_2]^+$ (calc. 673). However, presence of peak centered at 1908 as given in Fig. 6.5 also obtained though with very low intensity, for which a possible impurity of formula $[Zn_4(HL^3)_2(L^3)_2Br \cdot 2H_2O]^+$ (calc. 1909), however, not found match well. This

240

may be attributed to the presence of some tetranuclear impurity in dichloromethane solution or in the gas phase under ionization condition.
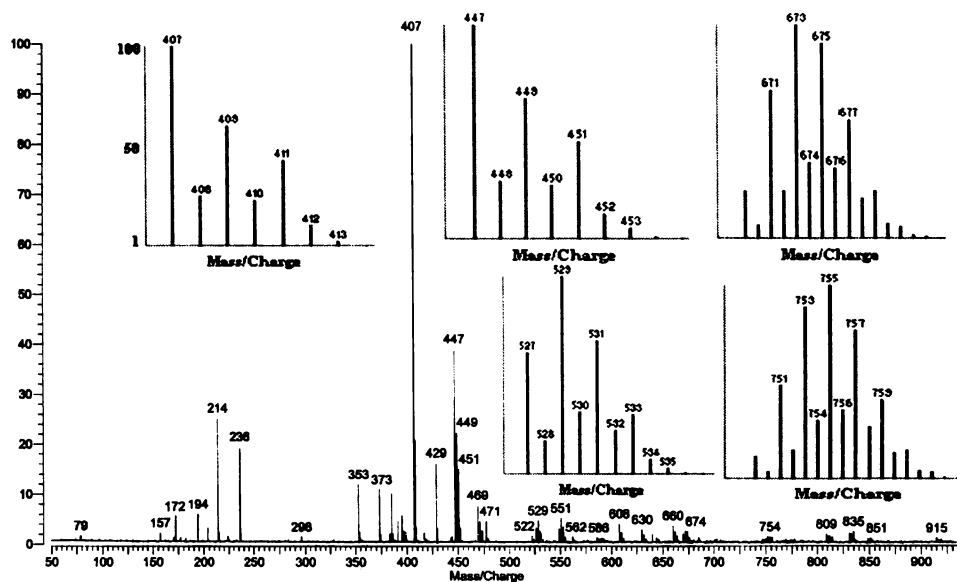
Fig. 6.4. The MALDI MS spectrum of complex **26**. The insets are calculated isotropic distribution patterns.
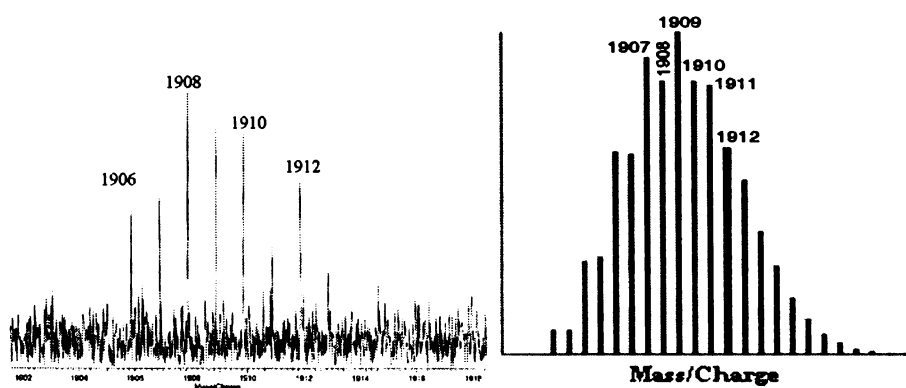
Fig. 6.5. Expected distribution pattern of a possible species $[Zn_4(HL^3)_2(L^3)_2Br\cdot 2H_2O]^+$ (right) and obtained weaker peaks (left).

241

The compound **27** exhibits a well resolved characteristic peak centered at 1791.5 assigned as $[Zn_4(HL^3)L^3_3]^+$ (calc. 1791) agreeing well with calculated isotropic distribution pattern. The base peak centered at 1578.4 corresponds to a dissociated species $[Zn_4L^3_3+\text{quinoline-2-aldehyde hydrazone-H}^+]^+$ (calc. 1578) also agreeing well with calculated isotropic distribution pattern. Both these simulations are given with spectrum in Fig. 6.6. However two other peaks seen centered at 1811.5 and 1996.6 are unassigned, as the isotropic distribution patterns are not found match well.
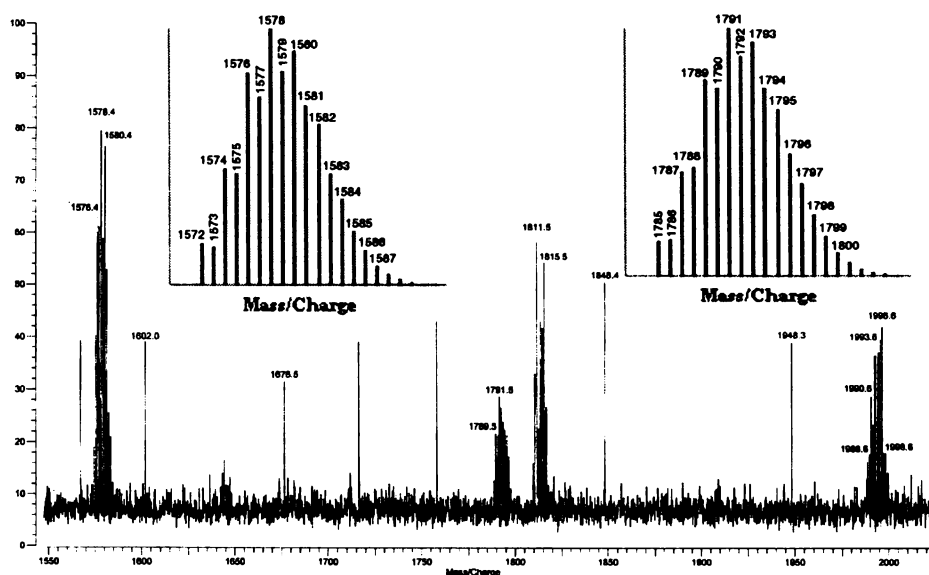
Fig. 6.6. The MALDI MS spectrum of **27**. The insets are well agreeing calculated isotropic distribution patterns.

For the carbohydrazone Zn(II) complex **28**, the base peak centered at 1942.8 assigned to $[Zn_4(HL^4)L^4_3]^+$ (calc. 1943) is found characteristic and agrees well with calculated isotropic distribution pattern. Other main peaks are seen centered at m/z 2006.7, 1520.8, 1718.8, 1690.8 and 973. All these peaks are found to be in well agreement with calculated isotropic distribution patterns (Fig. 6.7) of assigned species $[Zn_4(HL^4)L^4_3 \cdot 2CH_3OH]^+$ (calc. 2007), $[Zn_4L^4_3-H^+]^+$ (calc. 1521), $[Zn_4L^4_3-H^+ +$

242

dipyridyl ketone hydrazone]$^+$ (calc. 1719), [Zn$_4$L^4$_3$-H$^+$+(C$_5$H$_4$N)$_2$CH$_2$]$^+$ (calc. 1691) and [Zn$_2$(HL^4)L^4]$^+$ (calc. 973). The dissociated hydrazone species of respective ketone of ligands is found common with spectra of many of the complexes.
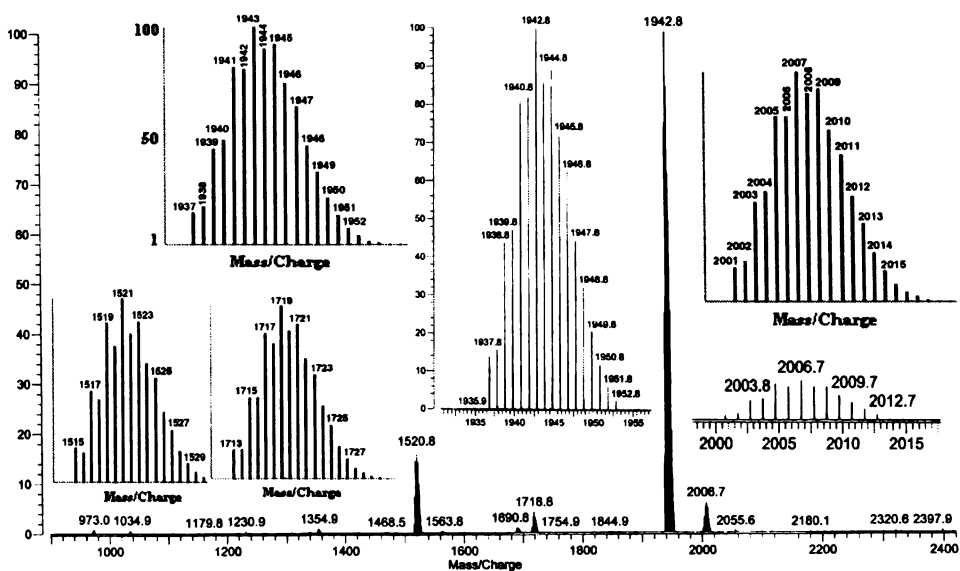
Fig. 6.7. The MALD1 MS spectrum of **28**. The insets are distribution patterns of main peaks (middle and right bottom) and their simulation patterns (top patterns) with other main simulation patterns (bottom left).

Like the carbohydrazone square grid **28**, the complex **29** also exhibits excellent spectrum suggesting the existence of molecular square structure in the solution. The spectrum of **29** shows main peaks centered at m/z 757, 1031, 1514.9, 1711.9 and 1934.9 along with well-resolved isotropic peaks. The molecular ion peak 1934.9 assigned to [Zn$_4$(HL^5)L^5$_3$]$^+$ (calc. 1935), 1514.9 corresponds to [Zn$_4$L^5$_3$-H$^+$]$^+$ (calc. 1515) and 1031 corresponds to [Zn$_3$L^5$_2$-H$^+$]$^+$ (calc. 1031). The peak at m/z 757 may be attributed to [Zn$_4$L^5$_3$]$^{2+}$ species. These results suggest the existence of molecular square structure in the solution phase as well [32]. The presence of [Zn$_3$L^5$_2$-H$^+$]$^+$ species indicates that the complex **29** may lose one metal ion under ionization condition. Also, calculation of isotropic distribution of peaks shows that the peak

243

centered at 1711.9 corresponds to a dissociated species [Zn$_4$L^5$_3$+benzoyl pyridine hydrazone-H$^+$]$^+$ (calc. 1712) formed by the degradation of one of the ligand in the tetrameric species [Zn$_4$(HL^5)L^5$_3$]$^+$. The isotropic distribution peaks along with calculated isotropic distribution patterns of main peaks are given in Figs. 6.8 and 6.9.
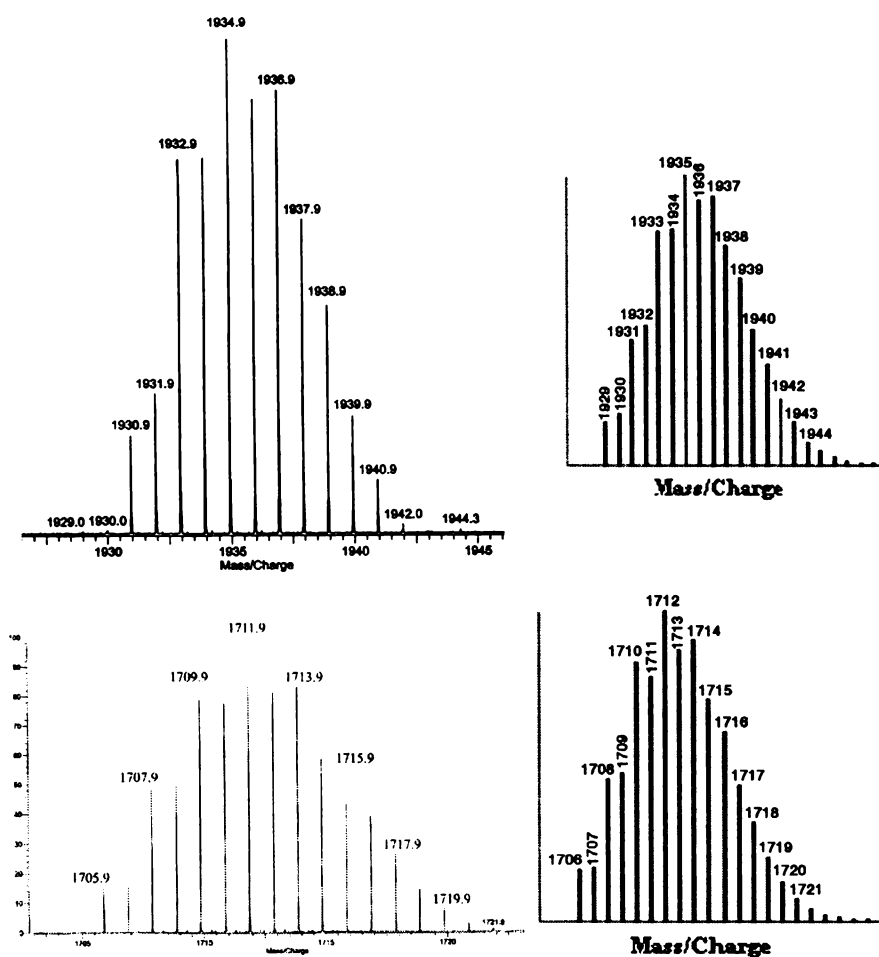
Fig. 6.8. The experimental and calculated isotropic distribution patterns of [Zn$_4$(HL^5)L^5$_3$]$^+$ (top) and its dissociated species C$_{87}$H$_{64}$N$_{21}$O$_3$Zn$_4$$^+$ (bottom) of **29**.
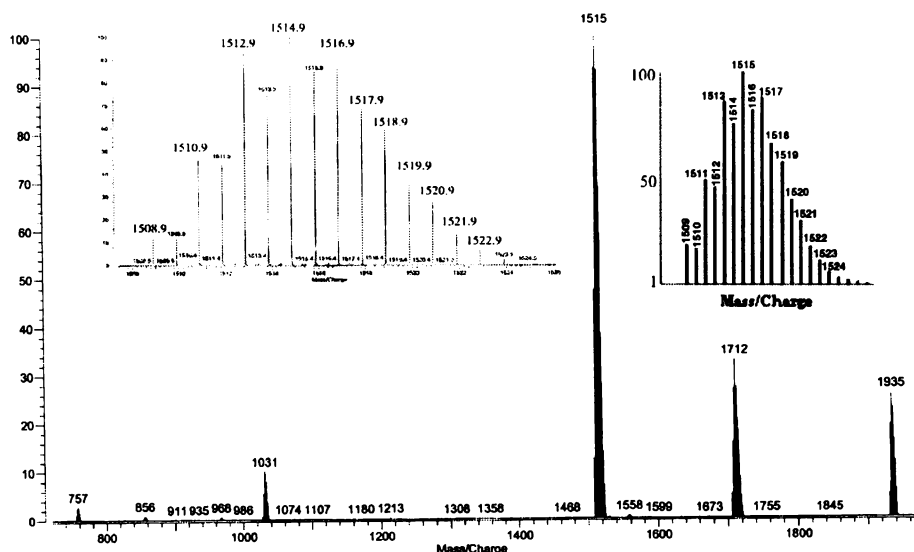
Fig. 6.9. The MALDI MS spectrum of 29. The insets are distribution pattern of base peak (left) and its simulation (right).

The isotropic distribution patterns of Cd(II) complexes are more complicated compared to corresponding Zn(II) complexes. The Cd(II) complex **30** exhibits peaks centered at m/z 1793, 1648, 1535, 1388, 1244, 1099, 955, 839, 695, 551, etc. These peaks are assigned as $[Cd_4(L^1)_3HL^{1\cdot}\ CH_3CH_2OH]^+$ (calc. 1794), $[Cd_2(HL^1)_3]^+$ (calc. 1535), base peak $[Cd_2(H_2L^1)HL^1(NO_3)_2\cdot\ H_2O]^+$ (calc. 1243), $[Cd_2(HL^1)L^1]^+$ (calc. 1099), $[Cd(HL^1)]^+$ (calc. 551) and agreeing well with calculated isotropic patterns. The spectra along with calculated isotropic distribution patterns of main peaks are given in Figs. 6.10 and 6.11.

The spectrum of complex **31** shows peaks centered at m/z 1740, 1636, 1488, 1344, 1250, 1239, 1095, 856, 837, 693, 549, etc. The base peak at 1095 assigned as $[Cd_2(HL^2)L^2]^+$ (calc. 1095) agreeing well. Other main species identified are $[Cd_4(L^2)_3HL^2]^+$ (calc. 1742), $[Cd_2(H_2L^2)HL^2(NO_3)_2\cdot\ H_2O]^+$ (calc. 1238), $[Cd(HL^2)]^+$ (calc. 549). All these assigned peaks are given in Figs. 6.12 and 6.13 and are found to be in well agreement with calculated isotropic distribution patterns.

245
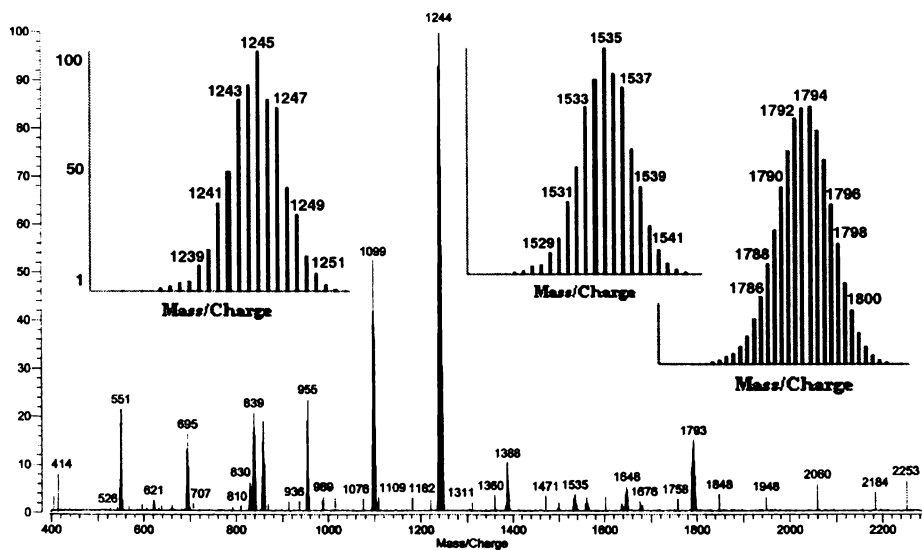
Fig. 6.10. The MALDI MS spectrum of Cd(II) complex **30**. The insets are agreeing calculated isotropic distribution patterns.
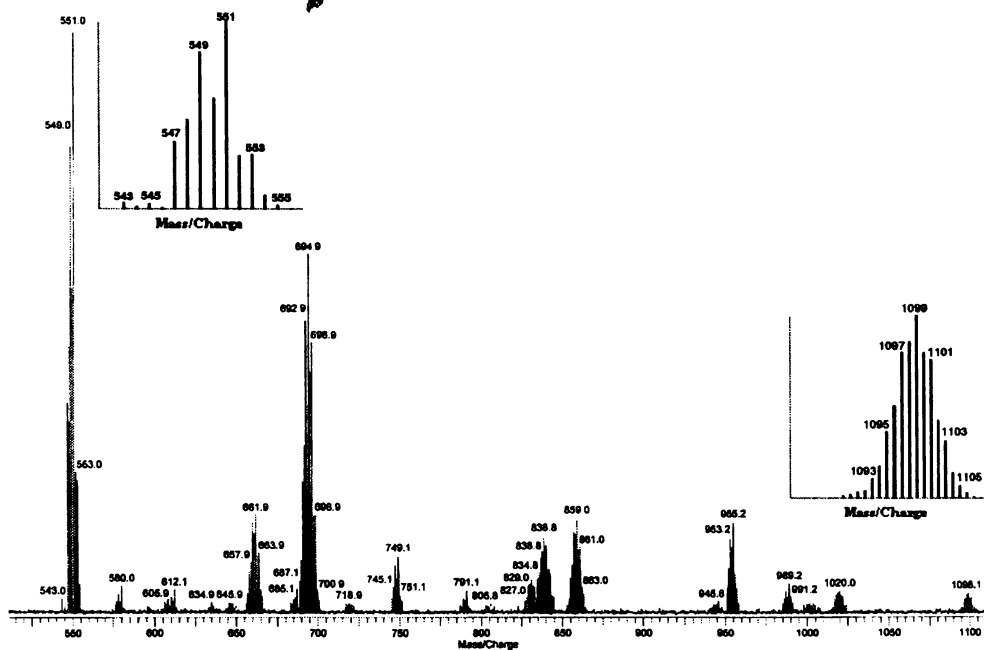
Fig. 6.11. The isotropic distribution peaks of **30** with well agreeing calculated isotropic distribution patterns.
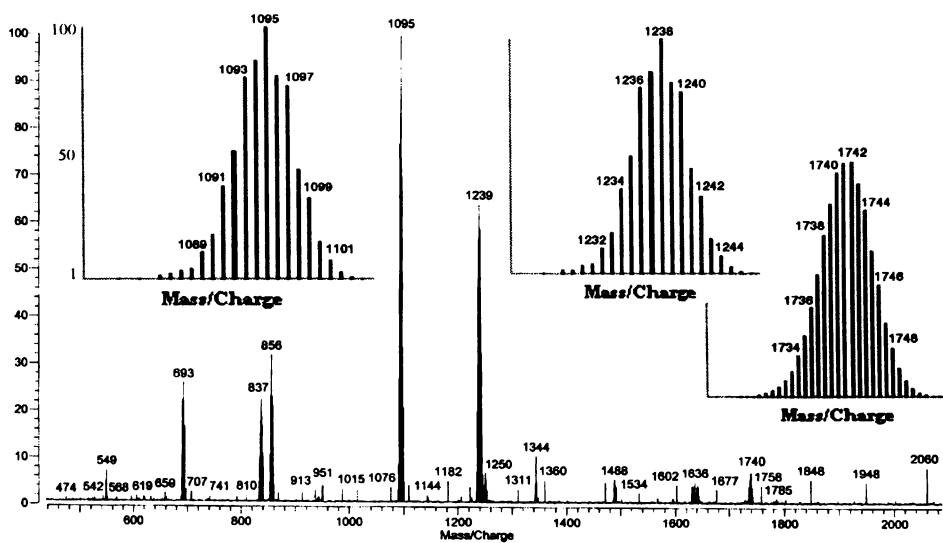
Fig. 6.12. The MALDI MS spectrum of complex **31**. The insets are agreeing calculated isotropic distribution patterns.
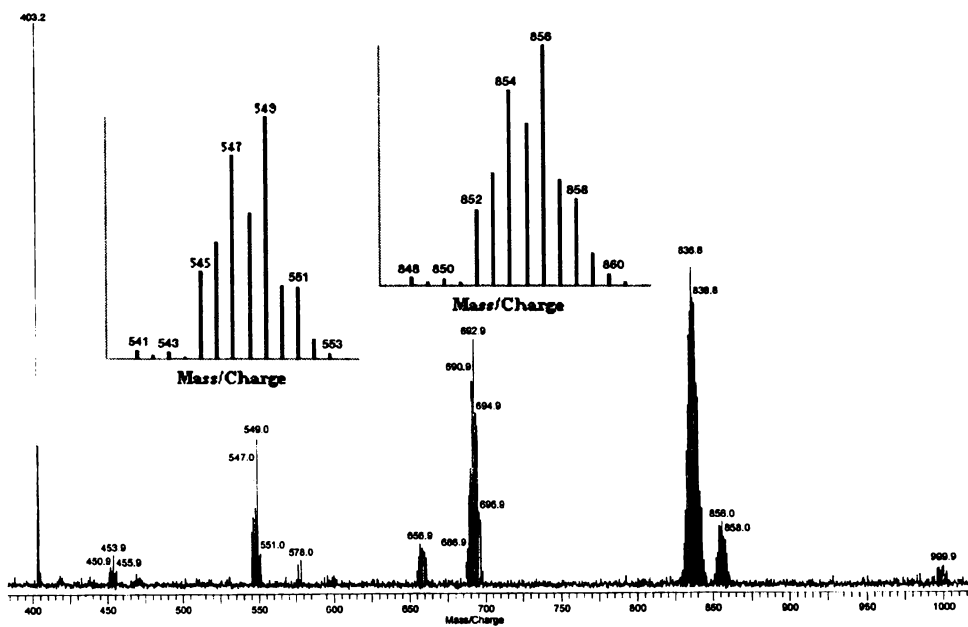
Fig. 6.13. The isotropic distribution peaks and agreeing simulations of peaks of **31**.

247

6.3.2. Electronic and IR spectral characteristics

The electronic spectra of tetranuclear compounds of Zn(II) (**25** and **27**) and Cd(II) (**30** and **31**) were taken in 10^{-5} M DMF solutions, while that of **29** were taken in 10^{-4} M DMF solution. The spectra of **24** and **26** were also taken in DMF as 2×10^{-5} M and 2×10^{-4} M respectively, while that of **28** was taken in ethanol solution. The absorbance values with extinction coefficients of all the complexes are summarized in Table 6.1. The Zn(II) and Cd(II) complexes are not expected to show any d-d transitions as both classes possess a d^{10} configuration. The spectra of all square grids are found to show intense charge transfer bands, which is less common in mononuclear Zn(II) and Cd(II) complexes. However there are many reports of the presence of charge transfer bands [1]. All the spectra show considerable differences with that of their corresponding ligands. The bands seen at ~28600 cm^{-1} for all the complexes, assigned as n→π* transitions, are shifted from that seen for free ligands.

Table 6.1. Electronic spectral features of Zn(II) and Cd(II) complexes.

Compounds	Absorbance features λ_{max} cm^{-1} (ε M^{-1} cm^{-1})
24	18150 (6800), 22780 (39860), 27100 (26800)
25	18480sh (31400), 18830 (32300), 22730 (54600), 27780sh (26800)
26	18760 (1280), 21550 (3180), 21600 (1880), 31250 (1860)
27	16260 (3300), 18180 (23100), 21600 (178000), 26880 (111400), 31550 (100300)
28	19610, 24750, 29760, 36760, 43100
29	19160 (30180), 23920 (20200), 28740 (11260)
30	19380 (62000), 22420 (54600), 28570 (26300)
31	19010 (58500), 22470 (61000), 27700 (28500)

The dinuclear Zn(II) compounds **24** and **26** show absorbances at ~18500 and at ~22000 cm^{-1} are assigned MLCT bands, but with low absorptivity. The spectra of these complexes in DMF solution are given in Fig. 6.14.
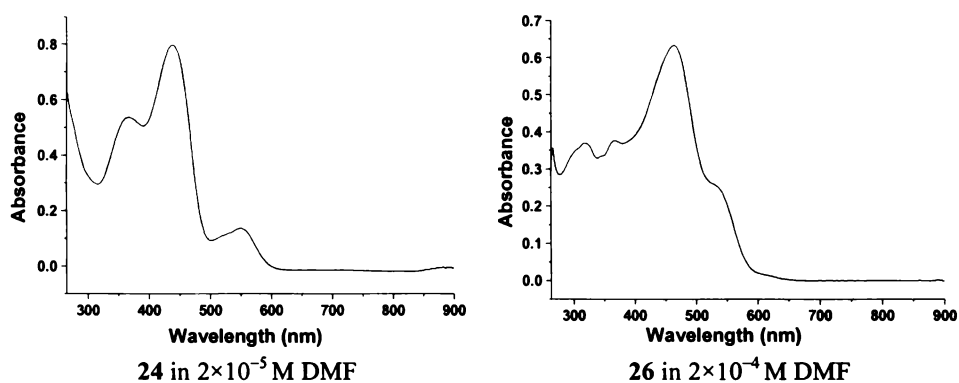
Fig. 6.14. Electronic spectra of dinuclear Zn(II) thiocarbohydrazone complexes.

In the case of Zn(II) molecular square grids, the absorbance features show significant differences attributed to the influence of ligands. The extinction coefficient of thiocarbohydrazone Zn(II) complex **25** is considerably higher than that of corresponding carbohydrazone complex **29**. Also the ligand with quinoline rings shows many absorbance bands as evidenced by the spectrum of **27** compared to its benzoylpyridine counterpart **25** (Fig. 6.15). The bands at ~22000 and at ~18300 cm^{-1} are assigned MLCT bands.
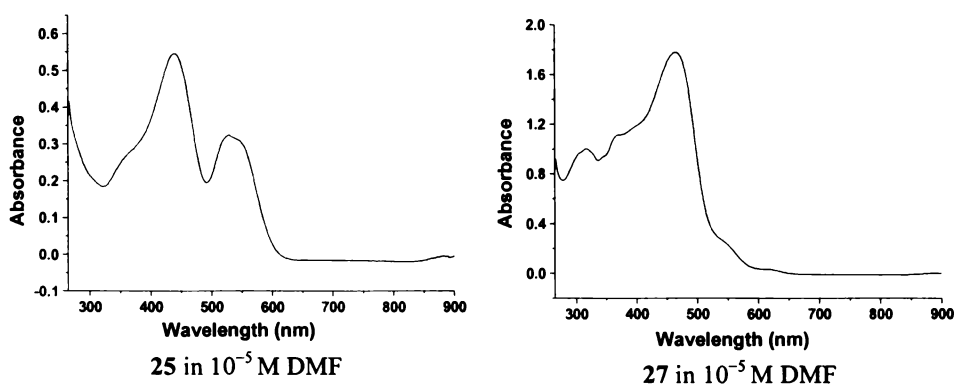
Fig. 6.15. Electronic spectra of Zn(II) thiocarbohydrazone square grids.

The carbohydrazone compound **29** exhibits intense charge transfer band, while complex **28** in ethanol not showed intense CT bands (Fig. 6.16). The intense

band at 19160 and 23920 cm^{-1} of **29** are assigned MLCT bands and is seen at 19610 and 24750 cm^{-1} for **28**. The bands at 43100 and 36760 cm^{-1} of **28** are assigned $\pi \rightarrow \pi^*$ and at 29760 cm^{-1} as n$\rightarrow \pi^*$ transitions.

29 in 10^{-4} M DMF   28 in ethanol
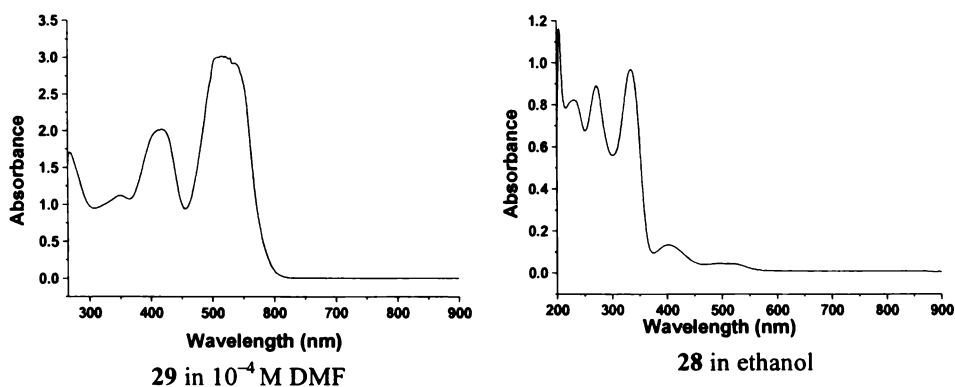
Fig. 6.16. Electronic spectra of Zn(II) carbohydrazone square grids.

The Cd(II) squares **30** and **31** show similar features (Fig. 6.17). The CT bands are seen at ~22450 and at ~19200 cm^{-1} but reverses in absorptivity. Also, the n$\rightarrow \pi^*$ transition band assigned at 28570 cm^{-1} for **30** show only marginal change from 28250 cm^{-1} of H$_2$L^1, while that of **31** at 27700 cm^{-1} shows considerable shift from 28900 cm^{-1} of H$_2$L^2. These differences may be attributed to change of ligand and deprotonation on coordination in **31** compared to the nondeprotonated ligand form in **30**.

30 in 10^{-5} M DMF   31 in 10^{-5} M DMF
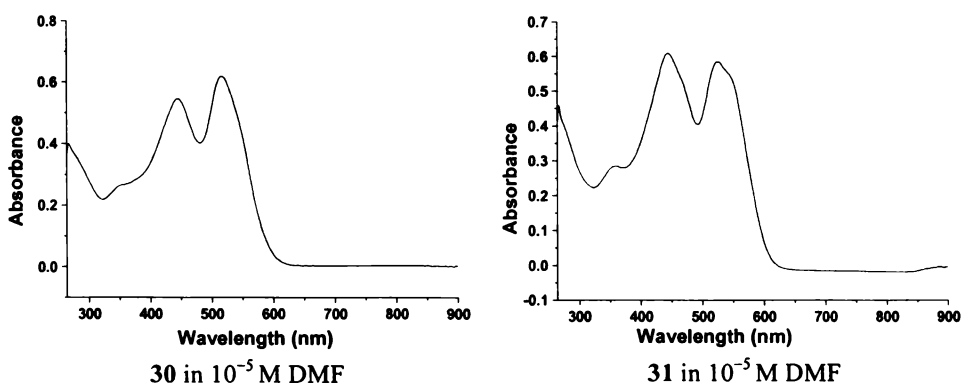
Fig. 6.17. Electronic spectra of Cd(II) thiocarbohydrazone square grid complexes.

250

The IR spectra of Zn(II) and Cd(II) complexes are very much rich with bands and assignments of these bands are very difficult. However, a comparison of spectra of all Zn(II) and Cd(II) complexes with their corresponding carbohydrazone and thiocarbohydrazone ligands also found relevant and resulted some assignments as given in Table 6.2. All the compounds show the presence of lattice water as evidenced by the broad bands centered in the region of 3405 to 3493 cm^{-1}. The v(NH) bands are seen in the region 3110 to 3327 cm^{-1}, although the broad stretching bands of water mask some of them. The shifts in frequencies in these regions may be due to changes in possible hydrogen bonding interactions. Also none of the spectra exhibit bands between 2500 and 2700 cm^{-1} due to the stretching of SH group [33,34] rules out the presence of any thiol forms in free or coordinated forms in both Zn(II) and Cd(II) complexes. Bands ranging from 1600-1400 cm^{-1}, attributed to v(C=C) and v(C=N) vibration modes, in the spectra of complexes suffer significant shifts and their mixing patterns are different from that seen in the spectra of their respective free ligands.

The spectra of **24** and **26** resemble and are different from other spectra of Zn(II) molecular squares. However the formation of squares cannot be differentiated with IR or electronic spectral studies alone. The strong v(C=S) bands of free ligands H$_2$L^2 and H$_2$L^3 seen at 1225 and 1209 cm^{-1} are found to be shifted to 1152 and 1143 cm^{-1} in the spectra of **24** and **26** respectively, suggesting the thione sulfur coordination. Also, strong bands at ~320 cm^{-1} in the far IR region of these compounds are consistent with sulfur coordination like in zinc thiosemicarbazone complexes [4]. The v(N–N) bands seen at ~1130 cm^{-1} for free ligands are shifted to ~1210 cm^{-1} confirming the coordination through azomethine nitrogen. Other uncoordinated N–N stretching bands are seen at ~1110 cm^{-1}. The azomethine coordination is further supported by bands of v(Zn–N$_{azo}$) at ~410 cm^{-1} [4]. The v(Zn–N$_{py}$) bands expected are present at ~220 cm^{-1} [35,36] in both complexes and changes in the 600-700 cm^{-1} regions compared to their respective ligands may be attributed to the pyridyl or quinolyl nitrogen coordination to Zn(II) in **24** and **26**.

251

Table 6.2. IR spectral assignments of Zn(II) and Cd(II) complexes (cm^{-1}).

c.	vH$_2$O	vN-H	vC-H	vC=N+ vC=C	vC-N/ vHetero cyclic	vC-S/ vC=S	vC-O	vN-N	δC-H	py/qu
24	3493br	3262s	3049s	1593m, 1505vs, 1470vs, 1440s, 1418m	1307s, 1260m	1152s		1214m, 1100s	978s, 845m, 800s, 743m, 701s	654m, 627m, 550m, 498m, 470m
25	3405br	3327m	3053m	1590s, 1559s, 1512s, 1459vs, 1441s, 1401s	1320s, 1261vs	1090 vs		1201m, 1154m	972m, 791m, 745s, 709s	640m, 558m, 521m
26	3446br	3235br	3021m	1553m, 1507m, 1469m, 1423vs	1334s, 1250s	1143s		1213s, 1119s	996m, 934m, 873s, 827m, 752m	625m, 481m
27	3408br	3238sh	3054m	1584m, 1528s, 1501vs, 1469m, 1432m, 1409s	1327s, 1302m	1095 vs		1214m, 1140m	992m, 939m,	624m, 522m, 480m
28	3418br	3110m	3063m	1713w, 1570s, 1524vs, 1456vs	1357m		1316s	1216m, 1121s	969m, 743s, 833m, 752s, 696m	636m, 520m, 558w
29	3410br	3192m	3058s	1664s, 1626s, 1570s, 1525vs, 1465s	1262s		1324s	1213 s, 1107s	796s, 703vs	654m, 616w
30	3440br		3053m	1590m, 1504s, 1461s	1318s	1156s		1231s, 1107m, 1086m	998m, 797s, 743s	651m, 629m, 613m, 497m, 471m
31	3445br	3324sh	3054m	1591m, 1556m, 1504s, 1461s	1258s	1081s		1158m	967m, 792s, 732m	662m, 637m, 451m, 413m

c. = compounds, br = broad, sh = shoulder, s = strong, vs = very strong, m = medium, w =weak.

The v(Zn–Br) bands obtained in the far IR spectra of compounds **24** and **26** at ~230 cm⁻¹ supports terminally coordinated bromine [35]. The IR spectrum of **24** and far IR spectrum of **26** are given in Figs. 6.18 and 6.19.
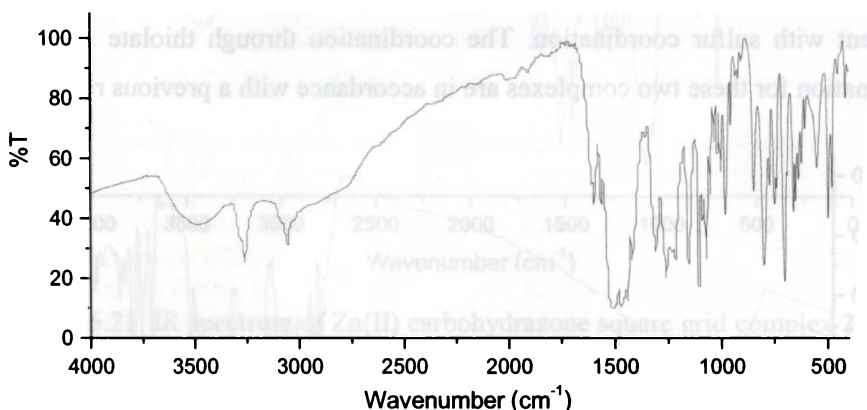
Fig. 6.18. IR spectrum of Zn(II) thiocarbohydrazone complex **24**.
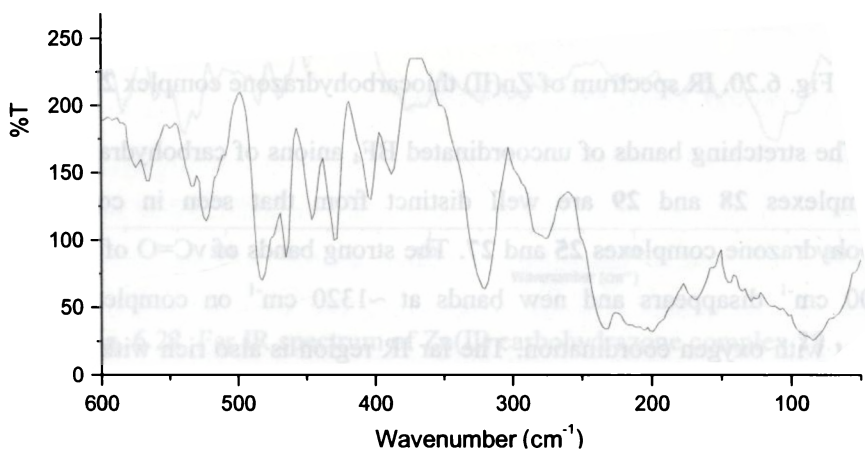
Fig. 6.19. Far IR spectrum of Zn(II) thiocarbohydrazone complex **26**.

The thiocarbohydrazone square grid complexes **25** and **27** exhibit similar spectral features. Very strong bands at ~1090 cm⁻¹ are assigned v(C–S) [13] and are merged with v_3(B–F) seen at ~1060 cm⁻¹ (Fig. 6.20), which are characteristic along

253

with v_1(B–F) at ~777 cm^{-1} and v_4(B–F) at ~533 cm^{-1} frequencies of uncoordinated BF$_4$ anions having T_d geometry [36]. The strong bands seen at 1095 cm^{-1} for compound **27** is attributed to v(C–S) band and the higher shift from that of free ligand is in agreement with sulfur coordination. The coordination through thiolate sulfur after deprotonation for these two complexes are in accordance with a previous report [13].
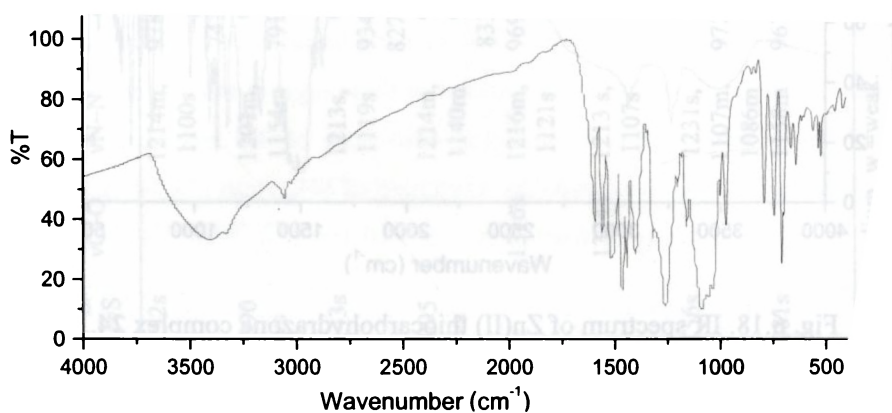
Fig. 6.20. IR spectrum of Zn(II) thiocarbohydrazone complex **25**.

The stretching bands of uncoordinated BF$_4$ anions of carbohydrazone square grid complexes **28** and **29** are well distinct from that seen in corresponding thiocarbohydrazone complexes **25** and **27**. The strong bands of vC=O of free ligands at ~1700 cm^{-1} disappears and new bands at ~1320 cm^{-1} on complexation is in agreement with oxygen coordination. The far IR region is also rich with bands (Fig. 6.22). The bands at 234 and 410 cm^{-1} of complex **29** are consistent with v(Zn–N$_{py}$) and v(Zn–N$_{azo}$) frequencies [35]. Bands corresponding uncoordinated BF$_4$ anions seen at 1069(vs), 767(w) and 535(w) cm^{-1} for complex **29** are assigned to v_3, v_1 and v_4 bands respectively [36]. For complex **28**, these bands are observed at 1062(vs), 794(s) and 531(w) cm^{-1}. The IR and far IR spectra of compound **29** are given in Figs. 6.21 and 6.22.
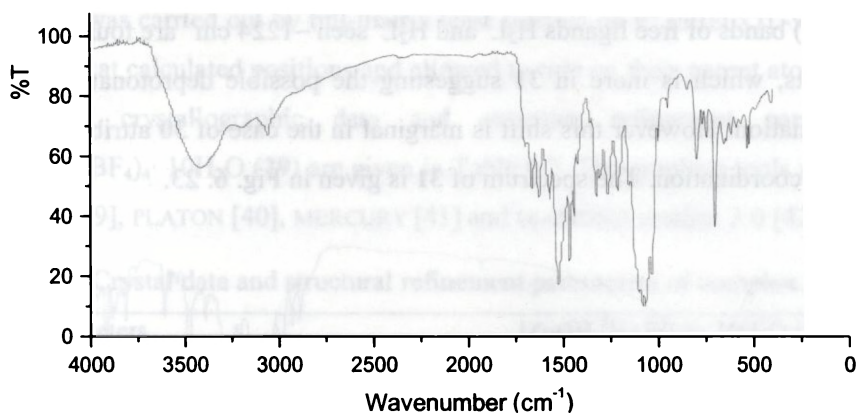
Fig. 6.21. IR spectrum of Zn(II) carbohydrazone square grid complex **29**.
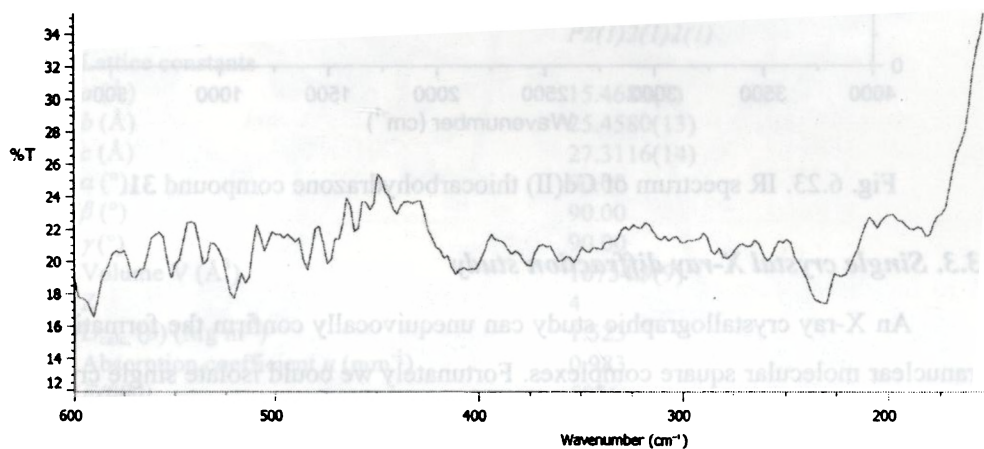
Fig. 6.22. Far IR spectrum of Zn(II) carbohydrazone complex **29**.

The IR spectra of two Cd(II) complexes show some similar features, which are attributed to the free nitrate groups present in both complexes. The very strong band at ~1380 cm^{-1} (v_3) is characteristic, different from the v(C=N) and v(C=C) vibrations, and weak bands at ~840 (v_2) and at ~710 cm^{-1} (v_4) clearly supports the uncoordinated nature of nitrate group [37]. Also, the absence of any bands in the region 1700-1800 cm^{-1} rules out the possibility of any coordinated nitrate groups. The

strong ν(C=S) bands of free ligands H_2L^1 and H_2L^2 seen ~1224 cm^{-1} are found to suffer negative shifts, which is more in **31** suggesting the possible deprotonated thiolate sulfur coordination. However this shift is marginal in the case of **30** attributed to the thione sulfur coordination. The spectrum of **31** is given in Fig. 6. 23.
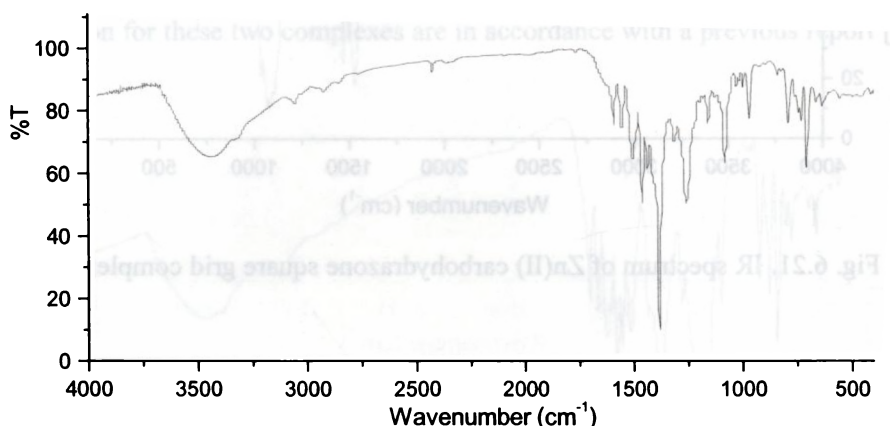
Fig. 6.23. IR spectrum of Cd(II) thiocarbohydrazone compound **31**.

6.3.3. Single crystal X-ray diffraction study

An X-ray crystallographic study can unequivocally confirm the formation of tetranuclear molecular square complexes. Fortunately we could isolate single crystals of compound **29** from its chloroform methanol mixture solution. All attempts to crystallize other complexes, however, went in vain. The X-ray diffraction study of **29**, the first example of a molecular square through self-assembly from a carbohydrazone ligand [32], confirms the formation of square grid and agrees well with MALDI mass results.

The data of **29** were collected at X-ray Crystallography Unit, School of Physics, Universiti Sains Malaysia, Penang, Malaysia using Bruker SMART APEX2 CCD area detector diffractometer equipped with graphite monochromated Mo Kα (λ = 0.71073 Å) radiation at temperature 100 K (Oxford Cyrosystems Cobra low temperature attachment). The trial structure was solved using SHELXS-97 [38] and

256

refinement was carried out by full-matrix least squares on F^2 (SHELXTL-97). H atoms were placed at calculated positions and allowed to ride on their parent atoms.

The crystallographic data and structure refinement parameters of $[Zn(HL^5)]_4(BF_4)_4 \cdot 10H_2O$ (**29**) are given in Table 6.3. The graphics tools used include ORTEP-III [39], PLATON [40], MERCURY [41] and DIAMOND version 3.0 [42].

Table 6.3. Crystal data and structural refinement parameters of complex **29**.

Parameters	$[Zn(HL^5)]_4(BF_4)_4 \cdot 10H_2O$ (**29**)
Empirical Formula	$C_{100}H_{96}B_4F_{16}N_{24}O_{14}Zn_4$
Formula weight (M)	2466.73
Temperature (T) K	100.0(1) K
Wavelength (Mo Kα) (Å)	0.71073
Crystal system	*Orthorhombic*
Space group	*P2(1)2(1)2(1)*
Lattice constants	
a (Å)	15.4680(7)
b (Å)	25.4580(13)
c (Å)	27.3116(14)
α (°)	90.00
β (°)	90.00
γ (°)	90.00
Volume V (Å^3)	10754.9(9)
Z	4
$D_{calc.}$ (ρ) (Mg m^{-3})	1.523
Absorption coefficient μ (mm^{-1})	0.983
F(000)	5056
Crystal size (mm^3)	0.58× 0.39× 0.28
θ Range for data collection	1.09 to 30.14°
Limiting Indices	$-21 \le h \le 21$,
	$-35 \le k \le 35$,
	$-38 \le l \le 38$
T_{max} and T_{min}	0.759 and 0.638
Reflections collected	124835
Independent Reflections	31705 [R(int) = 0.0912]
Refinement method	Full-matrix least-squares on F^2
Data / restraints / parameters	31705 / 0 / 1463
Goodness-of-fit on F^2	1.074
Final R indices [I > 2σ (I)]	$R_1 = 0.0575$, $wR_2 = 0.1323$
R indices (all data)	$R_1 = 0.0962$, $wR_2 = 0.1556$
Largest difference peak and hole (e Å^{-3})	1.227 and −0.947

6.3.3.1. Crystal structure of [Zn(HL⁵)]₄(BF₄)₄· 10H₂O (29)

The molecular structure of **29** with relevant atom numbering scheme is depicted in Fig. 6.24. Here, the ligand H_2L^5, in the deprotonated enol tautomer, adopted a *syn* configuration to form the complex **29** and is essential for getting molecular square architectures of octahedral centers. Relevant bond lengths and bond angles of **29** are given in Tables 6.4 and 6.5.
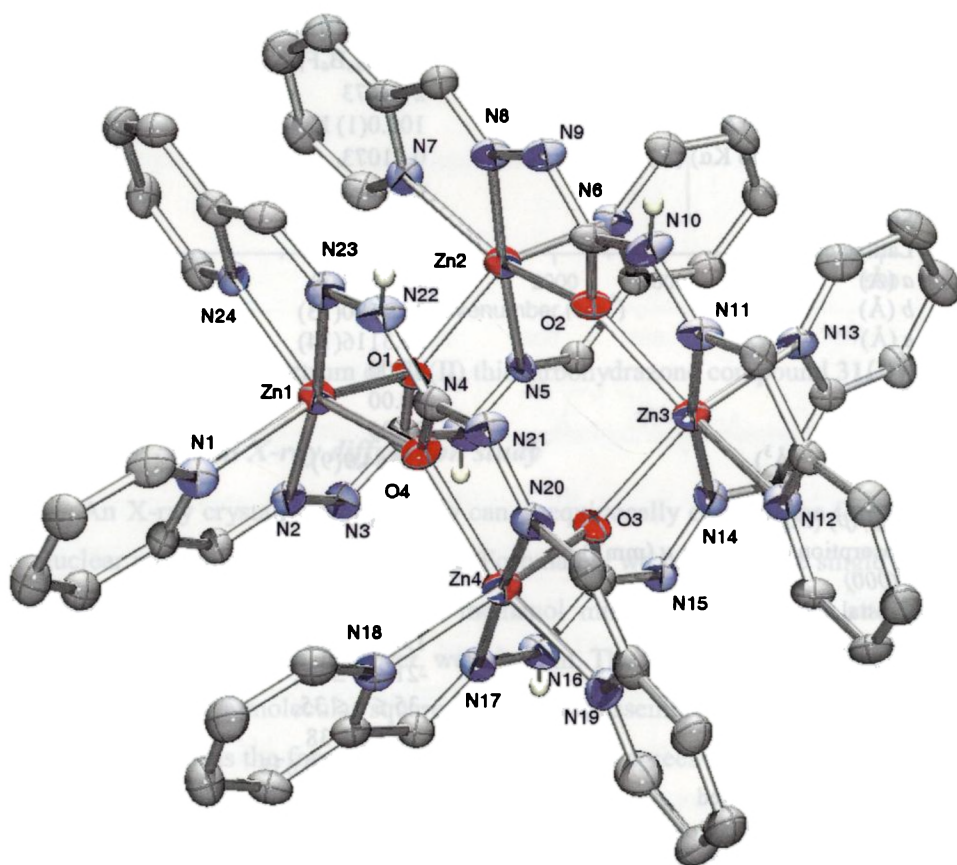
Fig. 6.24. ORTEP diagram for the compound **29** in 70% probability ellipsoids. Phenyl groups, carbon bound hydrogen atoms, anions and water molecules are omitted for clarity. The hydrogen atoms on N(4), N(10), N(16) and N(22) of ligand H_2L^5 are retained in the complex, while their counterparts deprotonated on coordination after enolization.

Table 6.4. Relevant bond lengths (Å) of molecular square grid complex **29**.

Zn(1)–N(2)	2.084(3)	Zn(4)–O(4)	2.163(3)
Zn(1)–N(23)	2.093(3)	Zn(4)–O(3)	2.164(3)
Zn(1)–O(1)	2.128(3)	O(1)–C(13)	1.288(5)
Zn(1)–O(4)	2.139(3)	O(2)–C(38)	1.286(5)
Zn(1)–N(1)	2.167(3)	O(3)–C(63)	1.271(4)
Zn(1)–N(24)	2.191(3)	O(4)–C(88)	1.287(5)
Zn(2)–N(8)	2.063(3)	N(2)–N(3)	1.376(5)
Zn(2)–N(5)	2.094(3)	N(4)–N(5)	1.360(5)
Zn(2)–O(2)	2.147(3)	N(4)–C(13)	1.364(5)
Zn(2)–N(7)	2.151(3)	N(3)–C(13)	1.338(5)
Zn(2)–N(6)	2.164(4)	N(8)–N(9)	1.377(5)
Zn(2)–O(1)	2.186(3)	N(10)–N(11)	1.349(5)
Zn(3)–N(14)	2.080(3)	C(38)–N(9)	1.314(5)
Zn(3)–N(11)	2.107(3)	C(38)–N(10)	1.386(5)
Zn(3)–O(3)	2.125(3)	N(14)–N(15)	1.383(5)
Zn(3)–O(2)	2.141(3)	N(16)–N(17)	1.354(5)
Zn(3)–N(12)	2.153(3)	C(63)–N(15)	1.337(5)
Zn(3)–N(13)	2.178(4)	C(63)–N(16)	1.382(5)
Zn(4)–N(20)	2.044(3)	N(20)–N(21)	1.370(5)
Zn(4)–N(17)	2.078(3)	N(22)–N(23)	1.343(5)
Zn(4)–N(18)	2.141(4)	C(88)–N(21)	1.328(5)
Zn(4)–N(19)	2.141(3)	C(88)–N(22)	1.375(5)

In the tetranuclear cation $[Zn(HL^5)]_4^{4+}$, the ligands are coordinated in the monoanionic form by deprotonation after enolization. The hydrogen atoms on N(3), N(9), N(15) and N(21) are deprotonated on coordination, while their counterparts retained. This is confirmed by the C(13)–O(1) bond distance of 2.288(5) Å, and a decrease of 0.026(7) Å for C(13)–N(3) bond compared to C(13)–N(4) bond, for example. Two $(HL^5)^-$ ligands bind to a Zn(II) in the *mer* configuration (with pairs of O atoms and pyridyl N atoms each bearing a *cis* relationship, whereas the azomethine N atoms are *trans* to each other) to form distorted octahedral metal centers, similar to sulfur coordinated Zn(II) tetramer of bis(2-acetylpyridine) thiocarbohydrazone [13] but different from the *cis-mer* configuration seen in mononuclear Zn(II) semicarbazone complex [8]. The $Zn–N_{py}$ bond lengths are greater compared to that of $Zn–N_{azomethine}$ indicating the strength of latter bonds. The Zn–O distances are

259

comparatively greater than similar bonds in mononuclear semicarbazone complexes [8]. A structure of complex **29** showing atomic arrangement in the molecule is given in Fig. 6.25.

Table 6.5. Relevant bond angles (°) of complex **29**.

N(2)–Zn(1)–N(23)	168.39(14)	N(11)–Zn(3)–O(3)	112.75(12)
N(2)–Zn(1)–O(1)	75.30(12)	N(14)–Zn(3)–O(2)	110.54(12)
N(23)–Zn(1)–O(1)	111.06(13)	N(11)–Zn(3)–O(2)	74.31(12)
N(2)–Zn(1)–O(4)	115.48(12)	O(3)–Zn(3)–O(2)	92.87(11)
N(23)–Zn(1)–O(4)	74.63(12)	N(14)–Zn(3)–N(12)	101.16(13)
O(1)–Zn(1)–O(4)	92.66(11)	N(11)–Zn(3)–N(12)	74.70(13)
N(2)–Zn(1)–N(1)	75.81(13)	O(3)–Zn(3)–N(12)	92.30(12)
N(23)–Zn(1)–N(1)	97.80(14)	O(2)–Zn(3)–N(12)	148.14(12)
O(1)–Zn(1)–N(1)	151.02(12)	N(14)–Zn(3)–N(13)	75.45(13)
O(4)–Zn(1)–N(1)	97.64(12)	N(11)–Zn(3)–N(13)	96.69(13)
N(2)–Zn(1)–N(24)	96.62(13)	O(3)–Zn(3)–N(13)	150.40(12)
N(23)–Zn(1)–N(24)	74.19(13)	O(2)–Zn(3)–N(13)	98.15(12)
O(1)–Zn(1)–N(24)	89.40(12)	N(12)–Zn(3)–N(13)	92.61(13)
O(4)–Zn(1)–N(24)	147.28(12)	N(20)–Zn(4)–N(17)	176.86(14)
N(1)–Zn(1)–N(24)	96.15(13)	N(20)–Zn(4)–N(18)	101.75(13)
N(8)–Zn(2)–N(5)	173.53(14)	N(17)–Zn(4)–N(18)	75.92(13)
N(8)–Zn(2)–O(2)	75.52(12)	N(20)–Zn(4)–N(19)	77.02(13)
N(5)–Zn(2)–O(2)	110.45(12)	N(17)–Zn(4)–N(19)	105.40(14)
N(8)–Zn(2)–N(7)	76.12(14)	N(18)–Zn(4)–N(19)	100.85(13)
N(5)–Zn(2)–N(7)	98.00(14)	N(20)–Zn(4)–O(4)	75.62(12)
O(2)–Zn(2)–N(7)	151.53(12)	N(17)–Zn(4)–O(4)	102.10(12)
N(8)–Zn(2)–N(6)	103.12(14)	N(18)–Zn(4)–O(4)	88.82(12)
N(5)–Zn(2)–N(6)	74.93(13)	N(19)–Zn(4)–O(4)	152.31(12)
O(2)–Zn(2)–N(6)	89.33(12)	N(20)–Zn(4)–O(3)	107.58(12)
N(7)–Zn(2)–N(6)	99.39(13)	N(17)–Zn(4)–O(3)	74.38(12)
N(8)–Zn(2)–O(1)	109.77(12)	N(18)–Zn(4)–O(3)	149.17(12)
N(5)–Zn(2)–O(1)	73.26(12)	N(19)–Zn(4)–O(3)	94.83(12)
O(2)–Zn(2)–O(1)	90.68(11)	O(4)–Zn(4)–O(3)	89.42(11)
N(7)–Zn(2)–O(1)	96.62(12)	Zn(1)–O(1)–Zn(2)	133.91(13)
N(6)–Zn(2)–O(1)	146.00(12)	Zn(2)–O(2)–Zn(3)	134.17(13)
N(14)–Zn(3)–N(11)	171.10(14)	Zn(3)–O(3)–Zn(4)	134.56(13)
N(14)–Zn(3)–O(3)	74.97(12)	Zn(4)–O(4)–Zn(1)	136.07(13)
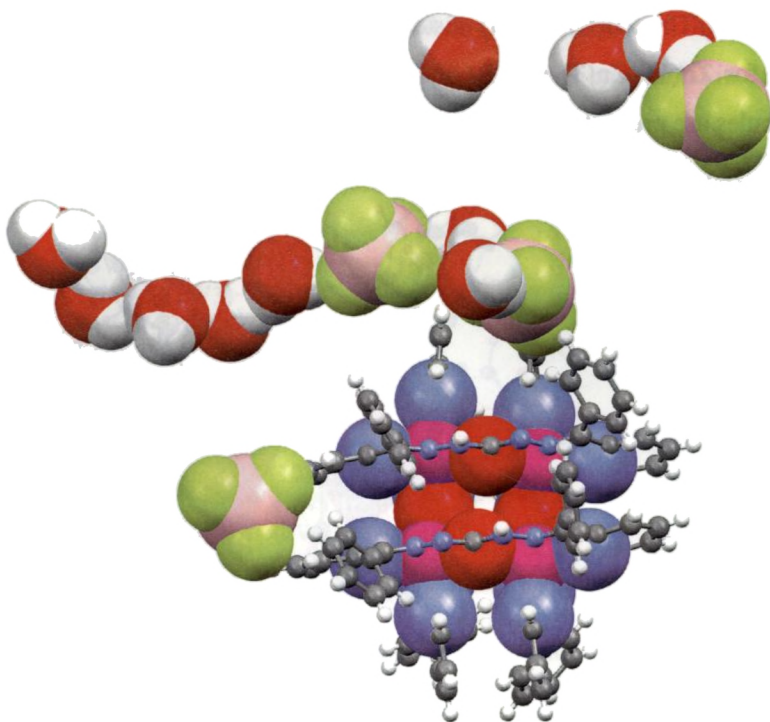
Fig. 6.25. The molecular structure of complex $[Zn(HL^5)]_4(BF_4)_4 \cdot 10H_2O$ (**29**) plotted using space fill and ball and stick models showing atomic arrangement and mid cavity space inside the square grid.

The symmetric molecule (Fig. 6.26) comprises four octahedral Zn(II) centers, which are connected through oxygen atoms (Fig. 6.26). This alternate zinc and oxygen atoms form a boat like structure of eight atoms. The angles subtended at Zn(1) and Zn(3) are ~92.7° and at Zn(2) and Zn(4) are ~90°, while those subtended at oxygen atoms varies from 133.91(13)° to 136.07(13)°. Yet, the four Zn(II) atoms are approximately in a plane with a maximum deviation of -0.1654(5) Å for Zn(3). The nearby Zn(II)···Zn(II) distances are ~3.96 Å {Zn(1)···Zn(2)=3.9700(7) Å, Zn(2)···Zn(3)=3.9496(7) Å, Zn(3)···Zn(4)=3.9566(7) Å, Zn(4)···Zn(1)=3.9898(7) Å} and Zn(II)···Zn(II)···Zn(II) angles are ~89° {Zn(1)–Zn(4)–Zn(3)=87.91(1)°, Zn(4)–Zn(3)–Zn(2)=91.57(1)°, Zn(1)–Zn(2)–Zn(3)=88.29(1)°, Zn(2)–Zn(1)–

Zn(4)=90.78(1)°}. The Zn(II)···Zn(II) distances along the corners of the square are 5.5158(7) Å for Zn(1)···Zn(3) and 5.6664(7) Å for Zn(2)···Zn(4). But no water or solvent molecules are present in the cavity space of square grid.
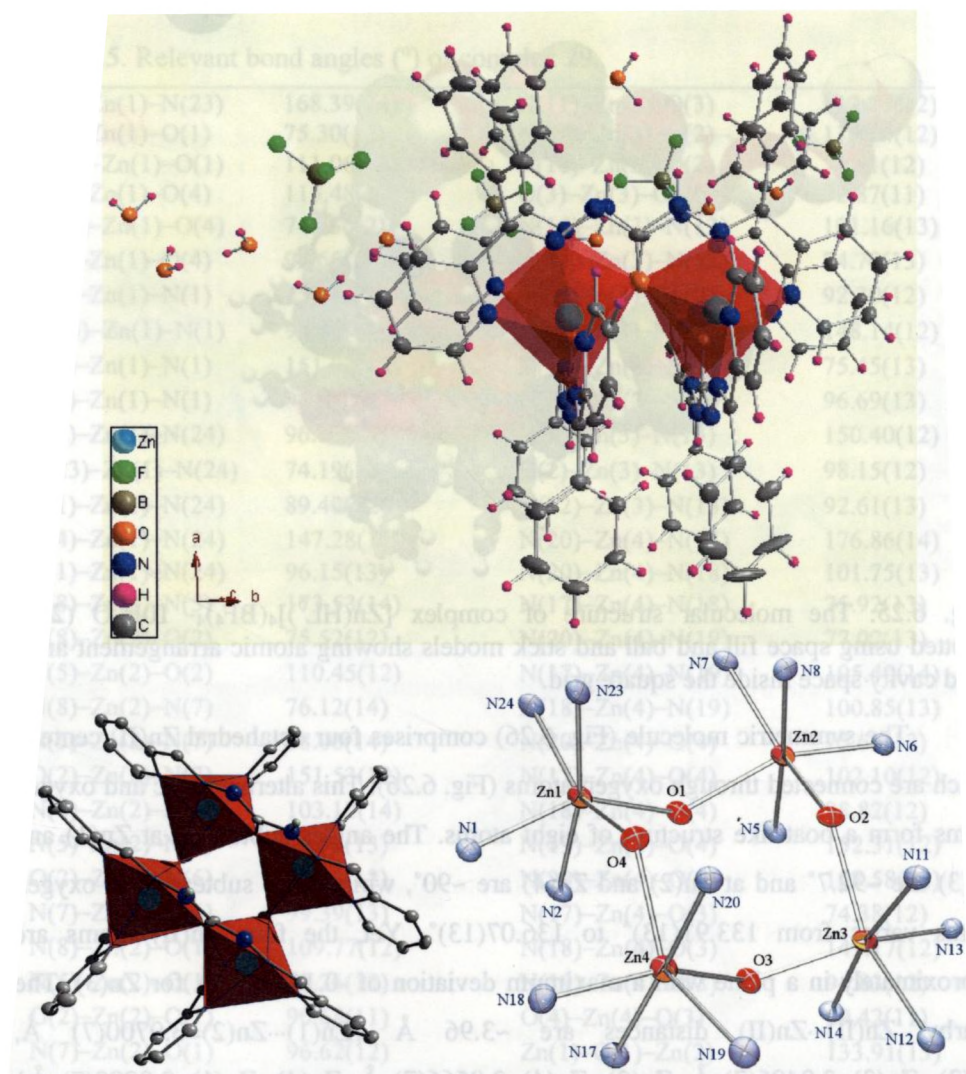
Fig. 6.26. A side view of **29** with coordination octahedral polyhedra (top) and top view of cationic part showing the symmetry (bottom left, carbon bound hydrogen atoms are removed for clarity) and the coordination core about the Zn(II) centers (bottom right).

All molecules are interconnected by a number of hydrogen bonding interactions (Table 6.6, Fig. 6.27) to form a three dimensional motif in the lattice.

Table 6.6. Hydrogen bonding interactions of complex **29**.

Residue	D–H···A	D–H (Å)	H···A (Å)	D···A (Å)	D–H···A (°)
6	O(1W)–H(1W1)···F(13)	0.85	2.12	2.944(9)	162
6	O(1W)–H(2W1)···O(10W)	0.85	2.21	2.847(7)	132
8	O(3W)–H(1W3)···F(11)	1.00	1.84	2.813(5)	162
8	O(3W)–H(2W3)···O(5W)[a]	0.86	2.00	2.798(6)	153
1	N(4)–H(4B)···O(8W)[c]	0.86	2.12	2.885(5)	148
9	O(4W)–H(1W4)···O(7W)	0.85	2.03	2.768(5)	144
9	O(4W)–H(2W4)···O(8W)	0.85	2.10	2.950(5)	176
10	O(5W)–H(1W5)···F(8)	0.85	2.10	2.944(6)	174
10	O(5W)–H(2W5)···F(9)	0.85	2.43	3.097(9)	136
10	O(5W)–H(2W5)···F(10)	0.85	2.30	3.044(7)	146
11	O(6W)–H(1W6)···O(7W)	0.85	2.36	3.051(6)	139
11	O(6W)–H(2W6)···O(2W)	0.85	2.16	2.782(6)	130
1	N(10)–H(10C)···O(9W)[d]	0.86	2.15	2.917(4)	148
12	O(7W)–H(1W7)···N(15)[b]	0.85	2.46	3.006(5)	123
12	O(7W)–H(2W7)···O(6W)	0.85	2.21	3.051(6)	171
13	O(8W)–H(1W8)···F(7)	0.85	2.02	2.760(7)	146
13	O(8W)–H(2W8)···O(4W)	0.85	2.15	2.950(5)	158
14	O(9W)–H(2W9)···F(15)[e]	0.84	2.29	2.847(6)	125
1	N(16)–H(16B)···O(7W)[c]	0.86	2.01	2.791(5)	151
15	O(10W)-H(1WA)···N(21)[a]	0.90	2.41	2.991(5)	122
1	N(22)–H(22B)···O(10W)[d]	0.86	2.09	2.801(5)	139
1	C(2)–H(2A)···F(1)[f]	0.93	2.51	3.224(6)	134
1	C(4)–H(4A)···F(1)	0.93	2.52	3.261(5)	137
1	C(12)–H(12A)···F(6)[c]	0.93	2.53	3.337(7)	144
1	C(20)–H(20A)···O(2W)[g]	0.93	2.45	3.358(6)	164
1	C(23)–H(23A)···F(3)[c]	0.93	2.49	3.207(6)	134
1	C(25)–H(25A)···F(16)[h]	0.93	2.43	3.224(6)	143
1	C(27)–H(27A)···F(5)[c]	0.93	2.49	3.258(6)	139
1	C(29)–H(29A)···F(9)[h]	0.93	2.50	3.235(9)	136
1	C(54)–H(54A)···F(4)[c]	0.93	2.46	3.166(5)	133
1	C(68)–H(68A)···O(10W)[a]	0.93	2.51	3.418(6)	166
1	C(70)–H(70A)···N(3)*	0.93	2.58	3.498(6)	168
1	C(72)–H(72A)···F(3)	0.93	2.51	3.163(6)	128
1	C(73)–H(73A)···F(2)	0.93	2.41	3.270(5)	154
1	C(76)–H(76A)···O(2W)[c]	0.93	2.58	3.263(6)	130
1	C(95)–H(95A)···F(4)[f]	0.93	2.41	3.305(6)	162

D= donor, A= acceptor; * intramolecular; Eqivalent position codes: a= ½+x, 3/2-y, 1-z; b= 2-x, -1/2+ y, 1/2-z; c= 2-x, 1/2+y, 1/2-z; d= -1/2+x, 3/2-y, 1-z; e= 2-x, -1/2+y, 3/2-z; f= -1/2+x, 3/2-y, -z; g= x, 1+y, z; h= 3/2-x, 2-y, -1/2+z.

In the crystal packing (Fig. 6.27) molecules are arranged along the *a* axis. The packing is directed by various C–H···π interactions, in addition to hydrogen bonding networks including water and BF_4^- anions. The crystal structure cohesion may also be reinforced by weak π···π interactions. The interactions are given in Tables 6.7 and 6.8.

Table 6.7. π···π interactions seen in the crystal packing of square complex **29**.

Cg(I)···Cg(J)	Cg···Cg (Å)	α (°)	β (°)
Cg(2)···Cg(6)[a]	3.804(2)	4.75	6.28
Cg(4)···Cg(8)[a]	3.864(2)	2.79	12.42
Cg(6)···Cg(2)[a]	3.804(2)	4.75	10.18
Cg(7)···Cg(12)[a]	3.870(2)	2.59	13.23
Cg(8)···Cg(4)[a]	3.864(2)	2.79	10.44
Cg(8)···Cg(24)[a]	3.945(2)	9.16	25.25
Cg(9)···Cg(14)[a]	3.806(2)	3.90	5.56
Cg(12)···Cg(7)[a]	3.870(2)	2.59	10.64
Cg(12)···Cg(18)[a]	3.912(2)	8.08	24.03
Cg(14)···Cg(9)[a]	3.806(2)	3.90	9.32
Cg(17)···Cg(22)[a]	3.692(3)	6.77	12.11
Cg(18)···Cg(12)[a]	3.913(2)	8.08	16.07
Cg(18)···Cg(21)[a]	3.686(3)	7.39	20.67
Cg(19)···Cg(24)[a]	3.758(2)	6.88	16.23
Cg(20)···Cg(23)[a]	3.722(2)	9.83	23.07
Cg(21)···Cg(18)[a]	3.686(3)	7.39	13.44
Cg(21)···Cg(24)[b]	3.929(2)	14.10	34.04
Cg(22)···Cg(17)[a]	3.692(3)	6.77	18.06
Cg(23)···Cg(20)[a]	3.722(2)	9.83	13.95
Cg(24)···Cg(8)[a]	3.945(2)	9.16	17.54
Cg(24)···Cg(19)[a]	3.758(2)	6.88	22.86
Cg(24)···Cg(21)[c]	3.929(2)	14.10	22.51

Cg···Cg is the distance between ring centroids. Only π···π interactions with Cg···Cg distances below 4 Å are included. α is the dihedral angle between the planes of Cg(I) and Cg(J). β is the angle Cg(I)-Cg(J).
Cg(2): Zn(1), O(4), C(88), N(22), N(23); Cg(4): Zn(1), N(23), C(89) C(96) N(24);
Cg(6): Zn(2), O(2), C(38), N(9), N(8); Cg(7): Zn(2), N(5), C(14), C(21), N(6);
Cg(8): Zn(2), N(7), C(30), C(31), N(8); Cg(9): Zn(3), O(2), C(38), N(10), N(11);
Cg(12): Zn(3), N(13), C(55), C(56), N(14); Cg(14): Zn(4), O(4), C(88), N(21), N(20);
Cg(17): N(1), C(1), C(2), C(3), C(4), C(5); Cg(18): N(6), C(21), C(22), C(23), C(24), C25);
Cg(19): N(7), C(26), C(27), C(28), C(29), C(30); Cg(20): N(12), C(46), C(47), C(48),
C(49), C(50); Cg(21): N(13), C(51), C(52), C(53), C(54), C(55); Cg(22): N(18), C(71),
C(72), C(73), C(74), C(75); Cg(23): N(19), C(76), C(77), C(78), C(79), C(80);
Cg(24): N(24), C(96), C(97), C(98), C(99), C(100).
Symmetry codes: a= x, y, z; b= 3/2-x, 2-y, 1/2+z; c= 3/2-x, 2-y, -1/2+z.

Table 6.8. CH···π interactions seen in the crystal packing of complex **29**.

X–H(I) Res(I)···Cg(J)		H···Cg (Å)	X···Cg (Å)	X–H···Cg (°)
C(1)–H(1A)	[1]···Cg(2)[a]	2.94	3.360(5)	109
C(100)–H(10B)	[1]···Cg(1)[a]	2.80	3.222(5)	109
O(9W)–H(1W9)	[14]···Cg(28)[b]	2.97	3.689(4)	138
C(25)–H(25A)	[1]···Cg(6)[a]	2.94	3.332(5)	107
C(50)–H(50A)	[1]···Cg(10)[a]	2.94	3.371(4)	110
C(53)–H(53A)	[1]···Cg(17)[c]	2.71	3.630(5)	169
C(67)–H(67A)	[1]···Cg(18)[d]	2.99	3.592(5)	123
C(75)–H(75A)	[1]···Cg(14)[a]	2.96	3.289(4)	102

Cg(1)= Zn(1), O(1), C(13), N(3), N(2); Cg(2)= Zn(1), O(4), C(88), N(22), N(23);
Cg(6)= Zn(2), O(2), C(38), N(9), N(8); Cg(10)= Zn(3), O(3), C(63), N(15), N(14);
Cg(14)= Zn(4), O(4), C(88), N(21), N(20); Cg(17)= N(1), C(1), C(2), C(3), C(4), C(5);
Cg(18)= N(6), C(21), C(22), C(23), C(24), C(25); Cg(28)= C(40), C(41), C(42), C(43),
C(44), C(45): Eqivalent position codes: a= x, y, z; b= ½+x, 3/2-y, 1-z; c= 3/2-x, 2-y,
1/2+z; d= 2-x, -1/2+ y, 1/2-z.
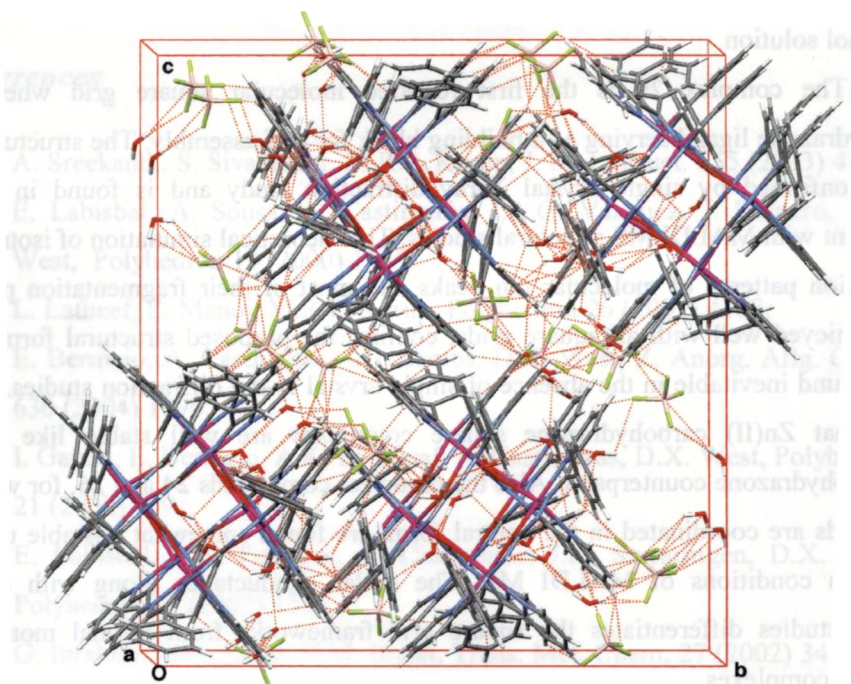
Fig. 6.27. A part of the unit cell packing of the molecular square complex **29** showing the molecules are packed along the *a* axis and the formation of 3D motif through hydrogen bonding and other short contacts.

6.4. Concluding remarks

This chapter presents syntheses and physico-chemical characterizations of dinuclear Zn(II), tetranuclear 2×2 square grids of Zn(II) and Cd(II) complexes of thiocarbohydrazone ligands. Also, Zn(II) tetranuclear molecular 2×2 square grids of carbohydrazone ligands H_2L^4 and H_2L^5 are reported, which are the first series of molecular square grids of carbohydrazone ligands. The reaction conditions for synthesis of complexes differentiate the anions BF_4^- and NO_3^- from bromide ion for supramolecular self-assembly as the latter prefer to coordinate to metal center. The Cd(II) complex **30** synthesized using methanol solvent found to be formed by respective neutral thiocarbohydrazone H_2L^1, while Cd(II) complex **31** is found to be formed by monodeprotonated form of thiocarbohydrazone ligand H_2L^2 when prepared in ethanol solution.

The complex **29** is the first reported molecular square grid where a carbohydrazone ligand serving as a building block for self-assembly. The structure of **29** is confirmed by single crystal X-ray diffraction study and is found in well agreement with MALDI MS structural studies. The theoretical simulation of isotropic distribution patterns of molecular ion peaks and most of their fragmentation peaks were achieved well with all square grids, confirm the proposed structural formulae and is found inevitable in the absence of single crystal X-ray diffraction studies. It is found that Zn(II) carbohydrazone square complexes are well stable like their thiocarbohydrazone counterparts. Also the dinuclear compounds **24** and **26**, for which the ligands are coordinated in the neutral form, are found somewhat unstable under ionization conditions of MALDI MS. The molar conductance along with other spectral studies differentiates the square grid frameworks from normal mono or dinuclear complexes.

The carbohydrazone derived metallosupramolecular square complexes **28** and **29** consist of carbonyl oxygen as the connecting atom between metal centers, and is

unequivocally confirmed for **29**. Hitherto reported carbohydrazone complexes show either mononuclear or binuclear metal complexes coordinated through N, N, O and N, N, N atoms. The carbohydrazone-derived complexes are novel in several respects. This is the first report where the carbonyl group is involved in the bridging mode for carbohydrazone ligands to form molecular square grids. The novel N_4O coordination mode offers carbohydrazones as a building block for interesting framework complexes through self-assembly. The M–O–M angles ranging from $133.91(13)°$ to $136.07(13)°$ for Zn(II) square grid **29** seem interesting since it leaves a possibility of orthogonal magnetic orbitals for future metal {especially for metals like Co(II)} complexes of these types and that might exhibit ferromagnetic behaviour with similar suitably substituted carbohydrazone ligands.

References

1. A. Sreekanth, S. Sivakumar, M.R.P. Kurup, J. Mol. Struct. 655 (2003) 47.

2. E. Labisbal, A. Sousa, A. Castineiras, J.A.G. Vazquez, J. Romero, D.X. West, Polyhedron 19 (2000) 1255.

3. L. Latheef, E. Manoj, M.R.P. Kurup, Polyhedron 26 (2007) 4107.

4. E. Bermejo, A. Castineiras, I.G. Santos, D.X. West, Z. Anorg. Allg. Chem. 630 (2004) 1096.

5. I. Garcia, E. Bermejo, A.K. El Sawaf, A. Castineiras, D.X. West, Polyhedron 21 (2002) 729.

6. E. Labisbal, A.S. Pedrares, A. Castineiras, J.K. Swearingen, D.X. West, Polyhedron 21 (2002) 1553.

7. G. Ibrahim, M.A. Khan, G.M. Bouet, Trans. Met. Chem. 27 (2002) 34.

8. N.C. Kasuga, K. Sekino, M. Ishikava, A. Honda, M. Yokoyama, S. Nakano, N. Shimada, C. Koumo, K. Nomiya, J. Inorg. Biochem. 96 (2003) 298.

9. A. Bacchi, A. Bonini, M. Carcelli, F.J. Farraro, J. Chem. Soc., Dalton Trans. (1996) 2699.

10. A. Bacchi, M. Carcelli, P. Pelagatti, C. Pelizzi, G. Pelizzi, F. Zani, J. Inorg. Biochem. 75 (1999) 123.

11. Z.H. Chohan, K.M. Khan, C.T. Supuran, Appl. Organometal. Chem. 18 (2004) 305.

12. A.A.A. Abu-Hussen, A.A.A. Emara, J. Coord. Chem. 57 (2004) 973.

13. G. Han, D. Guo, C.-Y. Duan, H. Mo, Q.-j. Meng, New J. Chem. 26 (2002) 1371.

14. M.A. Ali, P.V. Bernhardt, C.L. Keim, A.H. Mirza, Aust. J. Chem. 57 (2004) 409.

15. A.H.M. Siddalingaiah, S.G. Naik, B.S. Sherigara, B.E.K. Swami, J. Mol. Struct. (Theochem) 582 (2002) 69.

16. A.H.M. Siddalingaiah, S.G. Naik, H.D. Patil, Spectrochim. Acta Part A, 60 (2004) 2499.

17. A.H.M. Siddalingaiah, G.N. Sunil, J. Mol. Str.(Theochem) 581 (2002) 149.

18. A.H.M. Siddalingaiah, S.G. Naik, J. Mol. Str.(Theochem) 582 (2002) 129.

19. M. Melnik, K. Gyoryova, J. Skorsepa, C. E.Holloway, J. Coord. Chem. 35 (1995) 179.

20. E. Lopez-Toress, M.A. Mendiola, C.J. Pastor, B.S. Perez, Inorg. Chem. 43 (2004) 5222.

21. X.-H. Bu, H. Morishita, K. Tanaka, K. Biradha, S. Furusho, M. Shionoya, Chem. Commun. (2000) 971.

22. V. Patroniak, P.N.W. Baxter, J.-M, Lehn, M. Kubicki, M. Nissinen, K. Rissanen, Eur. J. Inorg. Chem. (2003) 4001.

23. Z. He, C. He, Z.-M. Wang, E.-Q. Gao, Y. Liu, C.-H. Yan, Dalton Trans. (2004) 502.

24. J.S. Casas, M.S. Garcya-Tasende, J. Sordo, Coord. Chem. Rev. 209 (2000) 197.

25. D.W. Christianson, Adv. Protein Chem. 42 (1991) 281.

26. M.B. Ferrari, G.G. Fava, Pelizzi, P. Tarasconi, J. Chem. Soc., Dalton Trans. (1992) 2153.

27. D. Solaiman, L. Saryan, D.H. Petering, J. Inorg. Biochem. 10 (1979) 135.

28. H. Beraldo and D. Gambino, Mini-Rev. Med. Chem. 4 (2004) 31.

29. D. Kovala-Demertzi, P.N. Yadav, J. Wiecek, S. Skoulika, T. Varadinova, M.A. Demertzis, J. Inorg. Biochem. 100 (2006) 1558.

30. Y.-P. Tian, W.-T. Yu, C.-Y. Zhao, M.-H. Jiang, Z.-G. Cai, H.-K. Fun, Polyhedron 21 (2002) 1217.

31. W.J. Geary, Coord. Chem. Rev. 7 (1971) 81.

32. E. Manoj, M.R.P. Kurup, H.-K. Fun, Inorg. Chem. Commun. 10 (2007) 324.

33. C. He, C.-y. Duan, C.-j. Fang, Y.-j. Liu,Q.-j. Meng, J. Chem. Soc., Dalton Trans. (2000) 1207.

34. M.A. Ali, A.H. Mirza, M.H.S.A. Hamid, F.H. Bujang, P.V. Bernhardt, Polyhedron 23 (2004) 2405.

35. P.F. Rapheal, Ph. D. Thesis, Diversity in structural and spectral characteristics of some transition metal complexes derived from aldehyde based thiosemicarbazone ligands, CUSAT, Kochi (2006).

36. K. Nakamoto, Infrared and Raman Spectra of Inorganic and Coordination Compounds, 5th ed., Wiley-Interscience, New York (1997).

37. D.N. Sathyanarayana, Vibrational Spectroscopy, New Age International New Delhi (2004).

38. G.M. Sheldrick, SHELXTL Version 5.1, Software Reference Manual, Bruker AXS Inc. Madison, Wisconsin, USA, (1998).

39. L.J. Farrugia, J. Appl. Cryst. 30 (1997) 565.

40. A.L. Spek, Acta Cryst. 36 (2003) 7.

41. C.F. Macrae, P.R. Edgington, P. McCabe, E. Pidcock, G.P. Shields, R. Taylor, M. Towler, J. van de Streek, J. Appl. Cryst., 39 (2006) 453.

42. K. Brandenburg, H. Putz, DIAMOND Version 3.0, Crystal Impact GbR, Postfach 1251, D-53002, Bonn, Germany (2004).

****

The work presented in this thesis comprises synthesis and characterization of suitably substituted thiocarbohydrazone and carbohydrazone ligand building blocks, self-assembled metallosupramolecular square grid complexes of Ni(II), Mn(II), Zn(II) and Cd(II) as well as some di/multinuclear Cu(II), Mn(II) and Zn(II) complexes. The primary aim was the deliberate syntheses of some novel transition metal framework complexes, mainly metallosupramolecular coordination square grids by self-assembly and their physico-chemical characterization. The work presented, however, also include synthesis and characterization of four mononuclear Ni(II) complexes of two thiosemicarbazones, which we carried out as a preliminary and supporting study.

In addition, the study of the coordinating preferences of thiocarbohydrazones and carbohydrazones towards selected first row transition metals, including magnetically important nickel, manganese and copper, provides an idea of the control over the topology of complexes can be achieved by the these ligand building blocks and probable similar kinds of ligands. Since the properties of any material are largely due to its structure, control over the topology sometimes allows to manipulate these properties. This allows the deliberate design of materials with a range of useful properties, including electronic properties, magnetic properties, non-linear optical effects luminescent properties, etc.

A variety of factors can influence the self-assembly process. Basically, the design of proper ligands as building blocks, together with the coordination preferences of the metal centers as nodes, is undoubtedly the most rational synthetic strategy in manipulating the framework topologies. The key step thus includes syntheses and characterization of useful ligands. We have designed three thiocarbohydrazone and three carbohydrazone ligands for this purpose. Additionally, two lower homologue thiosemicarbazone ligands were also prepared. The ligands synthesized were:

1. 1,5-Bis(di-2-pyridyl ketone) thiocarbohydrazone (H_2L^1)
2. 1,5-Bis(2-benzoylpyridine) thiocarbohydrazone (H_2L^2)
3. 1,5-Bis(quinoline-2-carbaldehyde) thiocarbohydrazone (H_2L^3)

4. 1,5-Bis(di-2-pyridyl ketone) carbohydrazone (H_2L^4)

5. 1,5-Bis(2-benzoylpyridine) carbohydrazone (H_2L^5)

6. 1,5-Bis(quinoline-2-carbaldehyde) carbohydrazone (H_2L^6)

7. Quinoline-2-carbaldehyde *N*(4),*N*(4)-(butane-1,4-diyl) thiosemicarbazone (HL^7)

8. 2-Benzoylpyridine-*N*(4),*N*(4)-(butane-1,4-diyl) thiosemicarbazone (HL^8)

Substituents having coordinating groups on attaching at the N^1 and N^5 positions of the carbohydrazide and thiocarbohydrazide enhance their denticity. We have used di-2-pyridyl ketone, 2-benzoylpyridine and quinoline-2-carbaldehyde to increase the denticity and substituted both the ends of carbohydrazide and thiocarbohydrazide. In doing so the new ligands, mainly possess two coordinating pockets, are found to act as building blocks for molecular square grid formation, by making use of sulfur/oxygen bridging, in a controlled manner. With these ligands we prepared a series of complexes of copper, nickel, manganese, zinc and cadmium. The complexes were characterized by various physico-chemical methods such as partial elemental analysis, molar conductance measurements, MALDI MS, IR, far IR, UV-visible, EPR and variable temperature magnetic susceptibility measurements. Single crystal X-ray diffraction studies of some complexes are also reported. MALDI mass spectra as DCTB mix on positive ion mode are found very useful for characterization of supramolecular coordination compounds. Isotropic distribution patterns of sensible peaks were characterized with theoretical calculated patterns. Magnetic data of molecular square grids are rationalized with fitting into modified van Vleck equation. EPR spectral parameters of Cu(II) and Mn(II) complexes under investigation conditions are reported with spectral simulations.

It is found that the present carbohydrazone and thiocarbohydrazone ligands are potential candidates as building blocks for molecular square grids of Ni(II), Mn(II), Zn(II) and Cd(II). Four of the six potential ligands are new candidates for self-

assembly of 2×2 grids as ditopic ligands. The coordination geometries of both thiocarbohydrazone and carbohydrazone derived square grids, complexes $[Ni(HL^1)]_4(PF_6)_4$· ½CH$_3$CH$_2$OH· 2.8H$_2$O (**1a**) and $[Zn(HL^5)]_4(BF_4)_4$· 10H$_2$O (**29**) respectively, have been explicitly solved by single crystal X-Ray diffraction studies. However Cu(II) ions are found very reluctant to form molecular square grids with the same set of ligands; but with flexible coordination modes multinuclear chelating complexes were synthesized and characterized. The ligands are found capable of coordinating metal centers in the neutral, monoanionic and dianionic forms subject to reaction conditions. Conversely, Cu(II) carbohydrazone complexes are found not very stable in their solutions of common organic solvents on exposure to air. However, all complexes are found very stable in the solid state. As expected, the Mn(II) complexes were also found labile in their solutions in organic solvents, especially at lower concentrations.

Hitherto reported complexes of carbohydrazones were all mononuclear or dinuclear in nature. However our study is observed first time for carbohydrazone derivatives behaving as the building blocks for self-assembly, and thereby offers a new dimension to metallosupramolecular squares. The novel N$_4$O coordination, with bridging mode of the carbonyl group, offers carbohydrazone ligands as a building block for interesting frameworks through self-assembly. The two-dimensional molecular square grids are precise and easy to prepare and provide best opportunities to enter the fascinating world of supramolecular chemistry. The carbohydrazide inner core thus offers a wide range of possibilities with suitable substituents having different coordination properties to build novel coordinating ligands for designing multinuclear coordination complex frameworks of desired metals, which would find applications in various fields.

The materials with uncoordinated ligand donor atoms after assembly possess chemically active sites and are expected to be useful for homogeneous or heterogeneous catalysis, or as molecular sensors. These kinds of complexes shall

further be used as a substrate for further complexation or to design mixed-metal complexes. The complexes reported here possess uncoordinated donor atoms and this is better in complexes derived from di-2-pyridyl ketone derived ligands. Accidentally and fortunately complex **1a**, got crystallized from a solution of complex **1**, is found to have two trapped water molecules inside the four uncoordinated pyridyl groups. This kind of water of crystallization as a receptee and associated hydrogen bonds are supramolecularly very potent.

The pyridyl group, selected here, is a very vital substituent in the light of various biological activities shown by thiosemicarbazone and other related potential compounds possessing it. Similarly, quinoline group, an equivalent analogue thereof, also has a unique position in drug chemistry. So we found it worthwhile to go for an immediate direction towards pharmaceutical applications. Also there was anticipation of anticancer drug analogues for thiocarbohydrazones. In the light of these aspects we carried out preliminary anticancer studies of selected compounds and included in the thesis. The chapter wise conclusions of the thesis are as described below.

Chapter 1 depicts a brief survey of the previous research works in the field of carbohydrazones and thiocarbohydrazones, their applications, importance of multinuclear coordination compounds, method of self-assembly and metallosupramolecular squares. The thiocarbohydrazone ligands possessing mainly two binding units, unlike thiosemicarbazones, are found to have the possibility of forming multinuclear compounds and for behaving as building blocks for self-assembly to form molecular square grids. The different analytical and spectroscopic techniques used for the analysis of the ligands and metal complexes are also discussed.

Chapter 2 includes syntheses of carbohydrazone, thiocarbohydrazone and thiosemicarbazone ligands and their spectral characterization by elemental analysis, IR, UV-vis and different NMR techniques with a comparative study. X-Ray crystal structures of two new ligands H_2L^3 and H_2L^4 are also reported. All compounds were

found to exist in their thione tautomeric form in solid state. It is found that the compounds H_2L^2 and H_2L^5 exhibiting keto-enol tautomerism, while the compound H_2L^1 shows an exclusive presence of its thione tautomer, in their $CDCl_3$ solutions. Study of *in vitro* anticancer activity towards MCF-7 cell lines of selected compounds are also reported, it is seen that the new thiosemicarbazone HL^7 shows antiproliferation effect.

Chapter 3 describes the synthesis, spectral and structural features of four self-assembled molecular square grids of Ni(II) using carbohydrazone and thiocarbohydrazone ligands. Single crystal X-ray diffraction study of one of them is described in details and is in agreement with a molecular square of four Ni(II) octahedral centers, as expected. The MALDI MS spectra are found very useful for the characterization of stable framework complexes. Magneto-structural correlation study shows intramolecular antiferromagnetic coupling between Ni(II) electrons, consistent with the bridging structural arrangement, by a super exchange mechanism through intervening sulfur/oxygen atoms. Four new thiosemicarbazone Ni(II) complexes were also synthesized and characterized. This include X-ray studies of two mononuclear octahedral Ni(II) compounds.

Chapter 4 comprises the syntheses and spectral characterization of twelve copper(II) complexes using all carbohydrazone and thiocarbohydrazone ligands. Tetranuclear, trinuclear and dinuclear copper(II) complexes are studied with special emphasis to EPR spectral and variable temperature magnetic properties. However, the Cu(II) compounds, especially from carbohydrazone-derived, are found not very stable in solution or under ionization conditions of MALDI. The lability in solutions is also clear because all the complexes showing antiferromagnetism in the solid state do not exhibit the coupling of electrons in their frozen DMF solution EPR spectra. The EPR parameters, under investigation conditions, were obtained by making use of simulations. In addition, selected compounds were screened for *in vitro* anticancer activity towards MCF-7 cell lines and the results clearly points to the fact that ligands

showed cell proliferation and their complexation leads to antiproliferation effect. Three complexes are reported as anticancer gadgets against breast cancer.

Chapter 5 explains the synthesis and spectral characterization of five Mn(II) complexes. Variable temperature magnetization study reveals strong antiferromagnetism. Frozen DMF solution EPR spectral studies suggesting possible fragmentations to monomeric species, under investigation conditions, as evidenced by EPR parameters obtained by making use of simulations. MALDI MS spectra reveal lower stability of Mn(II) complexes in their solutions or under MALDI ionization conditions, but show sensible fragmentation peaks. Magnetic data of four Mn(II) complexes were rationalized successfully on the basis of expected square grid structures in the solid state, as supported by mass and other studies, and is in agreement.

Chapter 6 deals the syntheses and characterization of six Zn(II) and two Cd(II) complexes. All complexes, except two Zn(II) compounds, exist as molecular square grids and their structural and spectral features are described in detail. This include single crystal X-ray diffraction study of one Zn(II) molecular square grid derived from a carbohydrazone ligand, H_2L^5. The results clearly indicate the utility of carbohydrazones as building blocks for self-assembled molecular frameworks. The MALDI MS spectrometry is found an important tool for the explicit characterization, existence and stability of framework complexes in solutions and can be confirmed by theoretical simulations of isotropic distribution patterns of characteristic peaks.

Based on the present work we would like to conclude that the carbohydrazones, thiocarbohydrazones and their coordination framework complexes of transition metals are promising systems for wide application in science and technology varied from physics to biotechnology. Novel classes of materials and biologically important potential compounds open up further scope of researches and we hopefully welcome any sort of related research to make this work more valuable.

****

Curriculum Vitae

PERSONAL PROFILE

Nationality	Indian
Date of Birth	28th February 1981
Permanent address	Puthen Madom
	Pandithitta East, Thalavoor (P.O.)
	Kollam-691 514, Kerala
	☏ +91-475-2328535
e-mail	manoje@cusat.ac.in
	manuthalavoor@yahoo.com
	manojepotti@gmail.com

EDUCATION

1996	SSLC (84.5 %) D.V.V.H.S.S., Thalavoor, Board of public examinations, Kerala state
1996-1998	Pre-Degree (71.6%) St. Gregorios College, Kottarakara University of Kerala
1998-2001	B. Sc. Chemistry (81.4%) St. Gregorios College, Kottarakara University of Kerala
2001-2003	M. Sc. Chemistry (79.7%, Fifth Rank) (Elective: Advanced Physical Chemistry) St. Stephen's College, Pathanapuram University of Kerala

ACHIEVEMENTS

2004 June	National Eligibility Test – UGC-JRF/Lectureship
2003	KSCSTE-JRF in Chemistry *Kerala State Council for Science,* *Technology and Environment.*

RESEARCH PUBLICATIONS

1. Structural and spectral studies of nickel(II) complexes with $N(4),N(4)$-(butane-1,4-diyl)thiosemicarbazones, E. Manoj, M.R.P. Kurup, Polyhedron, DOI: 10.1016/j.poly.2007.09.023

2. Synthesis and spectral studies of bisthiocarbohydrazone and biscarbohydrazone of quinoline-2-carbaldehyde: Crystal structure of bis(quinoline-2-aldehyde) thiocarbohydrazone E. Manoj, M.R.P. Kurup, E. Suresh, J. Chem. Cryst., DOI: 10.1007/s10870-007-9267-9

3. Synthesis and EPR spectral studies of manganese (II) complexes derived from pyridine 2-carbaldehyde based N(4)-substituted thiosemicarbazones: Crystal structure of one complex, P.F. Rapheal, E. Manoj, M.R.P. Kurup, Polyhedron 26 (2007) 5088.

4. Self-assembled macrocyclic molecular squares of Ni(II) derived from carbohydrazones and thiocarbohydrazones: Structural and magnetic studies, E. Manoj, M.R.P. Kurup, H.-K. Fun, A. Punnoose, Polyhedron 26 (2007) 4451.

5. Macrocyclic molecular square complex of zinc(II) self-assembled with a carbohydrazone ligand, E. Manoj, M.R.P. Kurup, H.-K. Fun, Inorg. Chem. Commun. 10 (2007) 324.

6. Synthesis and spectral characterization of zinc(II) complexes of N(4)-substituted thiosemicarbazone derived from salicylaldehyde: Structural study of a novel -OH free Zn(II) complex, L. Latheef, E. Manoj, M.R.P. Kurup, Polyhedron 26 (2007) 4107.

7. Copper(II) complexes of N(4)-substituted thiosemicarbazones derived from pyridine-2-carbaldehyde: Crystal structure of a binuclear complex, P.F. Rapheal, E. Manoj, M.R.P. Kurup, Polyhedron 26 (2007) 818.

8. Structural and spectral studies of novel Co(III) complexes of N(4)-substituted thiosemicarbazones derived from pyridine-2-carbaldehyde, P.F. Rapheal, E. Manoj, M.R.P. Kurup, E. Suresh, Polyhedron 26 (2007) 607.

9. 2-Hydroxyacetophenone 4-phenylthiosemicarbazone, E.B. Seena, E. Manoj, M.R.P. Kurup, Acta Cryst. Cryst. Struct. Commun. C62 (2006) o486.

10. Salicylaldehyde N(4)-hexamethyleneiminyl thiosemicarbazone, L. Latheef, E. Manoj, M.R.P. Kurup, Acta Cryst, Cryst. Struct. Commun. C62 (2006) o16.

11. N"-N""-bis[di(2-pyridinyl)methylene]carbonic dihydrazide, E. Manoj, M.R.P. Kurup, H.-K. Fun, S. Chantrapromma, Acta. Cryst. E61 (2005) o4110.

12. [Di-2-pyridyl ketone N^4, N^4-(butane-1,4-diyl)thiosemicarbazonato-k^3 N, N', S] dioxovanadium(V), Varughese Philip, E. Manoj, M.R.P. Kurup, M. Nethaji, Acta Cryst, Cryst. Struct. Commun. C61 (2005) m488.

13. N-(Pyridin-2-yl)hydrazinecarbothioamide, P.F. Rapheal, E. Manoj, M.R.P. Kurup, E. Suresh, Acta Cryst. E61 (2005) o2243.

PATENT

1. A metal complex and a process thereof, Priya Srinivas, M.R. Prathapachandra Kurup, Easwaran potti Manoj, Rakesh Sathish Nair, *submitted for Indian Patent.*

CONFERENCE PAPERS

1. Self-assembled molecular square grid complexes of carbohydrazone ligands, E. Manoj, M.R.P. Kurup, A. Punnoose, International Conference on Materials for the Millenium, MatCon 2007, CUSAT. Kochi.

2. Structural and Spectral studies of novel Co(III) complexes of N(4)-Substituted thiosemicarbazones derived from pyridine-2-carbaldehyde, P.F. Rapheal, E. Manoj, M.R.P. Kurup, H.-K. Fun, National conference on the role of Analytical Chemistry in Materials Science and Technology, ACIMSAT-2006, Munnar.

3. Self-assembly of a macrocyclic molecular square: Structural and magnetic studies, E. Manoj, M.R.P. Kurup, H.-K. Fun, A. Punnoose, National seminar on Frontiers in Chemistry, FIC-2006, CUSAT. Kochi.